1-1-2005

Weathering effects on the mineralogy, chemistry and micromorphology of Pierre Shale

Matthew Alan Birchmier
Iowa State University

Weathering effects on the mineralogy, chemistry and micromorphology of Pierre Shale

by

Matthew Alan Birchmier

A thesis submitted to the graduate faculty

in partial fulfillment of the requirements for the degree of

MASTER OF SCIENCE

Major: Civil Engineering (Geotechnical Engineering)

Program of Study Committee:
Vernon Schaefer, Major Professor
David White
Michael Thompson

Iowa State University
Ames, Iowa
2005

Graduate College
Iowa State University

This is to certify that the master's thesis of

Matthew Alan Birchmier

has met the thesis requirements of Iowa State University

Signatures have been redacted for privacy

TABLE OF CONTENTS

LIST OF FIGURES

LIST OF TABLES

ABSTRACT

Following significant slope failures during the construction of the Oahe Dam site in South Dakota, many studies were conducted to understand the mechanism of the failures. These studies indicated strength loss unassociated with major changes in the mineralogy. The changing environments during the construction was noted to contribute to weathering and subsequent strength loss. Significant measures such as placement of a bituminous sealer within two hours of exposing a cut were taken to prevent the weathering process from occurring.

In this study, the residual strength for various degrees of weathering of Pierre Shale is correlated with a detailed mineralogical, chemical, and fabric investigation of the material. A weathering profile and wet/dry-cycled samples are analyzed with x-ray diffraction (XRD), x-ray fluorescence (XRF), and energy dispersive spectroscopy (EDS) in a scanning electron microscope to compare minor mineralogical/chemical changes with the residual strength measured from a ring-shear device.

It is concluded that the potassium ion is the main contributor to the higher strength of the unweathered Pierre Shale in the weathering profile. The increase in coarser particles in the transitional zone of the weathering profile causes a more turbulent mode of shearing to control and leads to higher residual strengths as well. It is also concluded the breakdown of clay particle size during wet/dry cycles causes a increase in the plasticity index and a decrease in the residual strength. The main mineralogical change in the wet/dry cycles involves the removal of the soluble gypsum mineral in the first few washings.

CHAPTER 1

INTRODUCTION

WEATHERING AND CLAY SHALES

Terzaghi (1939) summarized the purpose of geotechnical engineering almost perfectly:

> *"... in engineering practice, difficulties with the soils are almost exclusively due not to the soils themselves but to the water contained in their voids. On a planet without any water there would be no need for soil mechanics."*

The engineering problems encountered in overconsolidated clays and clay shales are due foremost to the presence of water, specifically slope instability. The problems are magnified by the high quantity of shrink/swell and active clay minerals.

While mechanical aspects of slope failures have been well studied, physico-chemical mechanisms are commonly overlooked in a project's design. The dynamic nature of soils and rocks requires engineers to look at the critical state, which may exist in some future environment. Strength loss associated with the physico-chemical state is magnified in overconsolidated clay and clay shales due to their geologic history and high clay contents. The economic and social impacts of these materials are significant. Nearly 1.5 billion U.S. dollars are lost and 25 to 50 people lose their lives yearly to landslides in the United States (FEMA 2004). Overconsolidated clays and clay shales underlay much of the areas prone to landslides in the U.S. (Schuster 1996). The area in North America most renown for landslides is along the upper Missouri and South Saskatchewan River basins, specifically in

the Pierre, Bearpaw, and Claggett Shale formations (Botts 1986). Brooker and Peck (1993) described the mechanism behind many of these problems: swelling of the clay, weathering and softening take place after rebound and initial fissuring leading to slope failure. The peak strength can only be used for initial failures while the residual strength is relevant for previous slides. Many studies have focused on the mechanical aspect of reaching the residual strength through swelling and strain softening but few studies have considered the physico-chemical mechanisms of the residual strength. It has been shown that residual strength is a dynamic property, subject to change with the environment (Moore and Brunsden 1996). Pore water chemistry, mineralogy and cation concentration have been observed to affect the residual strength by many authors. A better understanding of the role of weathering in a clay shale system is important as significant problems can be caused by small disturbances in clay shale systems (Brooker and Peck 1993). An understanding of the physico-chemical aspects of residual strength may help recognition and mitigation of potential problems associated with weathering in clay shales.

The Oahe Dam site and its geology provide an excellent case study on the many issues associated with clay shales. The site is underlain by several members of a Cretaceceous period clay shale called the Pierre Shale formation. The material deteriorates rapidly with wetting and drying cycles, turning into a sticky-gumbo clay (Knight 1963). Bentonite seams are scattered throughout the site, providing a potential shear surface and were recognized early in the project's design as the weakest material. Bentonite also swells to many times its dry volume when wetted. Significant weathering units exist throughout the formation as well. These units were weaker than the firm shale, by nearly a ten-degree difference in the peak friction angle (Fleming *et al.* 1970). Slopes at the site were designed

with the weathered shale peak strength parameters, c = 24.8 kPa (3.6 psi) and ϕ'= 11.9°, and constructed, followed by slope failures. The slopes were redesigned and constructed at the softened strength of c = 14.5 kPa (2.1 psi) and ϕ'= 8.5° with subsequent slides. Final decisions were made at the site to remove all of the weathered material, some 6.5 million cubic yards of excavated material, from a slide-prone abutment (Fleming *et al.* 1970). Significant measures were also taken to prevent softening of the shale during construction. A bituminous sealer or mortar was placed within two hours on fresh cuts to prevent any drying of the material (Johns *et al.* 1963), showing the quickness of the strength reduction. The severity and speed of the stress loss show the importance of knowing the mechanism controlling it. "*Small disturbances*," as described by Brooker and Peck (1993), in the material's micromorphology, mineralogy, and pore water chemistry may have led to the failures at the Oahe Dam.

The objective of this research was to correlate the weathering-induced alterations in the mineralogy, chemistry and micromorphology of Pierre Shale with changes in its residual strength. The research was divided into two parts: one part analyzed a weathering profile at the Oahe Dam site; and the second part looked at the effects of laboratory wetting and drying cycles on an unweathered Pierre Shale sample.

DOCUMENT ORGANIZATION

The thesis is organized to address the two parts of research with two journal papers. An extensive literature review is included in Chapter 2 to provide a background of the material in the succeeding chapters. The paper given in Chapter 3, "Strength of Pierre Shale in Relation to Weathering, Mineral and Chemical State," analyzes a weathering profile at the

Oahe Dam, South Dakota. The wetting and drying cycles of Pierre Shale are discussed in Chapter 4, "A Mineralogical and Chemical Study of the Strength Loss of Pierre Shale due to Wetting and Drying." A discussion of the two papers' results and future research are provided to conclude this Thesis.

Five appendixes are included. Appendix A shows the Bromhead Ring Shear reports and the residual strength and settlement plots for the ring-shear tests. Appendix B is the multistage testing procedure used to obtain the residual strength with the Bromhead Ring Shear Device. The boring log for PZT50-5.42 and the engineering classifications are in Appendix C. Appendix D and E are provided as an attached electronic document. All of the work completed with the scanning electron microscope (SEM), including electrodispersive spectroscopy (EDS) results, is shown in Appendix D. The mineralogy and chemistry data and results from x-ray diffraction (XRD) and x-ray fluorescence (XRF) are in Appendix E.

CHAPTER 2

BACKGROUND

INTRODUCTION

Appreciation for the weathering changes in the mineralogy, chemistry, and micromorphology and the subsequent engineering behavior provides a geotechnical engineer with invaluable knowledge of how to ensure success of their designs. This literature review provides a general background of the weathering processes, mineralogy, and the engineering behavior of Pierre Shale. Physical and chemical weathering processes known to occur in Pierre Shale are initially discussed and are followed by the complex and colloid behavior of clay minerals. Shales and clay shales, including classification schemes, sedimentology, weathering concerns, and engineering problems are then presented. The clay shale topic is narrowed to the Pierre Shale formation, and finally to the Oahe Dam site, to provide the reader a general understanding of the problematic shale. The theory and testing procedures of residual strength are then discussed. The literature review is concluded with a consideration of various methods to determine mineralogical, chemical, and micromorphology features.

WEATHERING PROCESSES

Weathering is described as the alteration of rock or soil by chemical and physical processes (Birkeland 1999). Ollier (1969) outlined chemical weathering as a result of alterations due to the material being out of chemical equilibrium with the atmosphere,

hydrosphere, and/or biosphere. Weathering can take place underwater, but most often occurs on land (Ollier 1969). Soil and rock properties can change significantly during the alteration. These alterations affect the material's strength, permeability, and compressibility. Physical weathering occurs when stresses buildup within a material causing the material to break. A fracture will occur where the resistance is the least, between bedding planes or the mineral grains. Chemical weathering causes a change in the chemical consistency of the material (Birkeland 1999). Physical and chemical weatherings' occurrence and rate are controlled by five main variables: climate, organisms, topography, parent material type, and time (Taylor and Cripps 1987). Weathering rates tend to increase for increases in climate, organism activity, and in areas with good drainage and steep slopes. Weathering rates decrease for increases in parent material resistance and time (Ritter *et al.* 2002). The resistance will be dependent on the mineral's position in the Bowen's Reaction Series, a diagram showing the stability of silicate minerals based on their formation characteristics (Birkeland 1999). Olivine is the least stable mineral in the series; quartz is the most stable; and the abundant feldspar minerals are in the center of the series. An overview of the physical and chemical weathering processes is shown in Figure 1, where it can be seen that weathering is a very complex phenomenon.

The weathering processes, through physical, chemical, and biological breakdown, lead to erosion, sedimentation, and/or the formation of a soil profile. These physical, chemical, and biological processes may affect the mechanical behavior of the material differently.

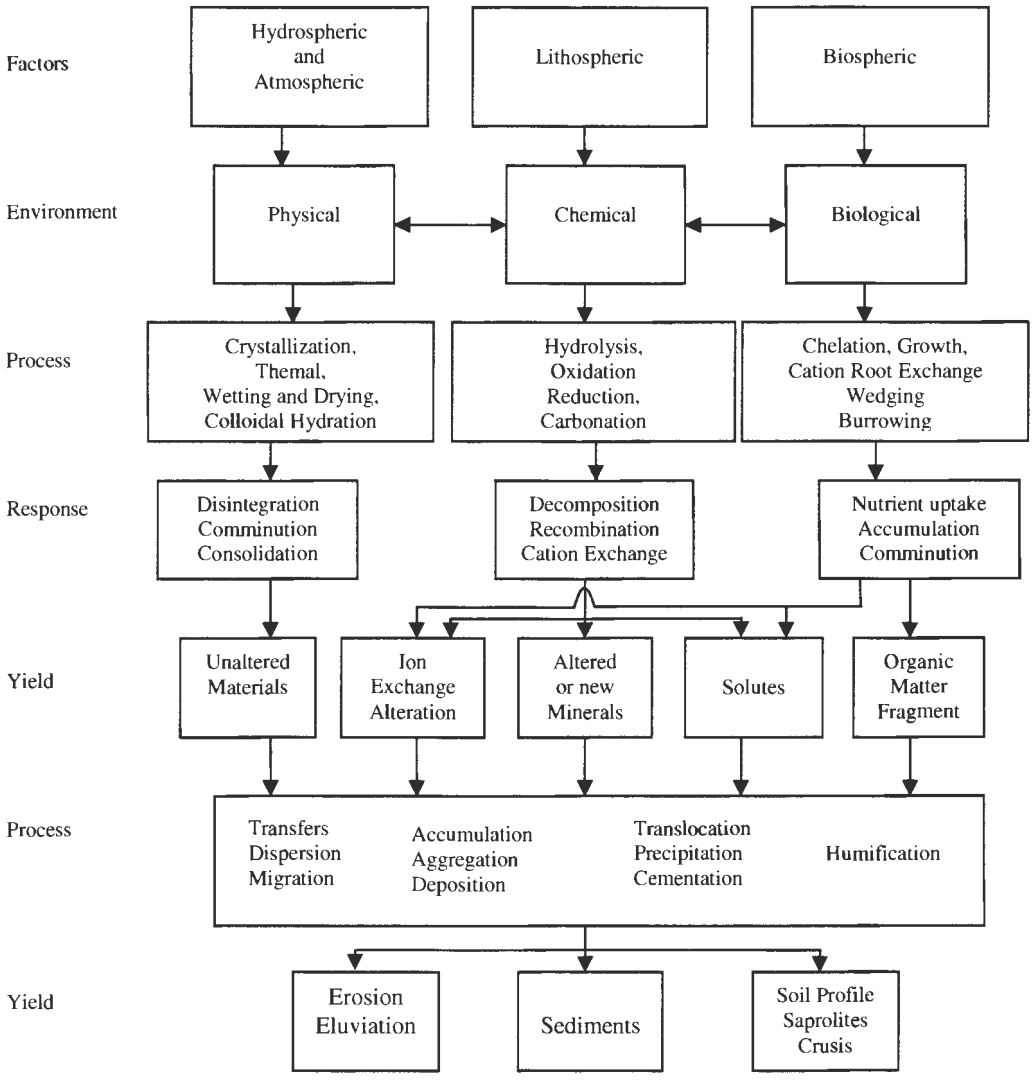

Figure 1. Weathering Processes (from Slaymaker 1988).

Physical Weathering

Unloading, frost weathering, and crystal formation are physical weathering processes. Unloading occurs when a mass is removed from an underlying material, by erosion, glacial retreat, or man. A buried rock mass consolidates elastically under the confining pressure. During unloading, stresses are released causing the rock to expand and fracture. Fracture size generally increases with depth due to the increase in confining pressure. Rocks near the

surface mostly expand upwards due to the lower confining stresses (Birkeland 1999). Isostatic rebound after the retreat of glaciers is an example of unloading. Additionally, the uplift of materials due to the load removal brings the materials in contact with a different environment, causing an increase in weathering rates.

Crystal growth and formation causes material disintegration in three ways. Internal stresses are created when salt precipitates and crystallizes from solution. The volume increase associated with the crystallization builds up *in situ* stresses as well. As an example, the growth of gypsum crystals has been observed to produce expansion pressures between 72 and 2,110 kPa (10.4 and 305.7 psi) (Luteneggar *et al.* 1979). Thermal expansion can occur when the salts are heated due to the high thermal expansion coefficient of many salts in comparison to common rocks, a possible cause for arid region weathering (Birkeland 1999).

Physical weathering compliments the occurrence of chemical weathering. The reduction of particle size during physical weathering exposes more surface area, increasing chemical weathering (Taylor and Cripps 1987). Unloading and tectonic movements also exposes material to new environments enhancing chemical weathering.

Chemical Weathering

Chemical weathering takes place due to a change in the systems' chemistry, putting the system out of equilibrium with its environment (Loughnan 1969). Chemical reactions can be significant in silt and clay fractions due to the high contact areas from the small particle sizes. Soil and rock decompose through chemical weathering processes such as hydrolysis, ion exchange, dissolution, and oxidation/reduction. Mitchell (1976) describes hydrolysis as the most important weathering process for soils. Hydrolysis is a reaction in

clay minerals between the mineral ions and the H^+ or OH^- ions of water. Equation 1a shows the formation of an illite molecule from the hydrolysis reaction between orthoclase and water (Ritter *et al.* 2002). Alternatively, all of the potassium cation can go into solution in the hydrolysis reaction of orthoclase to form kaolinite, as shown in Equation 1b.

(orthoclase) (illite)

$$3KAlSi_3O_8+2H^++12H_2O\rightarrow KAl_3Si_3O_{10}(OH)_2+6H_4SiO_4+2K^+ \quad (1a)$$

(orthoclase) (kaolinite)

$$2KAlSi_3O_8+2H^++9H_2O\rightarrow Al_3Si_3O_{10}(OH)_2+4H_4SiO_4+2K^+ \quad (1b)$$

The reaction will not occur in static waters as soluble materials must be removed and new H^+ ions introduced into the system. pH is also important in the reaction as it controls the amount of H^+ ions available and the solubility of SiO_2 and Al_2O_3 (Ritter *et al.* 2002).

Ion exchange is a significant weathering process, especially in clay minerals. The substitution of ions in solution for ions in the mineral grains occurs in clays due to the unsatisfied charge, the exposed hydroxyl on the edges, and isomorphous substitution (Mitchell 1976). Isomorphous substitution is the replacement of an ion in a mineral structure, upon formation, with an ion of another type. The substitution of Al^{3+} for Si^{4+} and Mg^{2+} for Al^{3+} are examples of isomorphous substitutions in clay minerals. Such substitution leads to a charge imbalance on the clay particle surface. Adsorption occurs when ions are attracted to colloidal surfaces, such as a clay surface, to counterbalance the negative charge. The adsorbed ions are loosely held and can be replaced by other ions. Cation exchange capacity (CEC) is a soil parameter describing the soil's ability to adsorb cations. Table 1

shows CEC values for various materials. Organic material has the highest CEC values while non-clay minerals such as quartz have the lowest. Smectites, very active clay minerals, have CEC values between 80 to 150 meg/100g dry weight in comparison to illite and kaolinite CEC values of 10 to 30 and 1 to 10 meg/100g dry weight. Ion exchange is controlled by the pH and composition of the interstial pore water and the type of ion. The pH is an indicator of the number of cations in the exchangeable position. Lower pH means more H^+ ions are replacing metal cations (Ritter *et al.* 2002).

Table 1. Cation-exchange capacity (from Birkeland 1999).

Material	Approximate Cation-Exchange Capacity (meg/100g dry weight)
Organic matter	150-500
Kaolinite	1-10
Halloysite	5-10
Hydrated halloysite	40-50
Illite	10-30
Chlorite	10-40
Smectite	80-150
Vermiculite	100-200+
Palygorskite	5-30
Sepiolite	20-45
Allophane	20-50
Hydrous oxides of aluminum and iron	4
Feldspars	1-2
Quartz	1-2
Basalt	1-3
Zeolites	230-620

The loss of an electron in an element to an oxygen ion is called oxidation. The process occurs above the water table in the presence of oxygen. Below the water table, with the presence of an energy source, reducing conditions exist and the element takes on an electron. When iron, in the ferrous state (Fe^{2+}), is exposed to the atmosphere, it oxidizes into

the ferric state (Fe^{3+}), as shown by Equation 2 (Ritter *et al.* 2002). Groundwater moves through fissures, a common macrostructure in overconsolidated clays and clay shales, or pore spaces of soil and serves as a pathway for oxidation.

$$2Fe^{2+}+4HCO_3^-+1/2O_2+2H_2O\rightarrow Fe_2O_3+4H_2CO_3 \quad (2)$$

Groundwater and weathering zones also leach secondary minerals and ions. Leaching is dependent on the mobility of the ion. Solubility follows a specific preference: $(Ca^{2+},Mg^{2+},Na^{+})>K^{+}>Fe^{2+}>Si^{4+}>Ti^{4+}>Fe^{3+}>Al^{3+}$, and is a function of the amount of water infiltrating into the rock (Ritter *et al.* 2002). Without leaching, weathering will cease due to an equilibrium in the system being reached.

CLAY MINERALS

The micron size of clay minerals provides large surface areas, from one to almost 900 m^2/gm, to weather. Many of the clay minerals encountered in the field belong to the phyllosilicate family (Nemecz 1981). These minerals consist of two fundamental units: the silica tetrahedron and the aluminum octahedron (gibbsite), as shown in Figure 2a and 2b, respectively.

A silica tetrahedron consists of four O^{2-} ions on the corners of a tetrahedral, equidistance from a Si^{4+} ions. Al^{3+} can replace Si^{4+} in the silica tetrahedron due to isomorphous suhstitution. An Al^{3+} ion is octahedrally coordinated with six O^{2-} or OH^- ions in the aluminum octahedron. Mg^{2+} can replace Al^{3+} in the aluminum octahedral due to isomorphous substitution (Mitchell 1976).

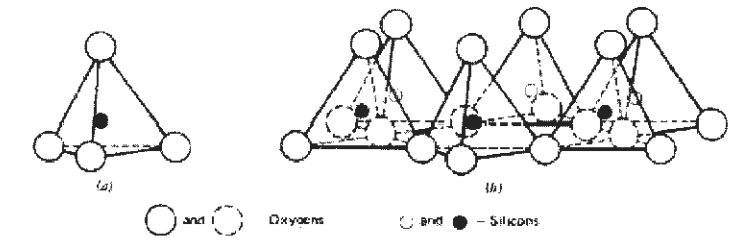

(a)

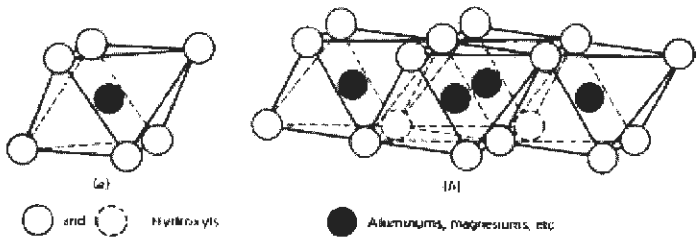

(b)

Figure 2. Clay mineral fundamental units, Silica tetrahedron b) Aluminum octahedron (from Grim 1953).

Interatomic bonds hold the mineral crystal structure together and occur when electrons between elements interact. Ionic and covalent bonds are examples of primary bonds where only outer shell electrons participate. Ionic bonds occur when an anion bonds with a cation to complete its outer shell. Covalent bonds form as a result of one or more electrons being shared by two atoms. The bonds are strong due to the large energy loss associated with primary bonds. Secondary bonds such as hydrogen and van der Waals bonds hold elements together but are weaker than primary bonds. Hydrogen bonds consist of the positive dipole end of H^+ attracting the negative dipole ends of elements or molecules. Van der Waals bonds are fluctuating dipole bonds (Mitchell 1976).

Clay minerals also have a negative charged surface and a distribution of counter-ion charge associated with the particle, called the diffuse double layer (DDL) (van Olphen 1977).

This area of repulsion and attraction charges, as shown in Figure 3, has a direct influence on the behavior of the clay. Decreases in the DDL thickness causes the strength of the clay minerals to increase.

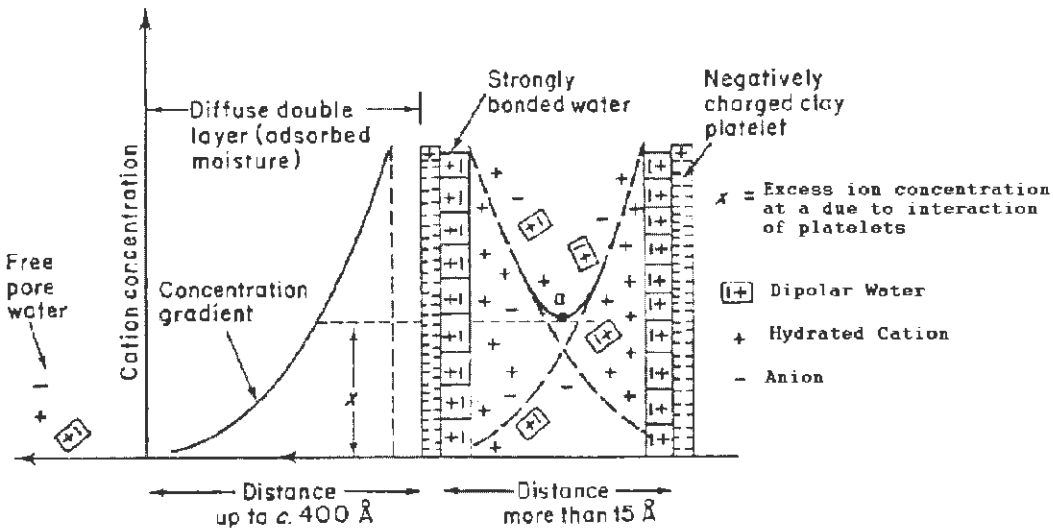

Figure 3. Clay mineral diffuse double layer and ion distribution (from Taylor and Cripps 1987).

Attraction forces in the diffuse double layer are due to van der Waal forces. Van der Waal forces are dependent on the dielectric constant and temperature. Repulsion forces are theorized to develop from electrostatic interference of diffuse counter-ion atmospheres of clay particles as they approach each other due to their Brownian motion. Electrolyte valence and concentration, pH, and dielectric constant control the repulsion forces (van Olphen 1977).

Suppression of the DDL causes clay particles to flocculate, while expansion of the DDL leads to dispersion. For a given cation, an increase in the concentration increases the attraction between clay particles (van Olphen 1977). Higher valency and larger

polarizability, such that $Ca^{2+}>K^{+}=Na^{+}$ and $K^{+}>Na^{+}$, respectively, suppress the double layer thickness (Mitchell 1976). A material's pH is also likely to control the diffuse double layer. Acidic conditions ionize the exposed alumina on the edges of clay minerals into a positive state. This promotes the formation of an unstable flocculated, cardhouse structure. pH has been proposed to be one of main controls of the fabric in kaolinite. The role of the pH has less importance in illite and has minimal importance in montmorillonite (Mitchell 1976)

Clay minerals are described in terms of their layer thickness, composition, and stacking (Mitchell 1976). Kaolinite, a 1:1 clay mineral, consists of alternating silica tetrahedra and gibbsite sheets bonded by strong hydrogen bonds and van der Waals forces (van Olphen 1977), as shown in Figure 4a. The chemical formula for a kaolinite unit cell is $(OH)_8Si_4Al_4O_{10}$. Cation exchange capacity (CEC) is minor, 1 to 10 centimole per kilogram, with only one Si^{4+} in every 400 substituted by Al^{3+}. Figure 4b shows illite, a 2:1 clay mineral with a chemical formula of $(K,H_2O)_2(Si)_8(Al,Mg,Fe)_{4,6}O_{20}(OH)_4$. Silica tetrahedra sandwich a gibbsite sheet forming a 3-sheet layer with the interlayer bond consisting of strong ionic bonds with potassium. Basal spacing is approximately 10 Å and the strong interlayer bonding of potassium gives illite a non-swelling behavior. The CEC of 20 to 40 centimole per kilogram is due to the isomorphous substitution (van Olphen 1977). Montmorillonite (a smectite), Figure 4c, also consists of silica tetrahedrons sandwiching a gibbsite sheet, but with weaker cation interlayer bonds. The chemical formula is given by $\underset{\downarrow\ Na_{0.66}}{(OH)_4Si_8(Al_{3.34},Mg_{0.66})O_{20}\cdot nH_2O}$ (Mitchell 1976). One in every six Al^{3+} in the octahedral sheet is replaced by Mg^{2+} giving montmorillonite a CEC between 80 to 150 centimole per kilogram. Water can cause expansion due the water molecules entering between the layers as it is adsorbed on the surface (Loughnan 1969). Montmorillonite, due to its weak interlayer

bonding, is the most active clay, followed by illite, and then kaolinite (Mitchell 1976). Many of these characteristics are used in the identification during analyses.

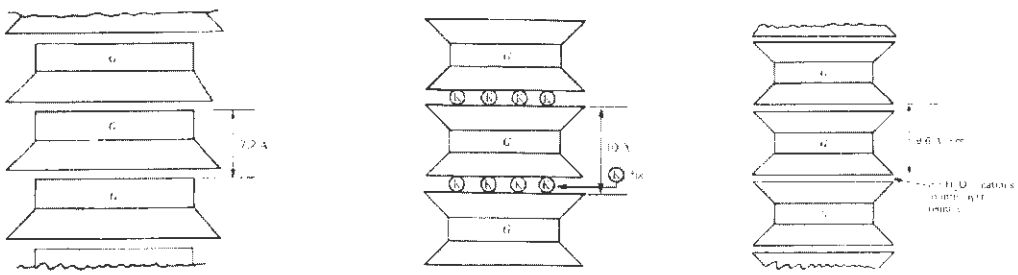

(a) (b) (c)

Figure 4. Structure of clay minerals, a) Kaolinite, b) Illite, c) Montmorillonite (from Mitchell 1976).

Mixed-layer minerals composed of multiple clay minerals are often found in nature in excess of other clay minerals. Two types of mix-layered structures were described by Grim (1953): regular interstratification, in which alternation of clay minerals is constant, and random, irregular interstratification, in which no order exist in the repetition of clay minerals. Random interstratified mixed-layer clays occur more often than regular interstratified mixed-layer clays. Illite and smectite (montmorillonite) mixed-layer clays have an irregular interstratification structure and are the most abundant mixed-layer clay (Grim 1953, Weaver 1989). The percentage of the two minerals is used to describe the composition. Mixed-layer clays form due to the increased temperatures associated with burial diagenesis, causing montmorillonite to convert to illite (Weaver 1989). The K-ion in smectite/illite mixed-layer clays is directly associated with the illite mineral.

SHALE AND CLAY SHALES

Classification

Fine-grained sediments make up nearly half of the geological rock in the world (Picard 1971). Due to the analysis complexities, little research was performed on fine-grained sediments before the 1960s (Picard 1971). Picard (1971) proposed a geological classification system of fine-grained sediments based on the clay, silt, and sand distribution and the mineralogical composition. In addition to the classification system, a full description of fine-grained sediments were obtained with the degree of fissility, bedding types and sedimentary structures, fossil content, and color (Picard 1971). The term "shale" has often been used to cover the spectrum of fine-grained sediments. Spears (1980) classified shale as fissile or laminated rock. Shale was therefore required to have stratum less than 1 cm in thickness (laminae) or be able to separate parallel to the bedding plane (fissility).

Engineering classification schemes for shales and clay shales are more useful for design purposes than geological schemes. Underwood (1967), Morgenstern and Eigenbrod (1974), and many others are a few sources for engineering classification of clay shales. Terzaghi (1936) classified clays into three categories: (1) soft, intact clays free from joints and fissures, (2) stiff, intact clays free from joints and fissures, and (3) stiff, fissured clays. Terzaghi noted the occurrence of stiff clays without fissures to be rare. Category 3, fissured clays, would include clay shale. Figure 5 shows a diagram of the classification of clay shale. By Underwood's (1967) definition, 50% or more of the particles in clay shale are clay size (<2μm). Clay shale is divided into soil and rock behavior based on the materials bonding. Underwood (1967) also produced an index of geotechnical properties, shown in Table 2, related to shale. Under unfavorable conditions, clay shale poses a potential problem for slope

stability as given by the low mechanical properties in Table 2. A main theme of the clay shale definitions in the literature was the large amount of overconsolidation in clay shale (Fleming *et al.* 1970). Fleming *et al.* (1970) concluded clay shale as material with silt- and clay-sized particles of sedimentary origin and their behavior and properties a function of the degree of overconsolidation and lithology. Lithology covers the origin of the sediment, transportation agents, and deposition environment. Cementing by iron oxide, calcite, or silica may be present with current consolidation pressures far less then past overburden loads. Clay minerals also constitute a large portion and the material may slake during wetting and drying cycles. Potter *et al.* (1980) classified clay shale as materials with medium laminae (4 mm) and clay-size particles between 66 and 100%. Medium laminae were described as platy parting in the shale lamination. Botts (1986) defined clay shale as a stiff clay or shale in which deteriorates in the presence of water. This definition includes the transitional phases of clay shale, which many definitions exclude.

Sedimentology and Development

Geologic history partially governs the behavior and properties of clay shale (Fleming *et al.* 1970). It is therefore beneficial to have a basic understanding of the formation and development of clay shale. The deposition of mud, a precursor of shale and other mudrock sediments, is proposed to be from weathering at the earth's surface of other muds, mudrocks, and shales as shown in Figure 6 (Potter *et al.* 1980). Potter *et al.* (1980) notes high temperatures and pressures were the main causes of weathering of silicate minerals. Glacial processes and volcanic dust were also given as possible sources of silicate minerals (Potter *et al.* 1980). The weathering processes generate mud with feldspars, micas, quartz and clay

minerals. Clay particles are deposited in areas of little energy such as offshore environments while coarser particles, such as quartz and silt particles, are deposited near the shoreline. Due to its small size, montmorillonite requires a very still body of water to settle to the seabed (Botts 1986). Deposition of muds occurs during the evaporation of water from basins, settlement of individual particles in still water, organism activity causing aggregation, or particle flocculation (Potter *et al.* 1980). Particles flocculate due to the colloidal behavior of the clay minerals. Interaction between the water chemistry and the DDL of the clay particles causes flocculation. The alkaline conditions and high calcium-ion concentrations of marine environments favored the formation of montmorillonite, illite, and chlorite minerals (Grim 1953). As discussed in the *Weathering processes* section, climate can amplify the weathering rates. Illite can be transformed to montmorillonite and montmorillonite can be further converted to kaolinite under high temperatures and rainfalls during the weathering phases (Botts 1986).

As sedimentation continues, diagenesis changes the minerals and structure. Diagenesis is described as changes occurring between the time of deposition until the recrystallization of sediment due to a change in the environmental conditions (i.e. Water chemistry, organisms, temperature, pressure). While weathering is associated with land processes, diagenesis is primarily an occurrence in the sea (Ollier 1969). The most significant diagenesis change is the transformation of smectite into illite (Weaver 1989). The recrystallization causes particles to conform to each other, forming bonds. The soil structure becomes denser, stronger, and more brittle as the bonds are subjected to higher pressures and temperatures. The bond formation is a function of the mineralogy and loading duration. Higher amounts of strain energy are absorbed upon loading for higher plasticity materials

(Fleming *et al.* 1970). The soil can be classified as soft rock if the bonds become strong enough (Bjerrum 1967).

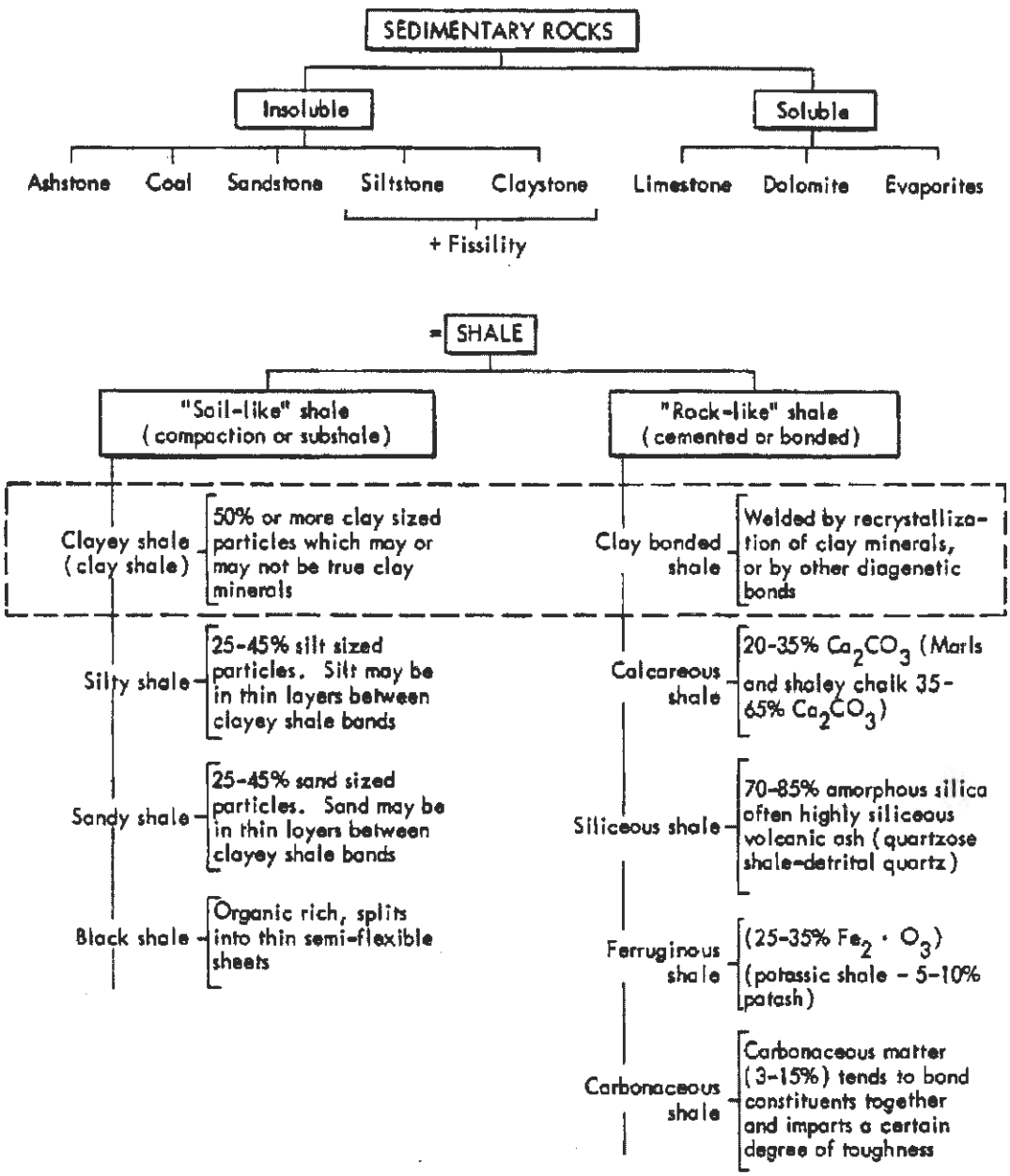

Figure 5. Clay shale classification system (from Underwood 1967).

Table 2. Clay shale engineering properties (from Underwood 1967).

Physical properties			Probable *in situ* behavior						
Laboratory tests and *in situ observations*	Average range of values		High pore-pressure	Low-bearing capacity	Tendency to rebound	Slope stability problems	Rapid slaking	Rapid erosion	Tunnel support problems
	Unfavorable	Favorable							
Compressive strength, psi	50 to 300		*	*					
		300-5000							
Modulus elasticity, psi	20,000 to 200,000			*					*
		200,000 to $2X(10^6)$							
Cohesive strength, psi	3 to 100				*	*			*
		100 to >1500							
Angle of internal friction, deg	10 to 20				*	*			*
		20 to 65							
Dry density, lb/ft^3	70 to 110		*					* (?)	
		110 to 160							
Potential swell, %	3 to 15				*	*		*	*
		1 to 3							
Natural moisture content, %	20 to 35		*			*			
		5 to 15							
Coefficient of permeability, cm/sec	10^{-5} to 10^{-10}		*			*	*		
		$>10^{-5}$							
Predominant clay minerals	Montmorill-onite or illite		*			*			
		Kaolinite to chlorite							
Activity ratio: PI/clay content	0.75 to >2.0					*			
		0.35 to 0.75							
Wetting and drying cycles	Reduces to grain sizes						*	*	
		Reduces to flakes							
Spacing of rock defects	Closely spaced			*		*		* (?)	*
		Widely spaced							
Orientation of rock defects	Adversely oriented			*		*			*
		Favorably oriented							
State of stress	Existing overburden load				*	*			*
		Overburden load							

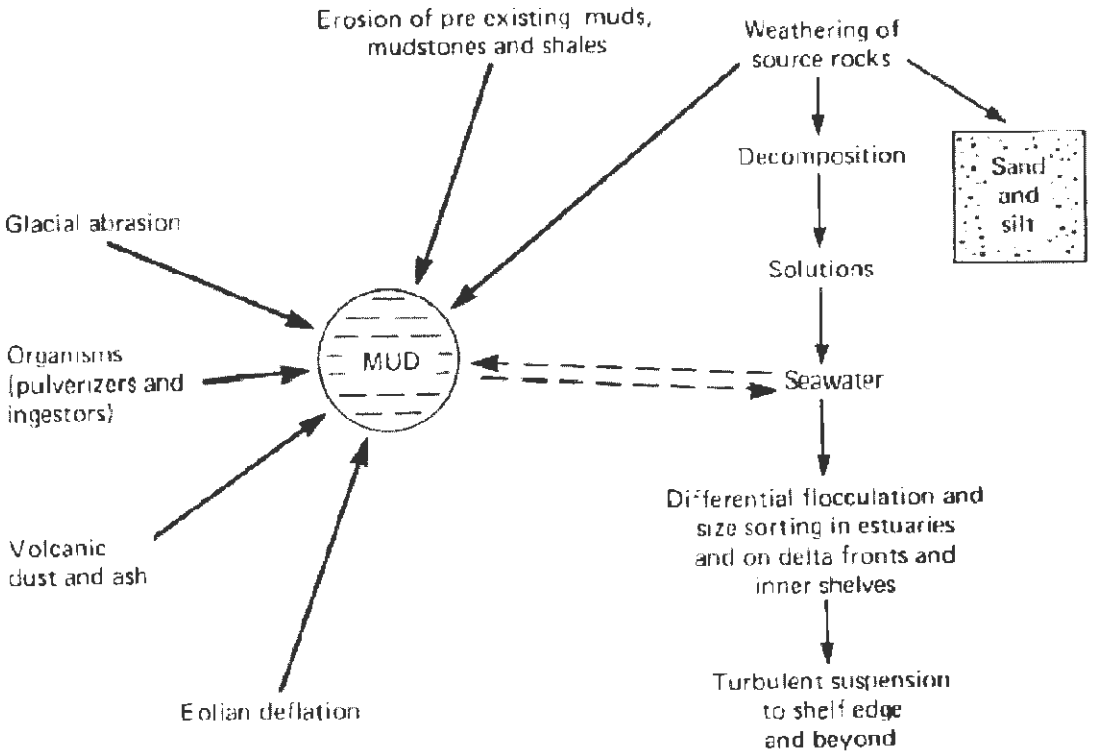

Figure 6. Deposition of mudstones/shales (from Potter *et al.* 1980).

A fundamental part of clay shale is the high degree of overconsolidation. Botts (1986) described the behavior of clay shale in terms of the degree of consolidation and degree of unloading. The bonds formed due to diagenesis hold strain energy within the soil structure after unloading occurs. As overburden material is removed, the clay structure expands due to the recoverable strain energy, with the final water content a function of the amount of strain recovery. The final water content will be less than the amount of water expelled during the consolidation phase in the geologic loading history of the material (Bjerrum 1967). Bjerrum (1967) described three different types of bonds: weak, strong, and permanent bonds. The amount of energy released upon unloading is dependent on the type of bond. Weak bonds release all of the entrained energy while strong bonds release energy

slowly after unloading. The energy within permanent bonds is never released. Weak bonds in montmorillonite and illite material absorb water into the crystalline structure upon unloading. The high swelling ability of montmorillonite can create high internal stresses in the material, creating fissures and slickensides. Fissures and joints are free surfaces where no shear resistance exists, a problematic feature for slope stability.

Weathering in Mudrocks and Overconsolidated Clays

Weathering poses many challenges to the engineering community. Bjerrum (1967) noted the significance of weathering on the strength of clay shales. Significant outcropping of clay shale due to isostatic rebound or tectonic uplift are synonymous with slope stability problems (Botts 1986). Landslides, ground heaving, and acid water are a few examples of the potential problems weathering poses (Oyama and Chigira 1999). Skempton (1964) and others also noted softening as a problem associated with clay shale. Physical weathering in mudrocks and overconsolidated clays can be very rapid and can be a front for chemical weathering processes due to their geologic history (Taylor and Cripps 1987). The high horizontal stresses in overconsolidated materials increases the weathering rates because of the fissurization processes inherent in such materials. Mechanical weathering was noted by Deere and Paton (1971) as a more significant process in clay shales than chemical weathering. Many studies have observed minor mineralogical changes in clay-shale weathering profiles (Fleming *et al.* 1970, Russell and Parker 1979).

Weathering's importance in clay shale is a function of the type of bond and the amount of relaxation. Structural relaxation and rebound features govern the rate and depth of weathering (Fleming *et al.* 1970). Structural relaxation increases near the surface in features

such as fissures (Fleming *et al.* 1970). Intraparticle swelling in expandable clays and osmotic pressures cause swelling and disintegration as well. Osmotic swelling occurs when the cation concentration between clay minerals is greater than the surrounding pore water (Taylor and Cripps 1987). Swelling of the clays, weathering, and strain softening occur after the rebound and initial fissuring. These processes lead to strain softening, causing slope instability (Brooker and Peck 1993). Large landslides can cause additional stress release, accelerating weathering and strength reductions (Chigira *et al.* 2003).

Slaking is a common physical weathering process in shale after the removal of confining stresses. The physical disintegration occurs due to stress buildup within the material or a decrease in strength. The slaking rate is controlled by straitagraphic (lithology and mineralogy) and structural (megascopic and microscopic) characteristics of the material. The degree of disintegration for indurated mudrocks is greater than weakly bonded clays, producing a wider particle distribution (Taylor and Cripps 1987). Indurated mudrocks are defined as sediments that have become hardened or cemented (Potter *et al.* 1980). Clay minerals increase the slaking rate due to their hydrating and physico-chemical behavior (Perry and Andrews 1984). Slaking modes are largely dependent on the mineralogy, but can be related to the physico-chemical aspects of the material (McClure 1980). Osmotic swelling occurs in sodium clays; calcium montmorillonites slake by osmotic swelling and hydration; calcium illite slakes by hydration and compressed air; and calcium kaolinite swells and slakes by compressed air. Slaking increases for higher activity minerals.

Three distinct weathering zones are prevalent in shales (Fleming *et al.* 1970). The first zone immediately below the surface shows varying degrees of disintegration based on the climate. This layer is severally strained by repeated freeze-thaw and wet-dry cycles.

Fleming *et al.* (1970) describes the second zone as a layer of "*...active advanced disintegration...*". Pore pressure variation from groundwater fluctuation and unloading are influential in the strains induced in the second zone. The lowest zone experiences no surface effects except swelling, dependent on the frequency of fractures and the mineralogy (Fleming *et al.* 1970).

Softening in clay shales has been observed to cause significant strength loss. Some deposits have shown up to 80% reduction in strength over a 30 to 70 year period (Skempton 1964). Two basic mechanisms were indicated by Botts (1986) to cause softening in clay shales:

> *"...equilibration of negative pore pressures and the deterioration of fissures by means of chemical alteration or slaking."*

Underlying both of these mechanisms was the existence of fissures in clay shale. Botts (1986) highlighted four main effects of fissures in the role of softening:

> *"...provide planes of weakness along which shear can occur...increase the permeability of clay shale deposits...significantly increase the surface area exposed to weathering agents...greatly enhance the process of deterioration in clay shales..."*

Negative pore water pressures form as the clay shale is unloaded and persist for long periods due to the low permeability of the material. The negative pore pressures increase the effective strength of the material initially, but as pore pressures are replaced by fluid, the material strength is reduced (Skempton 1964).

Acid formation can be destructive to a mineral's structure, specifically soluble carbonates such as calcite (Oyama and Chigira 1999). Sulfuric acid, H_2SO_4, is produced

from the oxidation of pyrite, FeS_2. Pyrite is the most common sulfide mineral and can rapidly oxidize when it is exposed to oxygen from groundwater or the atmosphere as shown in Equation 3 (Sammut *et al.* 1996). The oxidation reaction is exothermic and causes large volume changes and pressures, up to 500 kPa (72.5 psi). Taylor and Cripps (1987) concluded the oxidation of pyrite is a significant process in the weathering of mudrocks and overconsolidated clays.

$$FeS_2 + 15/4O_2 + 7/2H_2O \rightarrow Fe(OH)_3\downarrow + 2SO_4^{2-} + 4H^+. \quad (3)$$

Oyama and Chigira (1999) observed an oxidation front of pyrite in a mudstone weathering profile in a newly built tunnel wall. The unsaturated conditions of the tunnel caused a change in the tunnels environment to oxidizing conditions. Oxygen diffused into the rocks causing pyrite and FeO in the clay mineral to be oxidized. The sulfuric acid dissolved carbonate and glass bonds causing the material to weaken. Grainger and Harris (1986) observed a similar case with iron oxyhydroxide stains on a pyritic-oxidized mudrock and a color change from a dark grey in the intact material to a brown and pale grey in the oxidized material. Acids initially caused the dissolution of carbonate minerals and then caused the dissolution of silicate minerals. Sulfuric acid also attacks the edges of octahedral sheets of micas, smectites, and chlorites. When the sulfuric acid reacts with clay minerals, silica and metal ions are released (Sammut *et al.* 1996). Pye and Miller (1990) described the acid hydrolysis of illite when reacting with a sulfuric acid, releasing potassium ions, as given by Equation 4:

$$K_2Al_4Si_6Al_2O_{20}(OH)_4+2H^++3H_2O \Rightarrow 3Al_2Si_2O_5(OH)_4+2K^+. \quad (4)$$

Trace heavy metals and manganese can also be released due to the reaction. The fast reaction rate associated with pyrite causes many engineering problems. Chigira and Oyama (1999) found many case studies of heave, acid soil, slope failures, and leaching associated with weathering-induced damage in pyritic sedimentary soils.

Weathering zones within many pyritic weathering profiles were observed by Chigira and Oyama (1999). Figure 7 shows the weathering fronts with varying sulfuric acid (H_2SO_4) directions. Areas with oxygen and sulfuric acid in the same direction gave rise to an oxidized and dissolved zone. The oxygen was consumed in the oxidation zone while sulfuric acid moved farther down into the dissolved zone. When the sulfuric acid migrated through the oxidation zone, the dissolution and oxidized zones were combined. The downward movement of water was concluded to be the cause of the differentiated zones. Mudstones near the dissolution front showed dissolution of minerals and volcanic glass, leaching, and calcite depletion in Figure 7. The oxidation front displayed sulfuric acid and iron oxide stains from the oxidation of pyrite and the conversion of chlorite into a smectite clay mineral. Within the surface oxidation zone, a decrease in smectite crystallinity was observed in the mudstone. A sandstone material showed a similar weathering profile, except with a manganese oxides precipitate in the surface oxidized zone (Chigira and Oyama 1999).

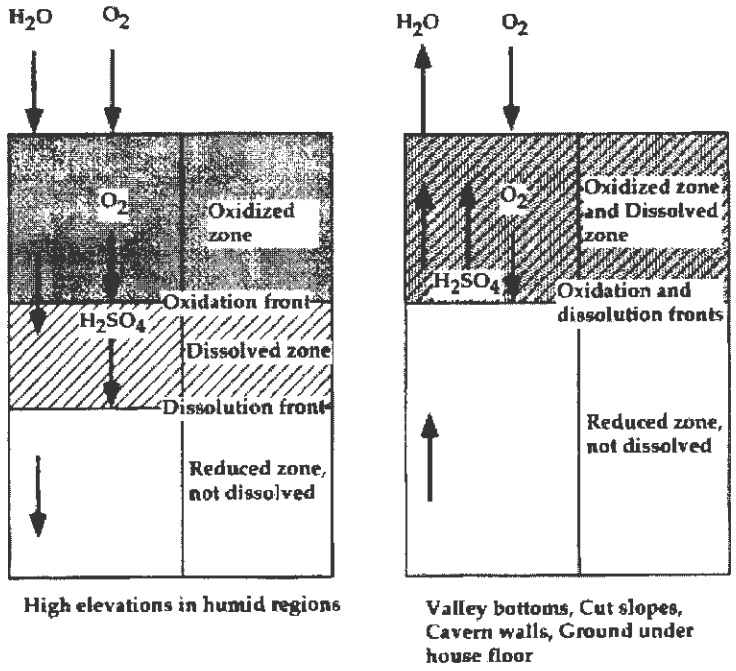

Figure 7. Weathering fronts for sulfuric acid (from Chigira and Oyama 1999).

Acid formation gives rise to subsequent chemical reactions. Cations can be released through dissolution or leaching of minerals, reacting with other materials. The reactions can result in crystal formation producing large expansive pressures causing heave, possibly up to 2,100 kPa (305 psi) (Luteneggar *et al.* 1979). Pye and Miller (1990) observed compaction problems with fill after pyrite oxidized and gypsum precipitated. Russell and Parker (1979) noted the importance of oxidation of pyrite in overconsolidated clays and the formation of gypsum, causing an uptake of cations. When sulfate ions from the acid react with available calcium in the material, possibly from the dissolution of carbonate minerals, gypsum is precipitated as expressed by Equation 5 (Russell and Parker 1979). If available potassium ions in the material react with the sulfuric acid, jarosite ($KFe_3(OH)_6(SO_4)_2$) can form. Jarosite frequently takes up potassium ions leached from illite and is a common mineral in over-consolidated clays and mudrocks (Russell and Parker 1979).

$$Ca^{2+}+SO^{4-}+2H_2O \rightarrow CaSO_4 \cdot 2H_2O \quad (5)$$

Clay minerals have also been observed to go into dissolution in weathering profiles. Pederstad and JØrgensen (1985) found large concentrations of K-feldspar, quartz, and plagioclase to be weathered away in marine clays. Trioctahedral illites were observed to break down to mixed-layer clays and dissolved in high weathering zones while dioctahedral illite was partially broken down to chloritized vermiculite. Dissolution of the other phyllosilicates caused the dioctahedral illite concentration to increase in the marine clay. Russell and Parker (1979) also indicated illite degradation in weathering zones.

Engineering Problems with Overconsolidated Clays and Clay Shales

In the third Terzaghi Lecture, Bjerrum (1967) concluded slope stability in overconsolidated clays and clay shales has strong correlations with the geological properties of the material. Bjerrum (1967) highlighted the recoverable strain ability as a source of engineering concern. The behavior of clay shales complicates the geotechnical issues. Clay shales can behave like rock or soil, with alterations to the material causing the behavior to shift towards a more soil behavior (Botts 1986).

Strength loss is commonly recorded in freshly weathered material, at shallow depths where construction projects occur. Slickensides formed during stress release can provide a passageway for water and be a front for weathering. Weathering tends to leach out cations, both decreasing the concentration and changing the adsorbed cation on the clay mineral (Moore and Brunsden 1996). Weathering causes the initial structure to deteriorate and the

material to become more homogenous, soft, and plastic (Manfredini *et al.* 1981). Hawkins *et al.* (1988) observed an increase in the montmorillonite content of a weathered Fuller Clay and suggested it was due to illite changing into mixed-layer clay. Slides were apparent in the Fuller Clay weathering profile, where calcite contents were found to decrease, causing an additional decrease in the residual strength.

Grainger and Harris (1986) described three features of a mudrock weathering profile favoring failure conditions: fracture frequency increases, pyritic and carbonaceous minerals are oxidized and leached, and materials are disaggregated causing diagnetic bonds to be lost. The higher fracture frequency increases the weathered materials' storage capacity and perviousness, enhancing the landslide possibility. Chigira *et al.* (2003) theorized slaking and sulfuric acid were influential in the Tsaoling landslide, a 125 million m^3 landslide in mudrock material in Taiwan. Iron-stained joints were observed throughout the scarp of the Tsaoling landslide indicating oxidation conditions.

A summary of problematic clay shale deposits throughout the world was included in Botts' (1986) dissertation. The overconsolidated, fissured clay shale deposits: Lias, Oxford, and London clays were noted to have the most significant engineering problems in Britain. Studies on slip surfaces of Lias clay found 1/5 to 1/26 of the compressive strength of similar undisturbed samples. Similar to these results, embankment cuts after 7 to 30 years showed a shear strength loss from 125 kPa to 34 kPa (18 to 5 psi). London clay was noted for its susceptibility to weather and its significant strength loss. Fifty to eighty percent strength loss was found in London clay cuts after 10 to 70 years. London clay turns from a fissured blue-grey clay to an oxidized brown clay when weathered. Weathering alterations and tectonic shearing in Italian overconsolidated clay shales was found to be a primary cause for many of

the landslides in the area. A loss of unconfined compressive strength from 12 (10^3) kPa to 23 kPa (1700 to 70 psi) was observed for unaltered to altered clay shale, respectively (Botts 1986). North American clay shales susceptible to landslides are shown in Table 3. Botts (1986) noted the most problematic areas in the United States were along the upper Missouri and South Saskatchewan River basins, specifically the Pierre, Bearpaw, and Claggett Shale formations. Slope failures after the construction of such dams as the Oahe and Fort Peck Dam on the Missouri River brought significant studies on these clay shale deposits. Slickensides and fissures are common macrostructures of these materials caused by the high swelling and plasticity. Weathering zones were observed throughout the Fort Peck Dam site with depths of 50 foot, a likely cause of the landslides at the site.

As summarized above, clay shales are a global problem, yet their behavior is not fully known. A better understanding of the physico-chemical processes of clay shale behavior may prevent failures from occurring and save significant economic resources.

PIERRE SHALE

The geologic history of Pierre Shale is directly related to the material's behavior. Knowledge of the geologic history is thus relevant to the slope stability problems associated with the material. Pierre shale is a heavily overconsolidated clay shale formed from a marine/non-marine environment sedimentation during the Cretaceous Period approximately 60-80 million years ago. Deposition occurred in the Cretaceous Epeiric Sea in a north-south direction, extending 1000 miles across Canada and as far south as the Gulf of Mexico as shown in Figure 8 (Shultz *et al.* 1980).

Table 3. Landslide susceptible clay shales of North America (from Fleming *et al.* 1970).

Unit	Description
Bearpaw shale	Upper Cretaceous; MT, WY, Alberta; marine clay shale, 600-700 ft; (Montana Group)
Carlile shale	Upper Cretaceous; CO, WY, NE, KS, SD, MT, NM; shale; 175-200 ft; (Colorado group)
Cherokee shale	Early Pennsylvanian; KS, NE, MO, OK; shale; 500 ft; (Des Moines Group)
Claggett formation	Upper Cretaceous; MT, WY; marine clay shale and sand stone beds; 400 ft; (Montana Group)
Dawson formation	Upper Cretaceous-Lower Tertiary; CO; non-marine clay shale, siltstone, sandstone; 1000 ft
Del Rio Clay	Lower Cretaceous; TX; laminated clay with limestone
Eden group	Upper Ordovician; OH, IN, KY; shale with limestone; 250 ft; (Cincinnati Group)
Ft Union group	Paleocene; MT, WY, ND, SD, CO; sandstone and shale; 4000 ft
Frontier formation	Upper Cretaceous; WY, MT; sandstone with beds of clay and shale; 2000-2600 ft; (Colorado Group)
Fruitland formation	Upper Cretaceous; CO, NM; brackish and freshwater shale and sandstone; 194-530 ft; (lat Montana age)
Graneros shale	Upper Cretaceous; CO, WY, MT, SD, NE, KS, NM; argillaceous or clay shale; 200 ft; (Colorado Group)
Gros Ventre formation	Middle Cambrian; WY, MT; calcareous shale; 800 ft
Jackson group	Upper Eocene; AL to TX; calcareous clay with shale, limestone.
Mancos shale	Upper Cretaceous; CO, NM, UT, WY; marine carbonate clay shale; 1200-2000 ft.
Merchantville	Upper Cretaceous; NJ; marly clay; 35-60 ft.; (Matawan Group)
Modelo formation	Upper Miocene; CA; shale, sandstone, chert.; 9000 ft.
Monterey shale	Upper, Middle, and Late Lower Miocene; CA; shale; 1000 ft
Morrison formation	Upper Jurassic; CO, WY, MT, SD, KS, OK, NM, AZ, UT; marl with sandstone and limestone beds; 200 ft.
Cowry shale	Upper Cretaceous; WY, MT, SD; shale; 150 ft.; (Colorado group)
Pepper formation	Upper Cretaceous; ND, SD, NE, MT, WY, CO; marine clay and sandy shale; 700 ft.; (Montana Group)
Rincon shale	Mid or low Miocene; CA; clay shale with limestone; 300-2000 ft.
Sundance formation	Upper Jurassic; SD, WY, MT, NE, CO; shale with sandstone; 60-400 ft.
Taylor marl	Upper Cretaceous; TX; chalky clay; 1200 ft.
Thermopolis shale	Upper Cretaceous; WY, MT; shale with sand beds; 400-800 ft.; (Colorado Group)
Trinity group	Lower Cretaceous; TX, OK, AD, LA; fine sand marl, limestone.
Wasatch formation	Lower Eocene; WY, MT, ND, CO, UT, NM; sand and clay; 0-5000 ft.

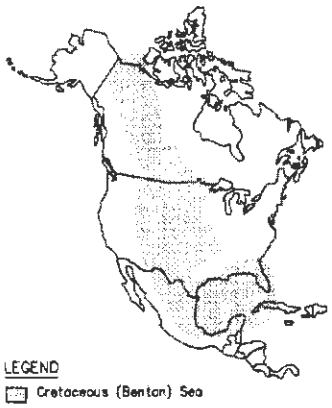

Figure 8. Cretaceous Sea of North America (from Brooker and Peck 1993).

Fossil Zones

Materials in the east, farther from the western source, are finer-grained mudstones and shales. In the west, siltstones and sandstones are more numerous (Shultz *et al.* 1980). Because of the westerly source, the material is thicker in the west. Clay shale near the Rocky Mountains in Colorado can exceed 2440 meters in thickness while in the eastern Dakotas and Nebraska the clay shale formation becomes thin to nonexistent (Nichols *et al.* 1986). Bentonite seams interbedded within the Pierre Shale Formation exist from wind-blown volcanic ash of the Elkhorn Mountain Volcanics (Shultz *et al.* 1980). These layers vary in thickness from a few millimeters to almost a meter (Tourtelot 1962). Some of the sediments in the Pierre Shale Formation were deposited in brackish waters due to sea transgression-regression during the period. The varying depositional environments created a complex-heterogeneous layering of marine- and non-marine sediments (Tourtelot 1962). The fossil zones make it possible to identify three main marine transgressions. The fossil zones also have different mineralogy and properties controlling their *in situ* behavior. The Telegraph Creek-Eagle regression resulted in the first fossil zone as shown by Figure 9. The regression

formed a thick-silty material called the Telegraph Creek Formation, grading into the Gammon shale in the east and then into the marl of the underlying Niobrara Formation near the Missouri River. During the Claggett transgression, the sea deepened and expanded forming the Claggett Formation known as fossil zone 2. Silty shale was deposited in the west while organically rich shale was deposited in the east, called the Sharon Springs Member. Underlying this fossil zone exist a bentonite bed called the Ardmore Bentonite Bed, with thicknesses as great as 5 meters. The Judith River regression formed fossil zone 3 of shallow water deposits. Sandstones and siltstones were deposited in the western areas and Black Hills during this period. During the Claggett transgression and Judith River regression, deposition near the Missouri River of South Dakota was very slow. The Bearpaw transgression produced the maximum-sea size and fossil zones 4 and 5. Fine-grained shale was deposited quickly in the east and many shale members were deposited during this transgression. In the southeast, local uplift produced shallow seas, which gave rise to erosion and subsequent deposition of the Crow Creek Member as shown in Figure 9. Remnants of the shallow seas are the carbonate beds throughout the Crow Creek Member. The Fox Hills regression was the last regression of the sea and formed fossil zone 6. The substantial shallowing in the east caused significant amounts of carbonates to be deposited, called the Mobridge Member. The shale of the Fox Hills Sandstone near the Missouri River consists of fine-grained, argillaceous siltstone. Non-marine formations followed these transgression-regression formations (Schultz *et al.* 1980). Overlying the Pierre Shale Formation exist formations from the Late Cretaceous, Tertiary, and Pleistocene ages. The Pierre Shale Formation is covered by glacial till east of the Missouri River (Fleming *et al.* 1970).

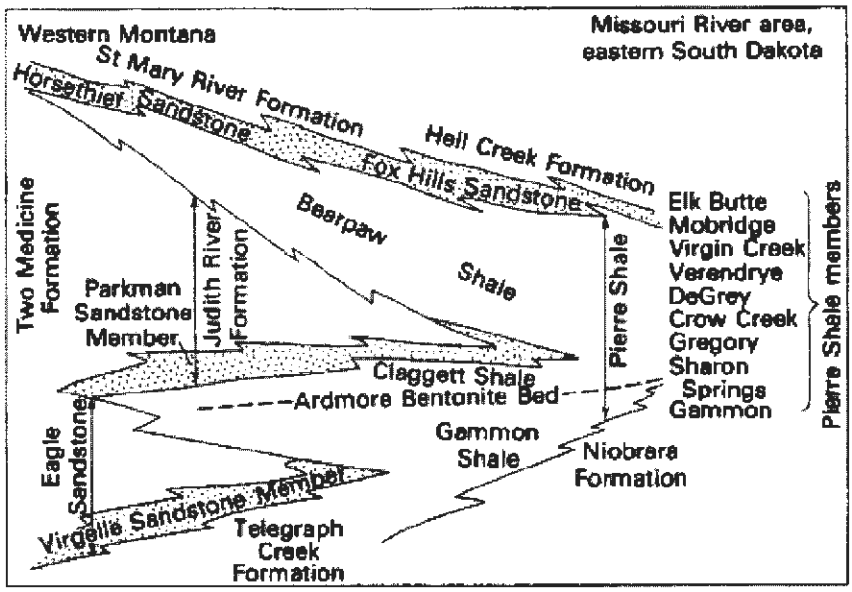

Figure 9. Pierre Shale formation in the Great Plains region (from Schultz *et al.* 1980).

Mineralogy and Chemistry

The marine and non-marine formations of Pierre Shale have similar mineralogy (Schultz *et al.* 1980). Marine clays tend to have larger clay fractions, with greater amounts of montmorillonitic clay and less mixed-layer clay. Illite, beidellite, and montmorillonite were constituents of the mixed-layer, making up at least 70% of the total clay minerals. Other clay minerals observed were kaolinite and chlorite in Pierre Shale. Minor amounts of potassium feldspar, calcite, dolomite, gypsum, pyrite, and zeloites were also found.

The elemental composition can be correlated to mineralogy through concentrations, stoichiometry, and back calculations. Silica was associated with quartz, cristobalite, and clay minerals while almost all the aluminum was linked to clay minerals by Tourtelot (1962). Clay minerals were associated with most of the ferric and ferrous iron, alkali and alkaline earth elements. Ferric iron also occurred in jarosite or other sulfates while ferrous iron occurred in pyrite. Tourtelot (1962) observed relations between the percent of concentration

of ferric oxide and the degree of oxidation in a sample as well. Carbonates were a source of the calcium and magnesium elements. Biogenic apatite, such as fish scales, correlated to phosphorous contents. Weathering caused much of the sulfur in sulfides to go into sulfates of calcium and iron. Clay minerals, carbonates, and oxides in weathered material were sources of manganese (Tourtelot 1962).

Uplift, Erosion, and Outcroppings

Outcropping is common throughout the Pierre Shale rock, especially in South Dakota, due to significant erosion and rebound (Shurr 1980). The Elk Butte and Mobridge members are the main members exposed at the surface of the Pierre Shale Formation. Weathering is common in outcrops due to the change in environments. Schultz *et al.* (1980) noted only minor weathering effects in outcroppings. Significant changes were only observed in organic-rich shales of the Pierre Shale Formation due to the high concentrations of pyrite. The outcropping caused the pyrite to oxidize, leading to the leaching of most of the chlorite, some of the Fe and Mg in the clay minerals, and the plagioclase. Gypsum and jarosite were formed from the released sulfur. A change in the pH was also observed in many of the outcrop samples. pH was observed to drop from 8 to 10 in the unweathered to 2 to 6 in the weathered in samples. The acidic conditions occured when the acidity from pyrite oxidation exceeded the alkalinity conditions of calcite, chlorite, and Na smectite in the material (Shultz *et al.* 1980). Physical property changes occured more frequently in outcroppings. Table 4 indicates physical property observations of weathered and unweathered Pierre shale near Hayes, South Dakota. Weathered Pierre Shale tends to be more open, less dense, and less saturated than unweathered materials.

Table 4. Physical properties of weathered and unweathered Pierre shale (from Nichols 1992).

	Weathered	Unweathered
Porosity	≥38%	33-37
Saturation	90-98%	99-102%
Bulk Density	1.86-2.06 g/cm^3	2.12-2.16 g/cm^3

Oahe Dam Site

The Oahe Dam near Pierre, South Dakota is known for slope stability problems. The dam has a foundation on the first four fossil zones, all marine shales, as outlined in the *Fossil Zone* section, of the Pierre Shale Formation in Figure 9, some 121 m (400 foot) thick. A cross section of the dam at the site is shown in Figure 10. The 74.7 m (245 foot) embankment of the dam is the eight largest in the world and consists of 70.3 million m^3 (92 million cubic yards) of earth fill and 0.858 million of m^3 (1.122 million cubic yards) of concrete (USACE 2004). Bentonite seams, as thick as 0.6 foot (0.2 m), lie throughout the stratigraphy (Fleming *et al.* 1970). The deepest member hit in the Pierre Shale Formation was the Crow Creek member. Firm shale, without any weathering, has an average dry density of 1.71 g/cm^3 (107 pcf), a moisture content of 25%, and specific density of 2.7 at the site. The unweathered material also exhibited high unconfined strength and Young's modulus of 478 to 17,428 kPa (70 to 2,500 psi) and 137,000 to 965,000 kPa (20,000 to 140,000 psi), respectively. Strength losses have been observed when the material weathers. Many of the slopes had to be redesigned at the site after slope failures, with initial engineering parameters of 11.3° for ϕ and 19.1 kPa (2.8 psi) for cohesion later designed with lower values of 8.5° for ϕ and 14.4 kPa (2.1 psi) for cohesion. Significant measures were taken to prevent weathering of the shale, such as immediately placing a bituminous sealer or mortar over exposed surfaces (Johns *et al.* 1963). A minimum of 10.2 cm (4 inches) of

pavement was placed under all exposed foundation surfaces at the site as well (Johns *et al.* 1963).

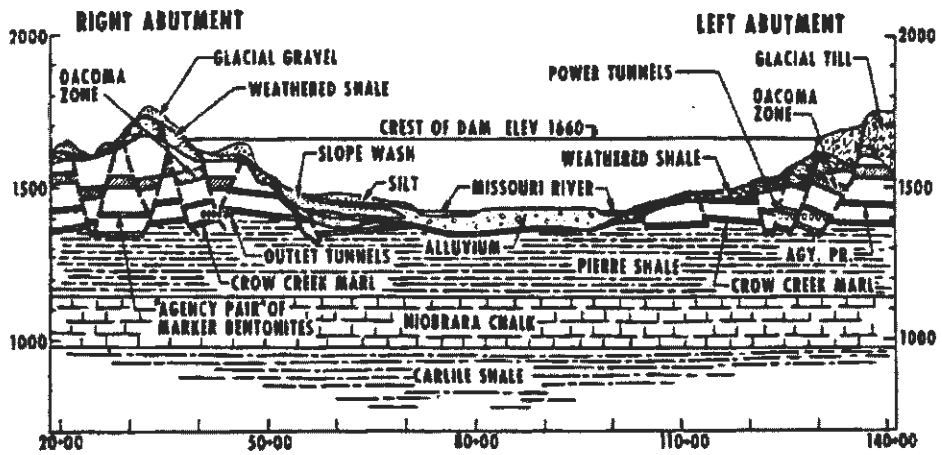

Figure 10. Geologic profile of the Oahe Dam (from Knight 1963).

Mineralogy

Many studies have been performed on the Pierre Shale Formation at the Oahe Dam but few engineering studies have focused on the weathering effects. Table 5 shows the average mineralogy, for the four fossil zones shown in Figure 9 and described in the *Fossil zone* section, encountered at the site. Similar to the rest of the Pierre Shale formation, clay minerals make up a large portion of the mineralogy. The clay minerals are mainly composed of mixed-layer clays. Quartz, cristobalite, and plagioclase, together, make up less than 25% of the mineralogy. Coarse quartz particles are common in the Crow Creek member. The gypsum concentrations are surficial evidence of the weathering of pyrite as discussed previously.

Weathering Case Study

Tourtelot (1962) discussed a case study of an excavation for the spillway of the Oahe Dam in the Verendrye member of the Pierre Shale formation. The profile, pH, and chemical diagrams are shown in Figure 11. The claystone was dark grey to black near the bottom of the excavation, turning into a lighter brown color near the top, with iron and manganese rich concretions oxidizing near the top. The top one meter (3-5 foot) showed a residual soil-like material. Silica contents increased initially in intermediately weathered (brown coloration) claystone and then dropped off as weathering decreased. Ferric oxide was found throughout the weathered material while ferrous oxide was observed in the unweathered samples. Alkalinity prevailed in the unweathered claystone which Tourtelot (1962) contributes to the exchangeable sodium ion. The material then becomes acidic in the weathered claystone and neutral in the soil-like material. Acidity was likely caused from the acid-soluble sulfur while the neutral environment from the absence of any strong bases or acids.

Strength Parameters

Weathering causes Pierre Shale to weaken from a durable, brittle rock into a plastic clay. The change in strength directly affects engineering design. Fleming *et al.* (1970) observed average peak strength values of weathered shale at the Oahe Dam site of ϕ=12° and cohesion=24.9 kPa (0.26 tsf). While the peak strength is good for engineering design of soils without slip surfaces, the Pierre Shale Formation contains shear surfaces causing the residual strength to control the design. Schaefer (2002) summarized the residual friction angle and their engineering indexes for Pierre Shale for the Oahe Dam site in Table 6.

Table 5. Mineralogy of Pierre Shale at Oahe Dam site (from Schultz *et al.* 1980).

	Fossil Zone			
	1	2	3	4
	Percent of mixed-layer clay			
Illite	40	41	33	43
Beidellite	38	38	32	30
Montmorillonite	22	21	35	27
	Percent of total clay			
Mixed-layer	73	78	83	72
Illite	18	16	13	16
Chlorite	2	2	2	1
Kaolinite	5	3	2	6
	Percent of sample, [percent detected in]			
Total Clay	71	77	65	78
Quartz	20	17	16	17
Cristobalite	0	0	5-25	0
Potassium feldspar	0	0	0	1
Plagioclase	4	2	2	1
Calcite	3	1	6	0
Dolomite	0	0	2	0
Gypsum	0	4 [4]	1-2 [8]	2 [11]
Jarosite	0	0	0	0
Pyrite	1 [12]	1-5 [28]	1-5 [28]	1-3 [68]
Zeolites	1 [12]	1-4 [68]	1-3 [13]	0

A discussion on the residual strength testing type displayed in Table 6 can be found in the *Residual Strength* section. The low residual friction angles shown in Table 6 suggest slope instability on flat slopes in the Pierre Shale at the site. A full understanding of the physico-chemical mechanisms will be an asset to the engineering community. Shales are one of the most common rocks on earth and their behavior is similar. Correlations between the behavior of Pierre Shale and other clay shales during weathering can be made to help mitigation of these problems.

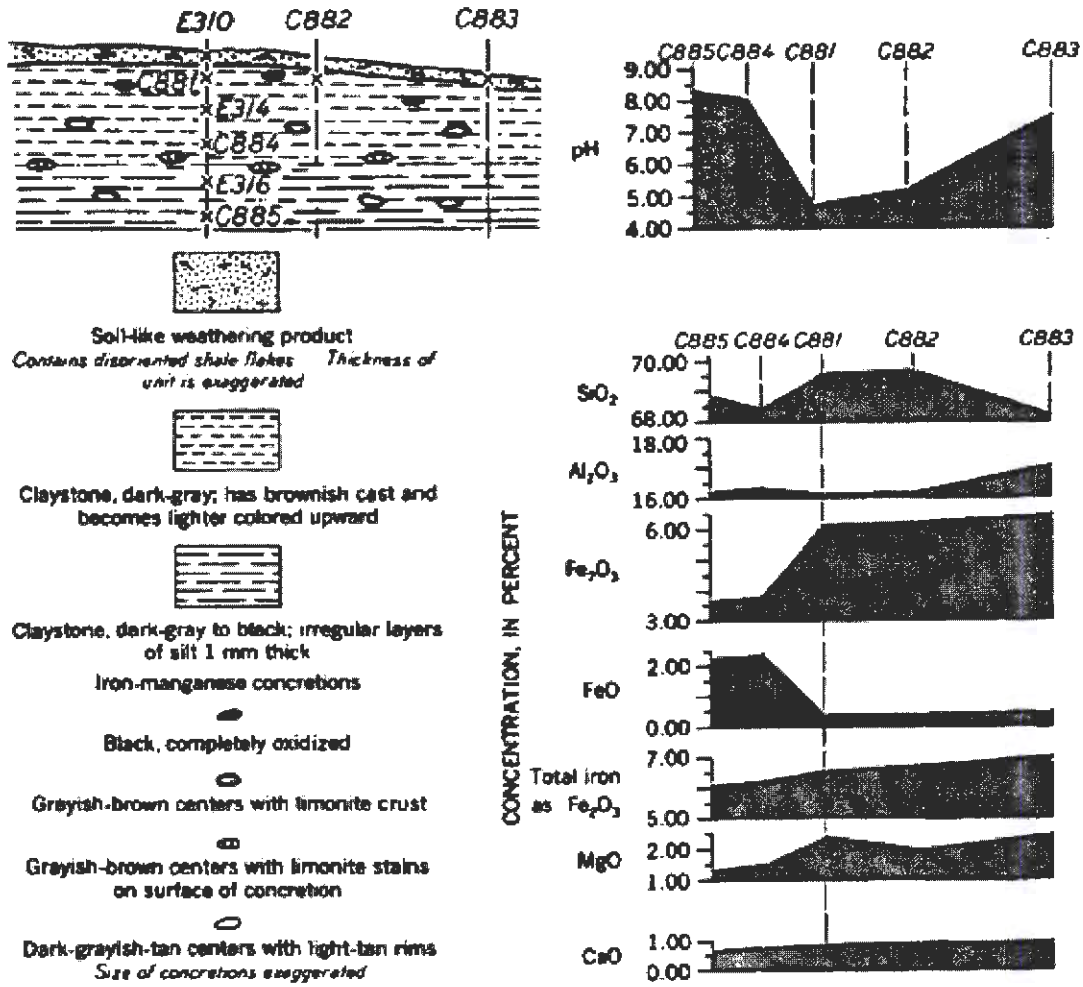

Figure 11. Oahe Dam weathering case study (from Tourtelot 1962).

RESIDUAL STRENGTH

Skempton (1964, 1985) describes the residual strength as the minimum strength of soil after large displacements. Slow shearing rates are required to prevent the disruption of the shear surface (Skempton 1985, Tika *et al.* 1996). Residual strength is often related to long-term stability design, and for areas with a landslide history, bedding planes, or folded strata (Skempton 1985). The drop in residual strength from peak strength, as shown in Figure 12a, can be significant for materials with large amounts of clay minerals, particularly platy

minerals, causing reactivation of old slides and destruction of property. The formation of the shear surface and achieving the residual strength relates to the formation of a new fabric, particularly in material with high clay contents. The drop in strength is attributed to the clay particles reorienting parallel to the direction of shearing (Bromhead 1986). While cohesion provides much of the peak strength, the material has little cohesion once a shear surface is formed as shown in Figure 12b (Skempton 1964).

Table 6: Residual strength values for the Oahe Dam Site (Schaefer 2002).

Reference	Description	LL	PI	CF	ϕ_r'	Test Type
Herrmann & Wolfskill (1966)	Resedimented	123	91	67	3.2°	RDS
Kenney (1967)	Resedimented	145	103	56	5.7°	RDS-precut
Fleming *et al.* (1970)	Shale-Remolded	74	53		7.4°	RDS-precut
		127	98		5.8°	RDS-precut
		144	110		5.1°	RDS-precut
		163			4.5°	RDS-precut
		204			4.1°	RDS-precut
Townsend & Gilbert (1973)	Shale-Remolded	351	320	85	3.1°	RtS
		351	320	85	3.1°	RDS-precut
		351	320	85	3.1°	RgS-precut
USACE (1997)	Shale-air dried then remolded	91	51	47	7.1°	RDS-precut
		143	109	67	4.3°	RDS-precut
		297	263	80	3.3°	RDS-precut
USACE (2000)	Shale-Remolded	80*	45*	60	6.4 to 8°	RDS-precut
	Bentonite Layer	150*	110*	80	2.8 to 4.0°	RDS-precut
Stark and Eid (1994)	Firm Shale	138	97	74	3.8°	RtS
	Bentonite Shale	192	145	65	6°	RDS
USACE (2000)	Weathered	126	92		3.8°	RtS

* = estimated from project records
RDS = Reversal Direct Shear Test
RtS = Rotational Shear Test
RgS = Ring Shear Test
precut: means undisturbed samples precut horizontally to form failure surface

Residual Strength Characteristics

Shear surfaces have been extensively studied. Tika *et al.* (1996) concluded shear surfaces are a permanent feature of soil once formed, unaffected by subsequent stress history. Some researchers have shown minor residual failure envelope curvature. Townsend and Gilbert (1976), Bishop *et al.* (1971), and Moore (1991) noted slight increases in the residual friction angle for lower normal stresses. Hawkins and Privett (1985) indicated curvature was evident for samples containing high clay contents and normal stresses lower than 200 kPa (2.1 tsf). Moore (1991) suggests expressing the residual friction angles in terms of normal stresses to mitigate this problem.

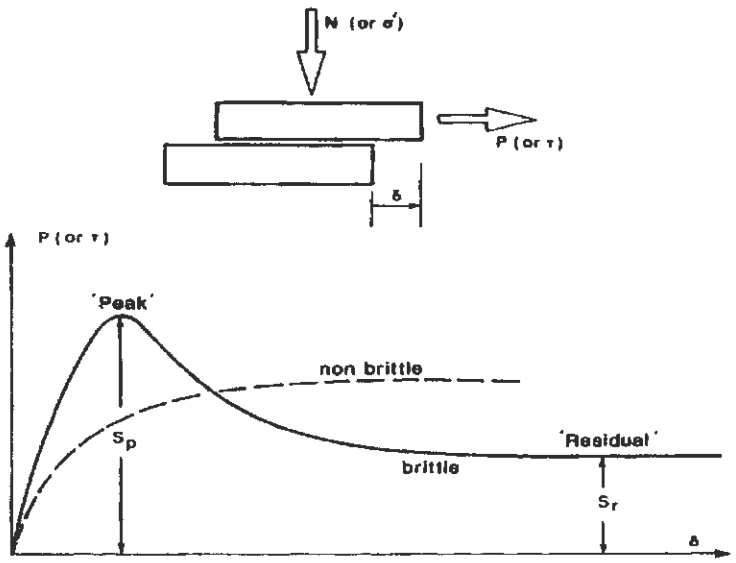

(a)

Figure 12. Residual strength behavior, a) Brittle behavior during shearing, b) Decrease from the peak to residual friction angle (from Skempton 1964).

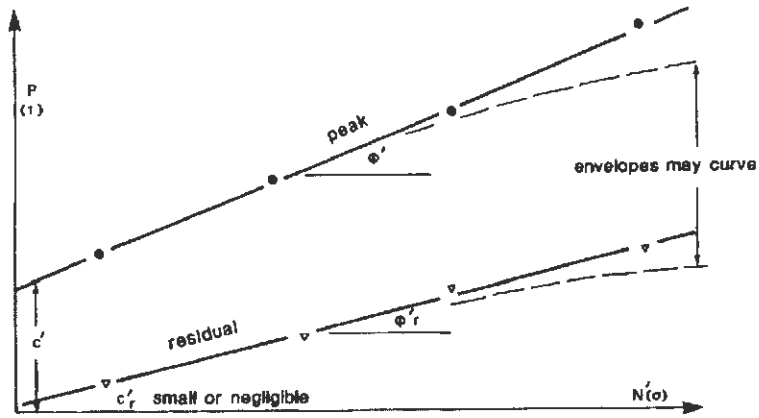

(b)

Figure 12 con't. Residual strength behavior, a) Brittle behavior during shearing, b) Decrease from the peak to residual friction angle (from Skempton 1964).

Soil Chemistry

The residual strength has been observed to be a dynamic soil parameter, dependent on the soil environment. Kenney (1967) found mineralogy to be the main determinant in a soil's residual strength, and to a lesser degree the overall soil chemistry, verified later by Skempton (1985) and Tika *et al.* (1996). Kenney (1967) observed particle shape, not size, to control residual strength for massive minerals, such as quartz and calcites. A drop in residual strength was shown with decreasing grain sizes for clay minerals (micas, muscovite, and montmorillonite), contrary to the massive minerals' behavior. These findings were explained by Lupini *et al.* (1981) with three types of soil shearing behavior: turbulent, transitional, and sliding. A turbulent shear behavior was observed for soils with high amounts of rotund particles such as quartz and calcite. The turbulent mode prevents particle alignment parallel to the direction of displacement due to particles rolling over each other. Residual strength for rotund minerals was dependent on shape and packing, independent of the interparticle

friction angle. The sliding-shear behavior was observed in soils with high amounts of platy particles. The platy particles allow the material to reorient in the direction of displacement. The residual friction angle for sliding shear behavior was dependent on soil mineralogy, pore water chemistry and interparticle friction angle. The transitional shear behavior was observed in materials with particle characteristics between the turbulent and sliding behaviors. The grain size distribution was a dominant factor determining whether the material acted in a sliding or turbulent mode. Lupini *et al.* (1981) noted particle rolling occurs in soils when clay contents were less than forty percent while sliding behavior occurred for clay fractions greater than fifty percent.

Strength loss is a concern for the clay minerals of montmorillonite, chlorite and illite due to their high activity and the characteristics of the minerals (Birkeland 1999). The physico-chemical effects on the residual strength of clay minerals can be significant when clay contents are greater than 10 percent (Moore 1991). The natural charged surface on clay surfaces is related to these effects. The net negative charge on the clay minerals' surface attracts cations to the interlayer. Cations are exchanged and replaced on the surface causing the mineral's properties to change. Moore (1991) showed that the pore water type and concentration greatly affected the residual strength of montmorillonitic soils. Higher valency and larger polarizability, such that $Ca^{2+}>K^{+}=Na^{+}$ and $K^{+}>Na^{+}$, respectively, suppress the diffuse double layer (DDL) thickness, increasing the residual strength (Kenney 1967). Steward and Cripps (1983) also noted that an increase in the cation concentration increased residual strengths. The increases or decreases in residual strength relate to suppression or expansion, respectively, of the DDL.

Clay Minerals' Influence

The high surface area of montmorillonite allows for residual strength coefficients to be lower than other minerals as well (Moore 1991). Kaolinite and chlorite have surface areas between 5 to 100 m^2/g with residual friction angles of 15.8 degrees. In comparison, calcium montmorillonites, with internal surface areas as high as 800 m^2/g, have been found to have residual friction angles lower than 10.1 degrees. Mesri and Cepada-Diaz (1986) also concluded that the lowest residual friction angles were found in soils with montmorillonite values between 30 to 80 percent. The mechanism behind the reduced residual strength is related to the particle size reduction and the high degree of platyness causing minimal interparticle contact pressure.

The elemental makeup, colloidal behavior, and structure cause each clay mineral to have characteristic behaviors. Montmorillonite's platy particles and highly active diffuse double layer (DDL) gives the mineral low strengths and shrink-swell behavior. Olson (1974) found physical effects to control the strength for clay minerals with calcium saturation. DDL effects were only observed for sodium-saturated montmorillonite and illite (Olson 1974). The residual strength has also been observed to be dependent on the colloidal behavior for clay material. Environmental changes causing a suppression of the DDL cause the residual strength to increase. Expansion of the diffuse double layer results in residual strength decreases. Residual strengths for montmorillonite vary with the absorbed cation. Table 7 describes the residual friction angle findings of Kenney (1967) and Olson (1974) for clay minerals. The lower bounds on the residual friction angles for montmorillonite were observed for zero salinity in the testing pore fluid for Kenney (1967) study. Olson (1974) varied illite interstitial fluid with calcium and sodium saturation. Residual friction angles

between 16° to 21° and 23° to 26° were observed for sodium- and calcium-saturated illite, respectively. Due to the natural heterogeneity of soils and rocks, pure clay studies are not always applicable to field studies. Changes in the chemistry and properties associated with pure clay minerals may not be comparable or proportional to the behavior of natural clay mixtures (Taylor and Cripps 1987).

Table 7. Clay minerals' residual friction angle

Type of Test:	Kenney (1967) (Drained Direct Shear)	Olson (1974) (Residual Triaxial Compression)
Calcium Montmorillonite	9.8° to 10.3°	~9.0°
Sodium Montmorillonite	4.1° to 10.3°	~5.0°
Kaolinite	15.5°	25.0°
Illite	17.8° to 25.8°	16.0° to 26.0°

RESIDUAL STRENGTH TESTING

A consistent and reliable test is needed to measure the residual strength over large displacements in one direction. Repeated direct-shear boxes were used in past research to measure residual strengths but shearing does not occur in one direction (Stark and Eid 1992). Direct-shear and ring-shear devices produce good residual strength results, but with less consistent on the shear box (Bromhead and Curtis 1983). Townsend and Gilbert (1976), Stark (1990) and others noted the direct-shear test overestimated residual strengths compared to torsional ring-shear tests. Many authors state the higher residual strength values produced by the direct shear is due to the samples being sheared in one direction in the direct shear, preventing reorientation of the clay particles parallel to the direction of displacement (Bromhead 1979, Stark 1990). The area of the sample is also changed as the sample is

sheared (Bishop *et al.* 1975). Triaxial compression tests have been used in past residual strength studies as well. Triaxial test produce higher residual strengths than direct-shear and ring-shear devices (Bishop *et al.* 1975).

Hvorslev (1939) concluded the torsional-shear test would be the most simple and efficient test to obtain the residual strength. The torsional ring-shear device has proven to be a better way in acquiring residual strength coefficients due to the soil being sheared continuously in one direction (Bishop *et al.* 1975, Bromhead 1979, Stark and Eid 1992). One of the requirements set forth by Hvorslev (1939) was a simple construction and operation process, a point partially unmet by many of the early apparatuses. More recently, the Bromhead Ring Shear Device designed by E. N. Bromhead and shown in Figure 13 has been getting more use. Bromhead (1979) and Stark and Eid (1992) attribute the success of the machine's use to the operation simplicity, cost, availability, and reliability. The Bromhead Ring Shear can be hooked up to a data acquisition machine, allowing for less supervision. The soil mold, Figure 14, consists of a mold 5 mm deep with an inner and outer diameter of 7 and 10 centimeters, respectively. A 10:1 counterbalanced lever arm provides the normal loading to the sample with a range of displacement rates from 0.024 to 60 degrees per minute (Bromhead 1979). Bromhead and Dixon (1986) and Stark and Eid (1992) noted the results from the Bromhead Ring Shear Apparatus were in good agreement with back calculations and field results.

Sample Preparation

A preparation procedure minimizing surficial measurements while measuring the residual strength of a material is required. Past studies on techniques to obtain residual strength are summarized in Table 8 and 9.

Residual strength can be obtained from undisturbed or remolded samples for the torsional ring-shear device. The residual friction angle has been determined to be independent of the initial soil structure so remolded samples can be used for testing (Bishop *et al.* 1971). Bishop *et al.* (1971) and Townsend and Gilbert (1976) found good agreement between undisturbed and remolded test results. Remolded samples are easier to obtain than undisturbed for the mold of the Bromhead Ring Shear. Remolded tests in the Bromhead ring shear were verified with back analysis by Bromhead and Dixon (1986). Many authors in Table 8 and 9 used remolded samples.

The following studies prepared samples for the torsional ring-shear device with remolded samples. ASTM Standard D6467-99 (ASTM 2003) requires gradation of the specimen through a sieve with "*...opening size less than 10% of the initial height of the sample.*" Stark and Vettel (1992) and Stark and Eid (1993, 1994 and 1997) used ball-milled, air-dried samples with material passing the U.S. Standard number 200 sieve for mudstone and shale particles. Unlike the others researchers, Townsend and Gilbert (1976) concluded the residual friction angle was independent of sample preparation procedure after testing undried, air-dried, and blenderized samples in their research.

Figure 13. Bromhead Ring Shear device

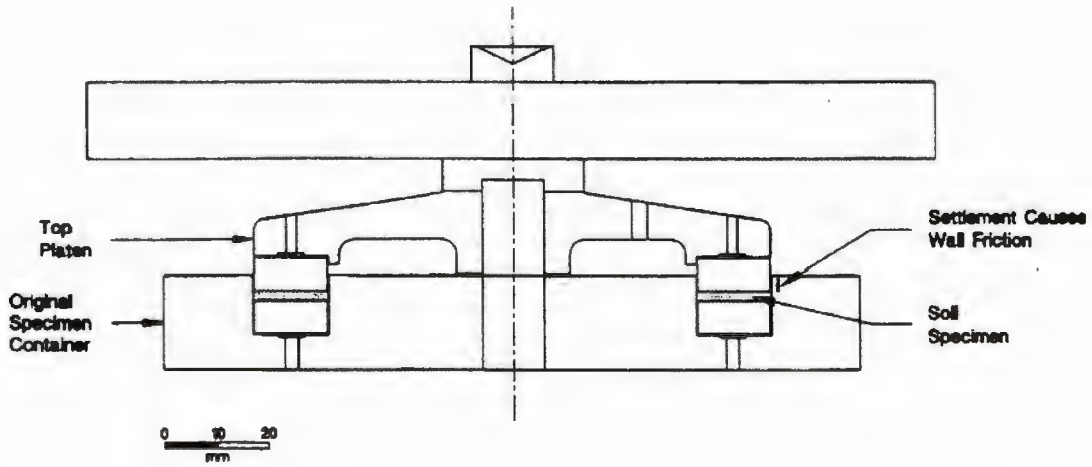

Figure 14. Bromhead Ring Shear (from Stark 1990).

Water was added to the sample after gradation. Stark and Eid (1994 & 1997) and Stark and Vettel (1992) added distilled water to the sample to obtain a liquid index of 1.5 and

allowed it to rehydrate for a week in a humidity room. Anayi *et al.* (1989) wetted their samples to their respective liquid limits and then air-dried the samples to the material's plastic limit. ASTM Standard D6467-99 suggests water contents near the sample's liquid limit with site specific or distilled water. Remolded samples should hydrate for a minimum of 24 hours. Townsend and Gilbert (1976) suggested a water content near or greater than the samples liquid limit as well. Bromhead (1979) suggests using drier samples for the Bromhead Ring Shear device due to the thinness of the molded sample to prevent excess settlement of the torque arm.

Consolidation stages varied throughout the literature. Townsend and Gilbert (1976) allowed stiff-clay samples to consolidate for two days with the Waterways Experimental Station Low-Capacity Annular Shear apparatus. Harris and Watson (1997) noted consolidation stages after each normal load had insignificant effects on the result. The authors suggested an initial consolidation to reach full consolidation with the Bromhead Ring Shear apparatus.

Modifications

Modifications have been suggested by Anayi *et al.* (1989) and Stark and Eid (1994) to improve the suggested "Bromhead Simple Ring Shear Apparatus" presented in Bromhead (1979). Anayi *et al.* (1989) observed the two proving rings' reading to vary after a short amount of shearing. The variation was believed to be caused by tilting or frictional resistance of the top platen on the mold's sides. The researchers prevented the differential readings by adding 24 three (3) mm high, evenly distributed vanes on the bottom and top

parts of the apparatus. Higher residual strengths with the proposed modifications were reported by Stark and Vettel (1992), concluding the vane modifications should not be used.

Table 8. Ring-shear preparation

Test	Sample Preparation					Ring Shear	
Literature	Water Content	Type of Water	State of Sample	Size Passing	Processing Method	Type of Ring Shear	Modifications
Anayi *et al.* (1989)	~ PL	---	Remolded	---	---	Bromhead Ring Shear	Added Vanes
ASTM (2003)	~LL	Site specific or distilled	Remolded	opening size <10% initial height	---	---	---
Bishop *et al.* (1971)	---	---	Undisturbed and Remolded	---	---	New Apparatus	---
Bromhead (1979)	---	---	Remolded	---	---	Bromhead Ring Shear	---
Bromhead and Curtis (1983)	---	---	Remolded	---	---	Bromhead Ring Shear	---
Eid (1996)	LI=1.5	Distilled	Remolded	US #200 for clay or shale	Air dried and ball milled	Bromhead Ring Shear	modified apparatus
Lupini *et al.* (1981)	---	---	Remolded	Used clay fraction	Dry powder	Bishop, *et al.* (1971) device	---
Stark (1995)	LI=1.5	Distilled	Remolded	US #200 for clay or shale	Air dried and ball milled	Bromhead Ring Shear	modified apparatus
Stark and Eid (1992)	LI=1.5	Distilled	Remolded	US #200	Air dried and ball milled	Bromhead Ring Shear	----
Stark and Eid (1994)	LI=1.5	Distilled	Remolded	US #200 for clay or shale	Air dried and ball milled	Bromhead Ring Shear	modified apparatus
Stark and Eid (1997)	LI=1.5	Distilled	Remolded	US #200 for clay or shale	Air dried and ball milled	Bromhead Ring Shear	modified apparatus
Stark and Vettel (1992)	LI=1.5	Distilled	Remolded	US #200	Air dried and ball milled	Bromhead Ring Shear	added vanes
Tika *et al.* (1996)	---	---	Remolded	---	---	Ring Shear of IC and NGI	---

Table 9. Ring-shear testing

Test	Ring Shear Details					
Literature	Type of Test	Consolidation Specifications	Fast Shearing Rate	Drained Shear Rate	Displacement required	Testing Procedure
ASTM (2003)	MS	---	<18 mm/min	0.020 mm/min	---	One Revolution for preshearing
Bishop *et al.* (1971)	MS	---	1.257 and 0.953 mm/min	0.004 and 0.008 mm/min	---	Used slow rate till peak, then fast, then slow
Bromhead and Curtis (1983)	MS	---	----	0.036 mm/min	>850 mm	---
Eid (1996)	MS and SS	-----	----	0.018 mm/min	---	---
Lupini *et al.* (1981)	SS	---	0.3 mm/min	Determined from 95% Consolidation test	---	Used slow rate till peak, then fast, then slow
Skempton (1985)	---	---	---	0.010 mm/min	100-500 mm to reach residual	Used slow rate till about 500 mm displacement, then fast, then slow
Stark and Eid (1997)	MS and SS	---	----	0.018 mm/min	---	---
Stark and Vettel (1992)	FT, SS, MS, PS	---	----	0.018 mm/min	---	---
Tika *et al.* (1996)	MS	>95% consolidation	9.5 mm/min		---	Used slow rate till peak, then fast, then slow
Townsend and Gilbert (1976)	MS	2-3 days	0.097 mm/min	0.012mm/min and 0.480 mm/min	---	Used slow rate till peak, then fast, then slow

* MS – Multistage SS – Single stage FT – Flush test PS - Preshearing

Stark and Eid (1994) suggested a "modified ring shear apparatus" of the Bromhead Ring Sear apparatus to minimize wall friction. Wall friction is negligible when settlement of the top confining ring is less than 0.75 mm (Stark and Vettel 1992). The modification

minimizes wall friction by permitting the side and center walls of the apparatus to become flush with the soil after consolidation and preshearing. Wall friction will be discussed in later parts of this review.

Types of Tests

Stark and Vettel (1992) outlined four different testing methods for a ring-shear device: single-stage, preshearing, proposed "flush" test, and multistage. A given normal stress is applied to a sample, consolidated and then sheared in a single-stage procedure. Once completed, shearing is stopped; the sample is removed; and a new sample is molded into the ring-shear apparatus. New samples are then used for other normal stresses until a residual failure envelope is obtained (Stark 1990). The single-stage procedure is time consuming and may not be appropriate for high normal stresses (Stark and Vettel 1992). The pre-shearing test procedure involves shearing the sample rapidly and then slowing the displacement rate down. Stark and Vettel (1992) suggest that the procedure produces higher values than their proposed flush test. The "flush" test consists of consolidating a sample at a given normal stress. Additional soil is molded into the ring-shear mold and allowed to reconsolidate after consolidation. Only one shearing stage is used per sample. This procedure prevents excess settlement of the torque arm, minimizing wall friction. Many authors (Stark 1990, Stark and Eid 1994, Bromhead and Curtis 1983) found multistage testing to produce satisfactory results with minimal time consumption. Results from multistage test in a ring shear are shown in Figure 15. The multistage test consists of consolidating a sample at a normal load, then shearing the sample at a fast rate to form a shear surface. The displacement rate is decreased to obtain the residual strength for the given

normal load. The normal load is increased, allowed to consolidate, and shearing is repeated at the slow displacement rate. One sample is used for the entire test, producing more reliable results than single-stage testing. The residual strength for each of the normal stresses is found from the test. A residual failure envelope, shown in Figure 16, is obtained from a single multistage test. A residual friction angle (ϕ') is obtained with trend lines through the origin and a cohesion intercept.

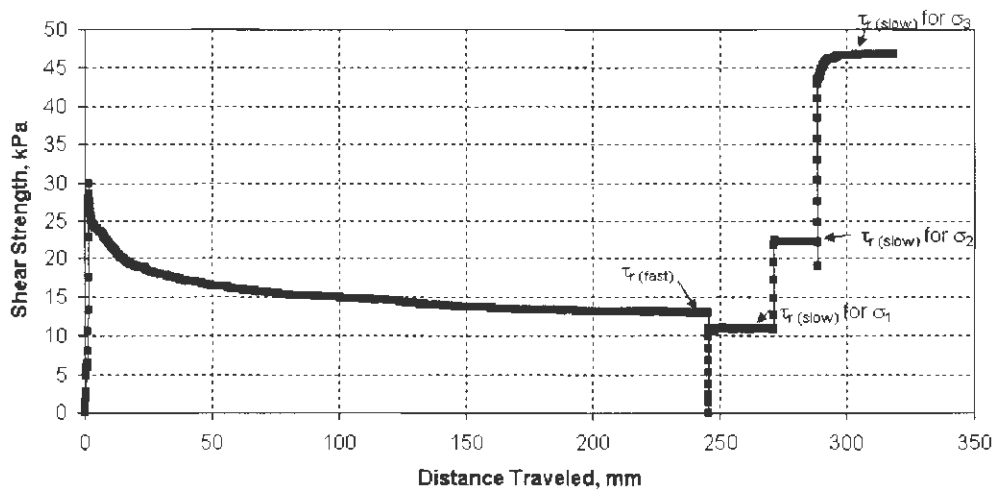

Figure 15. Multistage tests results

Displacement Rate

Both large displacements and slow rates are required to achieve the residual strength. A rate producing reliable residual strengths while minimizing the time requirement was needed. Many authors have used a fast displacement-shear rate to obtain a shear surface (Townsend and Gilbert 1976, Bromhead 1979, Stark and Eid 1997, Stark 1995, Tika, *et al.* 1996, Stark and Vettel 1992, Eid 1996, Harris and Watson 1997, Anayi *et al.* 1989). The rate was then slowed down to obtain the residual strength.

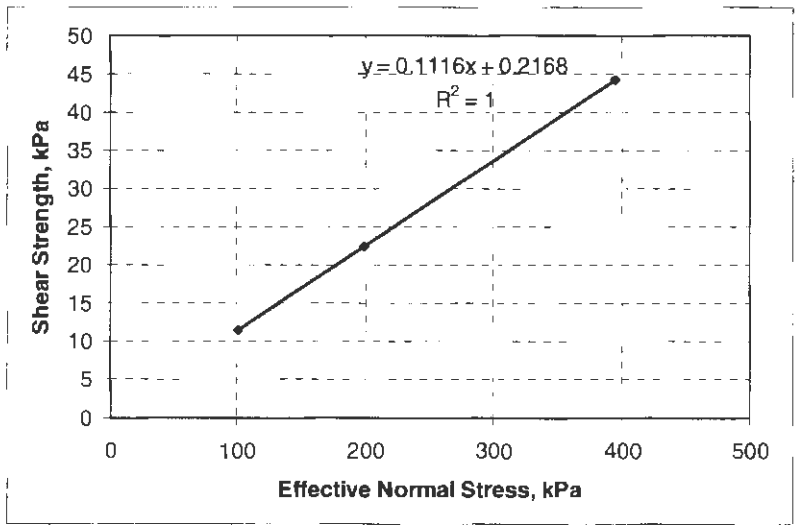

Figure 16. Residual strength failure envelope

ASTM Standard D6467-99 (ASTM 2003) requires a rate less than 18 mm/min for one revolution. The rate is then slowed until a residual strength is reached. ASTM suggests a rate of 0.020 mm/min. Townsend and Gilbert (1976) used two different procedures for various devices. Using the Waterways Experiment Station Low-Capacity Annular Shear Apparatus, an initial rate of 0.012 mm/min was used until the peak strength was reached. The rate was then increased to 0.097 mm/min until an apparent residual was reached. The fast rate was used to obtain the large displacement required to obtain the residual strength. The rate was decreased back to 0.012 mm/min until a constant residual strength was reached. Tests performed in a Harvard Rotational Shear Apparatus were conducted at 0.48 mm/min. Bishop *et al.* (1971) used similar procedures except with different rates. An initial shear rate of 0.008 mm/min was used until a peak strength was reached. Two faster rates of 0.953 mm/min and 1.257 mm/min were tested to achieve a large shear displacement. The testing performed in this research showed the soil was relatively insensitive to the shearing rate. After a large displacement was reached, the rate was slowed down to 0.008 mm/min. Lupini

et al. (1981) observed the residual strength for shear rates less than 1 mm/min to be within ten percent of the results at the slower rates of 0.01 to 0.025 mm/min. Bromhead and Curtis (1983) used rates of 0.036 mm/min to find the residual strength after a large shear displacement in the Bromhead Ring Shear apparatus. Harris and Watson (1997) suggested a rate of 0.036 mm/min after running through a fast stage. Stark and Eid (1992 and 1997) sheared samples at 0.018 mm/min, admitting that a faster rate could have been used. Eid (1996) fast sheared samples slowly by hand. A controlled rate was then applied at 0.008 mm/min.

Displacement

The residual strength is only achieved after large displacements. A shear displacement of 850 mm was required to obtain the residual condition for the study by Bromhead and Curtis (1983). ASTM Standard D6467-99 (ASTM 2003) requires a minimum of one revolution to create a shear surface. One revolution in the Bromhead Ring Shear equals a displacement of 267 mm (10.5 in). The ASTM Standard requires 10 mm of additional shear displacement to obtain the residual strength, requiring "a well-defined residual strength state." A displacement of 250 to 400 mm was suggested by Stark (1990) to achieve a shear surface. Stark and Eid (1992) observed a constant residual strength after a displacement of 70 mm. Eid's (1996) research required an additional 12 mm displacement after the formation of a shear surface to achieve the residual strength. Lupini *et al.* (1981) observed shear surfaces for displacements greater than 100 mm.

Wall Friction

A problem noted with the current ring-shear test in the literature was the increase in the strength caused by wall friction. Wall friction is a result of the shear surface moving deeper into the mold. Extruding material from shearing is also a source of wall friction. As noted by ASTM Standard D6467-99, for a single piece metal apparatus,

> *"...the amount of wall friction depends on the magnitude of torque arm settlement into specimen container, type of soil, and material lining the specimen walls."*

Limiting the settlement of the torque arm is suggested to prevent wall friction. Stark and Vettel (1992) concluded wall friction is insignificant if settlement of the torque arm was limited to 0.75 mm. Stark and Eid (1996) modified the Bromhead Ring Shear apparatus to account for this. This modification was discussed in the *Modifications* section.

Summary

A working procedure for the Bromhead Ring Shear device was established from the preceding review. Appendix C provides a comprehensive outline of the testing procedure used in this study. A multistage testing procedure was used to provide consistency, preserve sample material, and conserve time. Samples were crushed by mortar and pestle to pass the US standard #50 sieve. Samples were rehydrated with distilled water to a moisture content near their plastic limit and allowed to rehydrate for 48 to 72 hours. The prepared sample was molded into the ring-shear apparatus and trimmed in the direction of shearing. The apparatus was placed in a distilled water bath and consolidated under a normal stress of 101 kPa for approximately a hour. The sample was initially sheared at a displacement rate of

0.12 mm/min for 250 to 300 millimeters after the consolidation stage. The shear load was removed from the torque arm and the rate was slowed to 0.036 mm/min. Shearing was restarted and run for an additional ten to fifteen millimeters. Once a constant residual strength was achieved for the 101 kilopascal normal stress, shearing was stopped and the normal stress was increased to 198 kilopascals. The sample was reconsolidated for an hour and shearing was continued at the 0.036 mm/min rate. In a similar manner, a normal stress of 394 kilopascals was used.

MINERALOGICAL/CHEMICAL/MICROMORPHOLGY ANALYSES

Mineralogy, chemical, and micromorphology analyses were conducted to gain an understanding of the system's mechanisms at the micro-level. Many nondestructive techniques use electromagnetic radiation to determine the composition of a material. Mineralogical, elemental, and surface topography can be gathered through these techniques. X-ray diffraction (XRD), x-ray fluorescence (XRF), and scanning electron microscopy (SEM) are techniques, which use electromagnetic radiation, to determine different parameters of a material's composition. Emissions are produced due to a rapid deceleration of an electrically charged particle. Electrons from a cathode source, a glowing tungsten filament, are accelerated through a vacuum tube by a voltage, 15 to 50 kV, towards an anode source, a metal target, where it is decelerated by striking the target (Moore and Reynolds 1997). The interaction between the electron beam and the material, Figure 17, upon impact determines the type of information that can be gathered. Most of the energy, almost 99%, is lost in the form of heat upon impact. X-rays are one type of emissions produced. Two types of x-rays are produced when the electrons impact the material's surface: continuous and

characteristic radiation. XRD and XRF acquire information through these radiations. SEM uses auger, secondary, and backscattered electrons to determine surface topography and elemental composition.

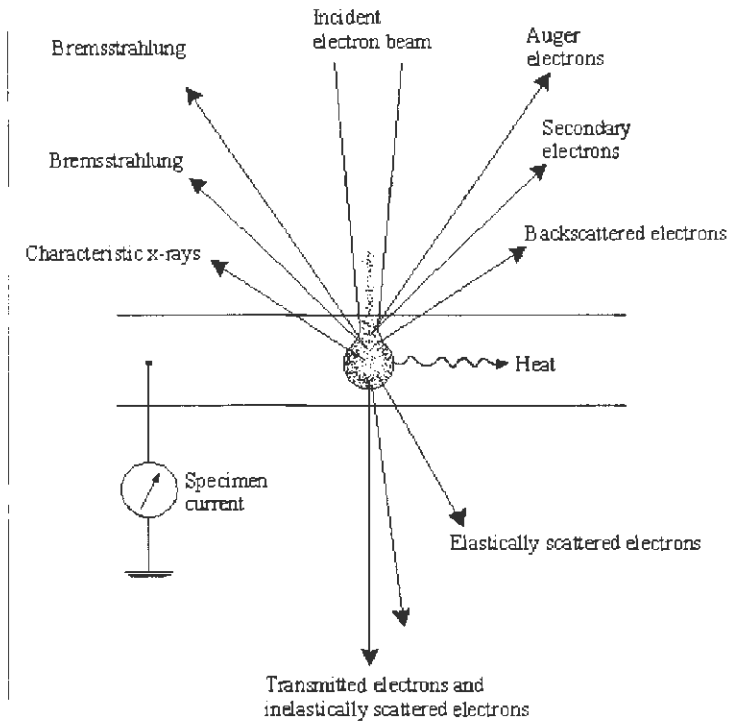

Figure 17. Electron scattering from an election gun (from Cullity 1978).

X-ray Radiation

The x-rays produced have varying wavelengths which are a function of the voltage in the x-ray tube and the current applied to the filament. The continuous radiation, also referred to as bremssstrahlung, heterochromatic, or white radiation, consists of many wavelengths and is shown by the broad, continuous spectrum in Figure 18. The impact of the electrons against any surface emits energy. Some electrons stop suddenly upon impact, giving up all of their energy, while other electrons lose fractions of their energy upon impact. The electrons stopping immediately give up the maximum amount of energy, releasing x-rays with small

wavelengths. The intensity of continuous radiation is zero up until a wavelength called the short-wavelength limit, λ_{SWL} (Cullity 1978). Increasing the voltage decreases the wavelength causing the intensity to increase and pushing the spectrum to the left. The combination of the energy emissions makes up the continuous spectrum. The intensity for the continuous spectrum is proportional to the current through the tube (i), the atomic number of the target material (Z), and the voltage (V) to the 'm' power. Changing the target material does not affect the wavelength distribution but causes intensity to vary. For analyses where large amounts of continuous radiation are needed, materials with high atomic numbers should be used (Cullity 1978).

Characteristic radiation is superimposed on the continuous spectrum in Figure 18 and is used in both XRD and XRF analyses to determine the mineralogy and elemental composition (Cullity 1978). This type of radiation is produced when the accelerated electrons strikes the metal target and knocks one of the electrons in the inner shell of the atom out of its orbit. The electron vacancy is then filled by an electron in an outer orbit, emitting a photon due to the energy loss.

Moore and Reynolds (1997) described the energy difference between the orbitals as a function of the number of protons in the nucleus attracting the electrons, a property unique to each element. The lines of the characteristic spectrum consist of the K, L, M, etc., in increasing wavelength. As shown by Figure 19, electrons from each shell can be knocked out of orbit and filled by an electron from any of the outer shells. The most pronounced response occurs when an electron is knocked out of the K-shell and filled by an electron in the L-shell. The K-line is the most commonly used characteristic line in x-ray diffraction. $K_{\alpha 1}$, $K_{\alpha 2}$, and $K_{\beta 1}$ are the strongest lines produced in the characteristic spectrum. The

intensity of a characteristic line is proportional to the tube current (i), the difference between the voltage applied (V), and the critical excitation voltage for the given characteristic line (V_K) to the n power. As characteristic lines are superimposed on the continuous spectrum, the intensity is measured above the continuous spectrum (Cullity 1978).

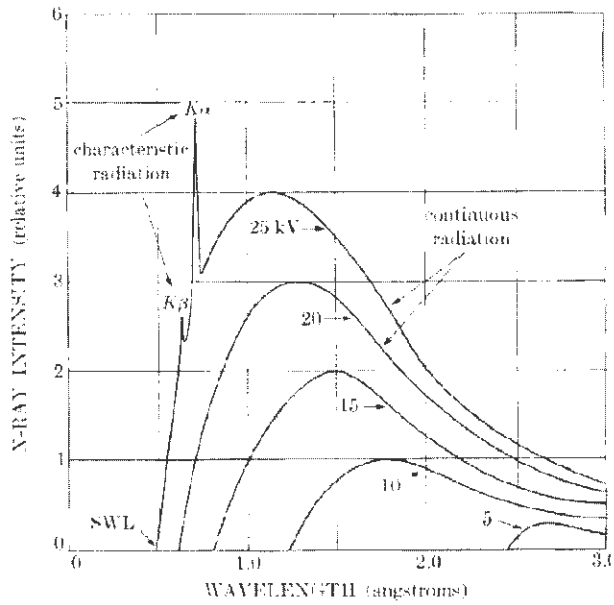

Figure 18. Continuous and characteristic curves (from Cullity 1978).

Crystal Geometry

The alternating pattern in a crystal's structure is important to the diffraction of x-rays. Amorphous solids, such as glass, do not have the periodicity in the atom arrangement like crystals. Cullity (1978) described a crystal in terms of a lattice framework instead of a group of atoms. A set of imaginary points within this framework, as depicted in Figure 20, are formed to make a point lattice: an array of points with equivalent surroundings. The bold rays outlined in Figure 20 represent one of the identical cells within the point lattice called a unit

cell. The unit cell can be described by three vectors called the crystallographic axes, their lengths, or the angles between the vectors. Indices are commonly used to describe a plane's orientation. Miller indices describe the orientation of a plane in a lattice by giving the "*...reciprocal of the fractional intercepts which the plane makes with the crystallographic axes...*" (Cullity 1978). The Miller indices (*hkl*), shown in parentheses, would represent fractional intercepts of 1/*h*, 1/*k*, and 1/*l* with the axes. Relationships to the unit cell are formed with the ordered 3-D periodic arrangement of atoms in crystals. A Miller index is used to describe the parallel lattice planes separated by a fixed translation distance, or the d-spacing, in a direction perpendicular to the plane. d_{001} would represent the Miller index (001) lattice plane (Mitchell 1976).

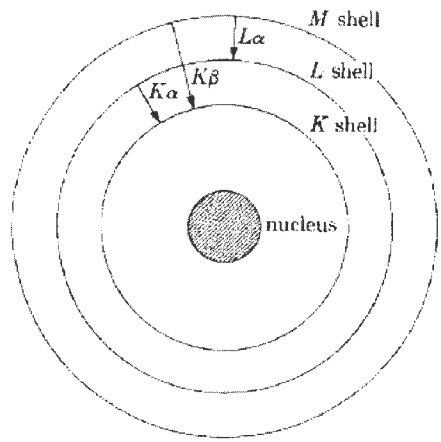

Figure 19. Electronic transitions in an atom (from Cullity 1978).

Repetition of the arrangement of atoms is what diffracts the x-rays and is used to define the material's symmetry. The repetition creates stacks of arranged atoms separated by a distance, d. As the d-spacing and intensity variations are unique to each crystal, crystals

can be identified through measuring these parameters. XRD is commonly used to identify clay minerals due to clay crystals' perfect (001) cleavage (Moore and Reynolds 1997).

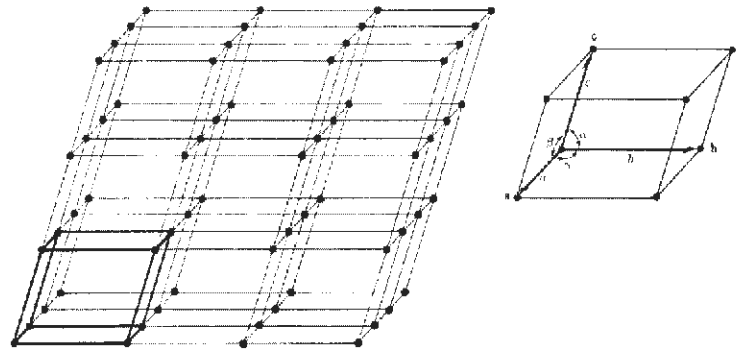

Figure 20. Point lattices and unit cell (from Cullity 1978).

X-ray Diffraction

Cullity (1978) defines a diffracted beam as a beam of many scattered rays mutually reinforcing each other. Figure 21 displays a beam hitting a crystal with a primary ray diffracted at an angle θ. The theory was first established by W.L. Bragg in 1912 and displays a crystal with planes A, B, C... at a uniform spacing of d'. 'KL' in Figure 21 is equal to d'. The wavelength difference between plane A and B, nλ, is equal to the summation of the segments ML and LN in Figure 21. Through trigonometry, Bragg's Law can be derived (Cullity 1978):

$$2d'\sin\theta = n\cdot\lambda \qquad (6)$$

Moore and Reynolds (1997) and many others regard Equation 6 as the most important formulae in x-ray diffraction. n is the order of reflection, equal to the wavelength difference

between scattered rays of adjacent planes, the smallest number in diffraction is one. Rays are required to have path lengths differing by a whole number (n) of the wavelength (λ) for diffraction to occur (Clegg *et al.* 2001). Monatomic gases do not satisfy Equation 6 as scattering is weak and in all direction, where as perfect crystals produce strong scattering and satisfy Equation 6 if the rays do not cancel each other out (Cullity 1978).

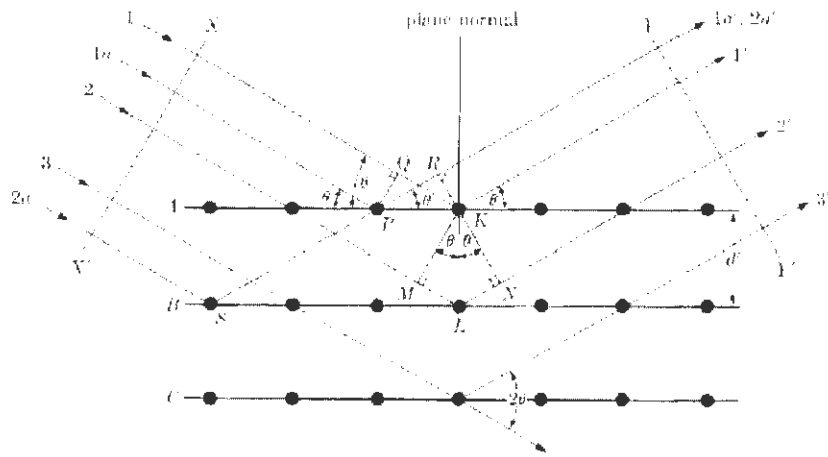

Figure 21. X-ray photons diffracting on a crystal's planes (from Cullity 1978).

Equipment and Procedure

Figure 22 shows the three main components of XRD equipment: an x-ray tube with a high voltage generator, a goniometer, and a detector. X-rays are produced in a sealed hot-cathode tube. As discussed earlier, a heated filament generates electrons, which are accelerated over a voltage difference, V. The electrons are targeted at an anode with a metal disk: copper, molybdenum, or cobalt. For Cu x-ray tubes, nearly 600 W (voltage of 30 kV and electron current of 15-20 mA) of power are directed at the target (Woolfson 1997). X-rays are emitted through a window of beryllium and then through the shutter opening into

Soller and divergence slits to gather and direct the beam. Soller slits prevent x-rays that are not traveling perpendicular to the axis G in Figure 22 from passing through. The beam diffracts off the sample and the portion of reflected rays is passed through another Soller slit and an anti-scatter slit before they are received by the detector (Moore and Reynolds 1997).

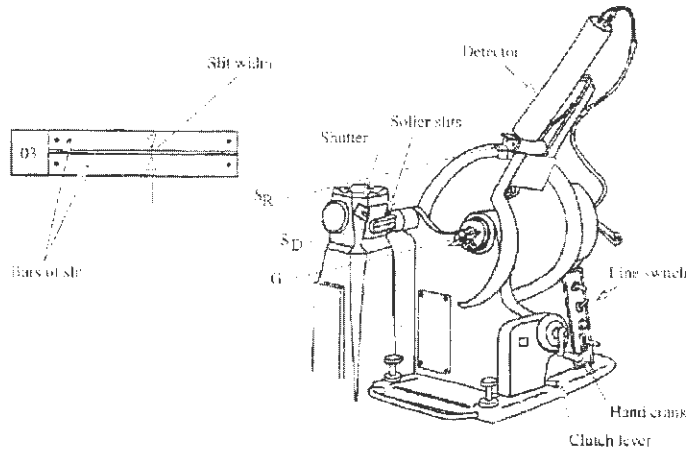

Figure 22. XRD equipment (from Moore and Reynolds 1997).

A goniometer, also called a diffractometer, is used to measure angles and is shown in Figure 22 by the label G. Automated diffractometers are commonly used in practice measuring 2θ steps of a certain size, x, over a period of time, t. Doubling the count time will cause peak heights and areas to double. Moore and Reynolds (1997) suggest step sizes of 0.1° for clay minerals and 0.05° for bulk rock powder samples. Step size does not affect accuracy of the integrated peak areas as long as the step size is 1/5 of the peak width at half-height.

Detectors catch and react to the diffracted x-rays. Five different types of detectors exist, but the scintillation detector will only be discussed (Moore and Reynolds 1997). A

scintillation counter detects diffracted x-rays by having the radiation initially fall on a fluorescent material. This produces a visible-light photon which falls on a photoemissive surface producing a photoelectron. The photoelectron is detected with a photomultiplier arrangement (Woolfson 1997). With the detector and goniometer, the photon intensity for a series of 2θs are measured. The d-spacing of the crystals can then be calculated by Bragg's law, Equation 6, and correlated to known d-spacings of a given crystal structure (Woolfson 1997).

Two main methods exist in XRD for analyzing the mineralogy of soil materials: powder and oriented samples. Both methods in XRD are primarily qualitative analyses. Powder mounted samples are used to analyze the bulk mineralogy of a material by using randomly oriented packed particles. Perfect random packing is difficult to obtain due to crystals breaking or cleaving. Some of the crystals may be oriented to have reflections conforming to Bragg's law (Moore and Reynolds 1997). When the x-ray beam hits the sample, each crystal sends off a reflection from its cystallographic planes, (*hkl*). Mineralogy of powder samples can be identified by consulting the Joint Committee on Powder Diffraction Standards (JCPDS) *Powder Diffraction File* system (The International Centre for Diffraction Data® 2004). Figure 23 shows an example diffractogram on a bulk sample of Pierre Shale. The proportion of clay to non-clay minerals is approximated from analyzing the powder-mounted XRD peaks. Essential to a good random powder analysis is a reduction of particle size to 5 to 10 μm. The size reduction (by impact not grinding) improves the possibility of obtaining the various spacings of the crystals (Moore and Reynolds 1997).

Oriented clay mineral aggregate samples are used to analyze the clay mineral fraction specifically. In random-mounted samples, some of the weak (00*l*) reflections of clay

minerals are covered by other minerals. Oriented-mounted samples intensify the (00*l*) reflections and reduce (hk0) by removing non-platy minerals and dispersing clay minerals into individual colloidal particles (Moore and Reynolds 1997). Chemical methods can be used for dispersal and cementation removal but non-chemical methods are preferred. Separating the clay fraction from suspension requires dispersal of the clay particles. Salts, which cause flocculation, must be washed out by centrifugation or multiple washings before separations can be performed. Consult the preceding topic *Clay minerals* for a discussion on flocculation. Particle-size separation is performed on the material based on Stoke's law, where particles <2µm equivalent spherical diameter are obtained. Centrifugation is the best method to separate particle sizes, if available. Various sample preparation methods are available, but only the filter transfer method will be discussed as it is being used. Moore and Reynolds (1997) recommended this method as it produces clay surfaces representative of the different minerals. The clay suspension is vacuumed through a filtration apparatus with a porous glass base and a side-necked vacuum flask, separated by a filter. The wet filter is removed, inverted and carefully placed on a glass slide. The filter and glass slide are dried at 50°C for 3 to 4 minutes; the filter is removed; and the sample is prepared for analysis. Various treatments on the suspension are used to differentiate the clay minerals. The x-ray diffraction flowchart shown in Starkey *et al.* (1984) was used for clay mineral identification.

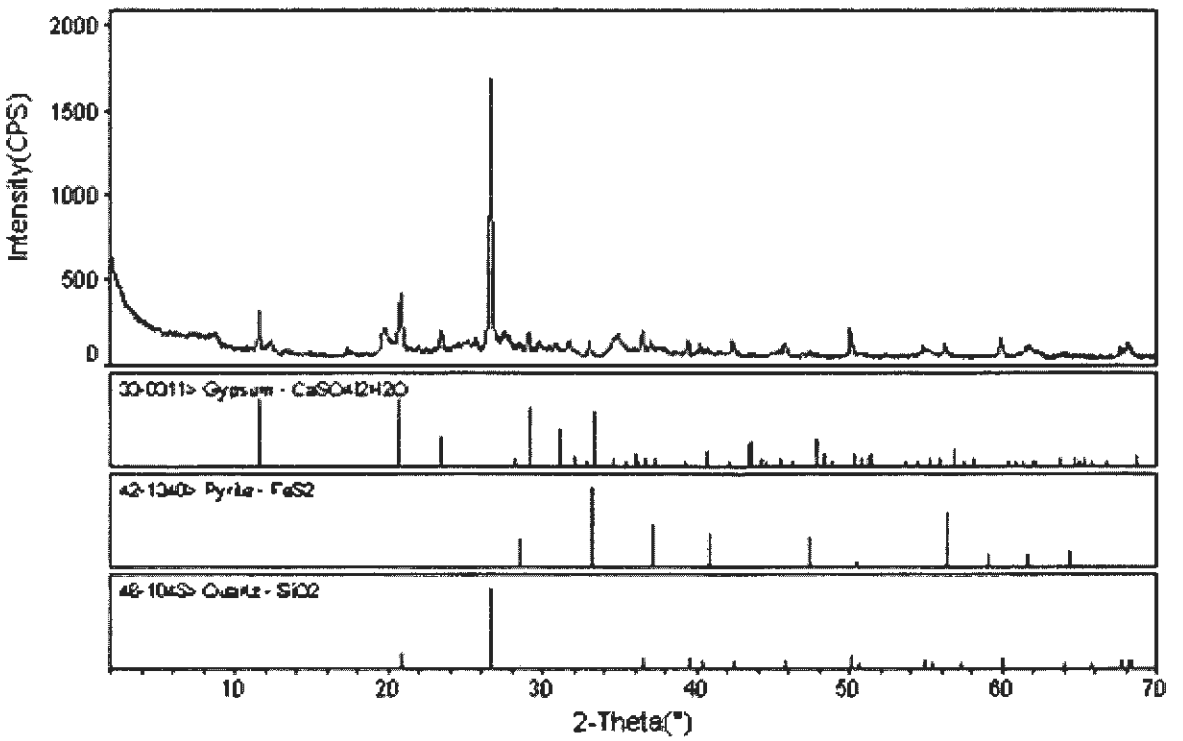

Figure 23. Random mount diffractogram on Pierre Shale

Mixed-layer clay mineral concentrations in the Pierre Shale were obtained from the procedure outlined by Schultz (1978). Figure 24 shows a diagram compiled by Schultz (1978) describing the proportion of illite-beidellite-montmorillonite mixed-layer clay common in Pierre Shale. Results from oriented mount samples were used to determine the concentrations.

X-ray Spectroscopy

While x-ray diffractions uses Bragg's law by knowing the x-rays' wavelengths to determine the d-spacing, x-ray spectroscopy uses a crystal with a known d-spacing to obtain a wavelength. Elemental information, regardless of the mineralogical composition, is obtained through this analysis. A quantitative measurement of the elements is obtained due

to the characteristic nature of each elemental's emission. The sample is bombarded with x-rays, causing the sample's elements to emit secondary fluorescent radiation that can be measured using x-ray spectrometers (Cullity 1978).

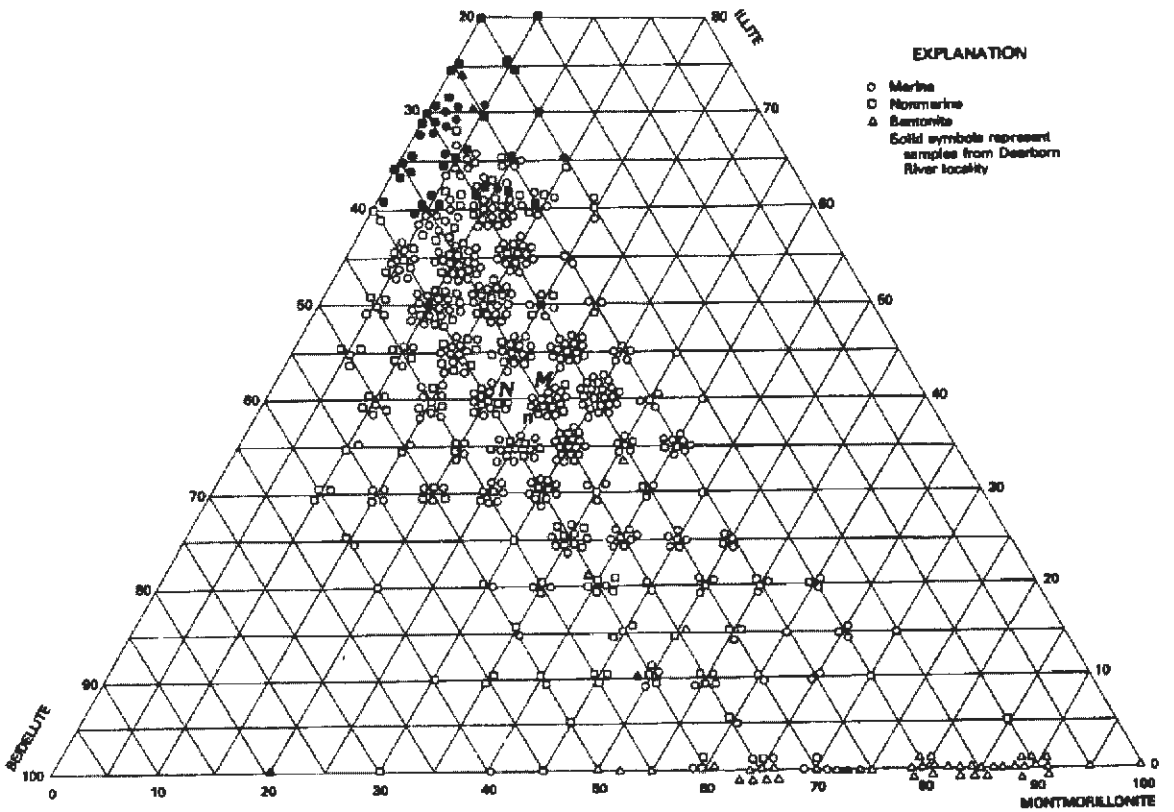

Figure 24. Proportion of mixed-layer clay minerals in Pierre Shale (from Schultz 1978).

Two types of spectrometers are used in practice: wavelength-dispersive and energy-dispersive. Figure 25a shows a diagram of a wavelength-dispersive x-ray spectrometer. X-rays from the x-ray tube are directed towards a crystal as the crystal is rotated about at an angle, 2θ, to the counter. For a given 2θ, the intensity is measured and the wavelength is calculated from Bragg's law (Equation 6). The scintillation (for short-wavelength elements) and sealed gas proportional (for long-wavelength elements) counters are used in practice.

The x-ray tube is similar to the one described in the *X-ray diffraction equipment and procedure* section. The d-spacing is the most important characteristic of the crystal used in x-ray spectroscopy. As an example, identifying elements with high atomic numbers (short wavelengths) require crystals with small d-spacings (Cullity 1978).

Determination of the elemental composition is obtained from the intensity of an element's radiation, which is proportional to the atomic fraction without any interfering effects. Matrix absorption and enhancement are the major causes of interference. The matrix absorption is a function of the absorption coefficient of the material for the particular wavelength. Enhancement is caused by overlapping characteristic radiation. Calibration curves and empirical-coefficient methods are used for quantitative analysis due to these complexities.

Energy-dispersive spectrometers (EDS), Figure 25b, do not diffract x-rays but separate wavelengths radiating from the sample by their energies. Cullity (1978) describes EDS as a semi-quantitative method. A Si(Li) counter and multichannel analyzer (MCA) are used to separate the wavelengths (Cullity 1978). The Si(Li) counter provides high-quality energy resolution, defined by $\Delta\lambda/\lambda$, and the MCA provides rapid pulse-height analysis. EDS has better resolution than wavelength-dispersive for small wavelength, high-energy elements.

Sample preparation for x-ray spectroscopy is important to obtain good results. The sample must represent the bulk sample while closely fitting the theoretical models applied to calculate elemental concentrations. Amonette and Sanders (1994) describes fusion as the "*only technique*" which truly homogenizes a sample. Cautions must be taken with fusion as it is a destructive procedure, dilutes the sample, and causes the loss of trace elements. Fusion consists of initially drying a sample in an oven followed by ignition to remove interlayer

water. Samples are then homogenized and mixed with an x-ray flux. A flux with a mixture of $Li_2B_4O_7$ and $LiBO_2$ (12:22) is commonly used in practice. The suspension is heated in a fluxer to form a fused glass disk and allowed to cool (Amonette and Sanders 1994).

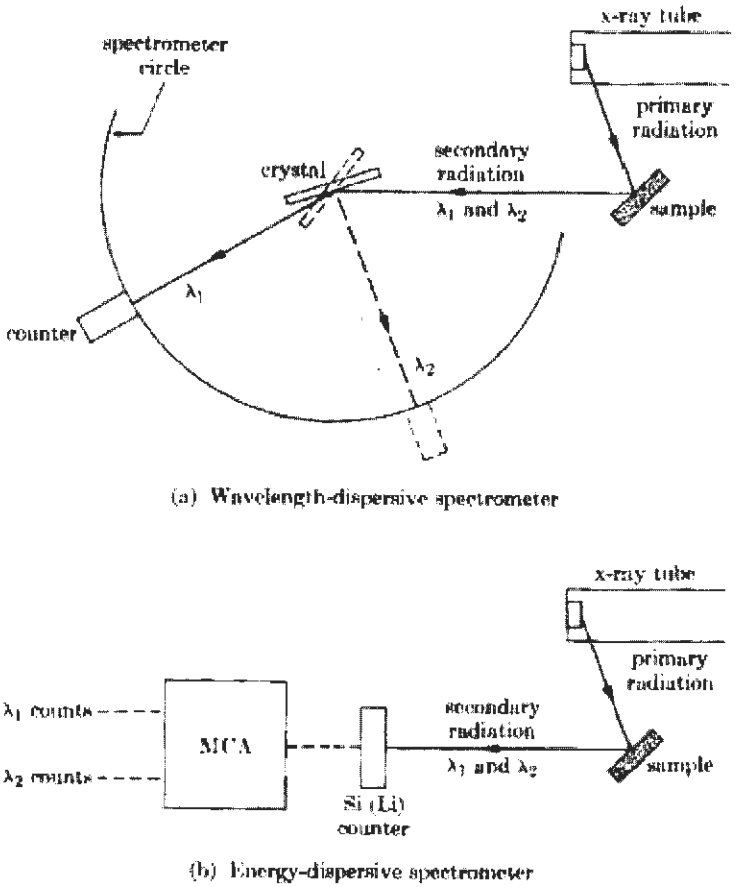

Figure 25. X-ray spectroscopy (from Cullity 1978).

Scanning Electron Microscopy

The scanning electron microscope (SEM) is a powerful tool in fabric analyses of clay minerals. A SEM, Figure 26, uses accelerated electrons directed at a sample to obtain a microscopic view of a material. The electron source, similar to the x-ray source in XRD and

XRF, is produced from a gun with a heated tungsten filament, a Wehnelt cylinder, and an anode which also acts as an electrostatic collector lens. A vacuum of 10^{-5} Torr must be used in the SEM, as electrons cannot pass through air. The electron beam is condensed onto the sample by lenses causing electrons to be reflected, similar to Figure 17, which are measured by a specific device unique to the type of electron. This signal is amplified and scanned onto a spot of a cathode ray tube, creating an image of the sample surface (Smart and Tovey 1982).

Several methods are available to prepare samples for analysis in the SEM. Due to the need for a vacuum in the testing chamber, samples must be dry before analysis. Removal or replacement of the pore fluid requires a non-destructive technique to preserve the soil structure. Clay fabrics cause difficulties with these methods due to their characteristic platy structure and their ability to hold water in the interlayer. Tovey and Yam (1973) describes the problem:

> *"...as the pore fluid is removed from samples the structure collapses until the shrinkage limit is reached after which little further collapse occur..."*

Six techniques to remove pore fluid from soils are used in practice: oven-drying, air-drying, humidity-drying, substitution-drying, freeze-drying, and critical drying.

Oven- and air-drying techniques produce large but varying shrinkage characteristics. Slower drying techniques, such as slow air-drying, exhibit greater amounts of shrinkage than oven-drying but less differential shrinkage between the vertical and horizontal components (Smart and Tovey 1982). A greater amount of reorientation of particles was also observed with slow-drying methods. Smart and Tovey (1982) cautioned against the use of oven-drying techniques as mineralogical alternations may take place at the high temperatures,

concluding that air-drying is preferred over oven-drying. High internal stresses also build up during oven-drying, possibly causing particle breakage. Air-drying can be used with minimal sample disturbance for samples with moisture contents below the material's shrinkage limit (Tovey and Yan 1973). Substitution air-drying, a pore fluid replacement method, involves impregnating the pore fluid with a substance with low surface tension before air-drying. Particle rearrangement may be caused from this method and the replacement fluid must be immiscible to the material.

Tovey and Yan (1973) considered critical point drying and freeze drying to be some of the "*more important*" methods in the preparation of soil specimens for SEM analysis. Critical point drying, also referred to as supercritical by some authors (Smart and Tovey 1982), substitutes the pore fluid with a substance having a low critical temperature and pressure, which is removed by turning it into a gas. Water has a critical temperature and pressure of 374°C and 22,100 kPa, respectively. These values are too high to remove water from a soil while sustaining a clay structure (Smart and Tovey 1982). Instead, the pore fluid is replaced by a substance with a lower critical temperature and pressure, such as water-ethanol or water-alcohol-amyl acetate-liquid carbon dioxide.

Freeze-drying rapidly freezes samples, avoiding surface tension problems associated with air- and oven-drying, while avoiding crystal formation. The ice is then removed by "*sublimation in vacuo*" to prevent structure disruption. The sublimation temperature must be low enough to avoid local melting and crystal recrystallization. Samples are initially cooled in a liquid with a low boiling temperature, such as liquid nitrogen or propane. Liquid nitrogen is often used to cool another liquid with a higher boiling point. Smart and Tovey (1982) provides details on freeze-drying. Three percent volumetric increases were observed

for marine-clay samples upon freezing. Freeze-drying has also been shown to cause some damage to the large-scale orientation and decreases in the 001 spacing of Ca-Montmorillonite (Erol *et al.* 1976).

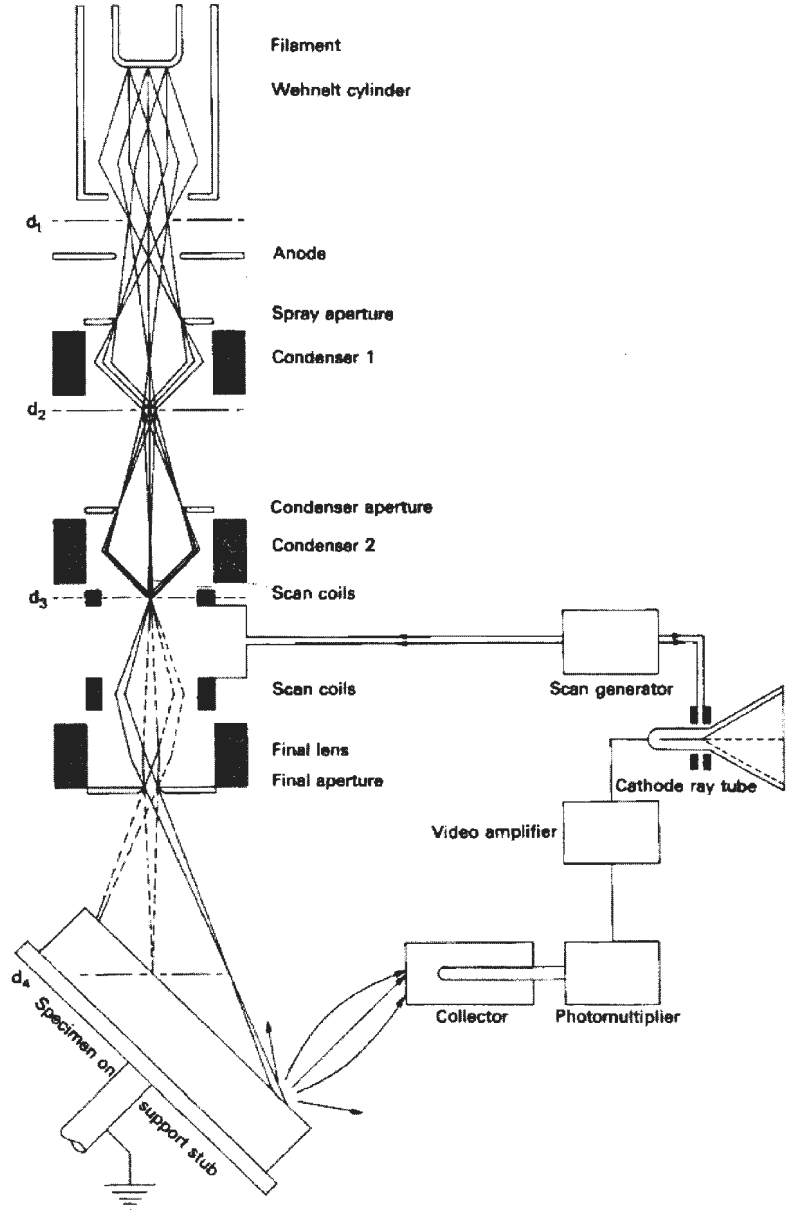

Figure 26. Scanning electron microscope (from Smart and Tovey 1982).

Fabric, Structure, and Micromorphology

Knowledge of a material's fabric is beneficial to understanding the mechanical behavior as the properties of soils and rocks are a function of the material's fabric (Mitchell 1976). The arrangement of particles, particle groups, and pore spaces is regarded as fabric (Brewer and Sleeman 1988, Mitchell 1976). Microscopic features are covered by fabric while macroscopic features are associated with structure (Brewer and Sleeman 1988). The term morphology covers both fabric and structural features. Yong and Sheeran (1973) considers structure as providing integrity to a soil and fabric to be an integral component of structure. The following discussion includes the nomenclature and common fabrics in clay and non-clay minerals.

Fabric analysis can be broken into three areas: elementary particle arrangements, particle assemblages, and pore spaces (Mitchell 1976). Fabric analysis builds on the smallest fabric unit to describe a soil in a series of levels. Elementary particle arrangements are interactions between the individual particles such as a cardhouse fabric consisting of an edge-face flocculated association. Particle assemblages are composed of one or more elementary particle arrangements with a definable boundary. Domains are aggregated, parallel clay plates. Many domains can be grouped together to form interweaving bunches as in turbostractic fabrics. Domains in an edge-face pattern make up a cardhouse fabric. The term clay matrix is used to describe a series of interacting clay particles while cluster defines a group of particles into a larger fabric unit (Brewer and Sleeman 1988). Brewer and Sleeman (1988) provide a comprehensive discussion on soil structure and fabric.

Most clay minerals have a characteristic structure and fabric. For active clays such as montmorillonite, dispersion or flocculation of the clay fabrics is related to environmental

conditions. As shown in Figure 27a and b, the morphology of montmorillonite consist of thin flakes, as low as 10Å in thickness. The montmorillonite in Figures 27a and b were described as "*...developed, webby pore-lining smectite...*" in the literature (Welton 1984). Figures 27c illustrates the characteristic cardhouse structure associated with montmorillonite. Figures 27d, e, and f show illite and its small, flaky particles with a hexagonal shape. Stacked thin sections of kaolinite are shown in Figures 27g, h, and i. The size difference between montmorillonite, illite, and kaolinite is obvious when noting the magnifications of the micrographs (Welton 1984).

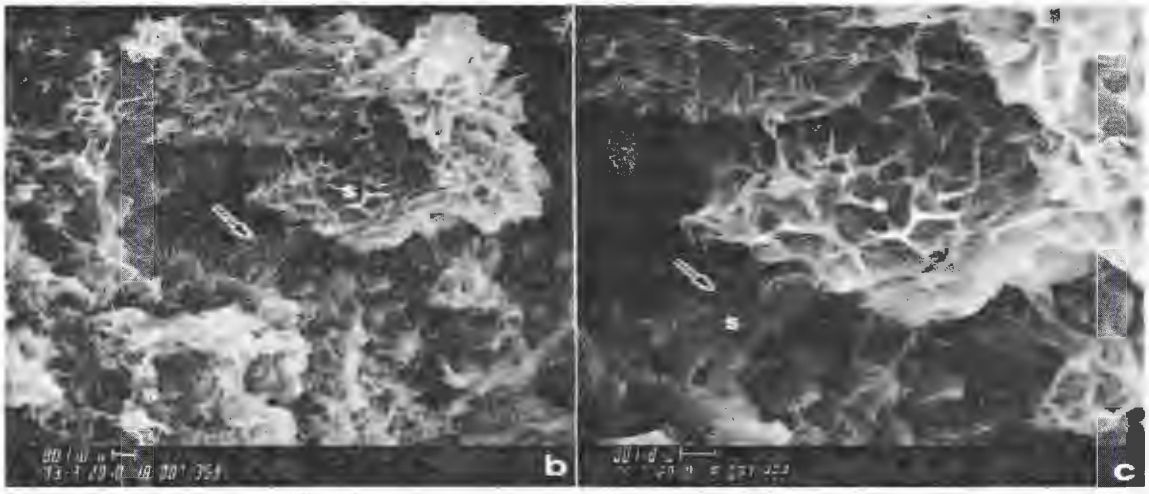

a) Smectite: magnification-3kx b) Smectite: magnification-5kx

Figure 27. Clay mineral micrographs (from Welton 1984).

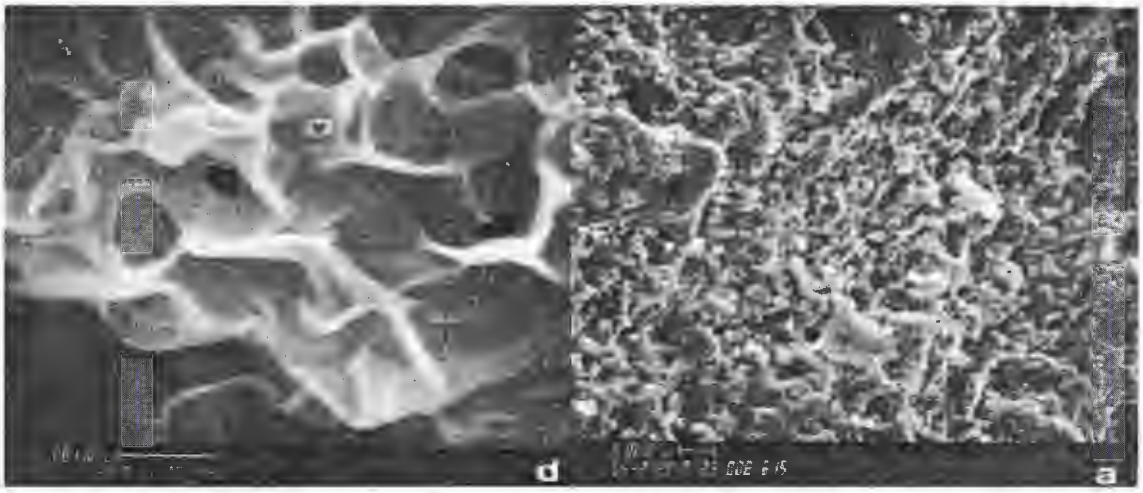

c) Smectite: magnification-15kx d) Illite: magnification-500x

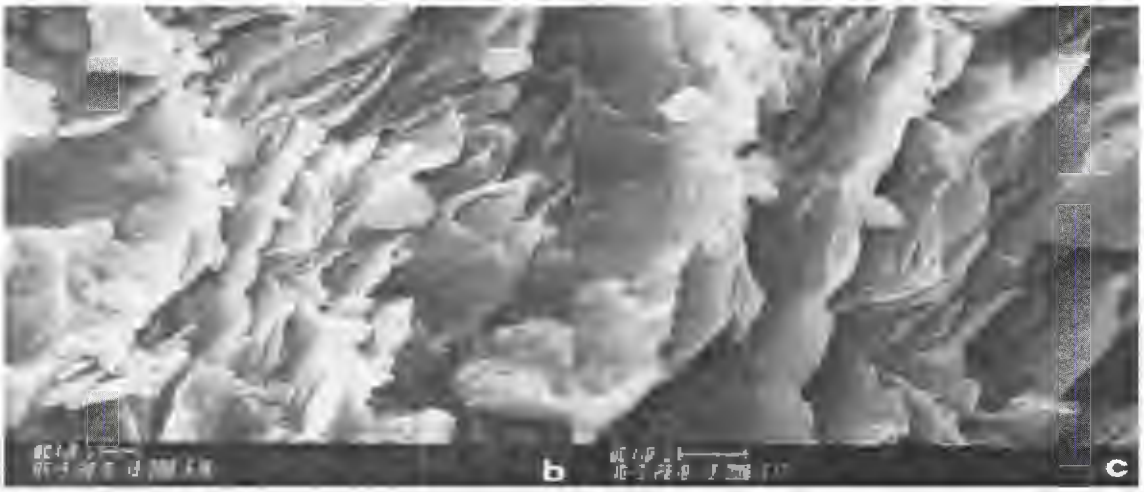

e) Illite: magnification-5kx f) Illite: magnification-10kx

g) Kaolinite: magnification-200x h) Kaolinite: magnification-500x

Figure 27. Clay mineral micrographs (from Welton 1984).

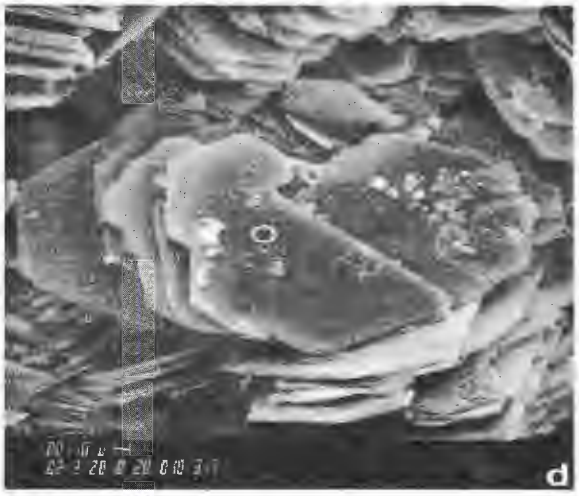

i) Kaolinite: magnification-2kx

Figure 27. con't . Clay mineral micrographs (from Welton 1984).

Non-clay minerals can also be identified by their morphology. Optical and visual observations are useful to identify many non-clay minerals due to their size. Color can also be used to characterize a crystal. Pyrite (FeS_2) has many morphological forms: cubic, octahedron or pyritohedron, and has a metallic, brassy-yellow color. Framboidal pyrite is also common. Figure 28a and b show octahedron and pyritohedron forms of pyrite. Octahedron pyrite and a pyritohedra of pyrite are denoted by an arrow and the letter 'P,' respectively, in Figure 28a. Lenses of pyrite framboids in a burrow are shown in Figures 28c and d. Framboids are round to oval shaped aggregates composed of small, crystalline pyrite. Gypsum ($CaSO_4 \cdot 2H_2O$) has a characteristic tabular or prismatic lath crystal with a transparent to white coloration. Gypsum crystals regularly form in a rosette, similar to the formation in Figure 28e and f (Welton 1984).

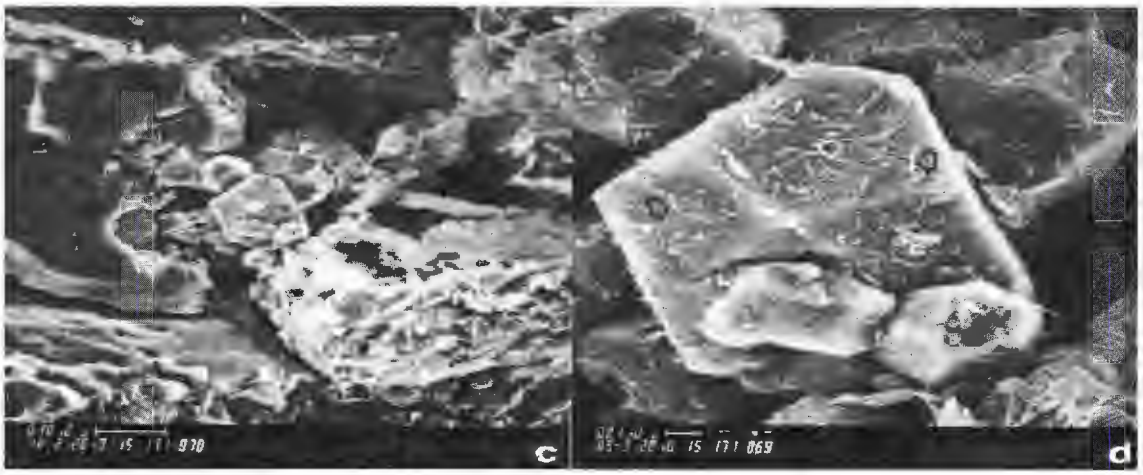

a) Pyrite: magnification-1000x b) Pyrite: magnification-5kx

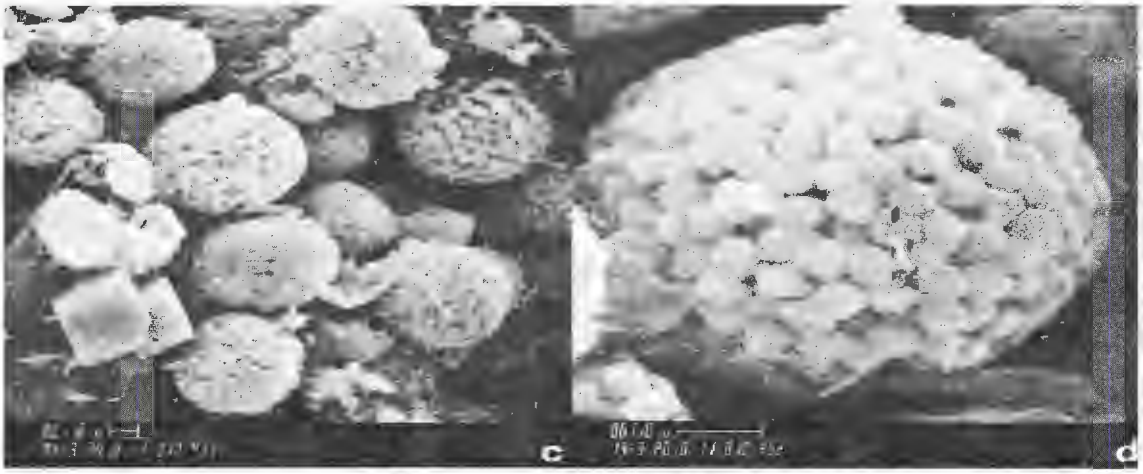

c) Pyrite: magnification-1000x d) Pyrite: magnification-5kx

e) Gypsum: magnification-700x f) Gypsum: magnification-5kx

Figure 28. Non-clay mineral micrographs (from Welton 1984).

SUMMARY

The complex nature of weathering requires a multidisciplinary analysis to understand the behavior. This review has shown a few of the engineering problems encountered in the Pierre Shale formation and how these problems can be studied. Ring-shear devices were shown to provide residual friction angles in agreement with field back analysis. X-ray diffraction and x-ray fluorescence procedures and sample preparation were included to obtain mineralogical and chemical data. The review concluded with a discussion on fabric analysis and the use of the scanning electron microscope.

CHAPTER 3

STRENGTH OF PIERRE SHALE IN RELATION TO WEATHERING, MINERAL AND CHEMICAL STATE

A paper to be submitted to: *Journal of Geotechnical and Geoenvironmental Engineering*

V. R. Schaefer[1,4], M. ASCE, M. A. Birchmier[2,4], and R. A. Lohnes[3,4], M. ACSE

ABSTRACT

Previous research has indicated that the strength loss of shales by weathering is not associated with major changes in clay mineralogy while laboratory studies on montmorillonite provide evidence that strength is related to type and concentration of exchangeable cations. Strength studies suggest that both potassium and calcium ions produce higher strength than sodium ions. In this study, the residual strength of Pierre Shale is investigated using ring-shear tests on weathered, transitional, and unweathered samples. The mechanical-strength tests are supplemented by x-ray diffraction (XRD), x-ray fluorescence (XRF), and energy dispersive spectroscopy (EDS) in a scanning electron microscope (SEM) to discern the effect of subtle differences in mineralogy and chemical state on measured residual shear strength. The results suggest the increase in the coarse fraction is the main contributor to the higher residual strength of the transitional zone. The lowest residual

[1] James M. Hoover Professor of Geotechnical Engineering, Iowa State University.
[2] Graduate Student, Department of Civil, Construction, Environmental Engineering, Iowa State University
[3] Professor of Civil Engineering Emeritus, Iowa State University.
[4] Primary researcher and author.

strength values were observed in the weathered zone and where particle size analyses indicate fine-grained particles as a cause.

INTRODUCTION

Overconsolidated Cretaceous clay shales of North America, in particular the Pierre and Bearpaw Shales, are problematic with regard to slope instability (Brooker and Peck 1993). Central to these problems is the decrease from peak to residual strength as the materials respond to stress relief caused by erosion. Following rebound, initial fissuring of the shales, and subsequent swelling of the clays, weathering and strain softening take place, often resulting in landslides.

Most research concerning such soils and clay shales has been directed to measurement of residual strengths, numerical analyses, and the mechanical effects of the drop from peak to residual strength. Less effort has been expended on understanding the physico-chemical processes associated with strength loss. The few physico-chemical studies were often conducted on artificial soils consisting of pure clays or mixtures of clays with sands; however they did indicate that cations adsorbed by the montmorillonite affect the soil's strength.

This paper reports the results of a study conducted to relate the strength of weathered, transitional, and unweathered Pierre Shale to its chemistry, mineralogy, and micro-morphology. Previous studies have shown that the Pierre Shale mineralogy varies little between the weathered and unweathered material, with montmorillonite the dominant clay mineral in both materials.

BACKGROUND

The mechanical behavior of overconsolidated clays is well known through the work of pioneers such as Skempton (1948, 1964) and Bjerrum (1967), and a key aspect of this behavior is the change in strength from peak to residual as the overconsolidated materials are subjected to large strains due to stress relief and erosion. Additionally, it is well known that the shear strength of clays is controlled in part by adsorbed cations (Mitchell 1993).

Long-term slope stability and residual strength have long been an area of study. Tiedemann (1937), Haefeli (1938), and Hvorslev (1939) were some of the first researchers to introduce the term residual strength. Skempton (1964) later demonstrated the importance of residual strength in controlling the slope stability of overconsolidated clays, particularly in jointed and fissured clays. The dominate feature in achieving the residual strength was clay size particles orienting in the direction of shear after large amounts of strain, which was found to be a permanent feature of the soil's fabric once formed. This finding showed that as the peak strength is exceeded, the strength will continue to decrease towards the residual strength, thus making residual strength the controlling factor in slope stability design (Skempton 1964).

The residual strength has been observed to be more sensitive to the particle properties in comparison to external properties such as the consolidation history. For small normal stresses, the residual strength was independent of the stress history for a given effective stress (Skempton 1964, Kenney 1967). Larger normal stresses have been hypothesized to allow for greater particle orientation, thus decreasing the residual stresses and making the failure envelope slightly curved (Townsend and Gilbert 1976). Higher normal stresses are theorized

to cause the platy particles to orient better, causing the residual strength to be lower than lower normal stresses.

Lupini *et al.* (1981) outlined different modes of shear behavior for varying mineralogy after the observation that particle shape controlled the residual strength for massive minerals, such as quartz and calcite, as opposed to clay minerals, in which particle size controlled the residual strength (Kenney 1967). Massive minerals or rotund particles were shown to behave more turbulently upon shearing, where the particles roll over each other, and the residual strength controlled by the packing and particle shape. Platy particles are more likely to orient in the direction of shearing, thus behaving in a sliding mode. For sliding mode behavior, the residual strength was dependent on the mineralogy, pore water chemistry and interparticle friction angle (Lupini *et al.* 1981).

Recent research indicates that the clay mineralogy and system chemistry of a soil may have a more significant influence on the strength behavior than once thought. The weathering process involves cation exchange of adsorbed ions on clays, especially montmorillonite. Laboratory experiments show that expandability and shear strength of smectites varies with the nature of the cations, with K^+ producing residual shear strengths higher than Na^+ (Steward and Cripps 1983) and Ca^{2+} also associated with higher strengths than Na^+ (Moore 1991). Moore (1991) quantified the difference, with the residual strength 39 percent higher for calcium-saturated than for sodium-saturated montmorillonite. The residual strength was also found to increase with increasing cation concentration (Steward and Cripps 1983, Moore 1991 and Di Maio and Fenilli 1994). Table 10 provides a summary of the various factors and their effect on the residual strength.

Table 10. Summary table of residual strength factors

Factors	Effect on residual strength
Cation concentration	Higher concentrations increase τ_r
Type of adsorbed cation	
Na^+ (monovalent and low polarizability)	Decrease τ_r
K^+ (monovalent and higher polarizability)	Increase τ_r in comparison to Na^+
Ca^{2+} (divalent and higher polarizability)	Increase τ_r in comparison to K^+
Clay content	Increase in clay content decreases τ_r
Type of mineral	
Platy mineral	τ_r increases: montmorillonite<illite<kaolinite
Massive minerals	τ_r greater than clay minerals
Liquid limit (related to other factors)	Higher liquid limit produces lower τ_r

MATERIALS AND SAMPLE PREPARATION

Materials

The material in this study is Pierre Shale and knowledge of the geologic history is important due to the significant influence on the mineralogy and interparticle friction angle, and thus the strength behavior. The Pierre Shale Formation was deposited during the Cretaceous Period some 60 to 80 million years ago, as a result of sedimentation in the Cretaceous Epeiric Sea that covered the central part of the United States and Canada. Much of the formation was formed under marine environments, but due to the transgressive-regressive nature of the inland sea, there are zones in the formation that have a non-marine origin (Tourtelot 1962). The material at depth is very strong, but as the shale is exposed to the environment, the material quickly degrades due to weathering and fissuring to rather weak soil materials. Pierre Shale has high smectite contents, with occasional almost-pure bentonite zones, due to volcanic ash deposition during formation of the deposit (Tourtelot 1962).

Pierre Shale from a boring in the Crow Creek Member at the Oahe Dam, South Dakota, USA, was used in this study. The boring was at station 50+00 along the dam as given in the diagram of the Oahe Dam by Knight (1963). Intact samples of the shale were obtained from coring operations during the installation of new instrumentation. Unweathered Pierre Shale at the site exhibits unconfined strengths of 0.5 to 17.4 MPa and a Young's modulus between 137 and 965 MPa (Johns *et al.* 1963). Weathering caused significant problems during the construction of the Oahe Dam (Johns *et al.* 1963). Many of the slopes had to be redesigned after slope failures, with initial engineering parameters of ϕ=11.3 degrees and 19.1 kPa for cohesion later designed with lower values of ϕ=8.5 degrees and 14.4 kPa for cohesion. Significant measures were also taken to prevent weathering of the shale, such as immediately placing a bituminous sealer or mortar over exposed surfaces (Fleming *et al. 1970*).

Materials in the depth range of 18 to 21 meters are weathered and shale below 26 meters is unweathered based on geologic interpretation of the boring logs and optical microscope observations (Birchmier 2005). Material altered after deposition by environmental conditions, not including unloading and rebound, was classified as weathered Pierre Shale. A transitional zone exists between the 21 and 26 meter depths. Samples from these ranges of depths were characterized with classification, strength, chemical and mineralogical tests. Sample preparation varied according to the tests that were conducted on the samples.

Sample Preparation

Classification and Residual Shear Strength

Sample preparation for classification tests and particle size distribution followed applicable American Society for Testing and Materials (ASTM 2003) standards. The sample preparation for the Bromhead Ring Shear used a modified version of ASTM D6467-99, Standard Test Method for Torsional Ring Shear Test to Determine Drained Residual Shear Strength of Cohesive Soils. The samples were crushed and passed through a US standard #50 sieve, remolded with distilled water to their plastic limit and allowed to hydrate for 48 to 72 hours. The ASTM standard suggests remolding at higher water contents, near the liquid limit, but Bromhead (1979) proposes drier samples in the Bromhead Ring Shear to prevent excess settlement of the top load platen.

Micromorphology

The relatively undisturbed micromorphology was evaluated using a scanning electron microscope (SEM). To help maintain the soil micromorphology, sample preparation is critical. Several techniques were tried, with freeze-dried sample preparation providing the best method to preserve the fabric. To evaluate relatively undisturbed micromorphology in the scanning electron microscope (SEM), samples were freeze-dried using the following procedure: samples were taken from the various depths and placed in an intermediate freezer for twelve hours at a temperature of -75 degrees Celsius; samples were then placed in a VirTis Ultra 35 8-shelf model freeze dryer at a temperature of -25 degrees Celsius until a vacuum of <100 millitorr was achieved; upon achieving this vacuum, the temperature was raised to 26 degrees Celsius and held constant for 48 to 72 hours; samples from each depth

were tension fractured and placed on carbon stubs for micromorphology and EDS analysis in the SEM.

Mineralogical and Chemical Analyses

X-ray diffraction (XRD), x-ray fluorescence (XRF), and energy-dispersive spectroscopy (EDS) were used to characterize the mineralogy and chemistry of the whole bulk samples. EDS analyses were also performed on sand- and clay-size fractions.

Smear mounted samples were used in the x-ray diffraction analysis with copper K-alpha radiation. This technique provides a fast and qualitative estimate of the mineralogy through partially orienting particles. The intensities of the layer silicate peaks for smear mount samples are higher than random mount samples due to the increase in the orientation (Hughes *et al.* 1980). Bulk mineralogy was inferred from the results obtained from the smear mounted samples. A computerized catalog of the Joint Committee on Powder Diffraction Standards (JCPDS) Powder Diffraction File system (The International Centre for Diffraction Data® 2004) was used for this analysis.

X-ray fluorescence used fused glass disc in the spectrometer analysis. Material from each depth was initially oven dried to a constant mass. The dry material was placed in a shatterbox for four minutes to break down the particles, after which the particles were ignited at 950° Celsius for thirty to sixty minutes. A mass of 1.2 grams of the ignited sample was mixed with 6.018 grams of Sigma x-ray flux 12:22 to a consistent blend. Four drops of lithium bromide were added to the mixture. The blend was placed in a platinum crucible and placed in an Automatic Fluxer FX-503. After 10.5 minutes of heating at 1200° Celsius, the

liquid mixture was poured into a platinum mold and cooled for 11 minutes. The glass discs formed were analyzed in the x-ray spectrometer (Amonette and Sanders 1994).

To separate the clay and sand fractions of the shale, a sample from each depth was immersed in distilled water for 48 hours with no chemical dispersing agent and then mechanically dispersed with an air jet unit. The entire sample was wet washed through the Number 200 (0.075 mm) sieve. Particles retained on the number 200 sieve were considered sand. The sand was washed off the sieve with distilled water into a pan. The portion of the sample that passed through the number 200 sieve was considered the silt and clay fractions of the sample. These two fractions were separated by sedimentation in distilled water. The separation of the silt and clay fractions could be visually observed in the sedimentation cylinder. The total settling time was an average of 24 hours for weathered samples and three to four days for transition and unweathered samples. Once the larger particles settled to the bottom after 24 hours, the finer fractions were removed by pipette and placed in test tubes for later analysis. The "silt" and "clay" fractions were separated by distinct boundaries of the suspension concentrations in the test tubes after additional agitation and settlement. The remaining silt fraction was washed with distilled water and oven dried. This procedure was used to qualitatively isolate the various fractions without any chemical treatment for elemental and morphological analyses in the SEM.

TESTING AND ANALYTICAL METHODS

Classification, pH and CEC

Atterberg limit and hydrometer analyses were conducted on the samples using ASTM standards. pH was measured with a *pHPlus*^{Direct} meter. A prepared slurry of 20 grams of dry

soil and 20 ml of distilled water was used for the test. Electrodes were initially calibrated with a neutral (7.00) and an acid (4.01) buffer. pH and temperature of the mixture were taken with the pH electrode and temperature probe (LaMotte 1999). The procedures outlined in Warncke and Brown (1998) were used to estimate cation concentrations and cation-exchange-capacity (CEC). NH_4OAc was used for the extraction at a pH of 7 and the major four cations: K, Ca, Mg, and K, were determined by inductively coupled plasma emission spectroscopy.

Ring-Shear Testing

The testing procedure for the ring-shear device used a modified version of ASTM D6467-99, Standard Test Method for Torsional Ring Shear Test to Determine Drained Residual Shear Strength of Cohesive Soils. Strength testing was performed using the Bromhead Ring Shear Device (Bromhead 1979). A ring-shear device allows for continuous shearing at a slow strain rate, which permits a better particle orientation parallel to the direction of shearing than direct shear devices. The Bromhead Ring Shear Device consists of a 10:1 counterbalanced lever arm which provides the normal loading to the sample and a range of displacement rates from 0.024 to 60 degrees per minute (Wykeham Farrance 2004). The mold for the device consists of an annular ring, 5 mm deep with an inner and outer diameter of 7 and 10 centimeters, respectively.

The prepared sample was placed into the mold and placed into the ring-shear device. The mold was immersed in distilled water and an initial normal stress of 100 kPa was applied. Progressive loading of a single sample during shearing, or multistage testing, was performed. Samples were subjected to an initial strain rate of 0.16 degrees per minute (0.119

mm per minute) for a displacement of one revolution (267.0 mm) to create a shear surface on the samples at the 100 kPa normal stress. The strain rate was then slowed to 0.048 degrees per minute (0.036 mm per minute) to obtain the residual shear strengths for normal stresses of 100 kPa, 200 kPa, and 400 kPa.

Scanning Electron Microscope

Freeze-dried samples were analyzed in a Hitachi S-2460N VP scanning electron microscope (SEM) with energy-dispersive spectrographic (EDS) and digital imaging capability. Micrographs were gathered from the SEM using two types of signal sources: backscattered electrons (BSE) and secondary electrons (SE). The BSE signal source used a low vacuum with a working distance of 25 millimeters to gather micrographs at lower magnifications and obtain elemental data with the EDS function. The SE signal source was used to produce higher- magnification micrographs. Samples were coated with gold to prevent charging on the specimen's surface (Smart and Tovey 1982) and were analyzed at a working distance of 12 mm using a high vacuum to maximize the resolution.

Digital elemental maps from EDS were produced to describe the elemental content of the particles in the freeze-dried samples. These data are largely qualitative with lighter colored images showing a higher content of the respective elements in those particles. Mineral contents were inferred from coincident scatter of multiple elemental maps and x-ray diffraction (XRD) results. The numbers in the upper left corner of the elemental maps were used as a semi-quantitative comparison of the elements. The number represents the brightest energy distribution sent off by the respective x-ray photon.

RESULTS

Geotechnical Tests, pH, and CEC

Standard engineering properties were determined on the samples. Table 11 shows the index properties for the shale over the range of depth from 18 to 34 meters. A large increase in the coarse fraction was observed in the transitional zone. The weathered material shows high amount of fines in comparison to the other zones as well. The unweathered material exhibited higher amounts of clay materials than much of the transitional zone as well. The silt fraction stayed relatively uniform over the weathering profile. The lowest fine fractions were observed at depths with high amounts of sand particles in the transitional zone. Tables 12 and 13 show the pH and the estimated cation exchange capacity (CEC). The material became acidic in the transitional zone and was nearly neutral in the upper portion of the weathered zone and all of the unweathered zone. The Na-ion concentration in Table 13 increased two-fold in the unweathered zone. The K-ion also showed higher concentrations in the unweathered zone. The Mg-ion indicated higher contents in the weathered material. The calcium concentrations were high over all of the zones and controlled the CEC of the weathering profile.

Ring Shear

Samples from each of the three weathering zones were tested in the ring-shear apparatus to determine residual strength parameters. The tests on the samples from each weathering zone were conducted with the normal stress increased in steps from 100, to 200, to 400 kPa. Figure 29a and 29b show typical results from a multistage test and its failure envelope, respectively. The data from each sample were analyzed using a spreadsheet

program for both the trend line through the origin and with a cohesion intercept. The residual friction angle (ϕ_r'), residual cohesion (c_r'), and correlation coefficients are summarized in Table 14. Many of the residual cohesions values were found to be negative and rounded to zero.

Table 11. Weathering profile engineering properties, Oahe Dam, Station 50+00

Depth M	Liquid Limit %	Plastic Limit %	Plastic Index %	>0.074 Mm	0.074-0.002 mm	<0.002 mm
17.9	76.4	46.6	29.8	7.8	42.2	50.0
18.5	66.2	41.6	24.6	4.2	49.8	46.0
19.1	75.0	45.7	29.3	2.2	65.8	32.0
21.7	76.3	43.6	32.7	1.5	48.5	50.0
22.7	71.1	41.2	29.9	5.9	43.1	51.0
23.3	66.7	41.1	25.6	25.5	62.5	12.0
23.9	71.4	41.5	29.9	30.9	53.1	16.0
24.8	82.0	46.0	36.0	23.1	56.9	20.0
25.8	68.2	44.2	23.2	9.3	75.7	15.0
26.4	61.5	40.0	21.5	9.3	74.7	16.0
27.0	63.8	41.5	22.3	2.0	62.0	36.0
28.8	88.2	42.4	45.8	4.7	67.3	28.0
31.8	71.2	43.5	27.7	5.1	67.9	27.0
33.9	74.2	46.6	27.6	3.0	75.0	22.0

Table 12. Weathering profile pH, Oahe Dam, Station 50+00

Sample depth m	pH
17.9	6.92
18.5	6.65
19.1	6.73
19.7	6.97
21.2	5.83
22.7	5.78
23.3	3.80
23.9	6.77
25.8	5.88
28.8	6.73
31.8	6.64
34.2	6.49

Table 13. Weathering profile CEC values, Oahe Dam, Station 50+00

Sample depth m	K cmole kg^{-1}	Ca cmole kg^{-1}	Mg cmole kg^{-1}	Na cmole kg^{-1}	Estimated CEC cmole kg^{-1}
18.3	1.5	44.6	10.2	8.3	64
19.1	1.3	33.5	9.3	8.9	53
22.7	1.0	24.4	9.5	9.2	44
23.9	1.5	31.3	7.2	8.1	48
27.3	0.8	66.6	7.6	13.4	88
31.8	3.1	19.4	4.3	20.2	47
33.9	2.5	13.4	4.8	18.5	39

SEM Images

Figure 30a and b shows SEM images of freeze-dried unweathered Pierre Shale at a magnification of 500X and 1500X, respectively. A fracture of the sample resulting from the freeze-dried process is apparent in the images. The 500X image of the unweathered sample shows a densely packed material with significant laminae vertically oriented in the image. A precipitate occurs throughout the sample, as shown by the bright particles scattered over the image. Particle shape is primary platy, except for some sub-rounded to sub-angular particles. The numbers on Figure 30b indicate locations where EDS analyses were conducted. EDS results are not included due to space limitations, but are reported in Appendix D (Birchmier 2005).

Figure 31a and b show SEM images of weathered Pierre Shale at magnifications of 500X and 1500X, respectively. The weathered sample has a massive-laminae fabric with the massive fabric dominating, shown by the dashed lines in Figure 31a and b. Laminae from the parent sedimentary rock occur intermittingly within the massive fabric. The massive fabric observed at the lower magnification in Figure 31a is more apparent in Figure 31b. The open fabric in Figure 30b has many sub-rounded particles. The sub-rounded shape of the massive minerals could be a source of strength reduction as well.

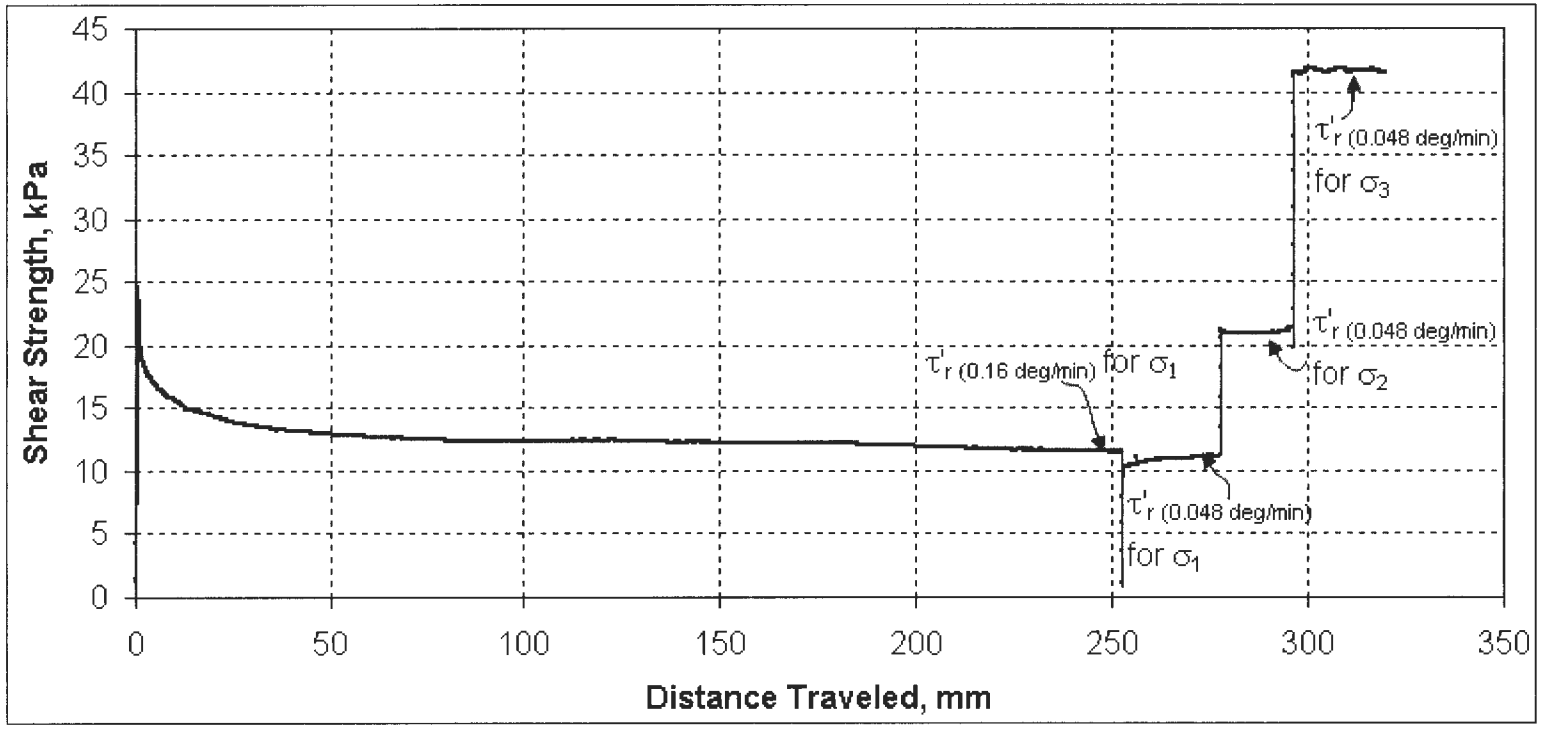

(a)

Figure 29. Multistage ring-shear results, a) residual strength plot, σ_1=100 kPa, σ_2=200 kPa, σ_3=400 kPa

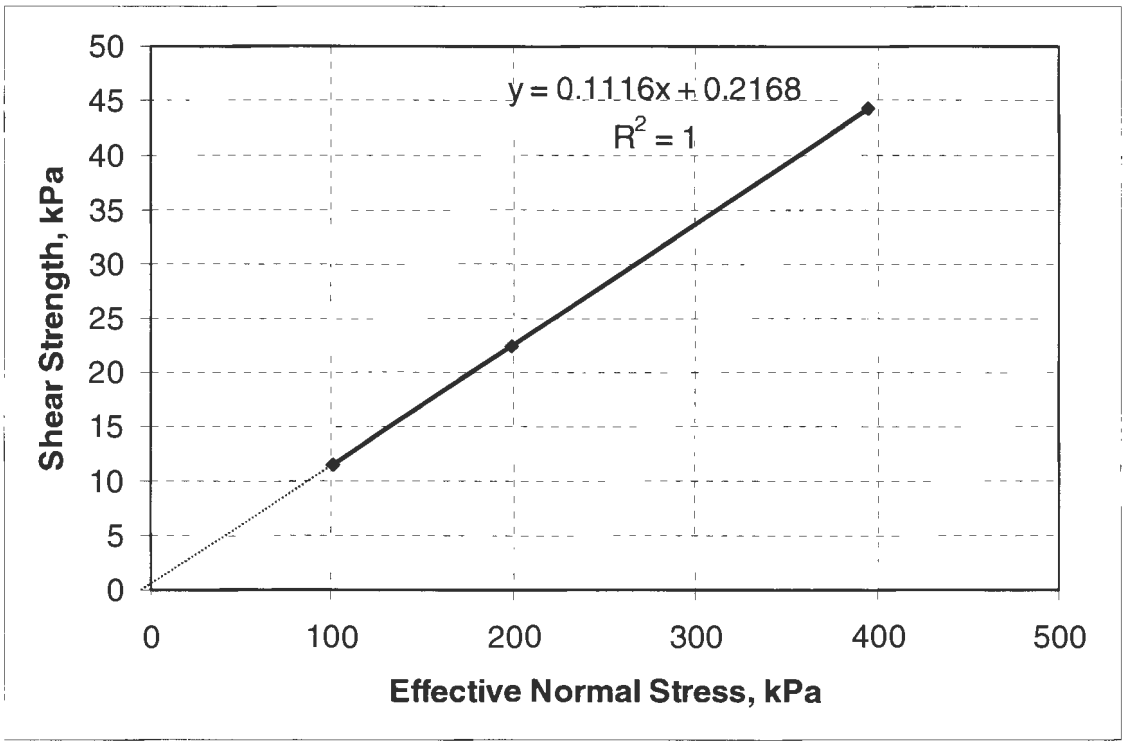

(b)

Figure 29. con't. Multistage ring-shear results, b) residual failure envelope

Table 14. Weathering profile residual strength parameters, Oahe Dam, Station 50+00

Depth, m	Weathering Zone	ϕ_r', degrees	c', kPa	r^2
17.9	Weathered	5.8	1.0	1.0
18.5		9.0	~0	1.0
19.1		6.8	~0	1.0
19.7		5.8	0.1	1.0
21.2		6.2	~0	1.0
21.8	Transitional	8.5	~0	1.0
22.7		11.1	~0	1.0
23.9		11.3	~0	1.0
25.8		8.7	~0	1.0
27.0	Unweathered	7.3	0.4	1.0
28.8		7.0	~0	1.0
31.8		7.3	~0	1.0
34.2		6.7	~0	1.0

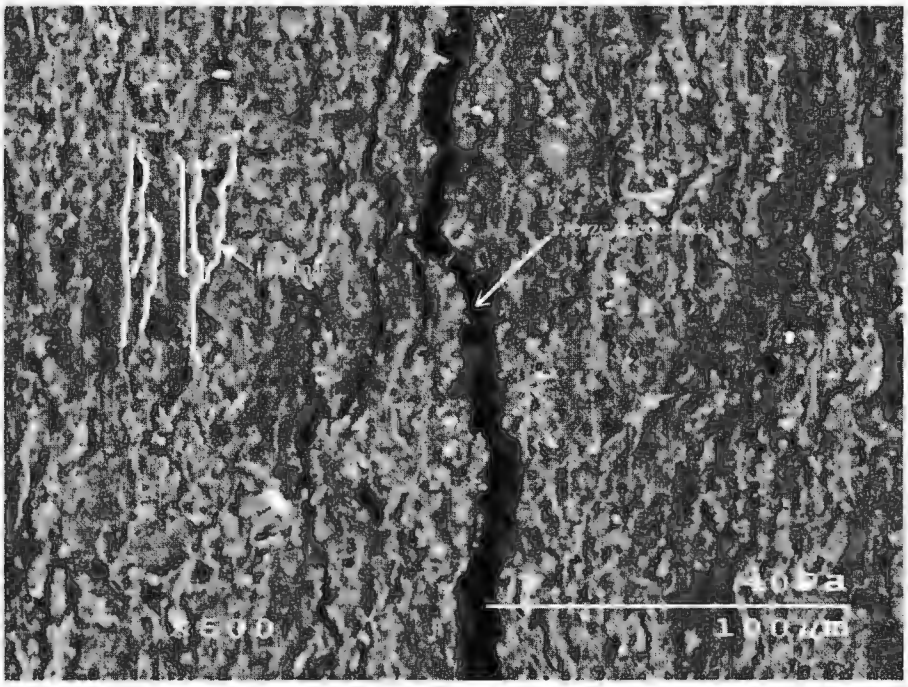

(a)

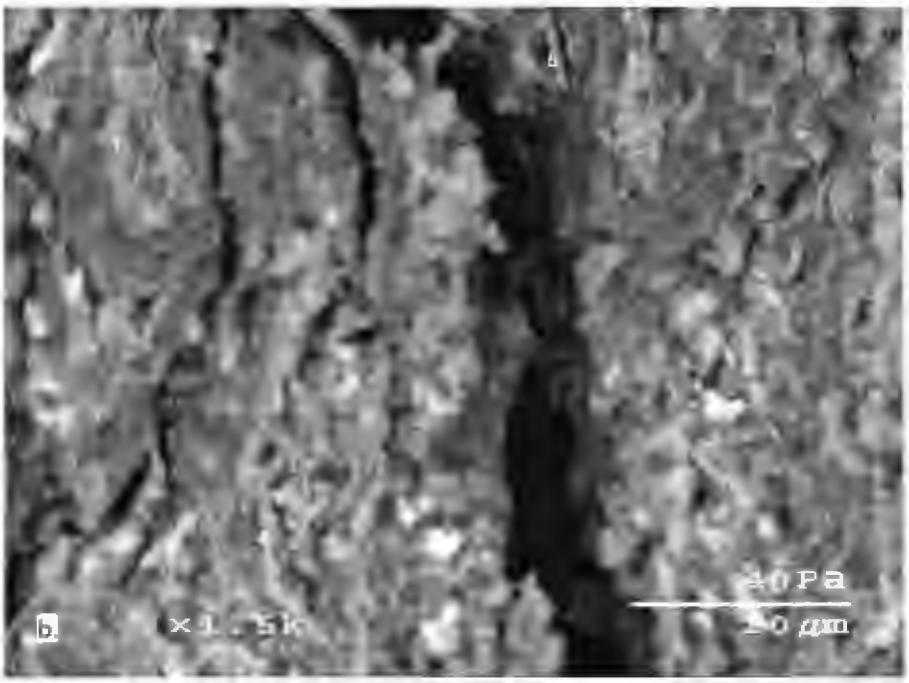

(b)

Figure 30. Oahe Dam, Station 50+00, 31.2 m, unweathered Pierre Shale micrographs, a) 500X magnification, b) 1500X magnification

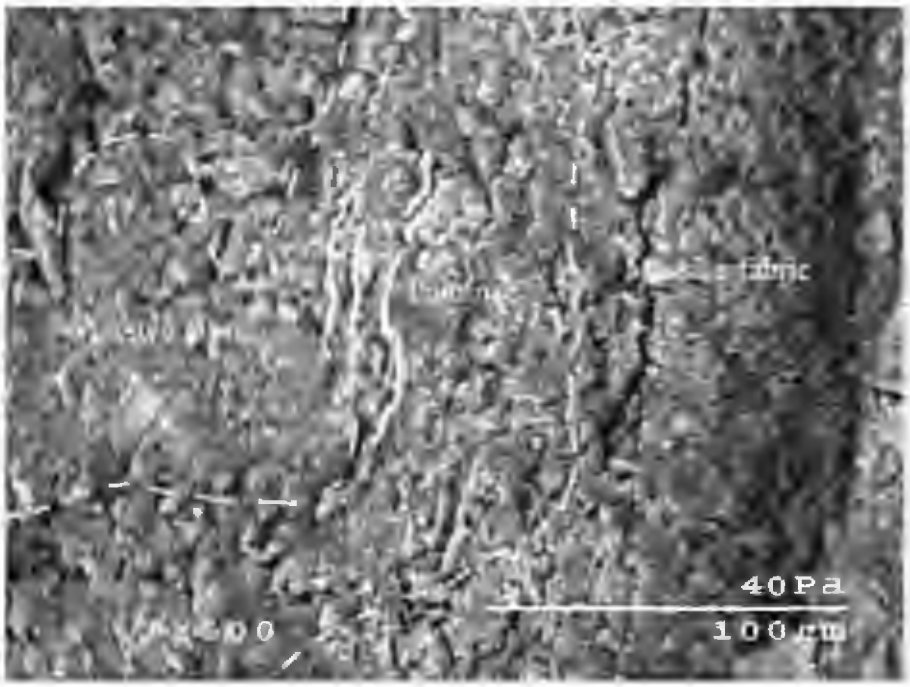

(a)

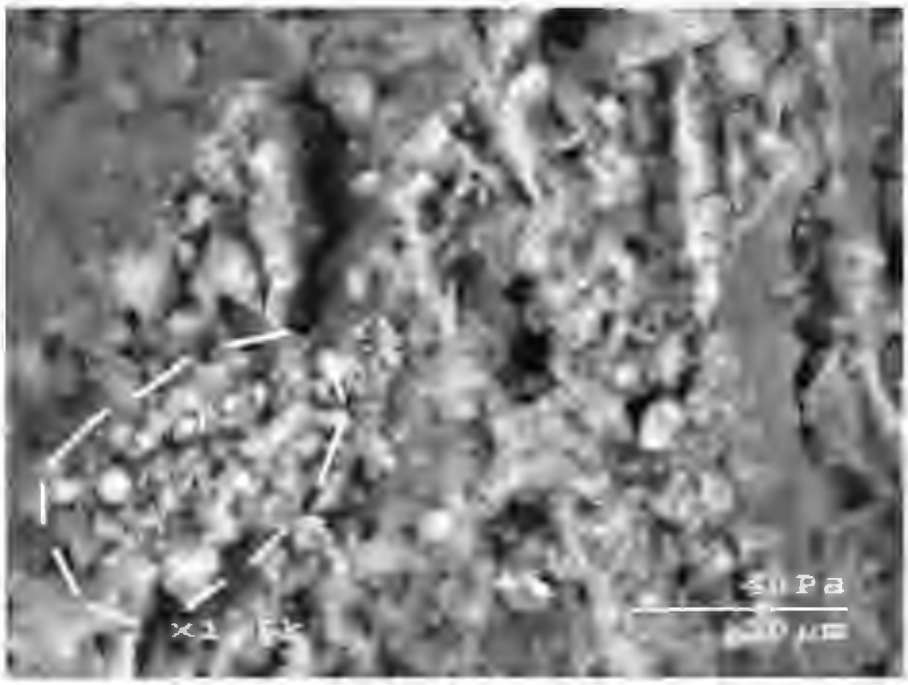

(b)

Figure 31. Oahe Dam, Station 50+00, 18.5 m, weathered Pierre Shale micrographs, a) 500X magnification, b) 1500X magnification

Mineral and Chemical Contents of Bulk Samples

XRD analyses of weathered, transitional, and unweathered whole Pierre Shale characterized mineral contents from the three zones. Quartz, montmorillonite and illite are present in weathered, transitional, and unweathered Pierre Shale. Gypsum was found in the weathered and transitional materials. Pyrite was not found in the diffractograms of the unweathered materials. Figures 32, 33, and 34 show the contrast in the weathered, transitional and unweathered zone's diffractograms. Hematite (Fe_2O_3) or goethite (FeO(OH)) may also exist in the transitional zone, shown by the d-spacings given in Figure 33.

The XRF analyses of the whole samples also showed little difference in the chemical compositions of the three weathered zones as shown in Table 15. The XRF concentrations are expressed on a loss-of-ignition (LOI) (carbonate-free) basis. These results are consistent with previous studies that found no major differences in the mineralogy or chemical composition of whole samples of weathered and unweathered Pierre shale (Schultz *et al.* 1980). Minor increases in the sodium contents were observed in the unweathered material. Manganese contents were high over the 18 to 34 meter depth but were especially high in the transitional zone. Iron, sulfur, calcium and potassium contents also peaked in the transitional zone.

Chemical Composition of Sand and Clay Fractions

The chemical composition of the sand- and clay-fractions from the three weathering zones was determined from EDS elemental maps. Mineralogy was inferred from the

elemental maps from coinciding elements. Some elemental maps are discussed but not included due to space limitations.

The elemental map of the sand fraction of the weathered sample (Figure 35) shows that calcium and sulfur occurred in the same particles, indicating that gypsum is a significant portion of the weathered sand fraction. Manganese was in concentrated aggregates, suggesting manganese nodules. Clay minerals, carbonates, and oxides in weathered material are sources of manganese. Silicon and oxygen occurred in many of the particles suggesting quartz, cristobalite, or clay minerals. Aluminum in the elemental maps can be primarily linked to clay minerals (Tourtelot 1962).

The elemental map of the sand fraction of the transitional zone (Figure 36) shows that calcium and sulfur coincide, indicating gypsum. Iron and sulfur occur in the same particles suggesting that pyrite is in the sand fraction of the transition material. Iron and barium also have coinciding particles in their elemental maps.

The unweathered sand fraction elemental maps (Figure 37) contain particles with high amounts of iron coincident with sulfur, suggesting pyrite. Calcium, manganese and silicon were observed again in the unweathered zone. Unlike the upper zones, there were no particles containing both calcium and sulfur.

Elemental maps of the clay fractions of Pierre Shale from all the weathering zones have similar amounts of uniformly distributed silicon, oxygen, and aluminum. These elements are associated with the crystalline structure of montmorillonite that exists in all the various stages of weathering. The elemental maps of sodium, potassium, and calcium exhibit variations among the three zones and are discussed in detail below.

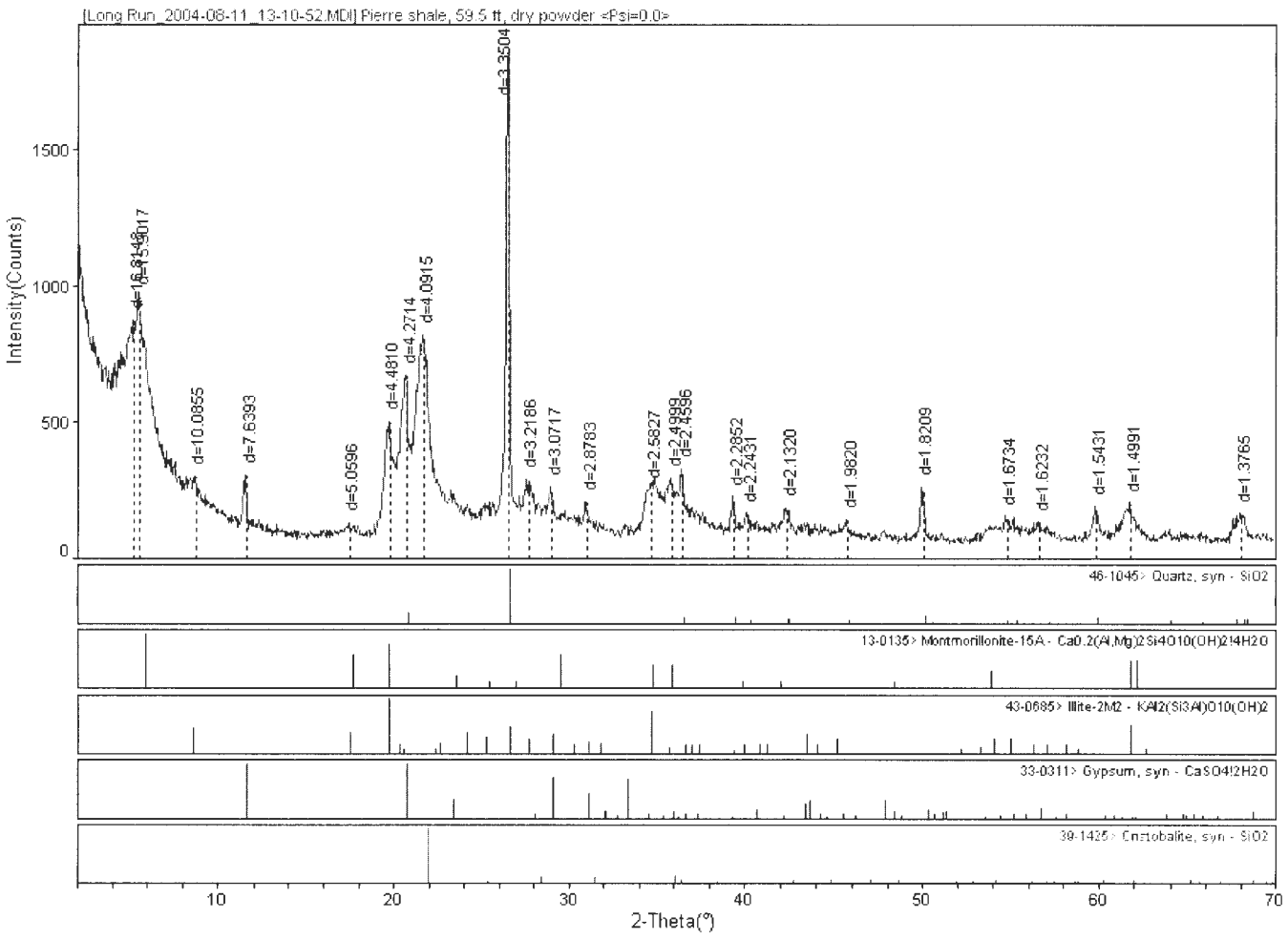

Figure 32. 17.9 m (59 ft), Pierre Shale, Oahe Dam site, PZT50-5.42, smear mount XRD dry powder

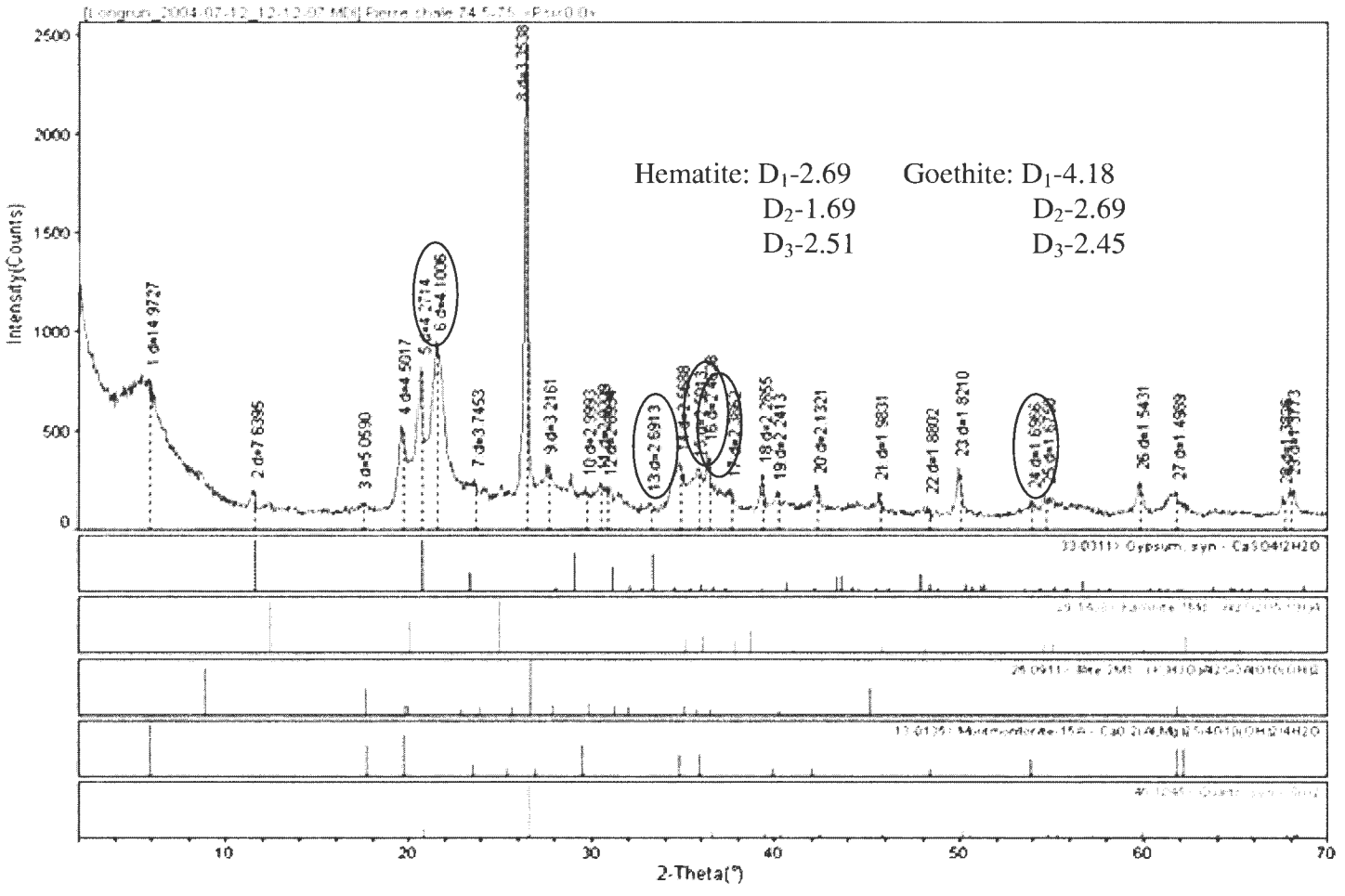

Figure 33. 22.7 m (75 ft), Pierre Shale, Oahe Dam site, PZT50-5.42, smear mount XRD dry powder

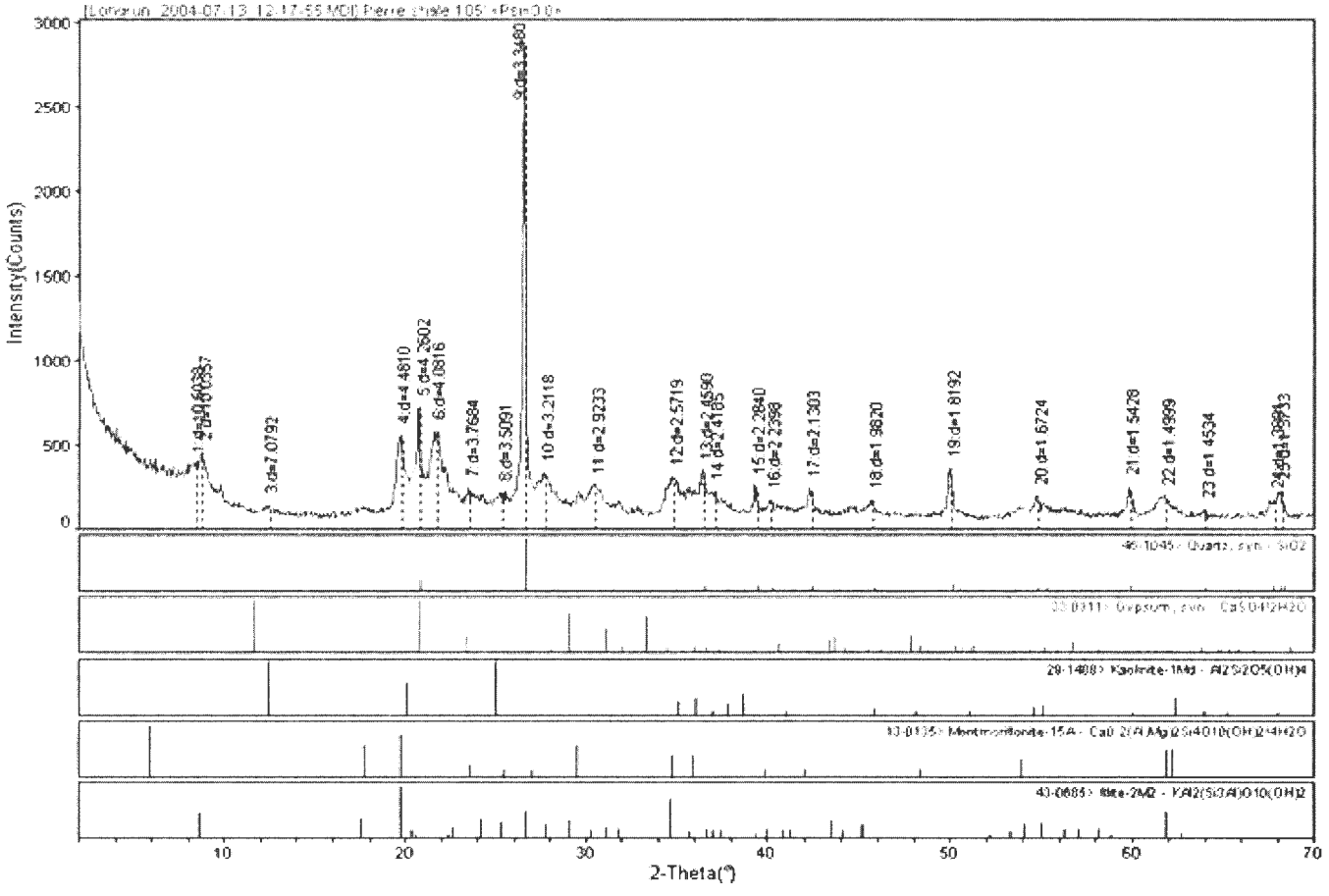

Figure 34. 31.8 m (105 ft), Pierre Shale, Oahe Dam site, PZT50-5.42, random mount XRD dry powder

Table 15. Weathering profile XRF results, whole sample, Oahe Dam, Station 50+00

Depth M	Moisture Content (%)	Loss On Ignition (%)	Sum of conc. (%)	Na_2O (%)	MgO (%)	Al_2O_3 (%)	SiO_2 (%)	P_2O_5 (%)
17.9	1.40	4.80	99.24	0.77	1.81	11.26	72.32	0.16
18.5	1.32	4.37	99.61	0.78	1.82	11.99	73.96	0.12
19.1	1.20	4.17	99.76	0.83	1.90	12.57	74.08	0.27
19.7	1.39	4.49	99.66	0.77	1.86	12.23	72.77	0.12
21.8	1.16	5.45	99.65	0.76	2.28	14.15	66.77	0.17
22.7	1.20	9.35	100.00	0.74	1.91	10.08	64.02	1.12
23.9	1.69	4.28	99.47	1.01	1.62	10.60	75.15	0.15
25.8	1.22	5.97	100.02	0.90	1.82	12.13	72.74	0.15
27.0	1.18	5.50	99.78	1.09	1.95	13.57	72.77	0.13
28.9	1.42	5.87	99.73	1.31	2.17	14.65	69.85	0.15
31.8	1.10	6.11	100.00	1.38	1.82	13.61	69.95	0.22
33.9	1.07	5.75	100.00	1.19	1.67	12.18	72.38	0.16

Depth M	SO_3 (%)	K_2O (%)	CaO (%)	TiO_2 (%)	Fe_2O_3 (%)	SrO (%)	Mn_2O_3 (%)	BaO (%)
17.9	0.78	1.92	1.78	0.44	4.77	0.02	3.19	0.04
18.5	1.09	1.95	1.74	0.46	4.79	0.02	0.89	0.04
19.1	0.19	2.07	1.16	0.48	4.97	0.02	1.18	0.03
19.7	1.11	1.97	1.87	0.46	5.24	0.02	1.16	0.08
21.8	1.03	1.86	2.45	0.45	5.38	0.02	4.29	0.03
22.7	1.28	1.70	4.13	0.40	9.32	0.02	5.27	0.02
23.9	0.08	1.80	0.84	0.42	4.38	0.02	3.38	0.03
25.8	0.95	2.04	1.74	0.48	4.98	0.02	2.04	0.04
27.0	0.68	2.10	0.86	0.52	5.37	0.02	0.68	0.05
28.9	0.49	2.28	1.38	0.56	5.48	0.02	1.33	0.06
31.8	0.81	2.14	1.73	0.53	5.24	0.02	2.48	0.08
33.9	0.87	1.95	1.64	0.48	4.81	0.02	2.59	0.06

The elemental maps of the clay fraction for the weathered shale are shown in Figure 38. The few particles with sulfur coinciding with calcium are interpreted as to be clay-sized gypsum. Potassium was dispersed throughout, suggesting illite or K-feldspar. Manganese and iron were found in minor amounts but no relationships could be established between the two elements and other elements.

The transitional zone elemental maps, Figure 39, show calcium and sulfur occurring in one particle. Calcium, manganese, and silicon were found in another particle showing high

concentrations. Calcium does not occur in a diffuse pattern. Sodium and potassium appear in disperse patterns. Sodium is thought to be adsorbed on the montmorillonite and the potassium is likely related to the illite.

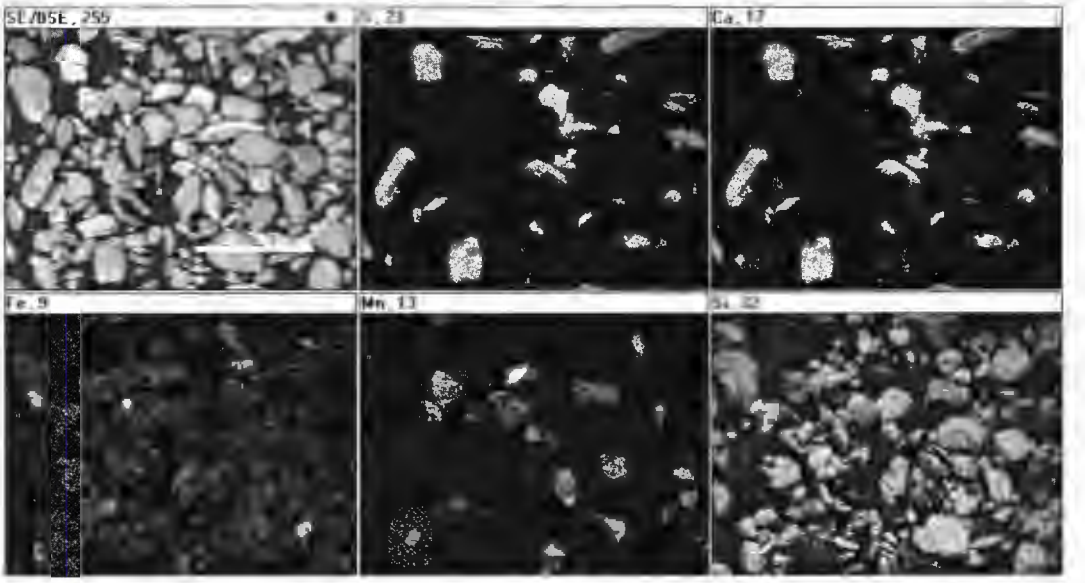

Figure 35. Elemental map of sand fraction for weathered material

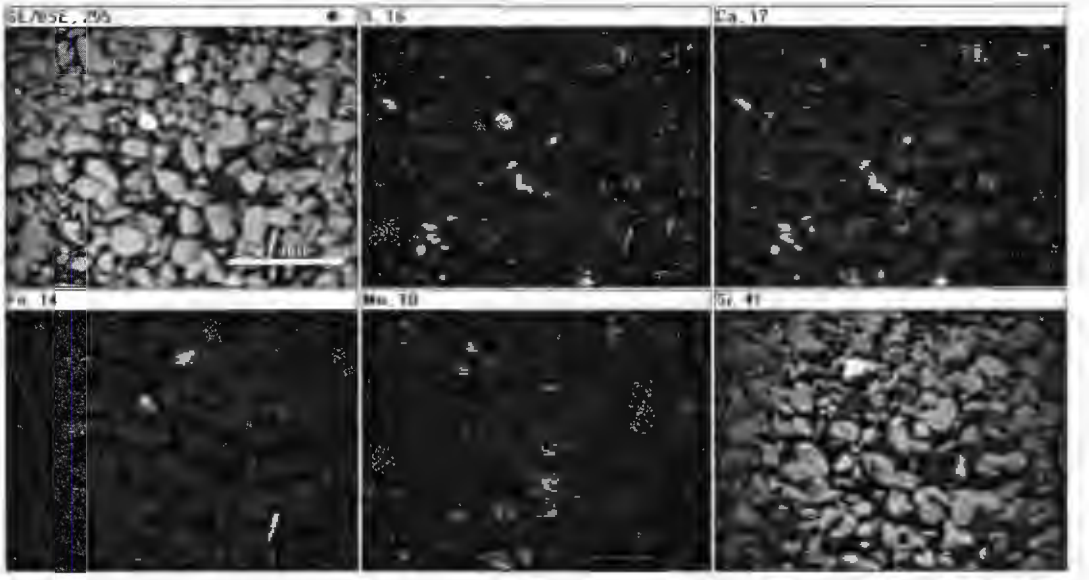

Figure 36. Elemental map of sand fraction for transitional material

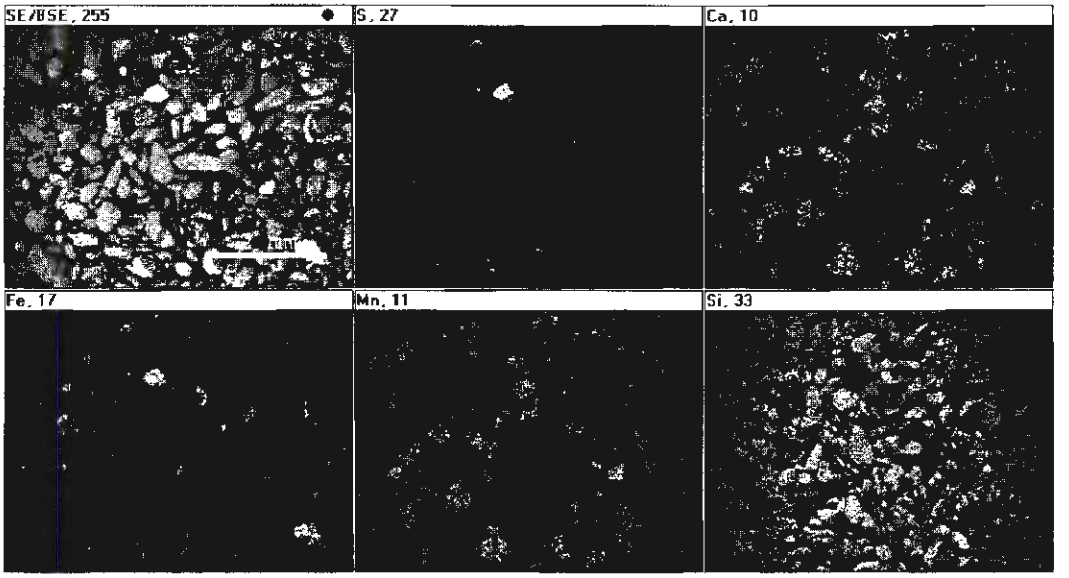

Figure 37. Elemental map of sand fraction for unweathered material

In the unweathered shale, sulfur is not associated with calcium in discrete particles, as Figure 40 shows. Iron and sulfur appear in the same particle and with higher intensities in comparison to the transitional zone. This iron and sulfur combination is thought to be pyrite. Manganese, calcium, and silicon also occur in individual particles in the unweathered zone, but in fewer particles than the transitional zone. The potassium content increased compared to the transitional zone content and was in smaller, more highly concentrated areas in its elemental map. These concentrated areas of potassium indicate illite aggregates. The sodium content did not change from the transition to the unweathered material and was evenly dispersed over the elemental map, suggesting it occurs as adsorbed ions on the montmorillonite.

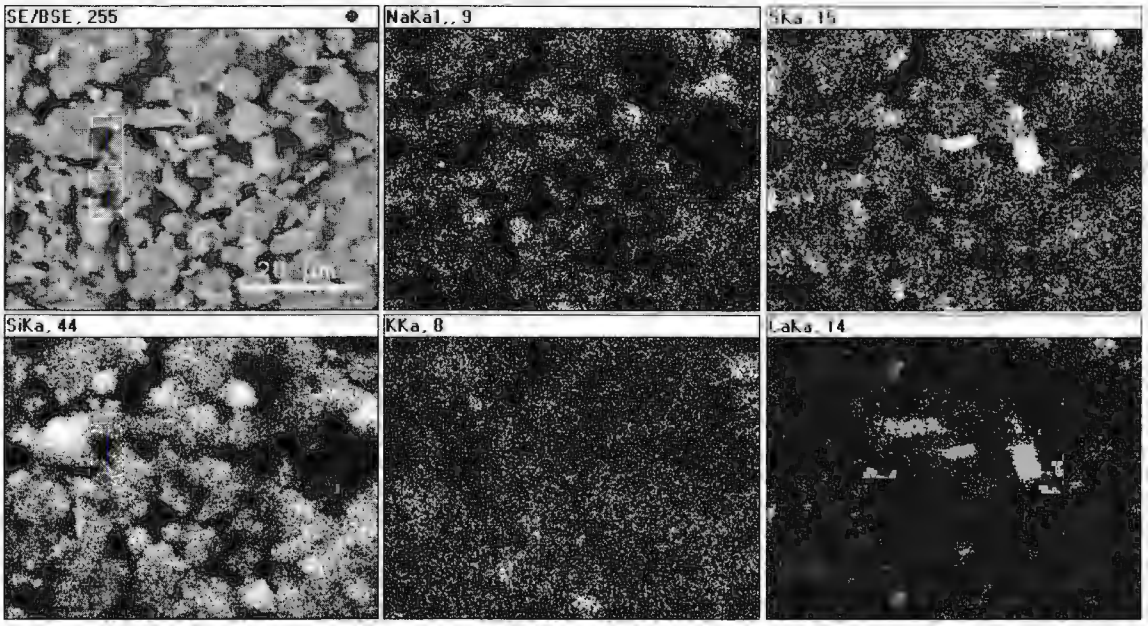

Figure 38. Elemental maps of clay fraction for weathered zone, 21.8 m

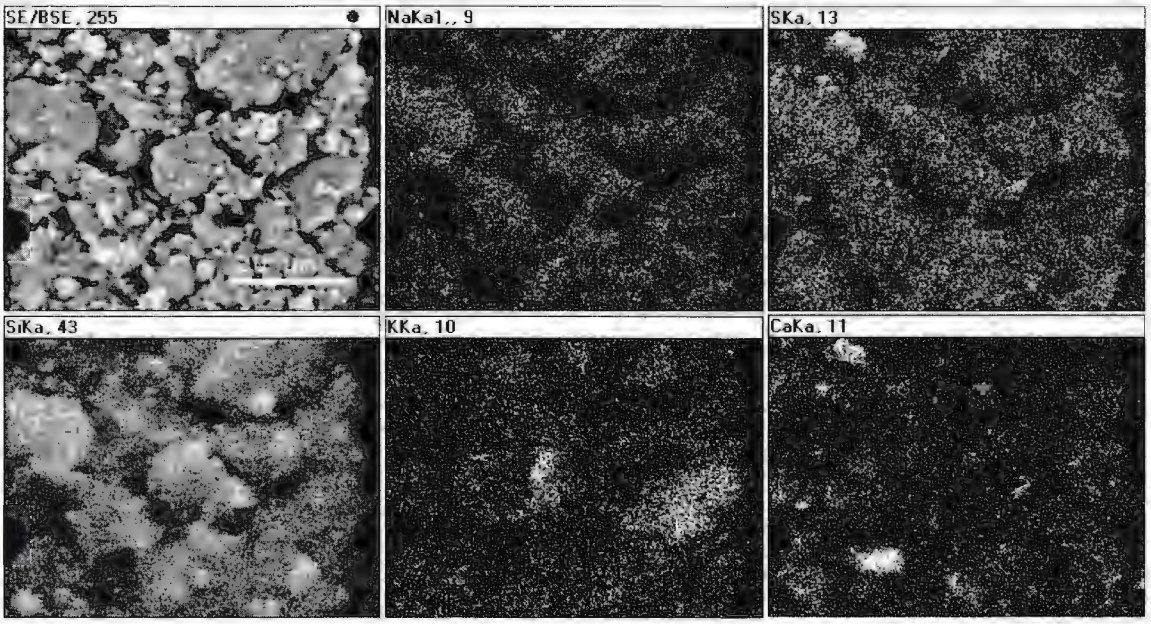

Figure 39. Elemental maps of clay fraction for transitional zone, 23.9 m

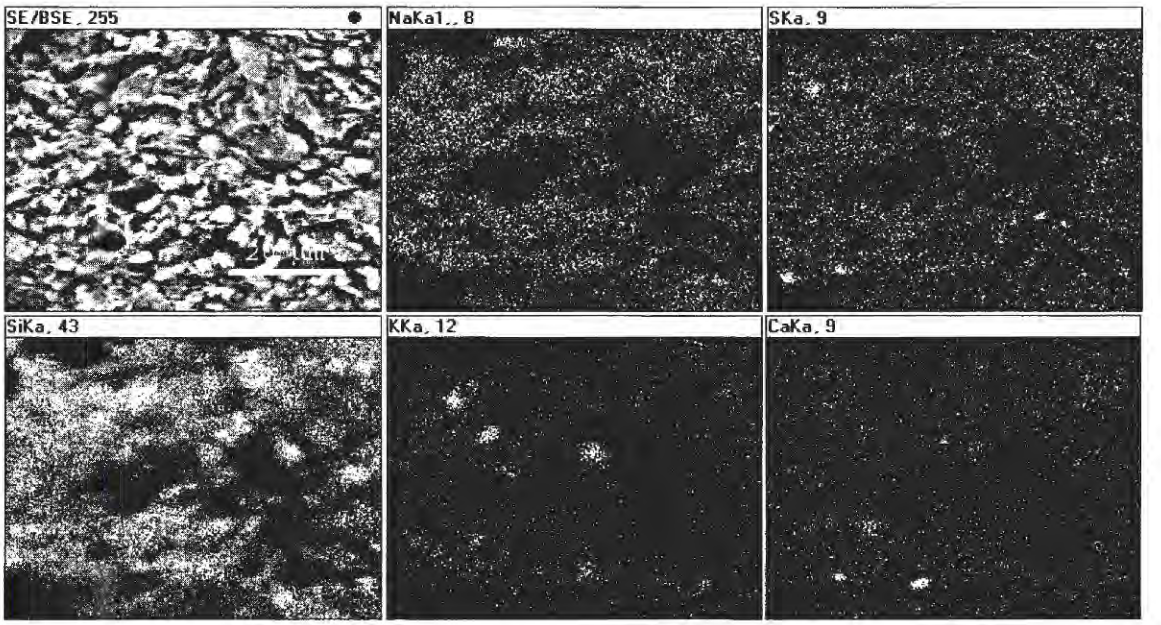

Figure 40. Elemental maps of clay fraction for unweathered zone, 28.5 m

DISCUSSION

Residual friction angles in the weathered zone are between 5.8 and 9 degrees; the residual friction angle increases to 11.3 degrees in the transitional zone; and the residual friction angle decreases to 6.7 to 7.3 in the unweathered zones. The increases in the coarse fraction and the concentration of massive minerals of quartz and cristobalite in the transition zone may be a source for the strength gain. The increase in the coarse fraction causes the particle shape and packing to control the residual strength (Lupini *et al.* 1981). The drop in the residual strength in the weathered zone signifies the strength loss associated with weathering and the montmorillonite mineral.

The pH shows the significance of pyrite oxidation to the weathering zones. Pyrite oxidation can produce insoluble iron oxides such as hematite or goethite and sulfuric acid (Bryant *et al.* 2004). As shown by the XRF results, the iron content increases in the

transition zone and then falls off in the unweathered material to similar values of the weathered material. The observations indicate mineralogical discontinuities may exist in the material. These results suggest the insoluble iron oxides accumulated in the transitional zone. Higher amounts of ferric oxides could also be indicative of the high coarse fractions found in the transition zone. Acidic conditions followed the weathered boundary in the transitional material and returned to almost basic conditions in the weathering zone due to the lack of any strong acids or bases such as the sulfuric acid (Tourtelot 1962). Acidic conditions occur when the acidity from pyrite oxidation exceeds the buffer potential of calcite, chlorite, and Na smectite in the material (Shultz *et al.* 1980). The weathering has caused much of the acidic and basic materials to be leached out of the weathered zone. The oxidation front appears to stop below 25.8 m, as interpreted from the pH values. These findings are consistent with the initial geologic and visual/optical interpretations.

The formation of gypsum in the weathering zone from sulfuric acid formed during the oxidation of pyrite and available calcium ions is also in agreement with the observed mineralogy and chemistry. Russell and Parker (1979) highlighted the importance of pyrite oxidation and the subsequent gypsum formation in overconsolidated clays. Gypsum has been shown to cause substantial amounts of heave which would result in further softening (Bryant *et al.* 2003). Chigira and Oyama (1999) observed a similar pH weathering profile in mudstones with pyrite. The weathering profile was described by three zones: an oxidized zone, a dissolved/transitional zone and firm mudstone. Pyrite was determined to be the cause of the rapid weathering associated with the material. The problems associated with pyrite oxidation range from heave and swell pressure to corrosion and acidic conditions (Bryant *et al.* 2003).

The exchangeable cation values in Table 12 correlated well with the weathering zones. Exchangeable sodium and calcium have higher concentrations near the unweathered zone. Sodium from the original deposition in the marine environment was likely leached out and replaced by the higher valence and larger polarity elements of Ca^{2+} and Mg^{2+} during weathering. The low Na^{+} concentrations at the depth of 23.9 m support the acidic conditions (Tourtelot 1962).

These results show the relevance of exchangeable cation analyses with respect to the mechanical behavior of the material. Decreases in the adsorbed cation concentration on the clay mineral causes the diffuse double layer (DDL) to expand, leading to a decrease in the residual strength. The type of cation adsorbed on the clay mineral is also important due the cation's valence and polarizability effect on the DDL (Kenney 1967).

Comparing the pairs of images in Figures 30 and 31 of the bulk micromorphology and the elemental maps of the clay fraction in Figures 38, 39, and 40 shows the contrast between the weathering zones. The particles of the bulk material appear more sub-rounded to sub-angular in the weathering micrographs, an indicator of weathering alterations. The micrographs of the clay fractions for the various weathering zones exhibit a similar morphology to the bulk material. The unweathered clay particles are sharper and better defined in comparison to sub-rounded to sub-angular clay particles in the weathering material. Higher magnifications show the weathering effects on the individual particles and particle contacts of the bulk material. Laminae were more distinct in the unweathered material. The unweathered shale has a greater amount of contact area between the particles in comparison to the weathered shale, showing the rock-like bonding associated with clay shales (Underwood 1967). The platy fabric observed in the unweathered micrograph (Figure

30) has deformed and softened into an overall massive structure in the weathered material (Figure 31). The orientation and bonding provides much of the material's strength. The micrographs of the unweathered indicate that peak strength may be more relevant to the field behavior of the unweathered shale than the residual strength as the material's bonding provides much of the strength. As the material fractures, softens and expands, these bonds are broken and the material loses much of its strength.

XRD and XRF results verify observations of earlier studies that differences in gross mineralogy and geochemistry are minor between the various weathering zones. Na concentrations were observed to decrease in the weathered zone suggesting the original sodium from the depositional marine environment of the shale had been leached. The effect of the weathering of pyrite was apparent throughout the weathering profile, though.

The EDS evidence indicates the presence of gypsum in the weathered material and pyrite in the unweathered material. Both of these minerals occur primarily in the sand fraction of the Pierre Shale. The EDS results of the clay fraction showed a less dramatic iron and sulfur occurrence due to pyrite's size. The concentration of the minerals in the sand fractions explains why the variations in these two minerals between the weathering zones are not so obvious in the diffraction patterns of the whole rock. These results are significant due to the rapid and problematic oxidation reaction associated with pyrite.

The EDS ion maps of the separate clay fractions also provide useful information regarding the variations in adsorbed cations on the montmorillonite mineral in weathered, transitional, and unweathered Pierre Shale. Potassium occurs in discrete particles in the unweathered material and is diffuse in the weathered material. The results suggest potassium

is related to the illite concentration in the weathered material. The EDS results suggest that sodium montmorillonite in the unweathered material.

The combination of these results show the unweathered material mechanically behaves similar to a rock. The high montmorillonite in the unweathered material causes the residual strength to be low, but the residual strength does not control the strength in this material unless a shear surface exists. The residual strength is more applicable when weathering degrades the microfabric due to strain softening, causing the material to become more homogenous as observed in the weathered micrographs. A progressive failure may occur as the material softens, causing the particles to orient in the direction of shearing and the strength dropping to the residual strength.

Multiple linear regression analyses of residual friction angle to various parameters were performed on the data sets included in this study using *SPSS 9.0* (SPSS 1999). The Pearson correlations are shown in Table 16, where the higher the absolute value, the better the correlation. The Pearson correlation coefficient measures the linear relationship between two variables. Negative correlation to the residual friction angle indicates an inverse effect (i.e. increases in liquid limit decreases the residual friction angle). Multiple linear regression equations are also shown in Table 16. Regression one and three consisted of twelve and six data sets, respectively, with the liquid limit, plastic limit, coarse fraction, and residual friction angle as parameters; regression two and four consisted of twelve and six data sets, respectively, with the liquid limit, plastic limit, fine fraction, and residual friction angle as parameters; regression five consisted of six data sets with the K ion, Ca ion, Mg ion, Na ion, and residual friction angle as parameters; and regression six consisted of six data sets with all of the parameters shown in Table 16. The number of data sets was decreased to six to

include the chemistry parameters. Both regression one and three showed a positive correlation between the coarse fraction and residual friction angle. Regression two showed a negative correlation between the clay fraction and residual friction angle. Regression four's correlation between the clay fraction and residual friction angle is negligible. Liquid limits and plastic limits consistently showed negative correlations with the residual friction angle for regressions one through four. Negative correlations were observed for potassium and sodium ions and positive correlations were observed for calcium and magnesium ions with the residual friction angle for regression five.

The coarse and clay fraction in regressions one and three have similar absolute correlations. The negative correlation of the clay fraction implies the sliding mode during shearing while the positive correlation of the coarse fraction implies the turbulent mode during shearing. These findings suggest the materials are shearing in a transitional mode in which both turbulent and sliding behaviors occur during shearing. Residual friction angle correlations with the liquid limit and the plastic limit were shown to be negative, in agreement with past studies. The negative correlation of the sodium cation and the positive correlation of the calcium cation on the residual friction angle is in agreement with Steward and Cripps (1983) and Moore (1991). The potassium ion's negative correlation to the residual friction angle may indicate the effect of the illite concentration.

CONCLUSIONS

The mineralogy and geochemistry of the unweathered and weathered shale is similar. The main differences are the sand fraction occurrences of gypsum in the weathered and pyrite in the unweathered material. The transition zone showed differences in the chemistry,

with higher amounts of manganese, iron, and calcium. Potassium decreased in the transition zone as well. The high concentrations of manganese and iron in the transitional material (from XRF of the bulk sample and EDS analyses of the sand fraction) suggest the presence of iron and manganese oxides. The high residual friction angles in the transitional zone were attributed to the coarse fraction. Much of the weathering disturbances were attributed to pyrite. The rapid oxidation of pyrite caused the formation of sulfuric acid and the subsequent formation of gypsum in the weathered material. The gypsum formation then compounds the softening mechanisms during weathering with its own expansive pressures.

Table 16. Multiple linear regression

	Simple Correlation Coefficients					
	Regression 1	Regression 2	Regression 3	Regression 4	Regression 5	Regression 6
Liquid limit (LL), %	-0.446	-0.446	-0.512	-0.512	-	-0.512
Plastic limit (PL), %	-0.473	-0.473	-0.800	-0.800	-	-0.800
Plastic index (PI), %	-	-	-	-	-	0.139
> 0.074 mm (SA)	0.677	-	0.871	-	-	0.871
0.074-0.002 mm (SI)	-	-	-	-	-	-0.685
<0.002 mm (CL)	-	-0.533	-	-0.087	-	-0.087
pH (pH)	-	-	-	-	-	0.081
K ion (K), cmole/kg	-	-	-	-	-0.424	-0.424
Ca ion (Ca), cmole/kg	-	-	-	-	0.468	0.468
Mg ion (Mg), cmole/kg	-	-	-	-	0.295	0.295
Na ion (Na), cmole/kg	-	-	-	-	-0.595	-0.595
Estimated CEC (CEC)	-	-	-	-	-	0.259
Number of data sets	12	12	6	6	6	6

$\phi_r' = f(...)$

Regression 1	$\phi_r' = -7.8(10^{-2})LL - 0.14PL + 0.134SA + 18.69$, $r^2 = 0.621$
Regression 2	$\phi_r' = -5.6(10^{-2})LL - 0.27PL - 6.0(10^{-2})CL + 25.72$, $r^2 = 0.506$
Regression 3	$\phi_r' = -0.14LL - 0.19PL + 0.11SA + 25.34$, $r^2 = 0.971$
Regression 4	$\phi_r' = 9.1(10^{-4})LL - 0.74PL - 6.5(10^{-2})CL + 42.54$, $r^2 = 0.871$
Regression 5	$\phi_r' = 19.53K - 0.69Ca + 2.39Mg - 2.96Na + 10.02$, $r^2 = 0.808$
Regression 6	$\phi_r' = -0.252PL - 0.251PI + 0.119SA - 0.492K - 1.4(10^{-2})CEC$, $r^2 = 1$

A distinct difference in micromorphology of the weathered and unweathered materials was observed. The material softens from a rock-state into a soil-state during weathering, indicating the engineering problems associated with the material. The contrast in the micromorphology of the weathered and unweathered shale materials provides evidence of the changes that occur from peak strength to residual strength as weathering occurs.

The combination of these results shows the usefulness of the various techniques and how they complement each other. Size fractionation is concluded to be the best method in determining the mineralogy and chemistry of the material. Each technique can then focus on major and minor constituents of the size fractions which may have been overlooked in the bulk sample. EDS provides the fastest data acquisition of the techniques used. Semi-quantitative results can be obtained through elemental maps, point elemental analyses, and line scans of a surface's chemistry. The analysis also provides an image of the surface under investigation.

ACKNOWLEDGEMENTS

The authors thank the engineers of the U.S. Army Corps of Engineers Project Office in Pierre, SD for their help in obtaining the samples of Pierre Shale and for access to information regarding the Oahe Dam, in particular, Mr. LeeJay Templeton. Ashley Schwaller, undergraduate student at Iowa State University, is thanked for running the XRD tests. Drs. Scott Schlorholtz and Warren Straszheim of ISU provided valuable assistance in the conduct of the analytical work. This material is based on work supported by the National Science Foundation under Grant Nos. CMS-0201482 and CMS-0227874. This support is gratefully acknowledged. Any opinions, findings and conclusions or recommendations

expressed in this material are those of the authors and do not necessarily reflect the views of the National Science Foundation.

REFERENCES

Amonette, J.E. and Sanders, R.W. (1994). "Nondestructive techniques for bulk elemental analysis," *Quantitative Methods in Soil Mineralogy*, SSSA Miscellaneous Publication, Madison, Wisconsin.

ASTM. (2003). *Annual Book of ASTM Standards, Section 4, Construction*, Vol. 04.09, American Society for Testing and Materials, Philadelphia, PA.

Bromhead, E. N. (1979). "A simple ring shear apparatus," *Ground Engineering*, 12(5), 40-44.

Bjerrum, L. (1967). "Progressive failure in slopes of overconsolidated plastic clays and clay shales," *Journal of the Soil Mechanics and Foundations Division,* American Society of Civil Engineers, 93(SM5), 1-49.

Brooker, E. W. and Peck, R. B. (1993). "Rational design treatment of slides in overconsolidated clays and clay shales," *Canadian Geotechnical Journal*, 30, 526-544.

Bryant, L., Mauldon, M. and Mitchell, J.K. (2003). "Impact of Pyrite on Properties and Behavior of Soil and Rock," *12th Panamerican Conference on Soil Mechanics and Geotechnical Engineering*, 1, 759-756.

Chigira, M., Wang, W.N., Furuya, T., Kamai, T. (2003). "Geological causes and geomorphological precursors of the Tsaoling landslide triggered by the 1999 Chi-Chi earthquake, Taiwan," *Engineering Geology*, 68, 259-273.

Di Maio, C. and Fenilli, G.B. (1994). "Residual strength of kaolin and bentonite: the influence of their constituent pore fluid," *Géotechnique*, 44(4), 217-226.

Fleming, R.W., Spencer, G.S., and Banks, D.C. (1970). *Empirical Study of Behavior of Clay Shale Slopes*, Vol. 1, NCG Technical Report No. 15, U.S. Army Engineer Nuclear Cratering Group, Livermore, CA, December.

Haefeli, R. (1938). "Mechanische Eigenschaften von Lockergesteinen," *Schweiz. Bauztg*, 111, 299-303 and 321-325.

Hughes, R.E., Moore, D.M., and Glass, H.D. (1980). "Qualitative and quantitative analysis of clay minerals in soils," *Quantitative Methods in Soil Mineralogy*, SSSA Miscellaneous Publication, Madison, Wisconsin.

Hvorslev, M. J. (1939). "Torsion Shear Tests and Their Places in the Determination of the Shearing Resistance of Soils," *Proceedings of the American Society for Testing Materials*, 39, 999-1022.

The International Centre for Diffraction Data®. (2004). *Joint Committee on Powder Diffraction Standards (JCPDS) Powder Diffraction File system.*

Johns, E.A., Burnett, R.G. and Craig, C.I. (1963). "Oahe Dam: Influence of shale on Oahe power structures design," *Journal Soil Mechanics and Foundation Division, ASCE*, 89, 95-113.

Kenney, T. C. (1967). "The influence of mineralogical composition on the residual strength of natural soils," *Proceedings of the Geotechnical Conference on Shear Strength of Cohesive Soils*, Oslo, pp. 123-129.

LaMotte Company. (1999). *pHPlus^{Direct} Meter Manual.*

Lupini, JF, Skinner, A.E. and Vaughn, V.R. (1981). "The Drained Residual Strength of Cohesive Soils," *Géotechnique*, 31(2), 181-213.

Mitchell, J.K. (1993). *Fundamentals of Soil Behavior*, 2nd Ed. John Wiley & Sons, New York.

Moore, R. (1991). "The chemical and mineralogic controls upon the residual strength of pure and natural clays," *Géotechnique*, 41(1), 35-47.

Russell, D.J. and Parker, A. (1979). "Geotechnical, mineralogical and chemical interrelationships in weathering profiles of an overconsolidated clay," *Quarterly Journal of Engineering Geology*, 12, 107-116.

Schultz, L.G., Tourtelot, H.A., Gill, J.R., and Boerngen, J.G. (1980). *Composition and Properties of the Pierre Shale and Equivalent Rocks, Northern Great Plains Regions*, Geological Survey Professional Paper 1064-B, United States Government Printing Office, Washington.

Skempton, A.W. (1948). "The rate of softening in stiff-fissured clays, with reference to London Clay," *Proceedings of the Second International Conference on Soil Mechanics and Foundation Engineering,* Rotterdam, 2, 50-53.

Skempton, A.W. (1964). "Long-term stability of clay slopes," *Géotechnique*, 14(2), 77-102.

SPSS Inc. (1999). *SPSS Base 9.0 Application Guide*, Chicago, Illinois.

Steward, H.E. and Cripps, J.C. (1983). "Some engineering implications of chemical weathering of pyritic shale," *Quarterly Journal of Engineering Geology*, 16, 281-289.

Tiedemann, B. (1937). "Über die Schubfestigkeit bindiger Böden," *Bautechnik*, 15, Nos 30 and 33, 400-403 and 433-435.

Townsend, F.C. and Gilbert, P.A. (1976). "Effects of Specimen Type on the Residual Strength of Clays and Clay Shales," *Soil Specimen Preparation for Laboratory Testing, ASTM STP 599*, 43-65.

Tourtelot, H.A. (1962). *Preliminary investigation of the geologic setting and chemical composition of the Pierre Shale, Great Plains region*, U.S. Geological Survey Professional Paper 390.

Underwood, L.B. (1967). "Classification and identification of shales," *Journal of Soil Mechanics and Foundation Engineering Division*, ASCE, 93, 97-116.

Warncke, D. and Brown, J.R. (1998). "Potassium and other basic cations," *Recommended Soil Testing Procedures for the North Central Region*, North Central Research Publication, No. 221 (Revised).

Wykeham Farrance Limited. (2004). "Torsional & simple shear," Wykeham Farrance, <http://www.wfi.co.uk/torsions.htm>, (Accessed March 9, 2005).

CHAPTER 4

MINERALOGICAL AND CHEMICAL MECHANISMS OF STRENGTH LOSS DURING THE WETTING AND DYRING OF PIERRE SHALE

A paper to be submitted to: *Quarterly Journal of Engineering Geology*

V.R. Schaefer[5,7] and M. A. Birchmier[6,7]

ABSTRACT

This study was an investigation into the physico-chemical and morphological role on the residual strength of Pierre Shale during wetting and drying cycles with distilled water. Ring-shear tests were conducted on intact and cycled material to assess the residual strength. The mineralogy and chemistry were determined from x-ray diffraction and x-ray fluorescence results. A scanning electron microscope with energy dispersive spectroscopy capabilities was used for morphological and elemental analyses. Minor mineralogical changes were observed during the cycling process. The material degraded from a firm, dense shale to a massive, gumbo material after three to four cycles. The results suggest the break down of particle size during slaking is the main determinate of the strength loss. The initial mineralogy was also observed to be a factor on the slaking rate and residual strength behavior.

---

[5] James M. Hoover Professor of Geotechnical Engineering, Iowa State University
[6] Graduate Student, Department of Civil, Construction, and Environmental Engineering, Iowa State University
[7] Primary researcher and author

INTRODUCTION

The tendency for clay shales to weather, soften, and slake upon drying and rewetting has been well documented. The degradation causes the material to soften and lose strength, possibly leading to slope failures. Skempton (1964) noted strength losses of up to 80% in some deposits after softening. The slaking rate has been observed to be dependent on the mineralogy and physico-chemical behavior, especially in materials with high activity clay minerals (Perry and Andrews 1984, McClure 1980). While the mineralogy mechanisms are well known, very few studies on clay shales have been conducted to analyze the role of physico-chemical occurrences on the strength loss.

Botts (1986) concluded an engineer must consider both the present strength and its susceptibility to turn into a soil-like material to have a successful design in overconsolidated clay shales. Weathering in overconsolidated clays and clay shales has been observed to be a significant process due to the mode of deposition and the bonding from diagenesis, especially in outcroppings. One of the largest and most problematic clay shales in the United States is the Pierre Shale Formation (Fleming *et al.* 1970). The drop in strength from the peak to residual strength is a source of the stability problems associated with these materials. Initial fissuring results from rebound in clay shales and leads to clay swelling, strain softening and weathering (Brooker and Peck 1993). Much of the past work on residual strength has focused on the mechanical aspects with less emphasis on the role of the more dynamic, physico-chemical effects on residual strength.

This paper reports the results of tests conducted to relate the strength of a series of laboratory wetting and drying cycles on unweathered Pierre Shale to its chemistry,

mineralogy, and micromorphology. The study analyzes the role of the initial mineralogy, breakdown of particle size, and the overall changes in the mineralogy.

BACKGROUND

Since the late 1940s, the geotechnical behavior of overconsolidated soil materials has been studied extensively. Terzaghi and Peck (1948) noted the frequency of small cracks or slickensides in stiff clays, causing a reduction in strength. Skempton (1948, 1964) and Bjerrum (1967) also identified large strain and stress relief as the mechanism behind the drop from peak to residual strength. Associated with the drop in strength was the adsorbed cation on the clay mineral (Kenney 1967).

Bjerrum (1967) highlighted the significance of weathering on the strength of clay shales. Slope stability problems are compounded by outcroppings caused by isostatic rebound or tectonic uplift (Botts 1986). Field studies have observed significant strength loss due to softening as well. The initial structure remolds and becomes a more homogenous, soft, and plastic material during weathering (Manfredini *et al.* 1981). The main mechanisms of softening in clay shales are pore pressure equilibration and weakening of fissures due to slaking or chemical changes (Botts 1986). Bjerrum (1967) and Skempton (1964) identified slaking as a common feature in clay shales. Physico-chemical effects have been shown to be a factor of the slaking rate and mode as well (McClure 1980).

Residual strength controls design parameters in overconsolidated clays and clay shales due to the likelihood of shear planes and slickensides. Physico-chemical effects on the residual strength of clay minerals are apparent when clay contents are greater than ten percent (Moore 1991). Mineralogy, system chemistry, and the volume of clay particles have

been determined to be the main influences of the residual strength for materials with high clay contents (Kenney 1967). Weathering tends to leach out cations, causing a decrease in the concentration and changing the adsorbed cation on the clay mineral (Moore and Brunsden 1996). Lower valency ($K^+=Na^+<Ca^{2+}$) and smaller polarizability ($Na^+<K^+$) of cations decrease the residual strength (Kenney 1967). Moore (1991) observed a 39% higher residual strength for calcium-saturated montmorillonite in comparison to a sodium-saturated montmorillonite. Low cation concentrations lead to a decrease in the residual strength (Stewards and Cripps 1983).

MATERIALS AND SAMPLE PREPARATION

Materials

As described by Bjerrum (1967), the behavior of overconsolidated materials is strongly correlated to their geologic history. Pierre Shale is a heavily overconsolidated clay shale formed from a marine/non-marine environment sedimentation during the Cretaceous Period approximately 60 to 80 million years ago (Fleming *et al.* 1970). The formation extends throughout Canada and as far south as the Gulf of Mexico. Significant slope failures have been observed throughout the formation, but are mainly focused in the upper Missouri and South Saskatchewan River basins (Botts 1986). The mineralogy of Pierre Shale is primary clay minerals, specifically smectite and mixed-layer clays.

Unweathered samples were obtained from a boring at the Oahe Dam site, South Dakota at depths below 60 meters (200 ft). Firm shale, without any weathering, has an average dry density of 1.71 g/cm^3 (107 pcf), a moisture content of 25%, and specific density of 2.7 at the site. Unweathered Pierre Shale at the site exhibits unconfined strengths of 0.5 to 17.4 MPa

(70 to 2530 psi) and a Young's modulus between 137 and 965 MPa (20,000 to 140,000 psi) (Johns *et al.* 1963). The wide variation in strength shows the engineering complications in classifying Pierre Shale as either a rock or soil. Extensive problems were encountered during the construction of the Oahe Dam due to the rapid strength loss in the material (Knight 1963). After many failures, slopes had to be redesigned with ϕ=8.5 degrees and 14.4 kPa (0.15 tsf) for cohesion (Johns *et al.* 1963). Weathering was observed to cause the durable, brittle, rock-like shale to turn into a weathered, soil-like material at the site. The peak strength of the weathered material was found to be ϕ=11.9 degrees and 24.9 kPa (0.26 tsf) for cohesion, but due to the possibility of slip surfaces in the shale, the residual strength controlled the design parameters. In a laboratory slaking test, Botts (1986) observed nearly a 75% drop in the shear strength of Pierre Shale samples, or a 6-degree drop in the internal friction angles and a reduction of the cohesion from 848 kPa (123 psi) to 0 kPa, after one wetting and drying cycle.

Sample Preparation

Residual Shear Strength

The testing procedure for the Bromhead Ring Shear device used a modified version of ASTM (D6467). The material was crushed and passed through a US standard #50 sieve, remolded with distilled water to their plastic limit and allowed to hydrate for 48 to 72 hours. Higher water contents are suggested by ASTM (2003) but Bromhead (1979) advises drier samples in the Bromhead Ring Shear device to prevent excess settlement of the top platen.

Micromorphology

Central to the quality of any fabric analysis in soils is a preparation method preventing disturbance. Dry samples are required for analysis in the vacuum environment of the scanning electron microscope (SEM). The freeze-drying technique was used to obtain relatively undisturbed samples. A sample from each weathering cycle was placed in an intermediate freezer for twelve hours at a temperature of -75 degrees Celsius and then placed in a VirTis Ultra 35 8-shelf model freeze dryer at a temperature of -25 degrees Celsius until a vacuum of <100 millitorr was achieved. The temperature was raised to 26 degrees Celsius and held constant for 48 to 72 hours. Tension fractured and placement on carbon stubs preceded the analysis in the SEM.

Mineralogical and Chemical Analyses

X-ray fluorescence (XRF) and x-ray diffraction (XRD) analyses used both bulk samples and size fractions to determine the composition of the material. Bulk, silt, and sand mineralogy was obtained from random-oriented mount samples mounted in the XRD unit and analyzed at a speed of 2^{o} two theta per minute with copper K-alpha radiation. Minerals were identified by a computerized catalog of the Joint Committee on Powder Diffraction Standards (JCPDS) *Powder Diffraction File* system (The International Centre for Diffraction Data® 2004). Particle-size separation was performed on the material on the basis of Stoke's law, where particles <2 μm equivalent spherical diameter were obtained. This fraction was further separated by the same method into the coarse clay fraction, particles less than 2 μm, and the fine clay fraction, particles less than 0.5 μm. The oriented-mounted samples intensify the (00*l*) reflections and reduce (hk0) reflections by removing non-platy minerals,

dispersing clay minerals into individual colloidal particles, and laying the clay particles flat (Moore and Reynolds 1997). The filter transfer method, as recommended by Moore and Reynolds (1997), was used to transfer the material to a filter. The type of clay mineral is identified by the characteristic expansion, contraction, or collapse of the clay mineral's d-spacing through five subsequent treatments: air drying, glycolation with ethylene glycol, heating to 400°C, and heating to 550°C (Poppe *et al.* 2001). Oriented-mount samples were also used to discern between beidellite and montmorillonite in the mixed-layer. This procedure differentiates the two clay mincrals by noting the expanding potential during the glyccrol stage after treatment with 3 N LiCl and heating to 200 °C (Green-Kelly 1955). The expansion difference is due to the location of isomorphic substitutions in the two minerals. Montmorillonite's laycr charge is neutralized and does not expand, remaining at its 10-Å thickness, while beidellite continues to expand during glycerol treatment (Shultz 1978). The methods described in Shultz (1978) were used to estimate the concentrations of the clay minerals in the mixed-layer.

Fused glass discs were used for the x-ray fluorescence (XRF) analysis. These discs were prepared according to the procedure set forth by Amonette and Sanders (1994) by heating an ignited sample to 1200°C after the addition of Sigma x-ray flux 12:22 (12 Parts Lithium Tetraborate With 22 Parts Lithium Metaborate). The prepared disc was then analyzed in the x-ray spectrometer. XRF was used to help with the interpretation of the mineralogy.

TESTING AND ANALYTICAL METHODS

Weathering Cycle

ASTM standard C593 (ASTM 2003) was used as an outline for the saturation of the Pierre Shale. The vacuum-saturation strength testing procedure described in the standard was modified to allow for saturation of the soil samples. The test consisted of obtaining multiple two cubic-inch samples of unweathered Pierre Shale and placing them on a filter in a vacuum chamber. Samples were vacuumed at 24 inch Hg (11.8 psi) for one hour in the chamber; the chamber was then flooded; and the samples were soaked for one hour in the distilled water bath. The samples were removed from the bath and allowed to air-dry for 48 to 72 hours, completing one weathering cycle.

Classification and Ring Shear

Classification testing followed applicable American Society for Testing and Materials (ASTM 2003) standards. Atterberg limit and hydrometer analyses were performed on the samples. The Bromhead Ring Shear Device was used for measurement of the residual strength. The device was first proposed by Bromhead (1979) and has provided results that are in good agreement with back-calculations for slope stability analysis (Bromhead and Dixon 1986, Skempton 1985). The Bromhead Ring Shear Device consist of a 10:1 counterbalanced lever arm which provides the normal loading to the sample and a range of displacement rates from 0.024 to 60 degrees per minute. The mold dimensions are 100-mm outer diameter, 70-mm inner diameter, and a thickness of 5-mm. Replicate testing was not conducted for the cycling studies due to sample limitations. Replicate samples were used for the third and

fourth wet/dry cycles of the 70.3 dept. Due to the apparent anomalous values obtained. The replication confirmed the results.

The prepared sample was molded into the ring at a water content near its plastic limit and placed in a distilled water bath. Multistage testing was used to obtain the residual strength. This technique uses progressive loading after the formation of a shear surface. The samples were initially consolidated at the normal stress of 100 kPa and then sheared at a rate of 0.16 degrees per minute (0.119 mm per minute) for a displacement of one revolution to form the shear surface. The rate was slowed down to 0.048 degrees per minute (0.036 mm per minute) and allowed to shear until the residual strength was reached, typically an additional 10 to 15 mm. The residual strength was obtained for 100, 200, and 400 kPa normal stress increments.

Scanning Electron Microscope

Freeze-dried samples were analyzed with a Hitachi S-2460N VP scanning electron microscope (SEM) with energy dispersive spectrographic (EDS) and digital imaging capability. Two sources were used to obtain surface topography: backscattered electron (BSE) and secondary electron (SE). BSE mode was used for lower-resolution imaging and elemental analyses while SE mode was used for higher magnifications. Samples were coated with gold to prevent charging for samples analyzed in the SE mode. Digital elemental maps were produced using the EDS function on the SEM. Mineral contents were inferred by coinciding elemental maps.

RESULTS

Engineering properties

Samples from three different depths below 60 meters were cycled through wetting and drying. Table 17 shows the index properties for the cycles. The material at the 63.0 and 70.3-meter depths consisted of approximately 2% sand, 50% silt, and 48% clay sized particles. The 63-meter samples exhibited a substantial increase in the liquid limit, as the material was wetted and dried. Minor increases in the liquid limit were observed in the 63.6-meter sample. The 70.3-meter sample showed insignificant changes in the Atterberg Limits. The plastic limit increased by ten and five percent for the 63.0 and 63.6 meter cycles. The plastic limit remained almost unchanged for the 70.3 meter depth. The liquid limits are plotted with wet/dry cycles in Figure 41 for the various depths

Table 17. Weathering cycle Atterberg Limits

Depth M	Depth Ft	Weathering Cycle	Liquid Limit (%)	Plastic limit (%)	Plastic Index (%)
63.0	208	0	79	33	46
63.0	208	1	85	35	50
63.0	208	2	88	36	53
63.0	208	3	100	40	60
63.0	208	4	113	40	73
63.0	208	5	125	43	82
63.6	210	0	63	32	31
63.6	210	1	78	34	44
63.6	210	3	79	35	44
63.6	210	5	86	36	50
70.3	232	0	72	31	41
70.3	232	1	72	30	41
70.3	232	2	72	31	41
70.3	232	3	74	32	42
70.3	232	4	68	29	39
70.3	232	5	71	31	40

The residual friction angle for each cycle for the three depths was determined from ring-shear tests. The formulated residual strength-normal stress plot for each sample was constructed using a spreadsheet program and analyzed for both the trend line through the origin and with a cohesion intercept. The residual friction angle (ϕ'), residual cohesion, and correlation coefficients are summarized in Table 18. A plot of the residual friction angles versus wet/dry cycles is shown in Figure 42. The residual friction angle dropped almost 1.5 degrees for the 63.0 meter depth, nearly one degree for the 63.6 meter sample, and 1.3 degrees for the 70.3 meter depth during the wet/dry cycles. An unexpected increase in strength was observed in the later stages of the 70.3 meter cycles. Similarities in the 63.6 and 70.3 meter residual friction angle plots are apparent for the first two cycles.

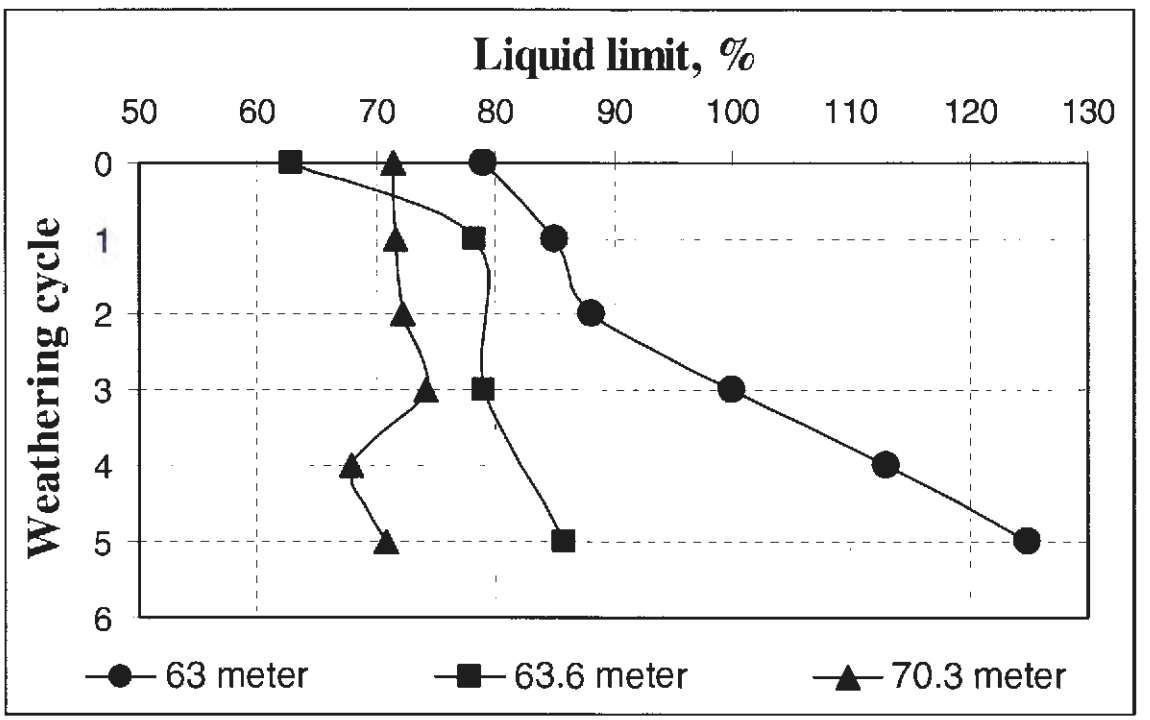

Figure 41. Wet/dry cycle Atterberg Limits

SEM Images and Visual Observations

Figure 43 shows the dense, high-laminae fabric encountered in the unweathered material below 60 meters. The three depths analyzed had similar fabrics. Various other fabrics and particle shapes were observed over the depths including burrows of pyrite framboids and cemented calcite accretions. The fabric shown in Figure 43 was dominant but the other fabrics signify the heterogeneity of the material. Weathering created a more homogenous fabric as shown by Figure 44. The open fabric shown in Figure 44 displays a sample after three wet/dry cycles exhibiting little of the layering visible in the unweathered sample in Figure 43.

Table 18. Wet/dry cycle residual friction angles

Depth M	Depth ft	Weathering cycle	ϕ_r' Degree	c' kPa	r^2	ϕ_r' for $c'=0$	r^2
63.0	208	0	6.8	0.7	1.0	6.9	1.0
63.0	208	1	6.5	~0	1.0	6.5	1.0
63.0	208	2	6.5	~0	1.0	6.3	1.0
63.0	208	3	6	0.5	1.0	6.1	1.0
63.0	208	4	5.6	0.1	1.0	5.6	1.0
63.0	208	5	5.4	~0	1.0	5.3	1.0
63.6	210	0	6.1	0.2	1.0	6.1	1.0
63.6	210	1	5.7	0.8	1.0	5.9	1.0
63.6	210	3	5.4	1.1	1.0	5.6	1.0
63.6	210	5	5.2	1.3	1.0	5.5	1.0
70.3	232	0	6.7	0.2	1.0	6.7	1.0
70.3	232	1	6.4	0.2	1.0	6.4	1.0
70.3	232	2	6.3	0.3	1.0	6.4	1.0
70.3	232	3	5.4	1.2	1.0	5.7	1.0
70.3	232	4	6.3	1.9	1.0	6.6	1.0
70.3	232	5	6.6	1.0	1.0	6.8	1.0

Visual observations of yellow, sulfuric, sand particles scattered over the sample between the laminae were made. Fabrics with large amounts of yellow particles showed a

significant amount of degradation after one to two wet/dry cycles as well. After the third cycle, the material turned into a soil-like material. As the material dried, large cracks were observed, an indicator of the shrink/swell potential of the clay minerals in the material.

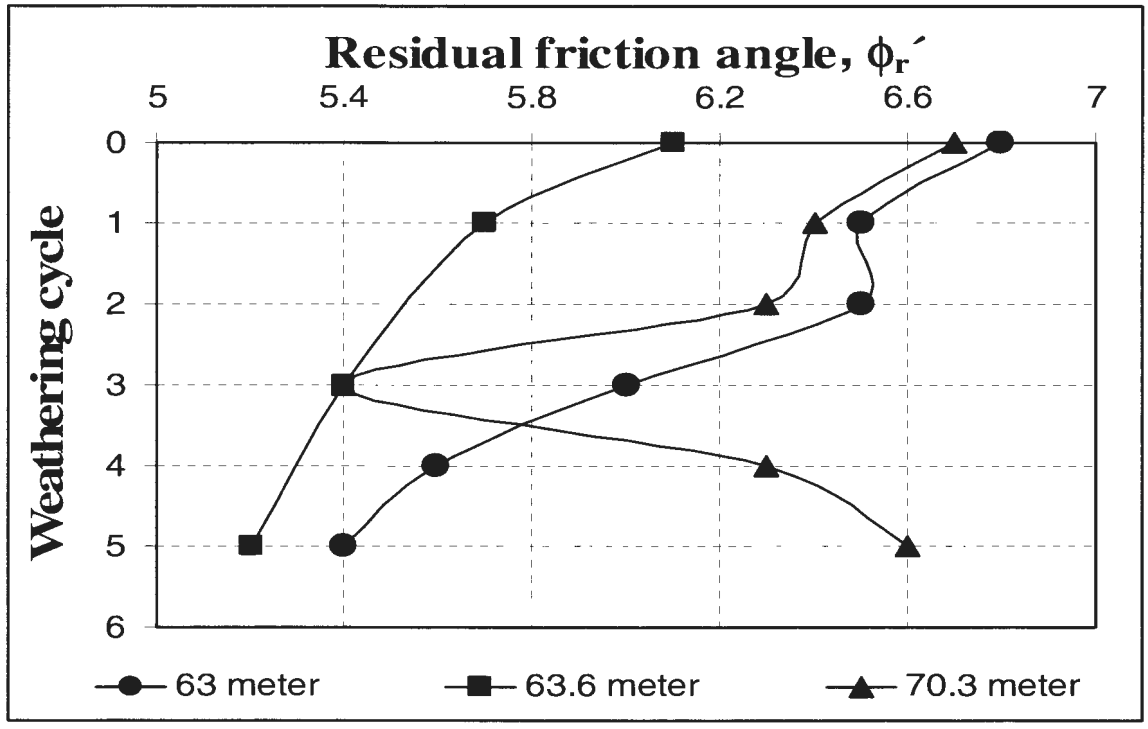

Figure 42. Wet/dry cycle residual friction angle

Following each weathering cycle, the sample was fractionated in a sedimentation cylinder to obtain the clay fraction for XRD analyses. Observations of the time rate of settlement of the particles during this process provide insight into the soils' behavior. Settlement analyses showed a contrast in the suspension time for wet/dry samples. The fine fraction of the wet/dry cycled samples stayed in suspension for many weeks longer than the un-cycled samples. A sample after five wet/dry cycles continued to be in suspension after three months.

Although not included, micrographs at 1500X magnification show that the unweathered material has particles with sharp, distinct edges while the cycled material of the 3, 4, and 5X cycles have rounded, degraded particles.

The elemental composition of the materials was inferred from elemental maps of the EDS analyses. Figure 45 shows elemental maps of the unweathered Pierre Shale of the area shown in Figure 43. K- and Na-ions are dispersed over the material, a possible indicator of the adsorbed cation on the montmorillonite mineral. The material has high aluminum, silicon, and oxygen suggesting clay minerals. The particles with high reflection in Figure 43 were determined to be pyrite due to the occurrence of iron and sulfur in the bright particles.

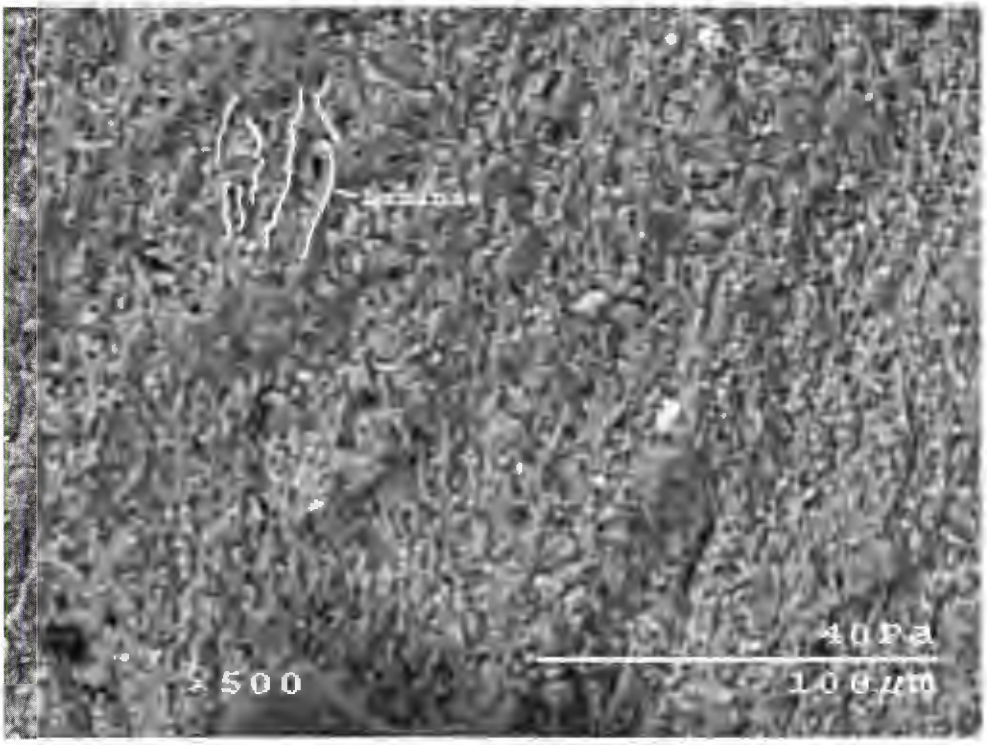

Figure 43. 70.3 m (232 ft) unweathered Pierre Shale, Oahe Dam site, SD

Figure 46 displays the elemental maps of the 70.3 m material after three wet/dry cycles, as shown in Figure 44. The potassium dispersed over the material are likely indicate potassium. The calcium and sulfur occurrences suggest gypsum. The sulfur and iron elements of the bright particles in Figure 44 indicate pyrite. The material also exhibited high amounts of clay mineral elements (Si, Al, and O) similar to the unweathered material shown in Figure 45. Unlike the Na- and Ca-ions, the K-ion is dispersed over the material in Figure 46.

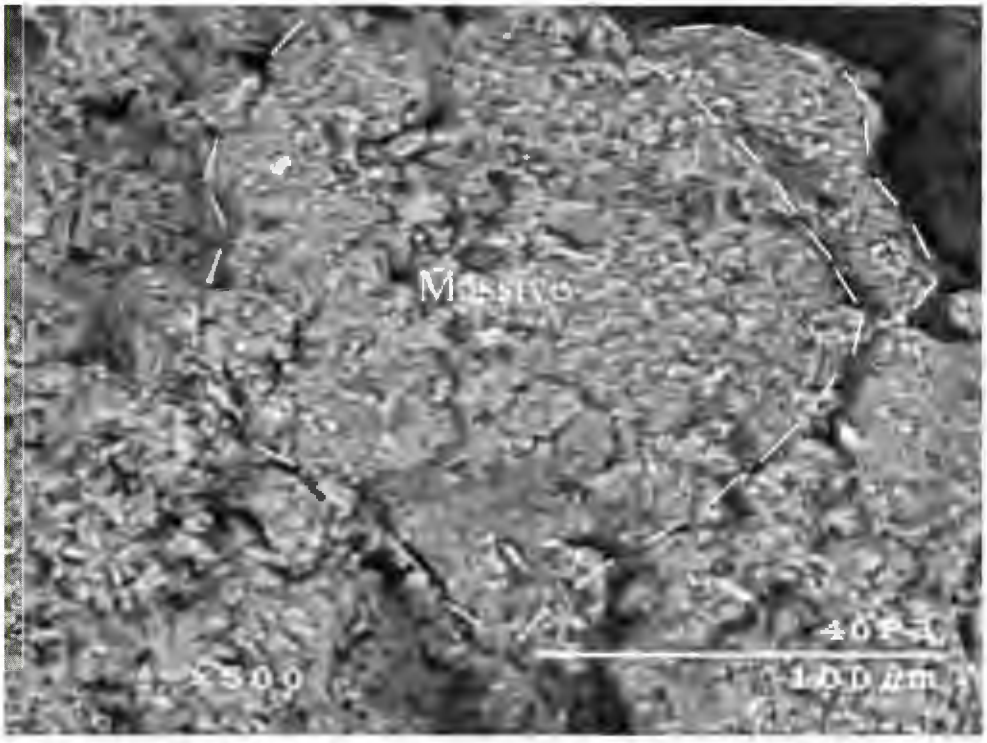

Figure 44. 70.3 m (232 ft) wet/dry X3 Pierre Shale, Oahe Dam site, SD

Mineralogy and Chemistry

A qualitative description of the mineralogy for the wet/dry cycles is shown in Table 19. Bulk mineralogy was determined from powder samples. Sand, silt, clay, and very fine

clay fractions were divided to determine the mineralogy of the fractions. Sand and silt mineralogy was determined by random-mount samples and clay mineralogy was found from oriented-mount samples. The diffractograms and raw data for the random- and oriented-mount samples can be found in Appendix D. Bulk mineralogy indicated quartz (SiO_2), gypsum ($CaSO_4 \cdot 2H_2O$), and pyrite (FeS_2). A comparison of the bulk mineralogy diffractograms at the depths of 63.0 m, 69.7 m, and 70.3 m is shown in Figure 47. The mineralogy was similar over the depths except for higher concentrations of gypsum at the 70.3 m depth.

The sand fraction was observed to be highly heterogeneous, with a significant amount of quartz. Large calcite accretions were observed visually in the bulk sample and were found in the sand fraction mineralogy. These observations were verified by EDS analyses on SEM specimens. Pyrite, gypsum, and bassanite ($CaSO_4 \cdot 1/2H_2O$) were also observed in the sand fraction. Gypsum is a hydrated form of bassanite. Quartz and pyrite were found in the silt fraction with minor amounts of feldspars including orthoclase ($KAlSi_3O_8$) and albite ($NaAlSi_3O_8$).

The clay minerals were primarily mixed-layer clays as well as minor amounts of illite clay mineral. Shultz (1978) provides a outline for the determination of mixed-layer clay minerals in Pierre Shale. The 63.0 meter depth showed a mixed-layer clay mineral with montmorillonite, illite, and beidellite concentrations of 20, 45, and 35 percent, respectively. The 70.3 meter depth had a mixed-layer clay mineral closer to bentonite with montmorillonite, illite, and beidellite concentrations of 60, 15, and 20 percent, respectively. Data and diffractograms for the mixed-layer clay determinations are shown in Appendix E (Birchmier 2005). These values fall within the data compiled by Schultz (1978) for mixed-

layer clay minerals in Pierre Shale. Figure 48 displays overlays of diffractograms of bulk samples for the wet/dry cycles of the 70.3 meter depth. Little change was observed over the weathering cycles except for the reduction of gypsum particle size during the initial cycles. The combination of the decrease in the gypsum peak intensity at 7.63 Å, and the constant 4.28 Å and 3.8 Å peak intensities during cycling suggest the breakdown of the gypsum particles. The decrease in the gypsum intensities caused the increase of other mineral peaks in subsequent wet/dry cycles as shown by Figure 48. After two wet dry cycles, gypsum peak intensities decreased, as indicated in Figure 48.

Similar to the pyrite decrease during wet/dry cycles observed in the x-ray diffraction results, x-ray fluorescence shows a drop in the concentrations of iron and sulfur. X-ray fluorescence data were not included due to space limitations but are shown in Appendix E (Birchmier 2005). A three percent drop in iron and sulfur concentrations were documented in the first two wet/dry cycles of samples from the 70.3-meter depth.

DISCUSSION

Residual friction angles for the wet/dry cycles decreased from 6.8° to 5.4°, 6.1° to 5.2°, and 6.7° to 5.4° for the depths tested. A degree drop in a material with an initial residual friction angle of 6.5° is significant. For a given normal stress and negligible residual cohesion, the factor of safety would be reduced by a ratio of 1.2. Exposure and removal of confining stresses during construction activities in Pierre Shale could cause wetting and drying to occur and lead to slope failures.

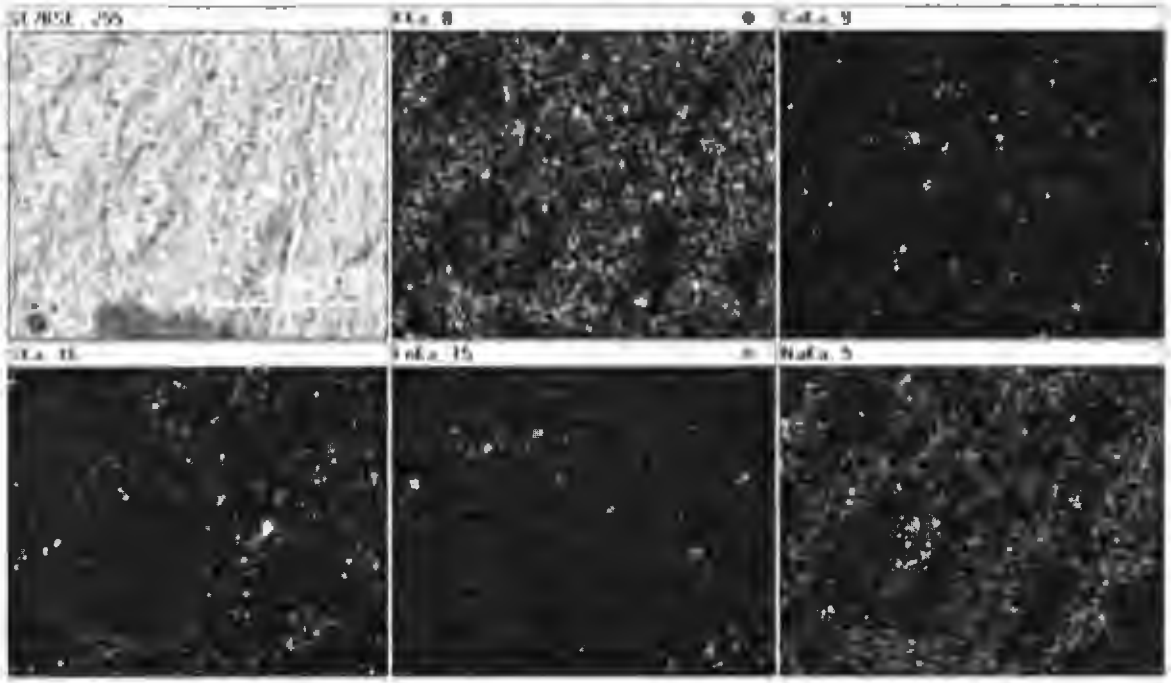

Figure 45. 70.3 m (232 ft) unweathered Pierre Shale, Oahe Dam site, SD elemental maps

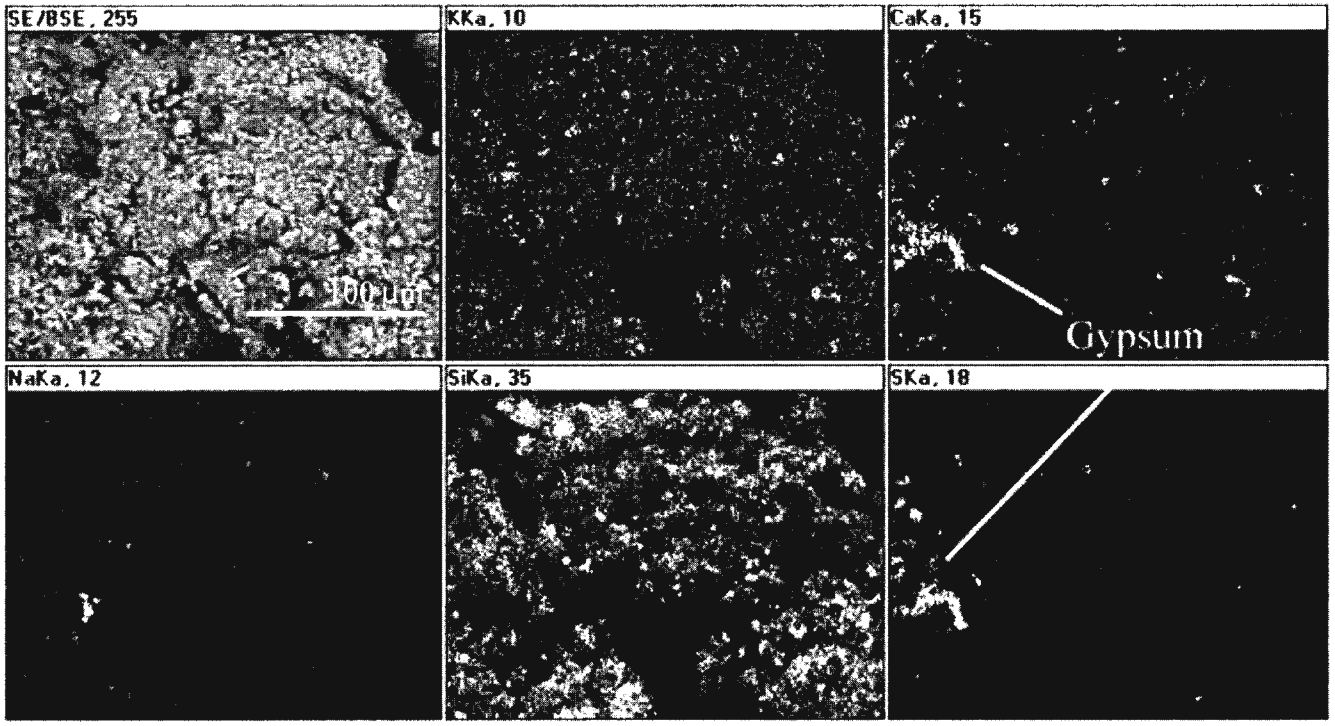

Figure 46. 70.3 m (232 ft) wet/dry X3 Pierre Shale, Oahe Dam site, SD elemental maps

Table 19. Weathering cycle mineralogy

		Bulk powders				Clay Fraction		
Depth	Cycle	Quartz	Gypsum	Pyrite	Others	MLC*	Illite	Kaolinite
63	Wx0	Major	Minor	Minor	feldspar(s)	Major	Minor	Intermediate
63	Wx1	Major	Minor	Minor	feldspar(s)	Major	Minor	Intermediate
63	Wx3	Major	Minor	Minor	feldspar(s)	Major	Minor	Intermediate
69.7	Wx0	Major				Major	Minor	Intermediate
69.7 (sand)	Wx0	Minor	None	Minor	Calcite major			
69.7 (silt)	Wx0	Major	None	Minor	feldspar(s)			
69.7	Wx1	Major				Major	Minor	Intermediate
70.3	Wx0	Major	Intermediate	Intermediate	feldspar(s)	Major	Minor	Intermediate
70.3 (sand)	Wx0	Major	Intermediate	Intermediate	feldspar(s)			
70.3 (silt)	Wx0	Major	None	Intermediate	feldspar(s)			
70.3	Wx1	Major				Major	Minor	Intermediate
70.3	Wx2	Major				Major	Minor	Intermediate
70.3	Wx3	Major				Major	Minor	Intermediate
70.3	Wx4	Major				Major	Minor	Intermediate
70.3	Wx5	Major				Major	Minor	Intermediate

*MLC-Mixed-layer clay (montmorillonite-illite-beidellite)

The excessive shrinking and swelling of the clay minerals in the material also caused the initial fabric to be destroyed after three cycles. The residual strength decrease has obvious application for engineering designs in clay shales due to the susceptibility for the material to soften, crack, and weather.

Figure 49 shows the residual friction angles plotted with the liquid limits for the various wet/dry cycles. The compilation of residual friction angles and liquid limits for Pierre Shale in Figure 49 for the residual direct shear, ring shear, and rotational shear are discussed in Schaefer (2002). The plot also includes results for a weathering profile at the Oahe Dam site, SD, which are shown in Appendixes A and C. Stark's and Eid's (1994) reference curves are included for materials with greater than 50% fines. All of the cycling data and the previous study of the weathering profile at the Oahe Dam site fall below the

curves. The high silt contents in the Pierre Shale likely contributed to the lower liquid limits while the high concentrations of mixed-layer clay minerals caused the residual friction angle to be low. Higher amounts of platy particles, such as mixed-layer clay minerals, allow better orientation of the particles leading to a low residual strength. The strength behavior during cycling was different for the 63.0 and 63.6 meter depths weathering cycle in comparison to the 70.3 m depth. The residual friction angle for the 63.0 meter depth shows the same pattern as the lower limit of Stark and Eid's (1994) proposed curve (Figure 49). The 63.6 meter sample showed minor changes over the wet/dry cycles, but followed the curve similar to the 63.0 meter samples. The increase in the liquid limit of the 63.0 and 63.6 m samples is likely associated with the decrease in aggregate size, as observed in the sedimentation process. No dramatic changes were observed in the liquid limits for the 70.3 meter sample. The residual friction angle initially decreased almost 1.5 degrees and then increased to the initial values, an unexpected observation. The differences in the mixed-layer clay mineral may have also influenced the behavior of the material from the two depths. The mixed-layer clay mineral at the 63.0 meter depth showed higher contents of illite and beidellite than montmorillonite, while at the 70.3 meter depth, montmorillonite was dominant mineral in the mixed-layer.

Major changes in the mineralogical composition were not observed as a consequence of the wet/dry cycles. These findings are similar to previous studies on weathering profiles in Pierre Shale (Schultz *et al.* 1980). The main change in the material's mineralogy was a decrease in the gypsum concentration. The wet/dry cycles caused the more soluble gypsum to be washed away after the first few cycles. Pyrite concentrations also decreased with wet/dry cycles. XRF results agree with the XRD results by showing iron and sulfur concentrations decreasing in the first two wet/dry cycles. This decrease is likely associated

with the oxidation of pyrite (Taylor and Cripps 1987, Oyama and Chigira 1999) and minor discontinuities in the shale. The rapid reaction of pyrite oxidation explains the stabilization of the iron and sulfur contents after two wet/dry cycles as indicated by the XRF results.

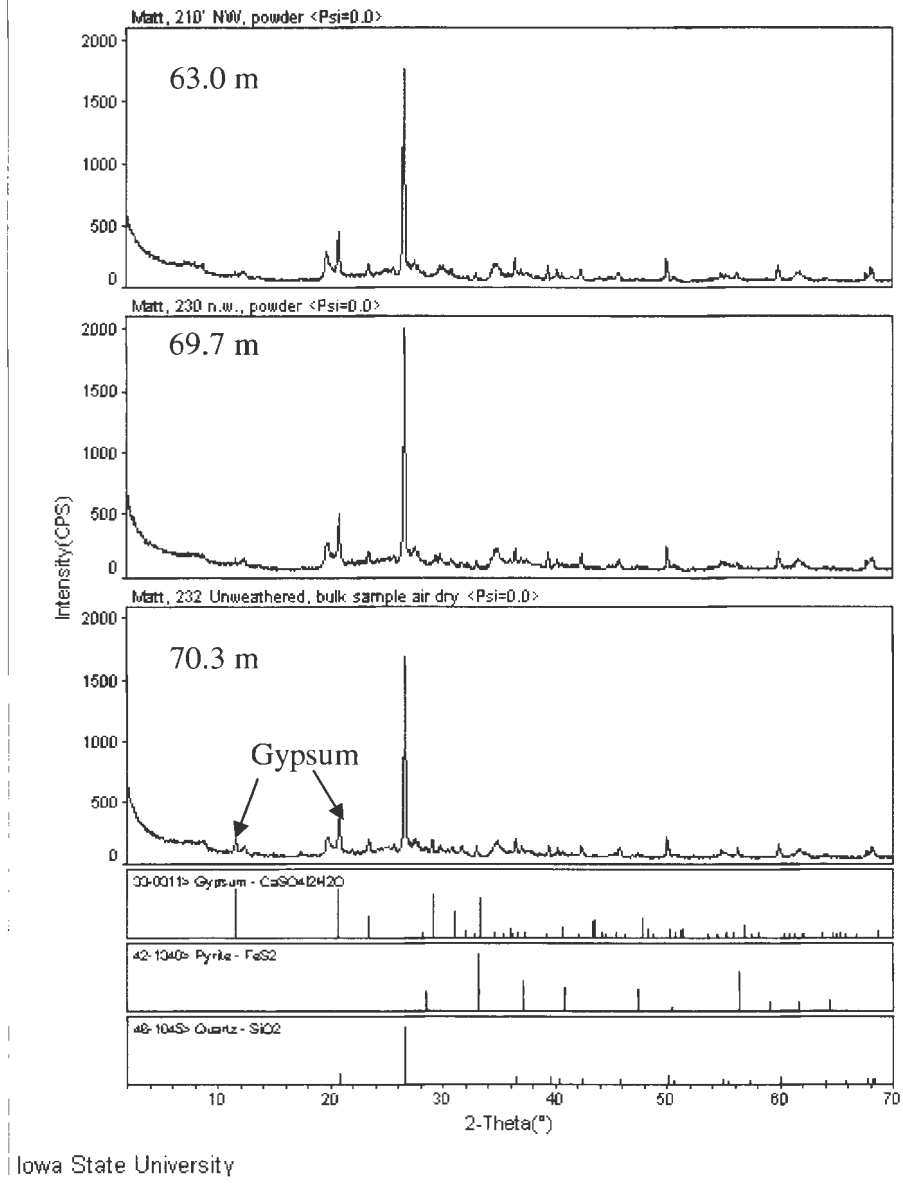

Figure 47. Bulk mineralogy diffractograms of unweathered Pierre Shale

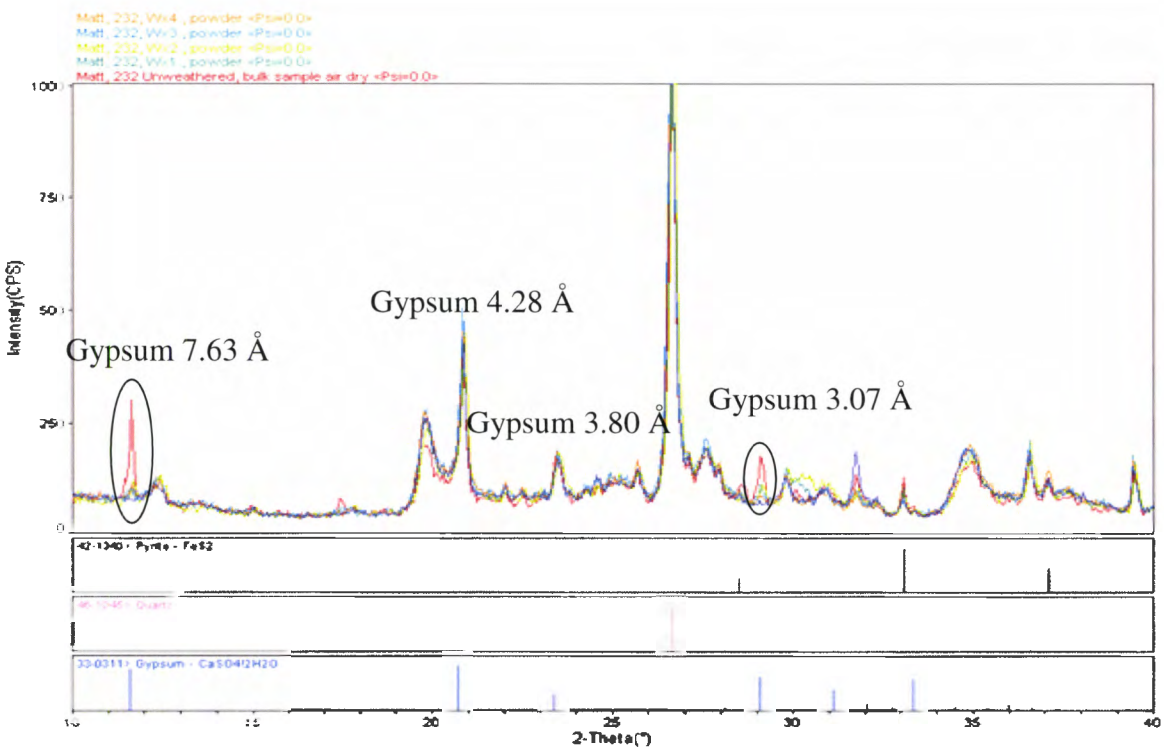

Figure 48. 70.3 meter wetting and drying cycle bulk mineralogy diffractograms

The yellow particles also appeared to open the fabric by separating the layers in the unweathered material, allowing water to penetrate into the sample and cause greater amounts of disturbance to the sample. The removal of the massive mineral, gypsum, and the decrease in particle size at the 70.3 meter depth during the first two wet/dry cycles likely resulted in the decrease in residual strength.

EDS results show the usefulness and limitations of the technique. Pyrite and gypsum were inferred from coinciding maps of the respective elements in the minerals. Pyrite was not observed in the wet/dry cycle shown in Figure 46, while gypsum was apparent. The . decrease in the pyrite contents with wet/dry cycles was also confirmed through XRD results. The SEM tool also provides a good method to identify crystal growth and other

micromorphological features. Many samples are required with this technique to identify discontinuities in the material.

Mineralogical changes may have been minimal, but the aggregate size was observed to change with the weathering cycles during the settlement analysis. The clay aggregates became successively smaller with the wet/dry cycles, causing the aggregates to stay in suspension longer. During the wetting and drying cycles, water moves in and out of the nanopores between quasicrystals. Each cycle continues to breakdown the clay minerals. The smaller aggregate size would be indicative of the lower residual strengths observed in the wet/dry cycles. The smaller aggregates size of the clay minerals causes better orientation of the platy quasicrystals, decreasing the residual strength. Ultimately, the residual strength could be decreased to the pure clay mineral's residual friction angle. Sodium montmorillonite has been determined to have residual friction angles as low as 4.1° to 5° (Kenney 1967, Olson 1974). Both the 60.3 and 63.6 meter samples showed higher liquid limits during cycling which could also be explained by the decrease in particle size. The 60.3 meter depth, the most llitic mixed-layer clay sample, showed nearly a hundred percent increase in the liquid limit during the wet/dry cycles. The liquid limit for 70.3 depth, the more montmorillonite mixed-layer clay sample, changed by only a few percent.

The degradation of the material during wet/dry cycles was best observed through fabric analyses. The original laminae of the un-cycled material nearly disappear after three cycles in distilled water. The material turns into almost a fluid-like material after the third cycling. Significant cracking was also apparent in these cycled samples. The particles become more sub-rounded to sub-angular during cycling as well, similar to observed weathering alternations on Pierre Shale.

The decrease in residual strength during wet/dry cycles is concluded to be primarily associated with physical mechanisms. The degradation of the material decreases the particle size, allowing particle orientation in the direction of shearing to increase, and thus causing the residual strength to decrease. While physico-chemical effects on the residual strength during wetting and drying cycles likely exist, the effects are overshadowed by the mineralogical changes (dissolution of gypsum) and increase in fine particles.

CONCLUSIONS

Minor mineralogical changes were observed in the wet/dry cycles similar to the weathering occurrences in Pierre Shale. Gypsum concentrations decreased initially in the wet/dry cycles. The low residual friction angles of 6.1° to 6.8° decreased an additional 0.8° to 1.4° during the wet/dry cycles. A significant fabric contrast was apparent after three cycles as the material's structure became more massive. The most noticeable difference in the cycles was the particle settlement rates. Excessive cycling caused particles to stay up in suspension for weeks to months longer than the un-cycled material. This observation indicates clay aggregates are becoming smaller and going towards their unit-cell size. The reduction in size increased the clay fraction, contributing to the residual strength decrease.

The mechanical behavior varied for the samples analyzed. The material with larger amounts of illite in the mixed-layer clay mineral showed a decrease in residual strength following Stark and Eid's (1994) curves. The material with higher amounts of montmorillonite in the mixed-layer clay mineral showed little change in the liquid limits, a contrast to the other sample. A decrease in residual strength was observed for the first two cycles but increased thereafter. The contrasting behavior shows the heterogeneity of the

material and the difficulties in determining design parameters. The mineralogical changes and the breakdown of aggregate size during wetting and drying are concluded to be more influential than physico-chemical effects.

ACKNOWLEDGEMENTS

The authors thank the engineers of the U.S. Army Corps of Engineers Project Office in Pierre, SD for their help in obtaining the samples of Pierre Shale and for access to information regarding the Oahe Dam, in particular, Mr. LeeJay Templeton. Ashley Schwaller, undergraduate student at Iowa State University, is thanked for conducting the XRD tests. Drs. Scott Schlorholtz and Warren Straszheim of ISU provided valuable assistance in the conduct of the analytical work. This material is based on work supported by the National Science Foundation under Grant Nos. CMS-0201482 and CMS-0227874. This support is gratefully acknowledged. Any opinions, findings and conclusions or recommendations expressed in this material are those of the authors and do not necessarily reflect the views of the National Science Foundation.

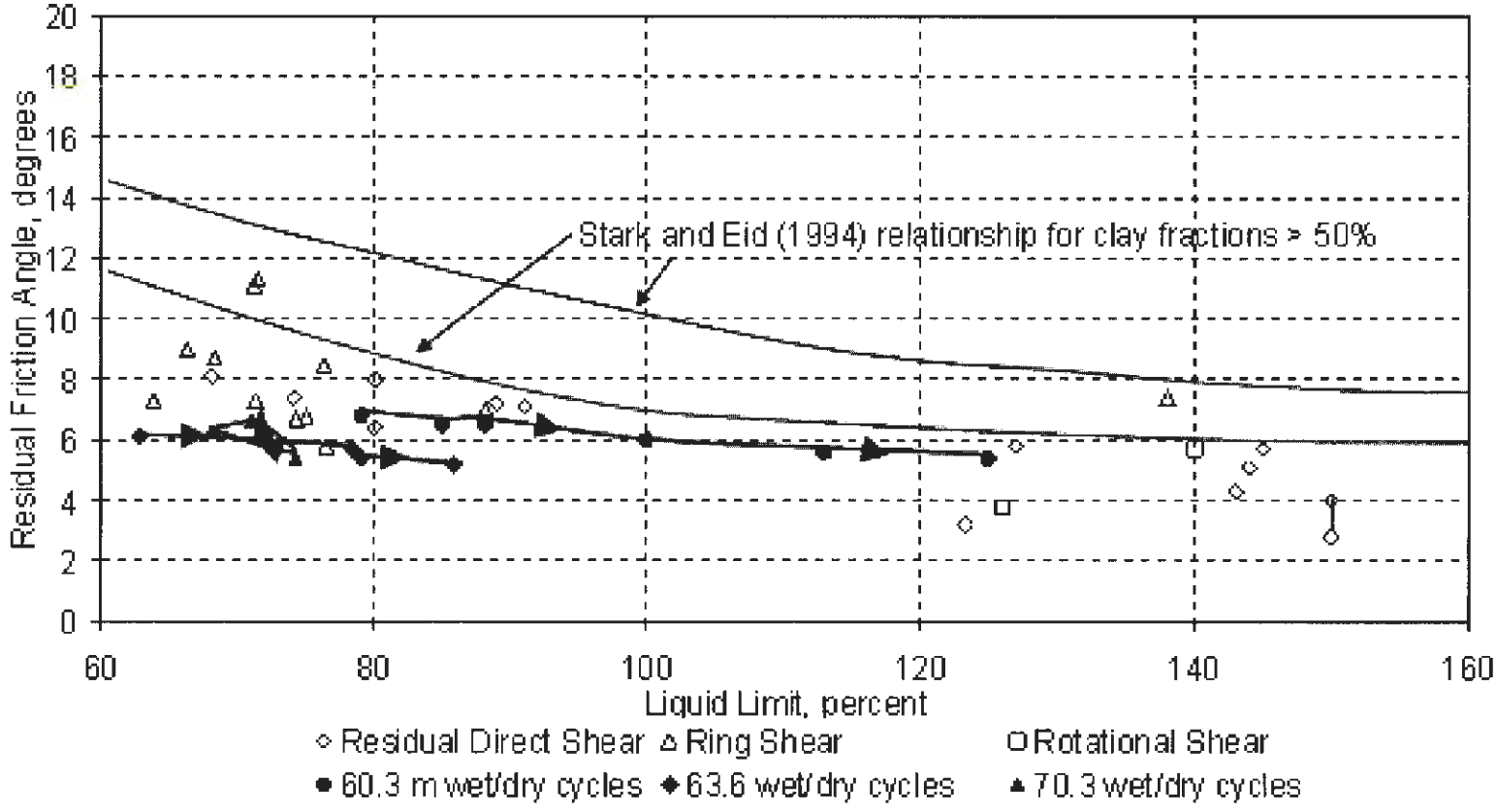

Figure 49. Plot of residual friction angle with liquid limit for wet/dry cycles (adapted from Schaefer 2002 and Stark and Eid 1994).

REFERENCES

Amonette, J.E. and Sanders, R.W. (1994). "Nondestructive techniques for bulk elemental analysis." *Quantitative Methods in Soil Mineralogy*, SSSA Miscellaneous Publication, Madison, Wisconsin.

ASTM. (2003). *Annual Book of ASTM Standards, Section 4, Construction*, Vol. 04.09, American Society for Testing and Materials, Philadelphia, PA.

Bjerrum L. (1967) "Progressive failure in slopes of overconsolidated plastic clay and clay shales," *Journal Soil Mechanics And Foundation Division*, ASCE, 93, 1-49.

Botts, M.E., (1986). *The Effect of Slaking on the Engineering Behavior of Clay Shales*, Ph.D. Dissertation, Department of Civil, Environmental, and Architectural Engineering, University of Colorado.

Bromhead, E.N. (1979). "A simple ring shear apparatus," *Ground Engineering*, 12(5), 40-44.

Bromhead, E.N. and Dixon, N. (1986). "The field residual strength of London Clay and its correlation with laboratory measurements, especially ring shear tests," *Gèotechnique,* 36(3), 449-452.

Brooker, E. W. and Peck, R. B. (1993). "Rational design treatment of slides in overconsolidated clays and clay shales," *Canadian Geotechnical Journal*, 30, 526-544.

Fleming, R.W., Spencer, G.S., and Banks, D.C. (1970). *Empirical Study of Behavior of Clay Shale Slopes,* Vol. 1, NCG Technical Report No. 15, U.S. Army Engineer Nuclear Cratering Group, Livermore, CA, December.

Green-Kelly, R.G. (1955). "Dehydration of the montmorillonite minerals," *Mineralogy Magazine*, 30(228): 604-615.

The International Centre for Diffraction Data®. (2004). *Joint Committee on Powder Diffraction Standards (JCPDS) Powder Diffraction File system.*

Johns, E.A., Burnett, R.G. and Craig, C.I. (1963). "Oahe Dam: Influence of shale on Oahe power structures design," *Journal Soil Mechanics And Foundation Division, ASCE*, 89, 95-113.

Kenney, T. C. (1967). "The influence of mineralogical composition on the residual strength of natural soils," *Proceedings of the Geotechnical Conference on Shear Strength of Cohesive Soils*, Oslo, pp. 123-129.

Knight, D.K. (1963). "Oahe Dam, geology, embankments and cut slopes," *Journal of the Soil Mechanics and Foundation Division*, ASCE, 89(2), 99-125.

Manfredini, G., Martinetti, S., Ribacchi, R., Santoro, V.M., Sciotti, M., and Silvestri, T. (1981). "An earthflow in the Sinni Valley (Italy)," *Proceedings of the 10th International. Conference on Soil Mechanics and Foundation Engineering*, 3, 457-462.

McClure, J.G. (1980). *Physicochemical Investigation of Shale Slaking*, PhD Thesis, University of California, Berkley.

Moore, D.M. and Reynolds, R.C. (1997). *X-ray Diffraction and the Identification and Analysis of Clay Minerals*, 2nd ed., Oxford Universities Press, Oxford.

Moore, R. (1991). "The chemical and mineralogic controls upon the residual strength of pure and natural clays," *Gèotechnique*, 41(1), 35-47.

Moore, R. and Brunsden, D. (1996). "Physico-chemical effects on the behavior of a coastal mudslide," *Gèotechnique*, Vol. 46, No. 2, pp. 259-278.

Olson, R.E. (1974). "Shearing strengths of kaolinite, illite, and montmorillonite," *Journal of the Geotechnical Engineering Division*, 100(11), 1215-1229.

Oyama, T. and Chigira, M. (1999). "Weathering rate of mudstone and tuff on old unlined tunnel walls," *Engineering Geology*, 55,15-28.

Perry, E.F. and Andrews, D.E. (1984). "Slaking modes of geologic materials and their impact on embankment stabilization," *Transportation Research Record 873*, Transportation Research Board, Washington, D.C., 15–21.

Poppe, L.J., Paskevich, V.F., Hathaway, J.C., and Blackwood, D.S. (2001). *A Laboratory Manual for X-Ray Powder Diffraction*, U.S. Geological Survey Open-File Report 01-041, United States Government Printing Office, Washington.

Schaefer, V.R. (2002). "Residual strength and back analysis of slopes in Pierre Shale," *Proceedings of the 3rd International Conference on Landslides, Slope Stability & the Safety of Infrastructures*, Edited by J.S.Y. Tan, July 11-12, Singapore, 407-414.

Schultz, L.G. (1978). *Mixed-Layer Clay in the Pierre Shale and Equivalent Rocks, Northern Great Plains*, Geological Survey Professional Paper 1064-B, United States Government Printing Office, Washington.

Schultz, L.G., Tourtelot, H.A., Gill, J.R., and Boerngen, J.G. (1980). *Composition and Properties of the Pierre Shale and Equivalent Rocks, Northern Great Plains Regions*, Geological Survey Professional Paper 1064-B, United States Government Printing Office, Washington.

Skempton, A.W. (1948). "The rate of softening in stiff fissured clays, with special reference to London clay," *Proceedings of the 2nd International Conference on Soil Mechanics*, 2, 50-53.

Skempton, A.W. (1964). "Long-term stability of clay slopes," Fourth Rankine Lecture, *Gèotechnique*, 14, 77.

Skempton, A.W. (1985). "Residual strength of clays in landslides, folded strata and the laboratory," *Gèotechnique*, 35(1), 3-18.

Stark, T.D. and Eid, H.T. (1994) "Drained Residual Strength of Cohesive Soils," *Journal of Geotechnical Engineering*, 120(5), 856-871.

Steward, H.E. and Cripps, J.C. (1983). "Some engineering implications of chemical weathering of pyritic shale," *Quarterly Journal of Engineering Geology*, 16, 281-289.

Taylor, R.K. and Cripps, J.C. (1987). "Weathering Effects: Slopes in Mudrocks and Over-consolidated Clays," Chapter 13 in *Slope Stability*, M.G.Anderson and K.S. Richards, John Wiley & Sons, Ltd., pp. 405-445.

Terzaghi, K and Peck, R.B. (1948). *Soil Mechanics in Engineering Practice*, Wiley, New York.

CHAPTER 5

CONCLUSIONS

BACKGROUND

Weathering in soils and rocks, specifically in clay shales, has been shown to be a complex, open-system process requiring a multidisciplinary approach to fully understand. Minor mineralogical and chemical changes in these materials can lead to catastrophic failures, as noted by Brooker and Peck (1993). Weathering in overconsolidated clays and clay shales is enhanced by events in geologic history and by the high clay contents. The Pierre Shale formation has been shown to be a problematic clay shale with significant outcroppings throughout South Dakota. Slope failures on flat slopes during the construction of the Oahe Dam highlighted the importance of understanding the failures' mechanisms. Due to the existence of slip-surfaces throughout the Pierre Shale formation, the residual strength controls a slope's design.

The residual strength has been described as a dynamic soil property, dependent on the soil particles and their environment. The physico-chemical state of soil/rock was shown to be critical in controlling the residual strength, especially in clayey materials. Many previous studies were reviewed in the literature review to describe ring-shear devices' accuracy and efficiency in measuring the residual strength due to the continuous shearing in one direction. A testing procedure for the Bromhead Ring Shear was also derived from these studies.

Many of the properties of Pierre Shale were attributed to the mineralogy, chemistry, and micromorphology. X-ray diffraction (XRD), x-ray fluorescence (XRF), and scanning

electron microscope (SEM) and their respective sample preparation were described as methods for analyzing these characteristics.

PAPER 1

Similar to past studies, minor mineralogical changes were observed in the weathering profile. The residual friction angle was the lowest, ϕ_r'=5.9°, in the weathered zone and increased significantly in the transitional zone. The increase in strength was attributed to the higher concentrations in the coarse fraction. The plasticity index decreased in this zone as well. The unweathered zone showed a residual friction angle higher than the weathered zone but lower than the transitional zone. The higher strengths were attributed to the higher potassium ion concentration found in the unweathered zone in comparison to the weathered zone.

Much of the mineralogical changes and the residual strength behavior were associated with the presence of pyrite in the material. The formation of oxides in the transitional zone and existence of gypsum in the weathered material are secondary minerals of the pyrite oxidation. The higher residual strength values from increase amounts of coarse fraction in the transition zone was likely associated with the coarse oxide minerals. Gypsum would have also caused the material to degrade due to its high expansive pressures.

SEM analyses showed the contrast in micromorphology between the two materials. The high laminae and dense fabric of the unweathered material almost disappears when it weathers. The micromorphology analyses also show the relevance of the peak strength to the field behavior if the material's fabric is not disturbed.

PAPER 2

Minor mineralogical changes were observed in the laboratory wet/dry cycles of unweathered Pierre Shale. Decreases in the residual strength and increases in the plasticity index were observed for the wet/dry cycles. The main mineralogical change was the removal of gypsum in the first few cycles. The wet/dry cycles were noted to cause a breakdown in aggregate size, causing clay minerals to be suspended for an increasingly amount of time. The decreases in the residual strength were attributed to the reduction in particle size. The mineralogical changes and particle size reduction during the wet/dry cycles were concluded to be more influential to the residual strength than physico-chemical effects.

OVERALL CONCLUSIONS

The weathering profile and wet/dry cycling studies showed similarities and differences. Gypsum was observed in both the weathered samples at depths of 20 meters and in the 70 meter samples used for cycling studies. The gypsum in the weathered profile at 20 meters was expected due to the oxidation of pyrite but was unanticipated at the lower depths used for the wet/dry cycling. The massive-laminae fabric apparent in the weathered material occurred in the 70.3 meter sample after one to two wet/dry cycles. The more wet/dry cycled material had an increase in massive fabric and the lost its initial laminae. The intact cycling samples, ranging from 60 to 70 meter depths, had a very dense fabric with high laminae in comparison to the dense structure with medium laminae observed in the unweathered material at 30 meters. The denser structure is a result of the higher overburden thickness.

Various techniques were used to analyze the complex system of weathering. Some methods were found to provide better results than others. Fractionation was noted to be

critical for a good analysis on "*...small disturbances...*" (Brooker and Peck 1993) caused by weathering. A better understanding of the mechanical behavior can be inferred by knowing the mineralogy and chemistry of the fractionate. Minor constituents can also be determined more readily. XRD provides a good qualitative determination of the mineralogy but should be complimented by XRF and EDS analyses. EDS analyses provides a wealth of information by allowing an interactive determination of the chemistry through line scans, point analyses, and elemental maps. The technique is qualitative to semi-quantitative, dependent on the type of analyses, but allows for the user to see the specimen under investigation.

FUTURE RESEARCH

This thesis has presented a narrow study of the complex weathering processes in clay shales. A more extensive study would better envelop the physico-chemical role in controlling the residual strength. Pore water chemistry was not included in this study but was noted as a factor influential in the residual strength. Future studies should include this factor with the mineralogical and chemical states. Full mineralogical and chemical descriptions should be obtained through a bulk (<2μm) and fine (<0.5μm) clay fractionate as well as analyzing the bulk sample and coarser fractionates. Thin sectioning of clay shale samples for micromorphology analysis would provide a greater resolution image and allow numerical modeling of the material's surface. Freeze-dried samples should also be used to aid the investigators in analyzing the surface's morphology and chemistry with SEM and EDS.

More studies are needed in this area, on multiple borings in problematic formations, due to clay shale's natural heterogeneity. Creating a database of the residual strength, the physico-chemical role, and the particle characteristics for these materials worldwide would

be an invaluable asset to geotechnical engineers. The effects of the ever-changing environmental conditions could then be better understood with respect to the long-term stability of the slope.

REFERENCES

Ammonette, J.E. and Sanders, R.W. (1994). "Nondestructive techniques for bulk elemental analysis," *Quantitative Methods in Soil Mineralogy*, SSSA Miscellaneous Publication, Madison, Wisconsin.

Anayi, J.T., Boyce, J.R., and Rogers, C.D. (1989). "Modified Bromhead Ring Shear Apparatus," *Geotechnical Testing Journal*, 17(2), 171-173.

ASTM. (2003). *Annual Book of ASTM Standards, Section 4, Construction*. Vol. 04.09, American Society for Testing and Materials, Philadelphia, PA.

Birkeland, P. (1999). *Soils and Geomorphology*, 3rd Ed, Oxford University Press, Inc., New York.

Bishop, A.W., Green, G.E., Garga, V.K., Anderson, A., and Brown, J.D. (1971). "A new ring shear apparatus and its application to the measurement of residual strength," *Gèotechnique*, 21(4), 273-328.

Bjerrum, L. (1967) "Progressive failure in slopes of overconsolidated plastic clay and clay shales," *Journal Soil Mechanics And Foundation Division*, ASCE, 93, 1-49.

Botts, M.E., (1986). *The Effect of Slaking on the Engineering Behavior of Clay Shales*. Ph.D. Dissertation, Department of Civil, Environmental, and Architectural Engineering, University of Colorado.

Brewer, R. and Sleeman, J.R. (1988). *Soil Structure and Fabric*, SR Frankland Pty. Ltd., Melbourne.

Bromhead, E.N. (1979). "A Simple Rnig Shear Apparatus," *Ground Engineering*, 12(5), 40-44.

Bromhead, E.N. (1986) *The Stability of Slopes*, Surrey University Press, Glasgow.

Bromhead, E.N. and Curtis, R.D. (1983). "A Comparison of Alternative Methods of Measuring the Residual Strength of London Clay," *Ground Engineering*, 16(4), 39-41.

Bromhead, E.N. and Dixon, N. (1986). "The field residual strength of London Clay and its correlation with laboratory measurements, especially ring shear tests," *Gèotechnique,* 36(3), 449-452.

Brooker, E. W. and Peck, R. B. (1993). "Rational design treatment of slides in overconsolidated clays and clay shales," *Canadian Geotechnical Journal*, 30, 526-544.

Chigira, M., Wang, W.N., Furuya, T., Kamai, T. (2003). "Geological causes and geomorphological precursors of the Tsaoling landslide triggered by the 1999 Chi-Chi earthquake, Taiwan," *Engineering Geology*, 68, 259-273.

Chigira, M. and Oyama, T. (1999). "Mechanism and effect of chemical weathering of sedimentary rocks," *Engineering Geology*, 55, 3-14.

Clegg, W., Blake, A.J., Gould, R.O., and Main, P. (2001). *Crystal Structure Analysis Principles and Practice*, Oxford University Press, Oxford.

Cullity, B.D. (1978). *Elements of X-ray Diffraction*, 2nd ed., Addison-Wesley Publishing Company, Inc., Reading, MA.

Deere, D.U. and Patton, F.D. (1971). "Slope stability in residual soils," *Proceedings of the Fourth Panamerican Confrence on Soil Mechanics and Foundation Engineering*, Vol. 1, State-of-the-Art Papers, pp. 87-170.

Eid, H.T. (1996). *Drained shear strength of stiff clay for slope stability analyses*, pHD, University of Illinois at Urbana-Champaign.

Erol, O., Lohnes, R.A. and Demirel, T. (1976). "Preparation of Clay-Type Moisture Containing Samples for Scanning Electron Microscopy," *Proceedings of the 9th Annual Scanning Electron Microscopy*, 1, 769-776.

Federal Emergency Management Agency. (2004). "Backgrounder: Landslides and Mudflows," *FEMA*, <http://www.fema.gov/hazards/landslides/landsli.shtm>, (Accessed March 10, 20050.

Fleming, R.W., Spencer, G.S., and Banks, D.C. (1970). *Empirical Study of Behavior of Clay Shale Slopes*, Vol. 1, NCG Technical Report No. 15, U.S. Army Engineer Nuclear Cratering Group, Livermore, CA, December.

Grainger, P. and J. Harris. (1986). "Weathering and slope stability on upper carboniferous mudrocks in south-west England," *Quarterly Journal of Engineering Geology*, Vol. 19, pp. 155-173.

Grim, R.E. (1953). *Clay Mineralogy*, McGraw-Hill, New York.

Harris, A.J. and Watson, P.J. (1997) "Optimal Procedure for the Ring Shear Test," *Ground Engineering*, Technical Note,. 26-28.

Hawkins, A.B. and Privett, K.D. (1985). "Measurement and use of Residual Shear Strength of Cohesive Soils," *Ground Engineering*, 18, 22-29.

Hawkins, A.B., Lawrence, M.S. and Privett, K.D. (1988). "Implications of weathering of on the engineering properties of the Fullers Earth formation," *Gèotechnique*, 38(4), 517-532.

Herrmann, H. G. and Wolfskill, L. A. (1966). *Engineering Properties of Nuclear Craters: Residual Strength of Weak Shales*, WES Technical Report 3-699, Report 5, U.S. Army Engineer Waterways Experiment Station, Vicksburg, MS.

Hvorslev, M.J. (1939). "Torsion Shear Tests and Their Place in the Determination of the Shearing Resistance of Soils," *Proceedings of the American Society for Testing Materials*, 39, 999-1022.

The International Centre for Diffraction Data®. (2004). *Joint Committee on Powder Diffraction Standards (JCPDS) Powder Diffraction File system.*

Johns, E.A., Burnett, R.G. and Craig, C.I. (1963). "Oahe Dam: Influence of shale on Oahe power structures design," *Journal Soil Mechanics And Foundation Division, ASCE*, 89, 95-113.

Kenney, T. C. (1967). "The influence of mineralogical composition on the residual strength of natural soils," *Proceedings of the Geotechnical Conference on Shear Strength of Cohesive Soils*, Oslo, pp. 123-129.

Knight, D.K. (1963). "Oahe Dam, geology, embankments and cut slopes," *Journal of the Soil Mechanics and Foundation Division*, ASCE, 89(2), 99-125.

Loughnan, F. C. (1969). *Chemical Weathering of the Silicate Minerals*, American Elsevier Publ. Co., Inc., New York.

Lupini, JF, Skinner, A.E. and Vaughn, V.R. (1981). "The drained residual strength of cohesive soils," *Gèotechnique*, 31(2), 181-213.

Lutenegger AJ, Wollenhaupt, N.C., Handy, R.L. (1979). "Laboratory simulation of shale expansion by induced gypsum growth," *Canadian Geotechnical Journal*, Vol. 16, pp. 405-409.

Manfredini, G., Martinetti, S., Ribacchi, R., Santoro, V.M., Sciotti, M., and Silvestri, T. (1981). "An earthflow in the Sinni Valley (Italy)," *Proceedings of the 10th International. Conference on Soil Mechanics and Foundation Engineering*, 3, 457-462.

McClure, J.G. (1980). *Physicochemical Investigation of Shale Slaking*, PhD Thesis, University of California, Berkley.

Mesri, G., and Cepeda-Diaz, AF (1986). "Residual shear strength of clays and shales," *Gèotechnique*, 36(2), 269–274.

Mitchell, J.K. (1976). *Fundamentals of Soil Behavior*, John Wiley & Sons, Inc., New York, 50-200.

Moore, D.M. and Reynolds, R.C. (1997). *X-ray Diffraction and the Identification and Analysis of Clay Minerals*, 2nd ed., Oxford Universities Press, Oxford.

Moore, R. (1991). "The chemical and mineralogic controls upon the residual strength of pure and natural clays," *Gèotechnique*, 41(1), 35-47.

Moore, R. and Brunsden, D. (1996). "Physico-chemical effects on the behavior of a coastal mudslide," *Gèotechnique*, Vol. 46, No. 2, pp. 259-278.

Morgenstern, N.R., and Eigenbrod, K.D. (1974). "Classification of argillaceous soils and rock," *Journal Geotechnical Engineering Division*, 100, 1137-1156.

Nemecz, E. 1981. *Clay Minerals*, Akadémiai Kiadó, Budapest.

Nichols, T.C., Collins, D.S., and Davidson, R.D. (1986). "*In situ* and laboratory tests of the Pierre shale near Hayes South Dakota- a characterization of engineering behavior," *Canadian Geotechnical Journal*, 23, 181-194.

Nichols, T.C. (1992). *Rebound in the Pierre Shale of South Dakota and Colorado-field and laboratory evidence of physical conditions related to processes of shale rebound, Open-file report 90-440*, United States Department of the Interior Geological Survey.

Ollier, C.D. (1969). *Weathering*, Oliver & Boyd, Edinburgh.

Olson, R.E. (1974). "Shearing strengths of kaolinite, illite, and montmorillonite," *Journal of the Geotechnical Engineering Division*, 100(11), 1215-1229.

Oyama, T. and Chigira, M. (1999). "Weathering rate of mudstone and tuff on old unlined tunnel walls," *Engineering Geology*, 55,15-28.

Pederstad, K. and JØrgensen, P. (1985). "Weathering in a marine clay during postglacial time," *Clay Minerals*, 20, 447-491.

Perry, E.F. and Andrews, D.E. (1984). "Slaking modes of geologic materials and their impact on embankment stabilization," *Transportation Research Record 873*, Transportation Research Board, Washington, D.C., 15–21.

Picard, M.D. (1971). "Classification of fine-grained sedimentary rocks," *Journal of Sedimentary Petrology*, 41: 179-195.

Potter, P.E., Maynard, J.B., and Pryor, W.A. (1980). *Sedimentology of Shale*, Springer Verlag, New York.

Pye, K. and Miller, J.A. (1990). "Chemical and biochemical weathering of pyritic mudrocks in a shale embankment," *Quarterly Journal of Engineering Geology*, 23, 365-381.

Ritter, D.L., Kochel, R.C., and Miler, J.R. (2002). *Process Geomorphology*, 4th Ed., McGraw-Hill Higher Education, Boston.

Russell, D.J. and Parker, A. (1979). "Geotechnical, mineralogical and chemical interrelationships in weathering profiles of an overconsolidated clay," *Quarterly Journal of Engineering Geology*, 12, 107-116.

Sammut, J., White, I. and Melville, M.D. (1996). "Acidification of an estuarine tributary in Eastern Australia due to drainage of acid sulfate soils," *Marine and Freshwater Research*, 47, 669-684.

Schaefer, V.R. (2002). "Residual strength and back analysis of slopes in Pierre Shale," *Proceedings of the 3rd International Conference on Landslides, Slope Stability & the Safety of Infrastructures*, Edited by J.S.Y. Tan, July 11-12, Singapore, 407-414.

Schuster, R.L. (1996). "Socioeconomic Significance of Landslides," Chapter 2 in *Landslides Investigation and Mitigation, Special Report 247*, edited by A.K. Turner and R.L. Schuster, Transportation Research Board, National Academy Press, Washington, D.C., pp. 12-35.

Schultz, L.G. (1978). *Mixed-Layer Clay in the Pierre Shale and Equivalent Rocks, Northern Great Plains*, Geological Survey Professional Paper 1064-B, United States Government Printing Office, Washington.

Schultz, L.G., Tourtelot, H.A., Gill, J.R., and Boerngen, J.G. (1980). *Composition and Properties of the Pierre Shale and Equivalent Rocks, Northern Great Plains Regions*, Geological Survey Professional Paper 1064-B, United States Government Printing Office, Washington.

Shurr, G.W. (1980). *Geological Setting of the Pierre Shale, Northern Great Plains*, Open-file report 80-675, United States Department of the Interior Geological Survey.

Skempton, A.W. (1964). "Long-term stability of clay slopes," Fourth Rankine Lecture, *Gèotechnique*, 14, 77.

Skempton, A.W. (1985). "Residual strength of clays in landslides, folded strata and the laboratory," *Gèotechnique*, 35(1), 3-18.

Slaymaker, O. (1988). "Slope erosion and mass movement in relation to weathering in geochemical cycles," *Physical and Chemical Weathering in Geochemical Cycles*, 83-111.

Smart, P. and Tovey, N.K. (1982). *Electron Microscopy of Soils and Sediments: Techniques*, Clarendon Press, Oxford.

Spears, D.A. 1980. "Towards a Classification of Shales," *Journal of the Geological Society*, 137, 123-130.

Stark, T.D. (1990). "Measurement of Drained Residual Strength of Overconsolidated Clays," *Transportation Research Record*, 1479, 26-34.

Stark, T.D. (1995). "Drained residual strength of overconsolidated clays," *Engineering Properties and Practice in Overconsolidated Clays, Transport. Res. Rec. 1479,* 26-34.

Stark, T.D and Eid, H.T. (1992). "Comparison of Field and Laboratory Residual Strengths," *Stability and Performance of Embankments and Slopes-II*, v. 1, 876-889.

Stark, T.D. and Eid, H.T. (1993) "Modified Bromhead Ring Shear Apparatus," *Geotechnical Testing Journal,* 16(1), 100-107.

Stark, T.D. and Eid, H.T. (1994) "Drained Residual Strength of Cohesive Soils," *Journal of Geotechnical Engineering*, 120(5), 856-871.

Stark, T.D. and Eid, H.T. (1997). "Slope Stability Analyses in Stiff Fissured Clays," *Journal of Geotechnical and Geoenvironmetal Engineering*, 123(4), 335-343.

Stark, T.D and Vettel, J. (1992). "Bromhead Ring Shear Test Procedure," *ASTM Geotechnical Testing Journal*, 15(1), 23-32.

Starkey, H. C., Blackmon, P. D., and Hauff, P. L. (1984). "The routine mineralogical analyses of clay-bearing samples," *U.S. Geological Survey bulletin 1563.*

Steward, H.E. and Cripps, J.C. (1983). "Some engineering implications of chemical weathering of pyritic shale," *Quarterly Journal of Engineering Geology*, 16, 281-289.

Taylor, R.K. and Cripps, J.C. (1987). "Weathering effects: slopes in mudrocks and over-consolidated clays," Chapter 13 in *Slope Stability*, M.G.Anderson and K.S. Richards, John Wiley & Sons, Ltd., pp. 405-445.

Terzaghi, K. (1936). "Stability of slopes of natural clay," *Proceedings of the First International Conference on Soil Mechanics and Foundation Engineering*, Harvard, 1, 161-165.

Terzaghi, K. (1939). "Soil mechanics a new chapter in engineering science," *Journal of the Institution of Civil Engineers*, 12,106-141.

Tika, T.E., Vaughan, P.R. and Lemos, L.J. (1996). "Fast shearing of pre-existing shear zones in soil," *Gèotechnique*, 46(2), 197-233.

Tourtelot, H.A. (1962). *Preliminary Investigation of the Geologic Setting and Chemical Composition of the Pierre Shale, Great Plains Region*, U.S. Geological Survey Professional Paper 390.

Tovey, N.K. and Yan, W.K. (1973). "The preparation of soils and other geological materials for the SEM," *Proceedings of the International Symposium on Soil Structure*, Gothenburg, Sweden, 59-68.

Townsend, F. C. and Gilbert, P. A. (1973). "Tests to measure residual strengths of some clay shales," *Géotechnique*, 23(2), 267-271.

Townsend, F.C. and Gilbert, P.A. (1976). "Effects of specimen type on the residual strength of clays and clay shales," *Soil Specimen Preparation for Laboratory Testing, ASTM STP 599*, 43-65.

Underwood, L.B. (1967). "Classification and identification of shales," *Journal of Soil Mechanics and Foundation Engineering Division*, ASCE, 93, 97-116.

U.S. Army Corps of Engineers. (1997). "Oahe Dam Powerhouse Slope Analysis," *Performance Report, Oahe Dam and Lake Oahe, Missouri River near Pierre, South Dakota*, Omaha District, Omaha, NE.

U.S. Army Corps of Engineers. (2000). *Geotechnical Re-evaluation Station 61+00 Oahe dam Pierre, South Dakota, Dam Safety Task Group, Dam Safety Major Rehabilitation, Phase II*, v. 1, General, Northwestern Division/MRR, Omaha District, Omaha, NE.

U.S. Army Corps of Engineers. (2004). "Oahe Dam and Power Plant," Omaha District, Omaha, NE. < http://www.nwo.usace.army.mil/html/Lake_Proj/oahe/dam.html>. (Accessed March 9 2005).

van Olphen, H. (1977). *An Introduction to Clay Colloid Chemistry*, John Wiley & Sons Inc., New York.

Weaver, C.E. (1989). *Clays, Muds and Shales*, Elsevier, Amsterdam.

Welton, J.E. (1984). *SEM Petrology Atlas*, The American Association of Petroleum Geologists, Tulsa, Oklahoma.

Woolfson, M.M. (1997). *An Introduction to X-ray Crystallography*, 2nd ed., Cambridge University Press, Cambridge.

Wykeham Farrance Limited. (2004). "Torsional & Simple Shear," Wykeham Farrance, <http://www.wfi.co.uk/torsions.htm>, (Accessed March 9, 2005).

Yong, R.N. and Sheeran, D.E. (1973). "Fabric unit interaction and soil behavior," *Proceedings of the International Symposium on Soil Structure*, Gothenburg, Sweden, 176-183.

ACKNOWLEDGEMENTS

The author would like to thank Vernon R. Schaefer, Professor of Geotechnical Engineering, for his guidance, advice, and understanding during the research of this project. His support and assistance helped guide the author through the research and the completion of this Thesis. The author is also indebted to the advice of Robert A. Lohnes, University Professor Emeritus, in the early stages of this study.

The author wishes to thank the MARL staff at Iowa State University for their help in the analyses of this study. The author is grateful for the contribution and advice from Drs. Scott Schlorholtz and Warren Straszheim of ISU. The author appreciates the help of Ashley Schwaller in running x-ray diffraction for the investigation. Drs. David White and Michael Thompson are thanked for their advice on mineralogy and service on the author's committee. The author is grateful for the help and contributions of Sherry Voros during the investigation. Thanks also goes to the engineers of the U.S. Army Corps of Engineers Project Office in Pierre, SD for their assistance in obtaining the samples of Pierre Shale.

The author would like to thank his parents for their love, understanding, and support throughout his educational career. Their encouragement was always appreciated but not always showed. The author also thanks his brother and sister, friends and colleagues for their patience during the coarse of this study.

APPENDIX A

RING-SHEAR RESULTS

DETERMINATION OF THE RESIDUAL SHEAR STRENGTH
IN THE BROMHEAD RING SHEAR APPARATUS

Sample Description:	WEATHERED X0 PIERRE CLAY SHALE	Boring:	PZT50/5.42
Sample Location:	OAHE DAM SITE, SD, USA	Performed By:	MB
Sample No:	Weathering Cycle 208 foot	Date:	5/9/2004
Depth ft:	208	Depth, m:	63
Preparation :	Remoulded at	Initial water content (%)	41.5
		Remolded Dry Density (g/cm^3)	1.49
	Controls:	Hydrated	Multistage
		Material Passed #50	

Stage	Normal effective stress kPa	Residual Shear stress kPa	Tan phi
1	100.95	12.8	0.13
2	198.91	23.9	0.12
3	394.84	47.4	0.12

Dimensions:

Inner radius mm :	50
Outer radius mm :	35
Thickness mm :	5

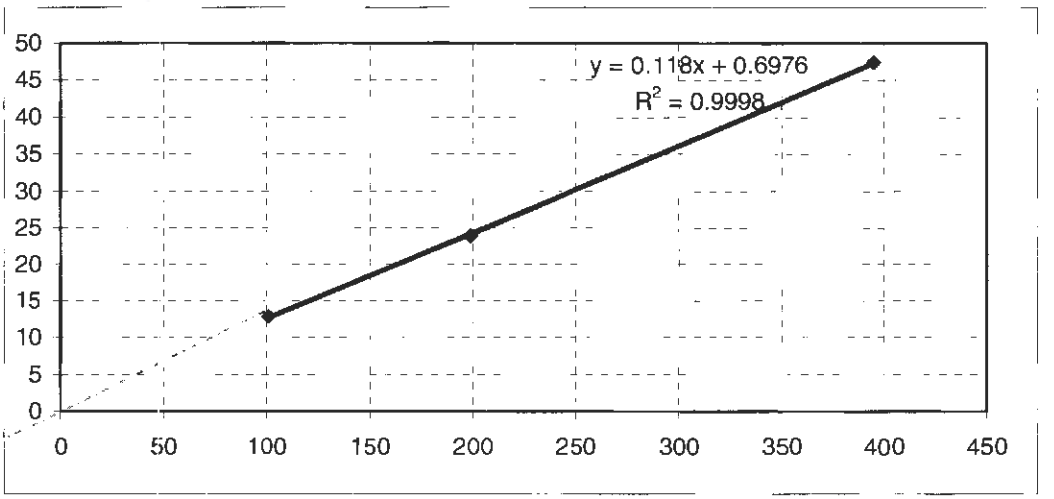

Shear parameters	c', kPa	ϕ'	r^2
Best fit straight line	0.7	6.8	0.999
Line through origin	0	6.9	0.999

Rate of Angular Displacement		
Shearing Stage for 1 revolution	0.12 mm/min	0.16 deg/min
Strain Rate for Normal Stresses	0.04 mm/min	0.048 deg/min

Figure A.1. 63.0 meter (208 ft), weathering cycle X0, Pierre Shale, Oahe Dam Site, PZT50-5.42, Bromhead Ring Shear report

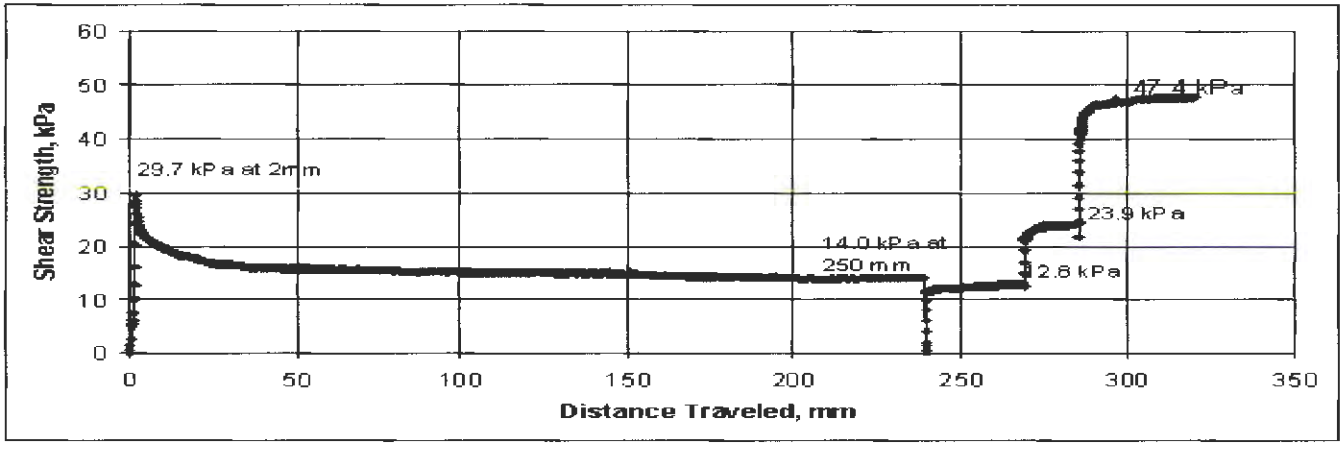

Figure A.2. 63.0 meter (208 ft), weathering cycle X0, Pierre Shale, Oahe Dam Site, PZT50-5.42, residual strength plot

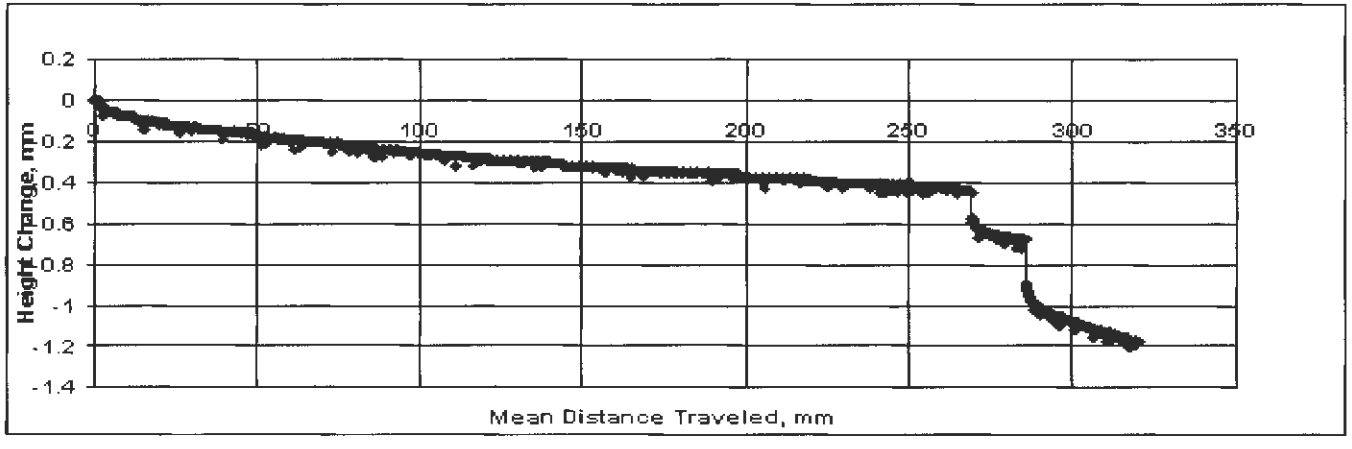

Figure A.3. 63.0 meter (208 ft), weathering cycle X0, Pierre Shale, Oahe Dam Site, PZT50-5.42, settlement plot

DETERMINATION OF THE RESIDUAL SHEAR STRENGTH
IN THE BROMHEAD RING SHEAR APPARATUS

Sample Description:	WEATHERED X1 PIERRE CLAY SHALE	Boring:	PZT50/5.42
Sample Location:	OAHE DAM SITE, SD, USA	Performed By:	MB
Sample No:	Weathering Cycle 208 foot	Date:	5/9/2004
Depth ft:	208	Depth, m:	63
Preparation :	Remoulded at	Initial water content (%)	38.0
		Remolded Dry Density (g/cm^3)	1.61
	Controls:	Hydrated	Multistage
		Material Passed #50	

Stage	Normal effective stress kPa	Residual Shear stress kPa	Tan phi
1	100.95	11.2	0.11
2	198.91	22.3	0.11
3	394.84	44.7	0.11

Dimensions:
Inner radius mm : 50
Outer radius mm : 35
Thickness mm : 5

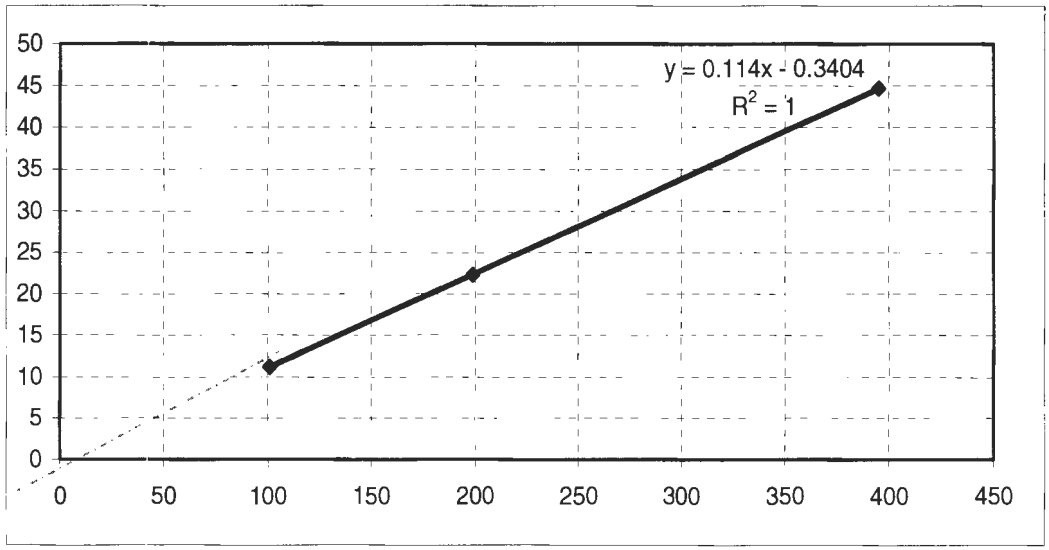

Shear parameters	c', kPa	ϕ'	r^2
Best fit straight line	~0	6.5	1
Line through origin	0	6.5	0.999

Rate of Angular Displacement

Shearing Stage for 1 revolution	0.12 mm/min	0.16 deg/min
Strain Rate for Normal Stresses	0.04 mm/min	0.048 deg/min

Figure A.4. 63.0 meter (208 ft), weathering cycle X1, Pierre Shale, Oahe Dam Site, PZT50-5.42, Bromhead Ring Shear report

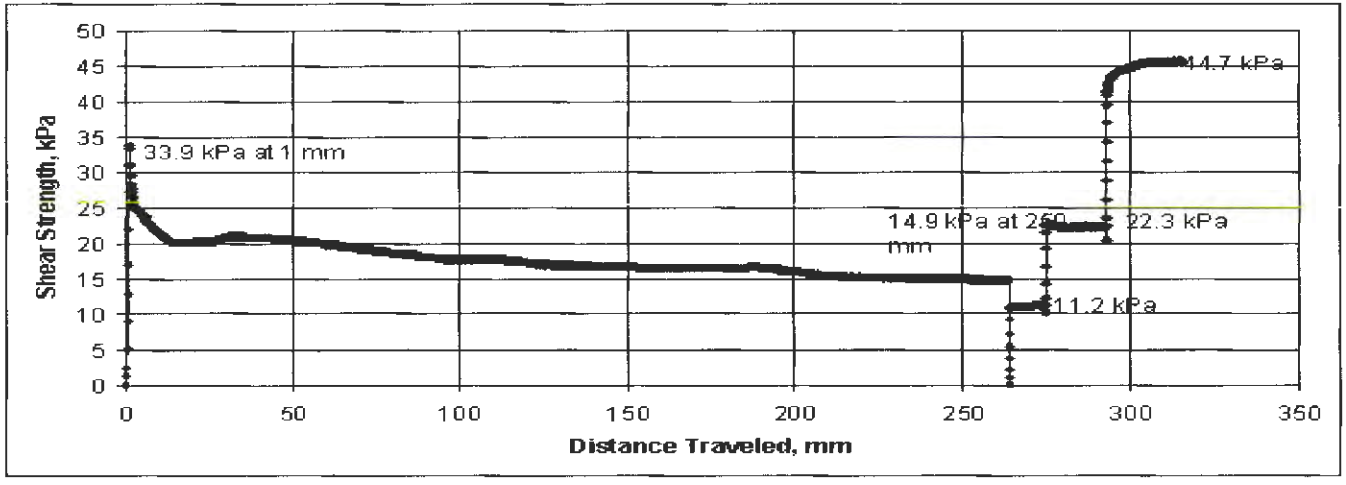

Figure A.5. 63.0 meter (208 ft), weathering cycle X1, Pierre Shale, Oahe Dam Site, PZT50-5.42, residual strength plot

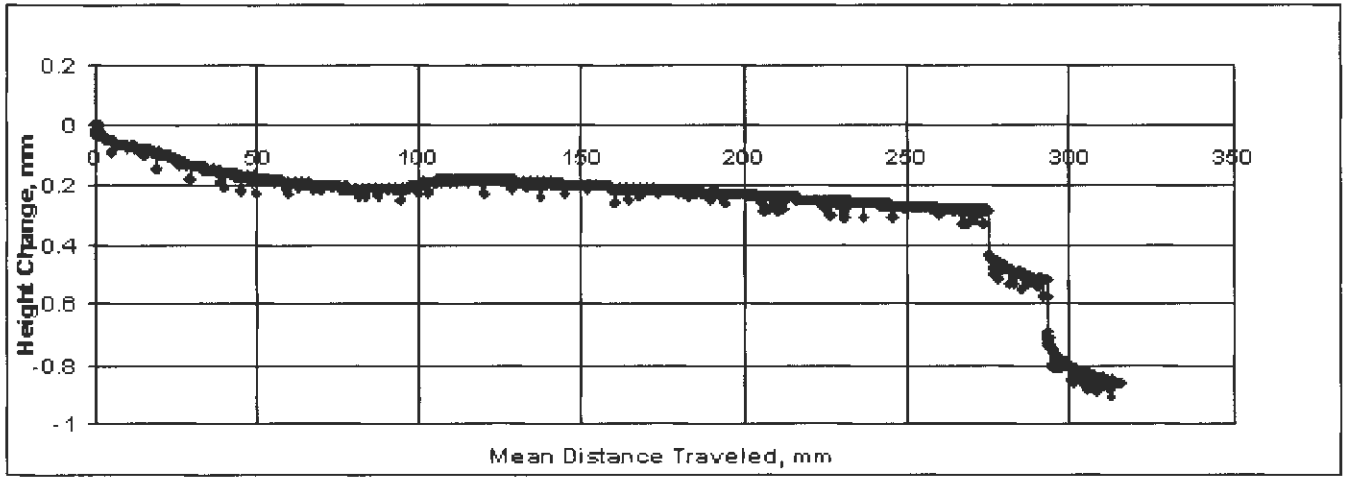

Figure A.6. 63.0 meter (208 ft), weathering cycle X1, Pierre Shale, Oahe Dam Site, PZT50-5.42, settlement plot

DETERMINATION OF THE RESIDUAL SHEAR STRENGTH
IN THE BROMHEAD RING SHEAR APPARATUS

Sample Description:	WEATHERED X2 PIERRE CLAY SHALE	Boring:	PZT50/5.42
Sample Location:	OAHE DAM SITE, SD, USA	Performed By:	MB
Sample No:	Weathering Cycle 208 foot	Date:	6/8/2004
Depth ft:	208	Depth, m:	63
Preparation :	Remoulded at	Initial water content (%)	37.2
		Remolded Dry Density (g/cm^3)	1.53
	Controls:	Hydrated	Multistage
		Material Passed #50	

Stage	Normal effective stress kPa	Residual Shear stress kPa	Tan phi
1	100.95	10.6	0.11
2	198.91	21.2	0.11
3	394.84	43.9	0.11

Dimensions:

Inner radius mm :	50
Outer radius mm :	35
Thickness mm :	5

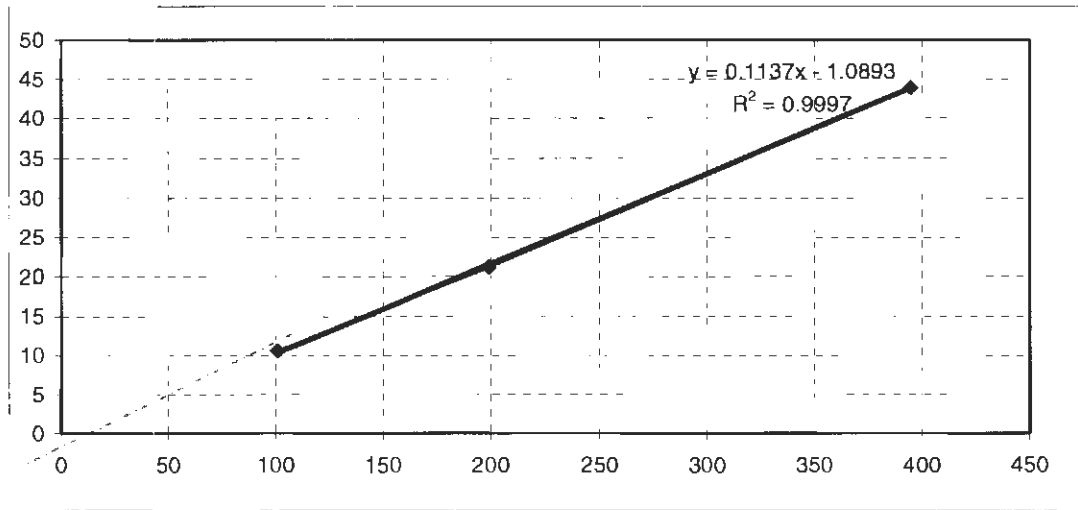

Shear parameters	c', kPa	ϕ'	r^2
Best fit straight line	~0	6.5	0.999
Line through origin	0	6.3	0.999

Rate of Angular Displacement

Shearing Stage for 1 revolution	0.12 mm/min	0.16 deg/min
Strain Rate for Normal Stresses	0.04 mm/min	0.048 deg/min

Figure A.7. 63.0 meter (208 ft), weathering cycle X2, Pierre Shale, Oahe Dam Site, PZT50-5.42, Bromhead Ring Shear report

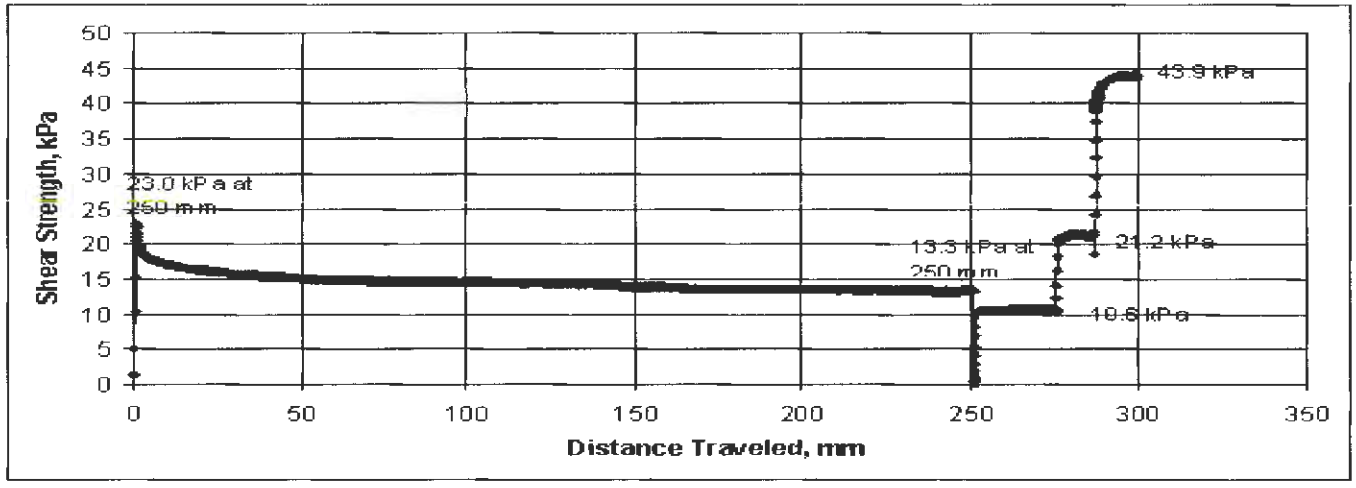

Figure A.8. 63.0 meter (208 ft), weathering cycle X2, Pierre Shale, Oahe Dam Site, PZT50-5.42, residual strength plot

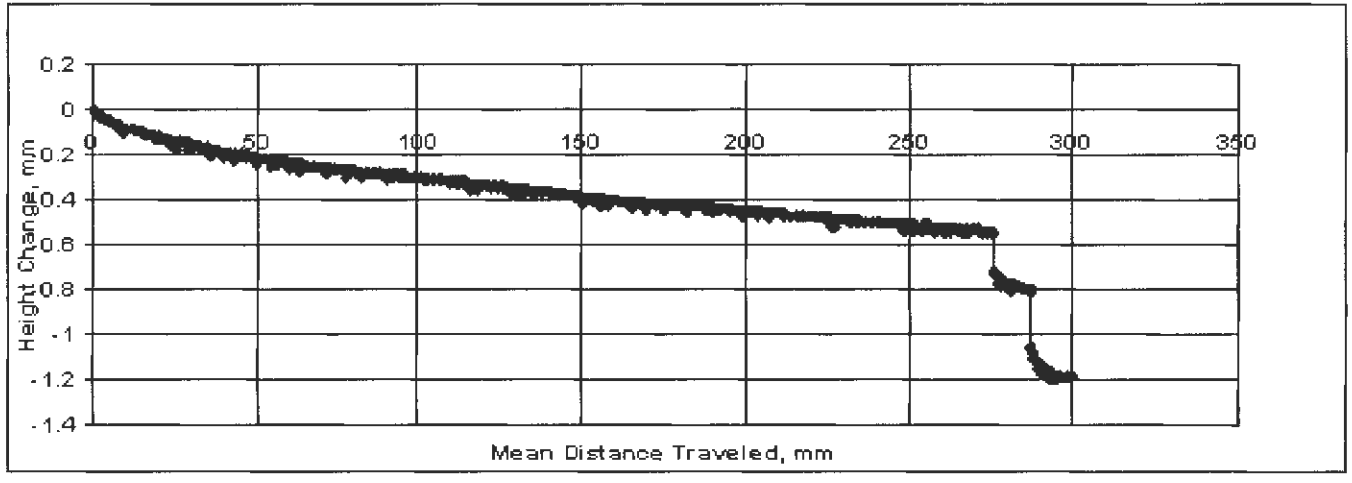

Figure A.9. 63.0 meter (208 ft), weathering cycle X2, Pierre Shale, Oahe Dam Site, PZT50-5.42, settlement plot

DETERMINATION OF THE RESIDUAL SHEAR STRENGTH
IN THE BROMHEAD RING SHEAR APPARATUS

Sample Description:	WEATHERED X3 PIERRE CLAY SHALE	Boring:	PZT50/5.42
Sample Location:	OAHE DAM SITE, SD, USA	Performed By:	MB
Sample No:	Weathering Cycle 208 foot	Date:	5/9/2004
Depth ft:	208	Depth, m:	63
Preparation :	Remoulded at	Initial water content (%)	38.0
		Remolded Dry Density (g/cm^3)	1.52
	Controls:	Hydrated	Multistage
		Material Passed #50	

Stage	Normal effective stress kPa	Residual Shear stress kPa	Tan phi
1	100.95	11.1	0.11
2	198.91	21	0.11
3	394.84	41.6	0.11

Dimensions:

Inner radius mm :	50
Outer radius mm :	35
Thickness mm :	5

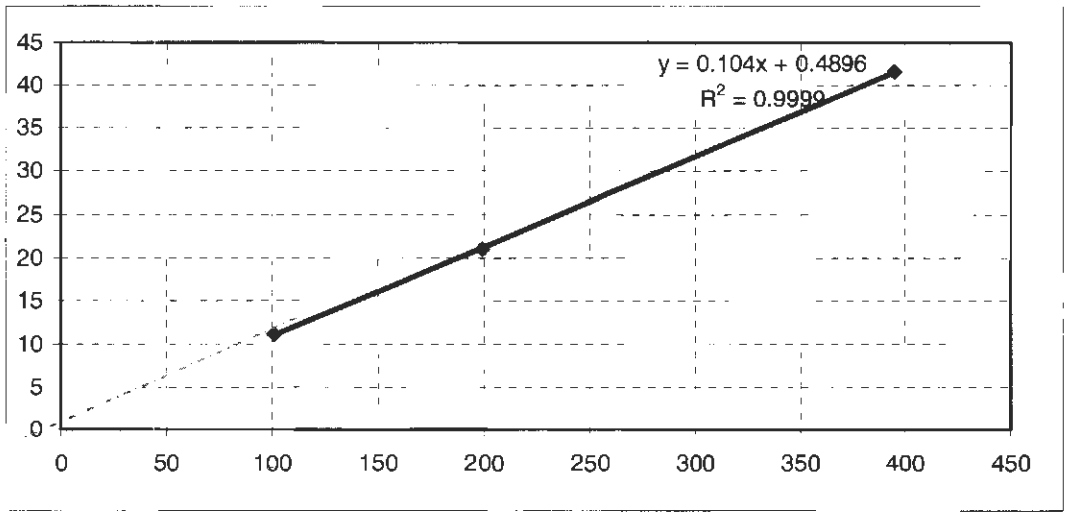

Shear parameters	c', kPa	ϕ'	r^2
Best fit straight line	0.5	6.0	0.999
Line through origin	0	6.1	0.999

Rate of Angular Displacement		
Shearing Stage for 1 revolution	0.12 mm/min	0.16 deg/min
Strain Rate for Normal Stresses	0.04 mm/min	0.048 deg/min

Figure A.10. 63.0 meter (208 ft), weathering cycle X3, Pierre Shale, Oahe Dam Site, PZT50-5.42, Bromhead Ring Shear report

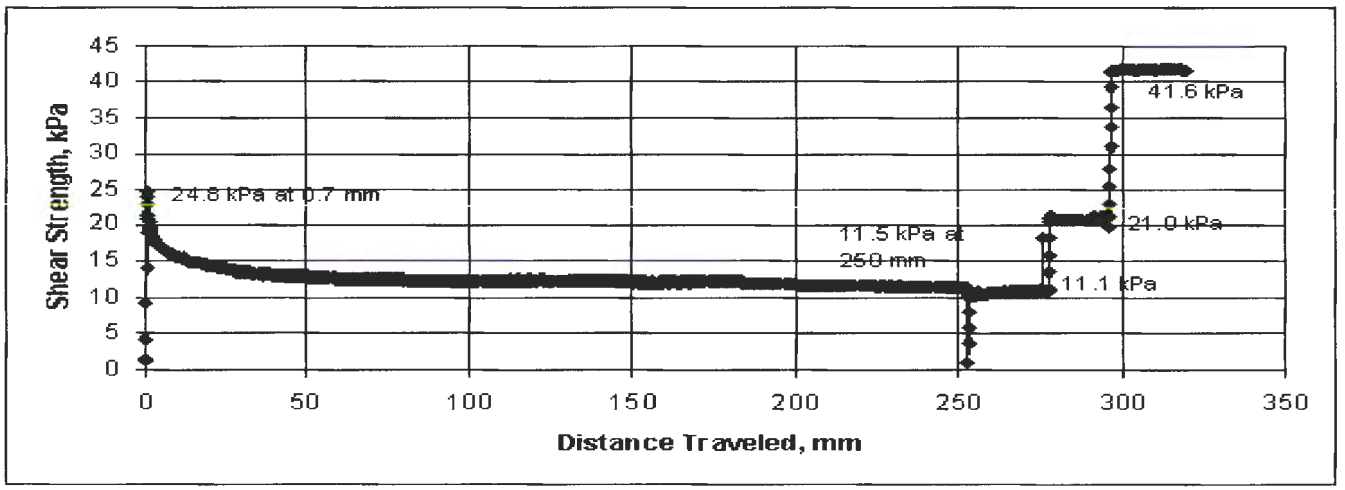

Figure A.11. 63.0 meter (208 ft), weathering cycle X3, Pierre Shale, Oahe Dam Site, PZT50-5.42, residual strength plot

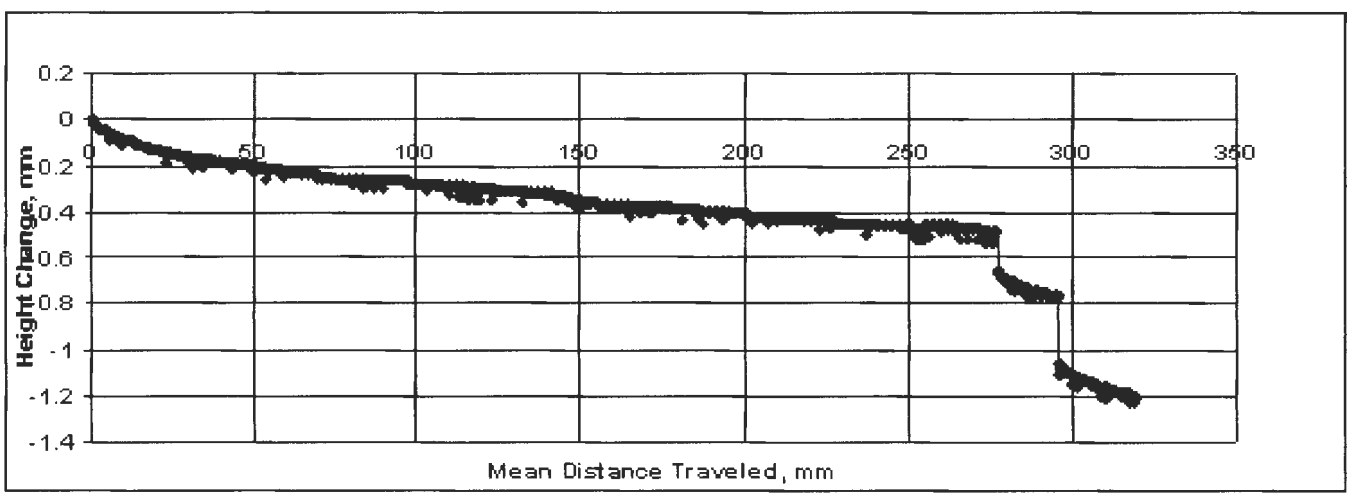

Figure A.12. 63.0 meter (208 ft), weathering cycle X3, Pierre Shale, Oahe Dam Site, PZT50-5.42, settlement plot

DETERMINATION OF THE RESIDUAL SHEAR STRENGTH
IN THE BROMHEAD RING SHEAR APPARATUS

Sample Description:	WEATHERED X4 PIERRE CLAY SHALE	Boring:	PZT50/5.42
Sample Location:	OAHE DAM SITE, SD, USA	Performed By:	MB
Sample No:	Weathering Cycle 208 foot	Date:	5/26/2004
Depth ft:	208	Depth, m:	63
Preparation :	Remoulded at	Initial water content (%)	41.1
		Remolded Dry Density (g/cm^3)	1.48
	Controls:	Hydrated	Multistage
		Material Passed #50	

Stage	Normal effective stress kPa	Residual Shear stress kPa	Tan phi
1	100.95	10.1	0.10
2	198.91	19.1	0.10
3	394.84	38.6	0.10

Dimensions:

Inner radius mm :	50
Outer radius mm :	35
Thickness mm :	5

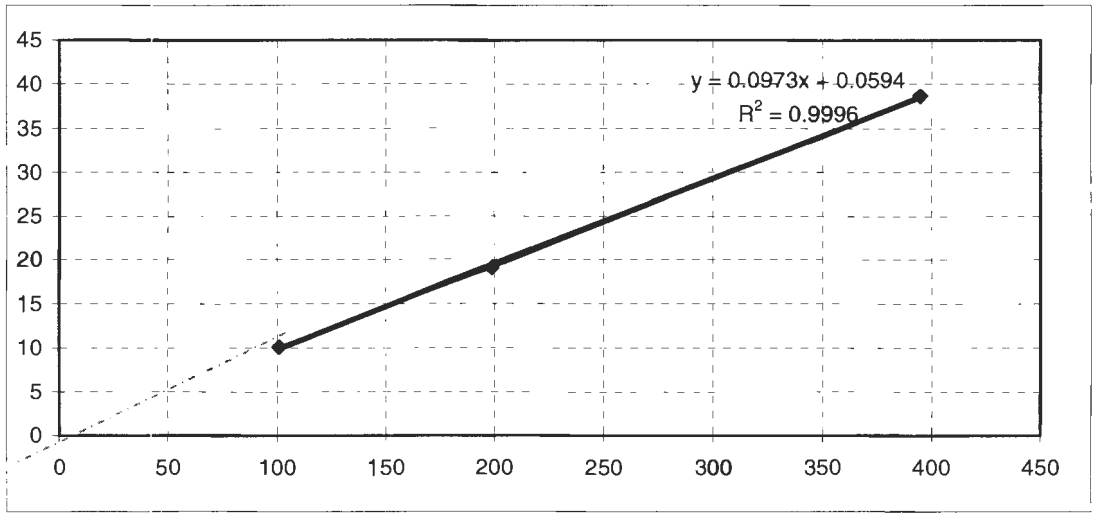

Shear parameters	c', kPa	ϕ'	r^2
Best fit straight line	~0	5.6	0.999
Line through origin	0	5.6	0.999

Rate of Angular Displacement

Shearing Stage for 1 revolution	0.12 mm/min	0.16 deg/min
Strain Rate for Normal Stresses	0.04 mm/min	0.048 deg/min

Figure A.13. 63.0 meter (208 ft), weathering cycle X4, Pierre Shale, Oahe Dam Site, PZT50-5.42, Bromhead Ring Shear report

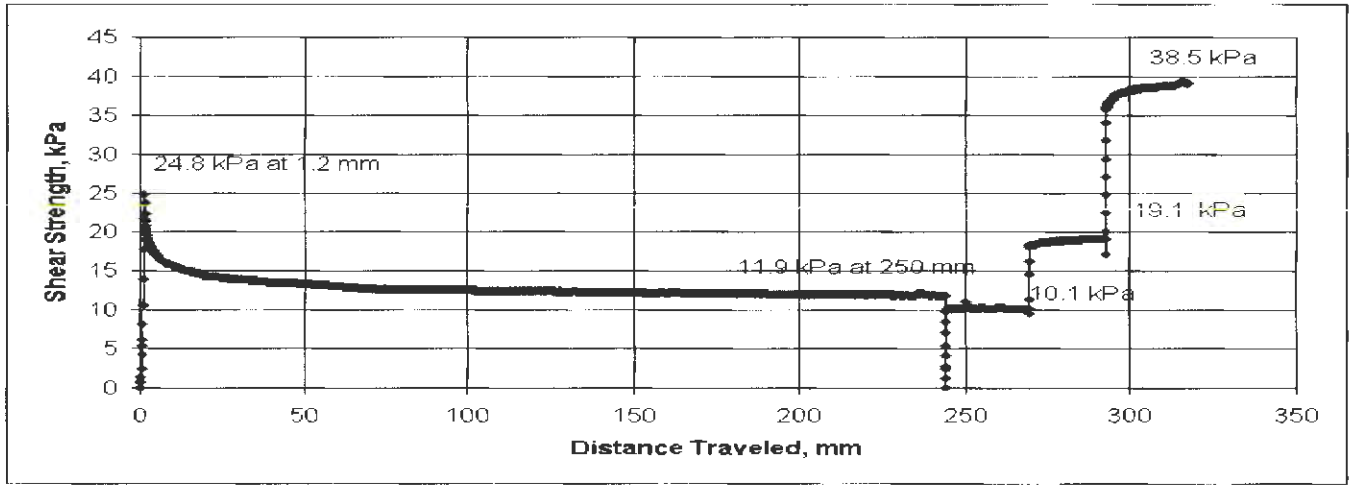

Figure A.14. 63.0 meter (208 ft), weathering cycle X4, Pierre Shale, Oahe Dam Site, PZT50-5.42, residual strength plot

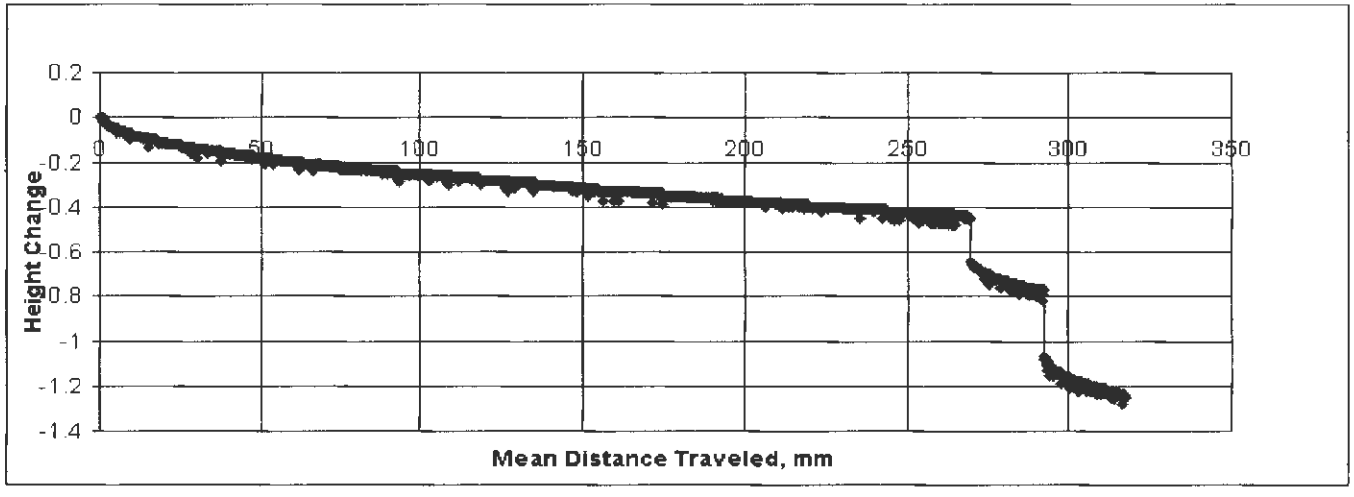

Figure A.15. 63.0 meter (208 ft), weathering cycle X4, Pierre Shale, Oahe Dam Site, PZT50-5.42, settlement plot

DETERMINATION OF THE RESIDUAL SHEAR STRENGTH
IN THE BROMHEAD RING SHEAR APPARATUS

Sample Description:	WEATHERED X4 PIERRE CLAY SHALE	Boring:	PZT50/5.42
Sample Location:	OAHE DAM SITE, SD, USA	Performed By:	MB
Sample No:	Weathering Cycle 208 foot	Date:	5/9/2004
Depth ft:	208	Depth, m:	63
Preparation :	Remoulded at	Initial water content (%)	37.2
		Remolded Dry Density (g/cm^3)	1.55
	Controls:	Hydrated	Multistage
		Material Passed #50	

Stage	Normal effective stress kPa	Residual Shear stress kPa	Tan phi
1	100.95	9.7	0.10
2	198.91	17.8	0.09
3	394.84	37	0.09

Dimensions:

Inner radius mm :	50
Outer radius mm :	35
Thickness mm :	5

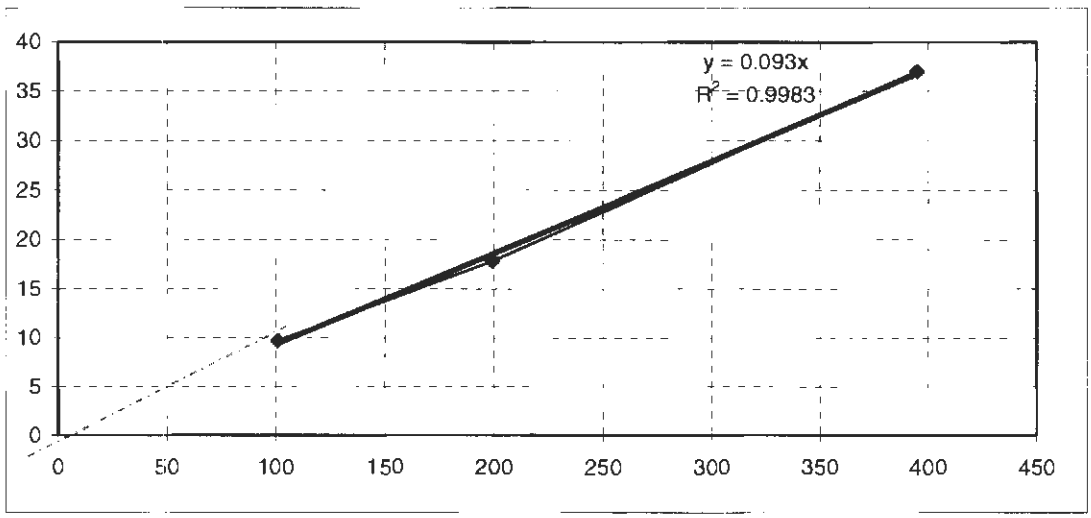

Shear parameters	c', kPa	ϕ'	r^2
Best fit straight line	~0	5.4	0.998
Line through origin	0	5.3	0.998

Rate of Angular Displacement

Shearing Stage for 1 revolution	0.12 mm/min	0.16 deg/min
Strain Rate for Normal Stresses	0.04 mm/min	0.048 deg/min

Figure A.16. 63.0 meter (208 ft), weathering cycle X5, Pierre Shale, Oahe Dam Site, PZT50-5.42, Bromhead Ring Shear report

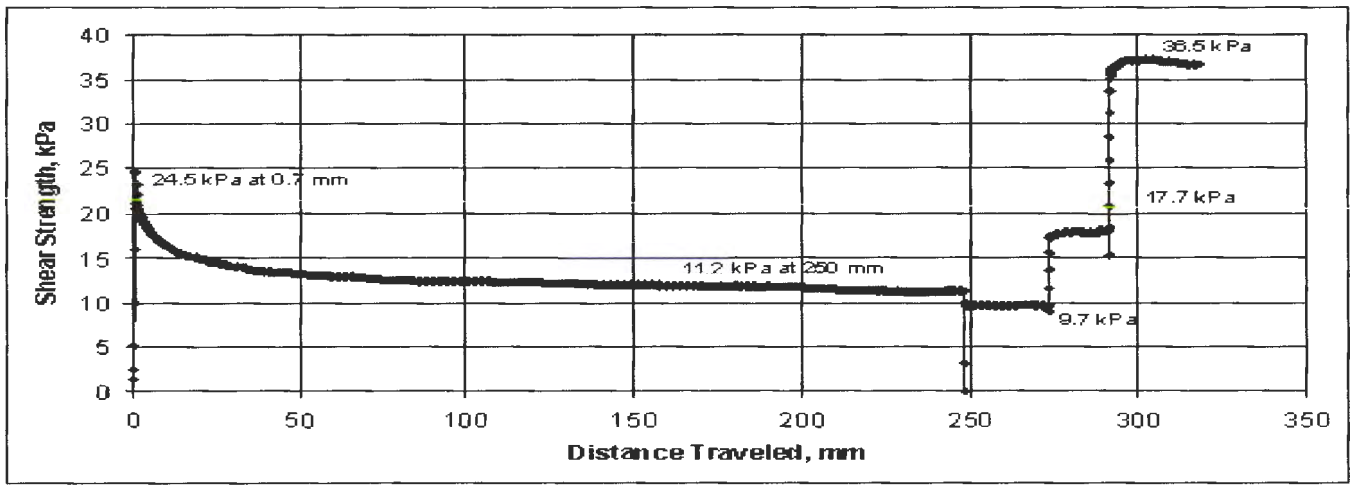

Figure A.17. 63.0 meter (208 ft), weathering cycle X5, Pierre Shale, Oahe Dam Site, PZT50-5.42, residual strength plot

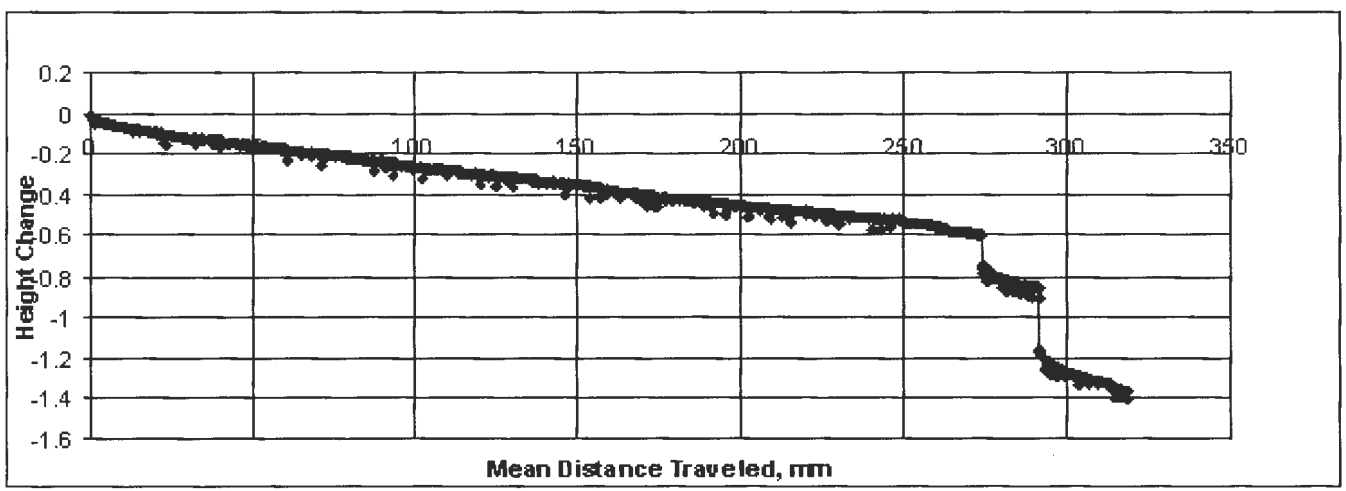

Figure A.18. 63.0 meter (208 ft), weathering cycle X5, Pierre Shale, Oahe Dam Site, PZT50-5.42, settlement plot

DETERMINATION OF THE RESIDUAL SHEAR STRENGTH
IN THE BROMHEAD RING SHEAR APPARATUS

Sample Description:	WEATHERED X0 PIERRE CLAY SHALE	Boring:	PZT50/5.42
Sample Location:	OAHE DAM SITE, SD, USA	Performed By:	MB
Sample No:	Weathering Cycle 210 foot	Date:	6/10/2004
Depth ft:	210	Depth, m:	64
Preparation :	Remoulded at	Initial water content (%)	35.5
		Remolded Dry Density (g/cm^3)	1.57
	Controls:	Hydrated	Multistage
		Material Passed #50	

Stage	Normal effective stress kPa	Residual Shear stress kPa	Tan phi
1	100.95	11.4	0.11
2	198.91	20.5	0.10
3	394.84	42.3	0.11

Dimensions:

Inner radius mm :	50
Outer radius mm :	35
Thickness mm :	5

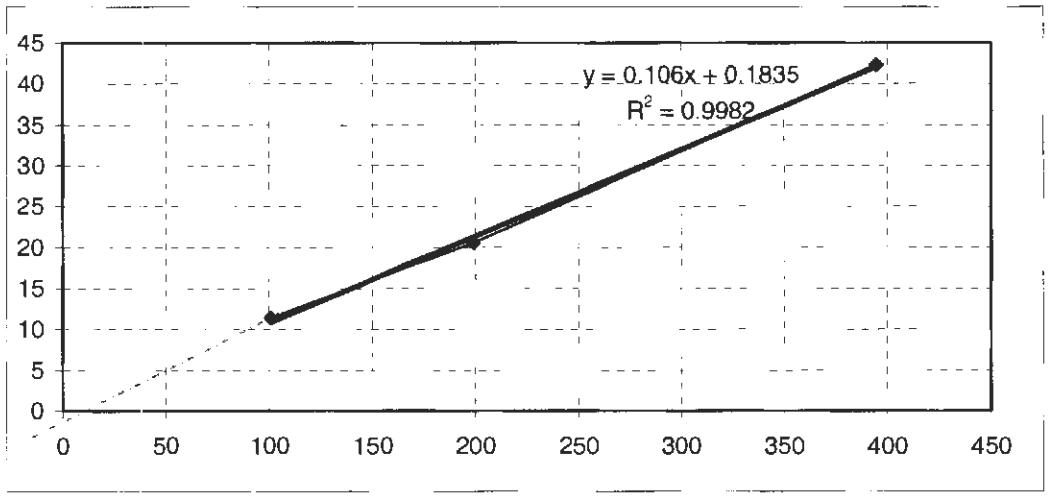

Shear parameters	c', kPa	φ'	r^2
Best fit straight line	0.2	6.1	0.998
Line through origin	0	6.1	0.998

Rate of Angular Displacement		
Shearing Stage for 1 revolution	0.12 mm/min	0.16 deg/min
Strain Rate for Normal Stresses	0.04 mm/min	0.048 deg/min

Figure A.19. 63.6 meter (210 ft), weathering cycle X0, Pierre Shale, Oahe Dam Site, PZT50-5.42, Bromhead Ring Shear report

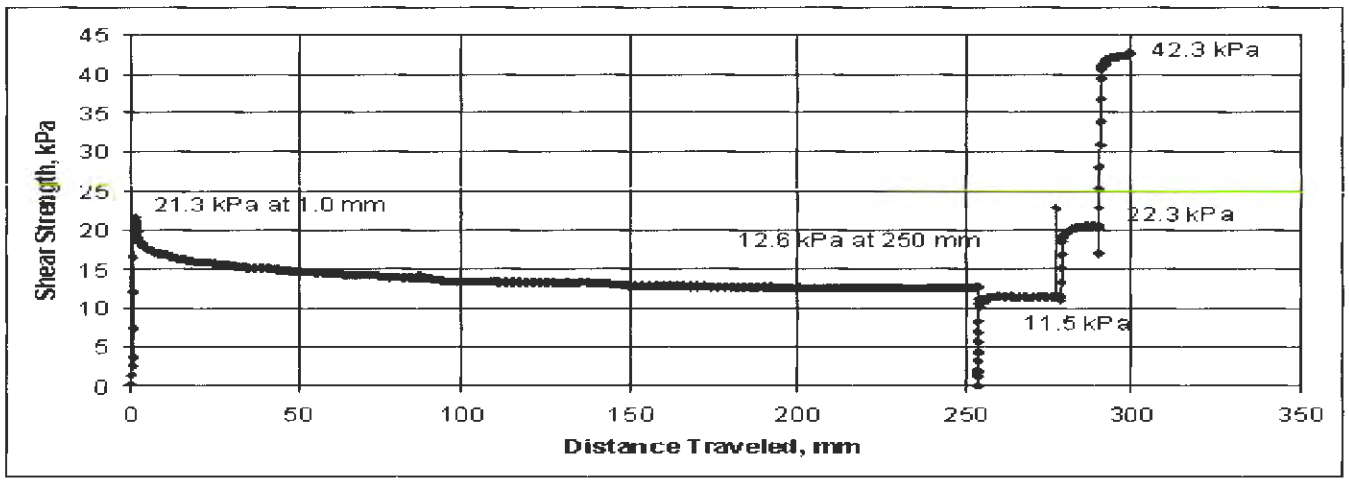

Figure A.20. 63.6 meter (10 ft), weathering cycle X0, Pierre Shale, Oahe Dam Site, PZT50-5.42, residual strength plot

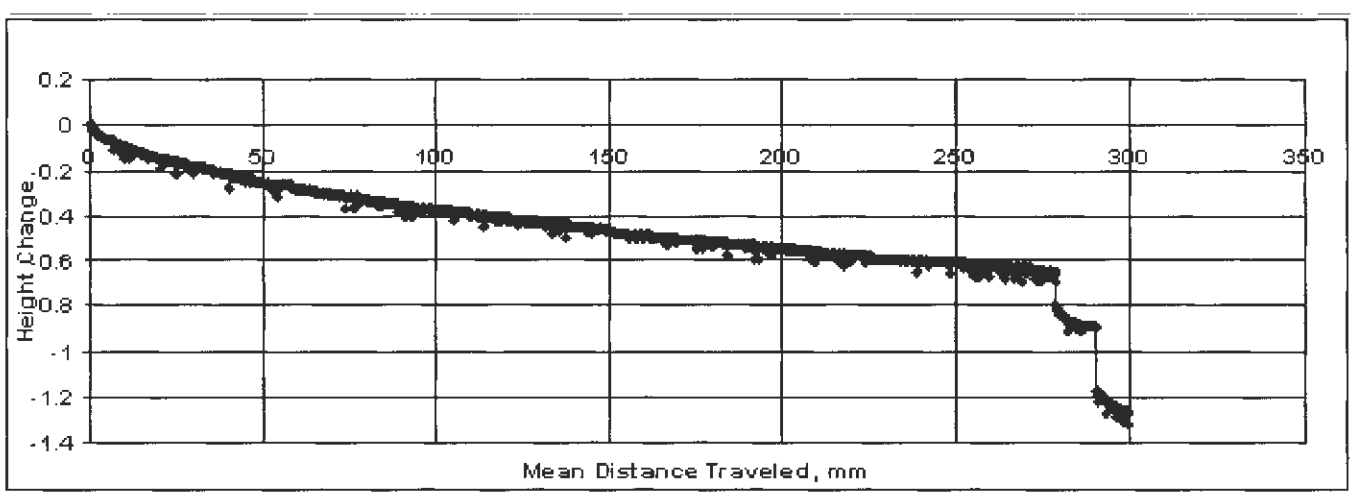

Figure A.21. 63.6 meter (210 ft), weathering cycle X0, Pierre Shale, Oahe Dam Site, PZT50-5.42, settlement plot

DETERMINATION OF THE RESIDUAL SHEAR STRENGTH
IN THE BROMHEAD RING SHEAR APPARATUS

Sample Description:	WEATHERED X1 PIERRE CLAY SHALE	Boring:	PZT50/5.42
Sample Location:	OAHE DAM SITE, SD, USA	Performed By:	MB
Sample No:	Weathering Cycle 210 foot	Date:	6/14/2004
Depth ft:	210	Depth, m:	64
Preparation :	Remoulded at	Initial water content (%)	44.0
		Remolded Dry Density (g/cm^3)	1.57
	Controls:	Hydrated	Multistage
		Material Passed #50	

Stage	Normal effective stress kPa	Residual Shear stress kPa	Tan phi
1	100.95	11.4	0.11
2	198.91	19.8	0.10
3	394.84	40.5	0.10

Dimensions:

Inner radius mm :	50
Outer radius mm :	35
Thickness mm :	5

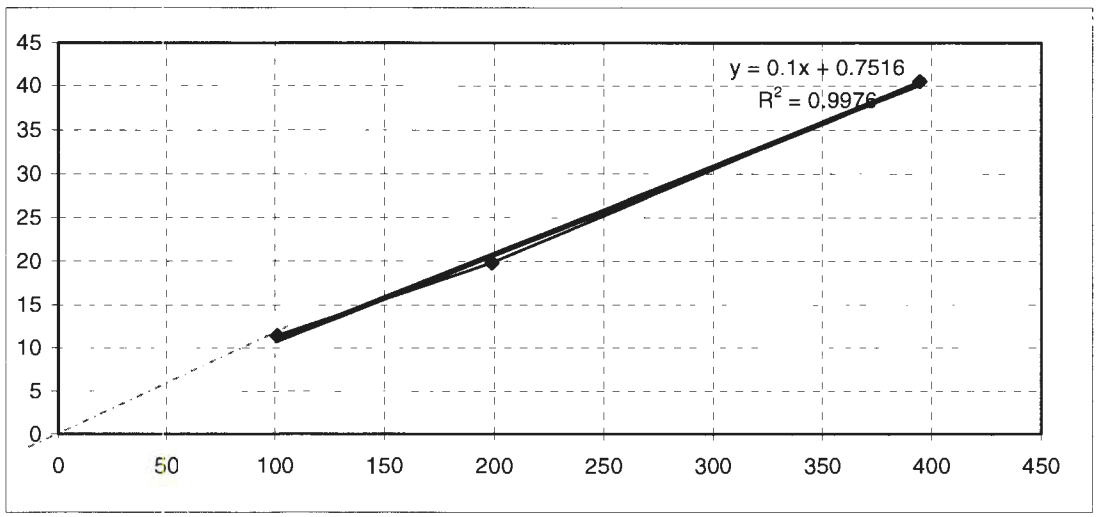

Shear parameters	c', kPa	ϕ'	r^2
Best fit straight line	0.75	5.7	0.998
Line through origin	0	5.9	0.996

Rate of Angular Displacement		
Shearing Stage for 1 revolution	0.12 mm/min	0.16 deg/min
Strain Rate for Normal Stresses	0.04 mm/min	0.048 deg/min

Figure A.22. 63.6 meter (210 ft), weathering cycle X1, Pierre Shale, Oahe Dam Site, PZT50-5.42, Bromhead Ring Shear report

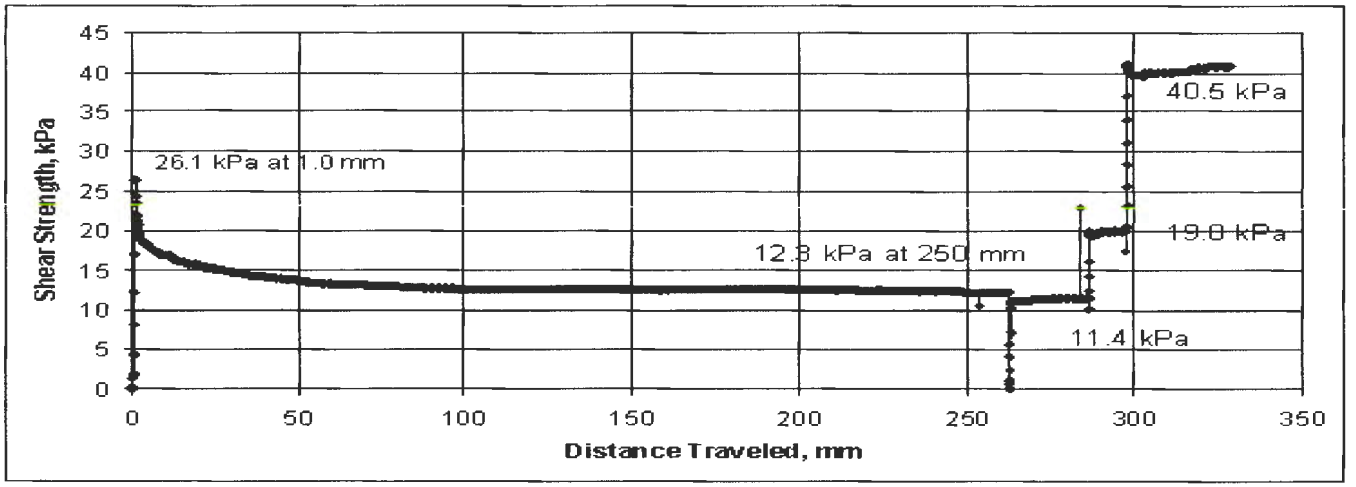

Figure A.23. 63.6 meter (210 ft), weathering cycle X1, Pierre Shale, Oahe Dam Site, PZT50-5.42, residual strength plot

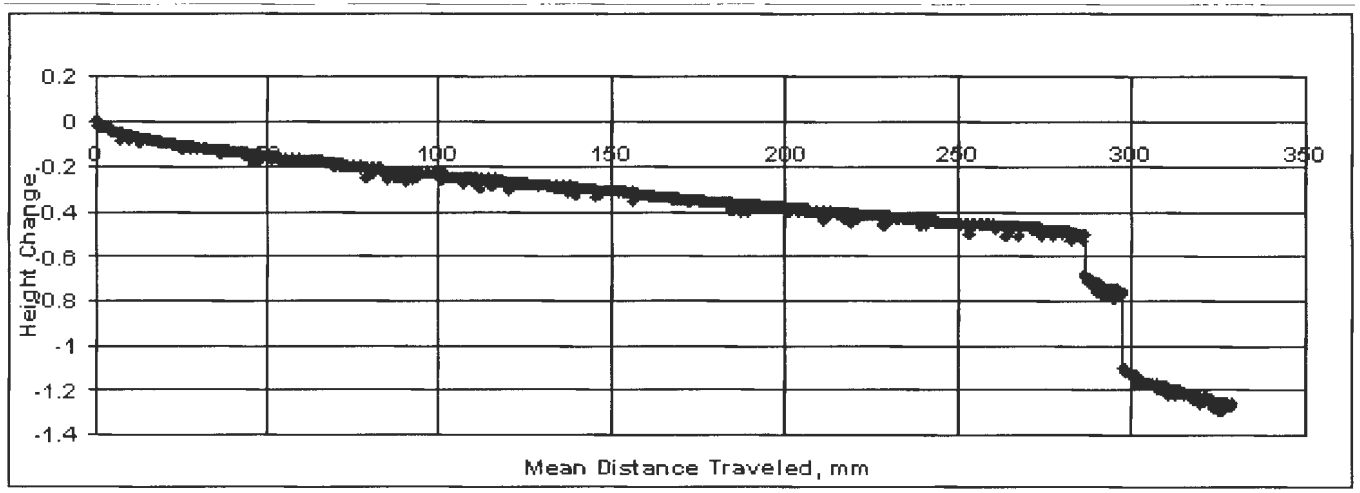

Figure A.24. 63.6 meter (210 ft), weathering cycle X1, Pierre Shale, Oahe Dam Site, PZT50-5.42, settlement plot

DETERMINATION OF THE RESIDUAL SHEAR STRENGTH
IN THE BROMHEAD RING SHEAR APPARATUS

Sample Description:	WEATHERED X3 PIERRE CLAY SHALE	Boring:	PZT50/5.42
Sample Location:	OAHE DAM SITE, SD, USA	Performed By:	MB
Sample No:	Weathering Cycle 210 foot	Date:	6/20/2004
Depth ft:	210	Depth, m:	64
Preparation :	Remoulded at	Initial water content (%)	38.0
		Remolded Dry Density (g/cm^3)	1.52
	Controls:	Hydrated	Multistage
		Material Passed #50	

Stage	Normal effective stress kPa	Residual Shear stress kPa	Tan phi
1	100.95	10.9	0.11
2	198.91	19.5	0.10
3	394.84	38.5	0.10

Dimensions:

Inner radius mm :	50
Outer radius mm :	35
Thickness mm :	5

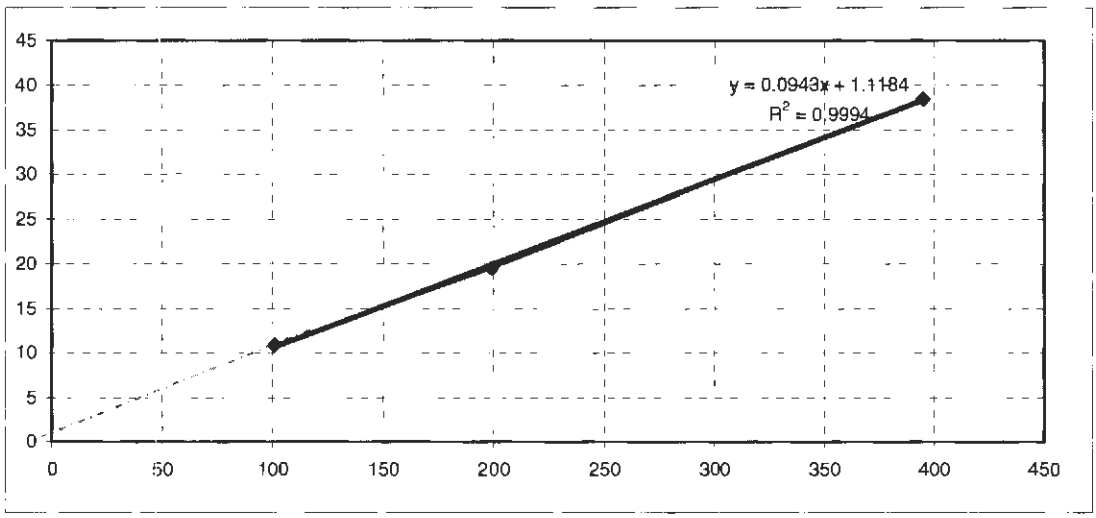

Shear parameters	c', kPa	φ'	r²
Best fit straight line	1.1	5.4	0.999
Line through origin	0	5.6	0.997

Rate of Angular Displacement		
Shearing Stage for 1 revolution	0.12 mm/min	0.16 deg/min
Strain Rate for Normal Stresses	0.04 mm/min	0.048 deg/min

Figure A.25. 63.6 meter (210 ft), weathering cycle X3, Pierre Shale, Oahe Dam Site, PZT50-5.42, Bromhead Ring Shear report

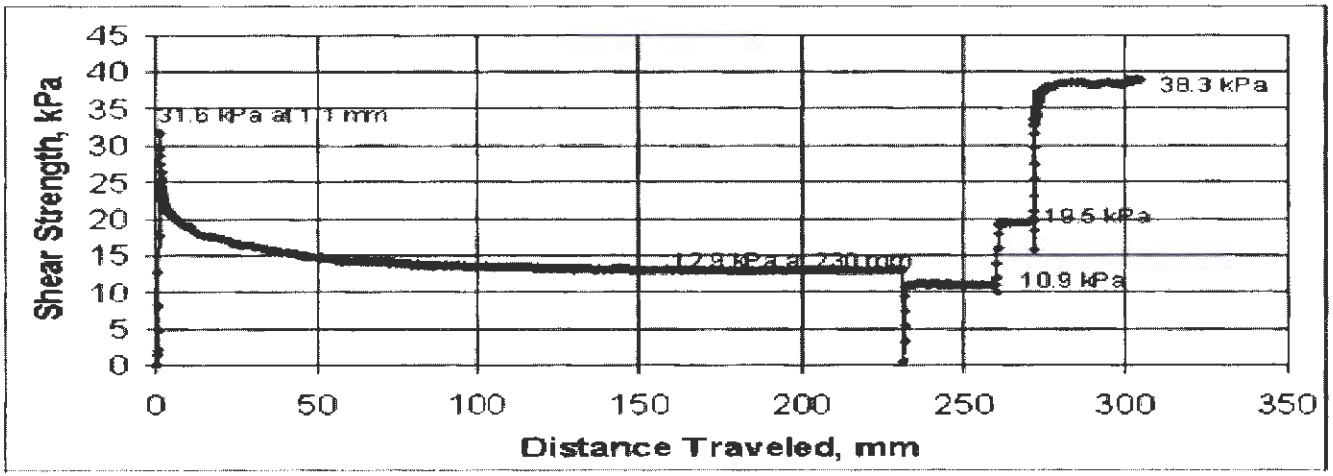

Figure A.26. 63.6 meter (210 ft), weathering cycle X3, Pierre Shale, Oahe Dam Site, PZT50-5.42, residual strength plot

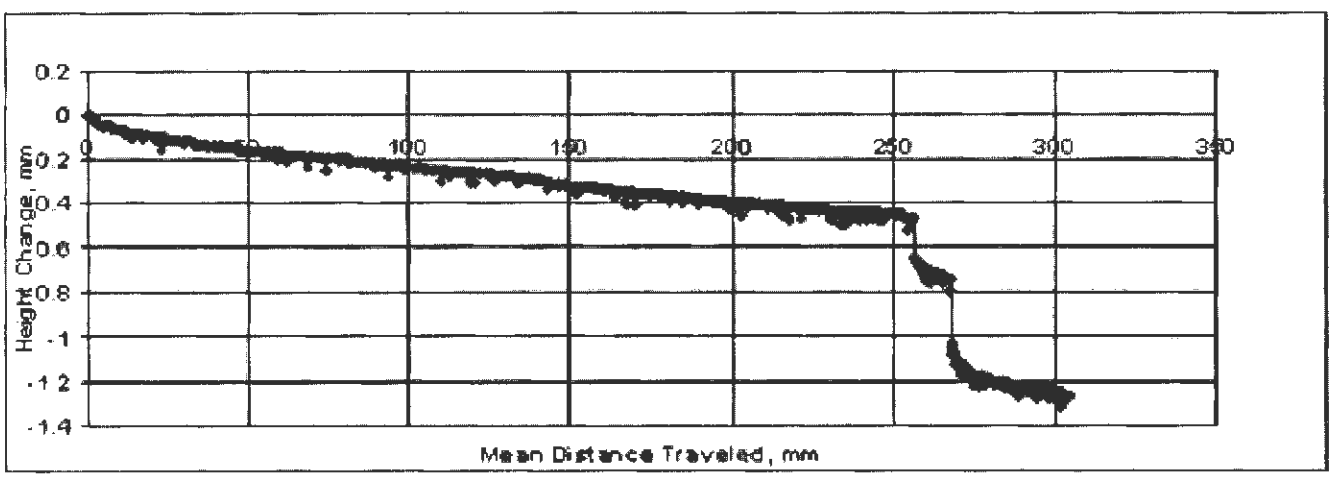

Figure A.27. 63.6 meter (210 ft), weathering cycle X3, Pierre Shale, Oahe Dam Site, PZT50-5.42, settlement plot

DETERMINATION OF THE RESIDUAL SHEAR STRENGTH
IN THE BROMHEAD RING SHEAR APPARATUS

Sample Description:	WEATHERED X5 PIERRE CLAY SHALE	Boring:	PZT50/5.42
Sample Location:	OAHE DAM SITE, SD, USA	Performed By:	MB
Sample No:	Weathering Cycle 210 foot	Date:	6/26/2005
Depth ft:	210	Depth, m:	64
Preparation :	Remoulded at	Initial water content (%)	34.0
		Remolded Dry Density (g/cm^3)	1.54
	Controls:	Hydrated	Multistage
		Material Passed #50	

Stage	Normal effective stress kPa	Residual Shear stress kPa	Tan phi
1	100.95	10.9	0.11
2	198.91	18.8	0.09
3	394.84	37.4	0.09

Dimensions:

Inner radius mm :	50
Outer radius mm :	35
Thickness mm :	5

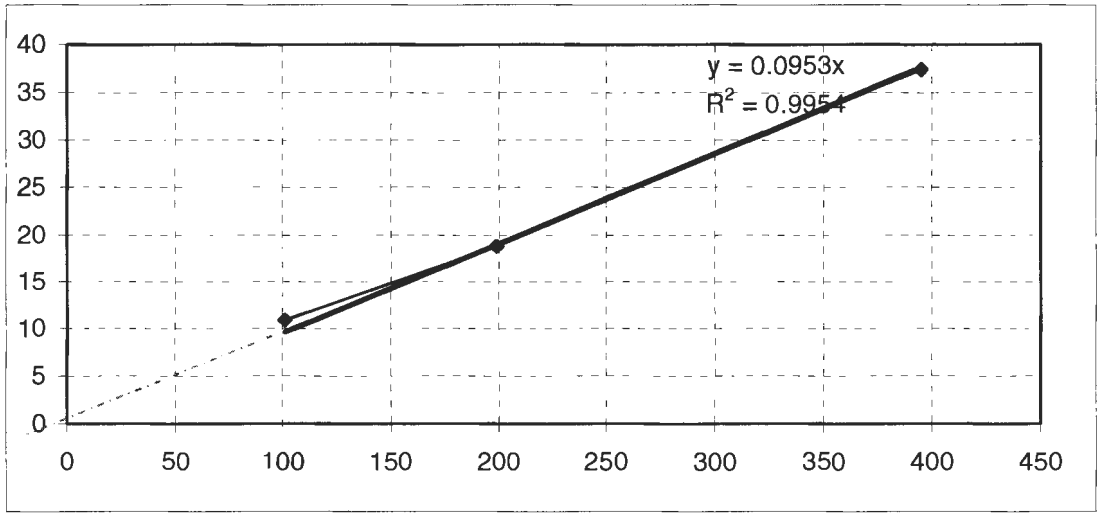

Shear parameters	c', kPa	φ'	r^2
Best fit straight line	1.3	5.2	0.9985
Line through origin	0	5.5	0.9954

Rate of Angular Displacement		
Shearing Stage for 1 revolution	0.12 mm/min	0.16 deg/min
Strain Rate for Normal Stresses	0.04 mm/min	0.048 deg/min

Figure A.28. 63.6 meter (210 ft), weathering cycle X5, Pierre Shale, Oahe Dam Site, PZT50-5.42, Bromhead Ring Shear report

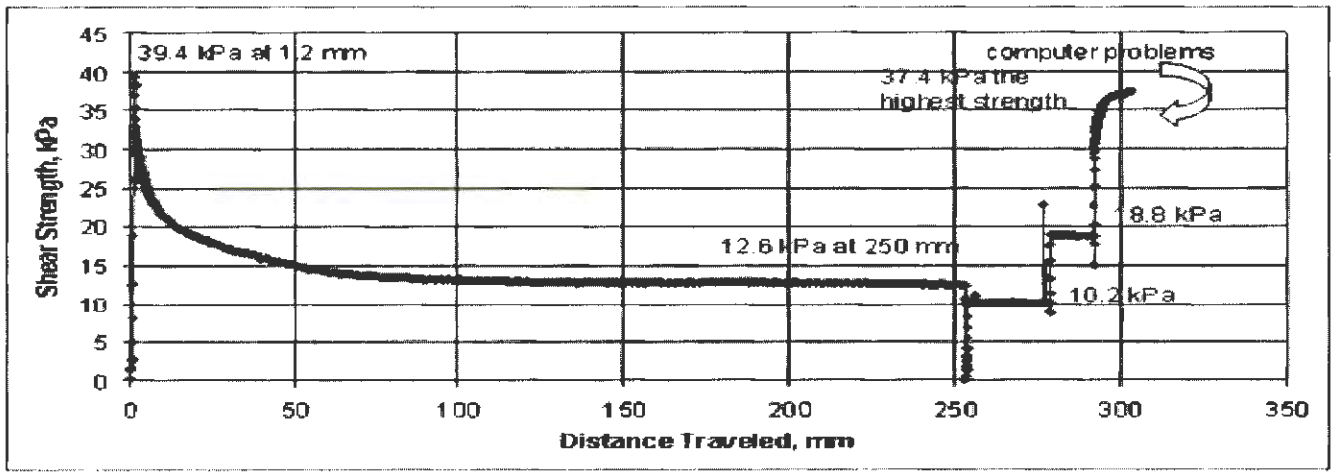

Figure A.29. 63.6 meter (210 ft), weathering cycle X5, Pierre Shale, Oahe Dam Site, PZT50-5.42, residual strength plot

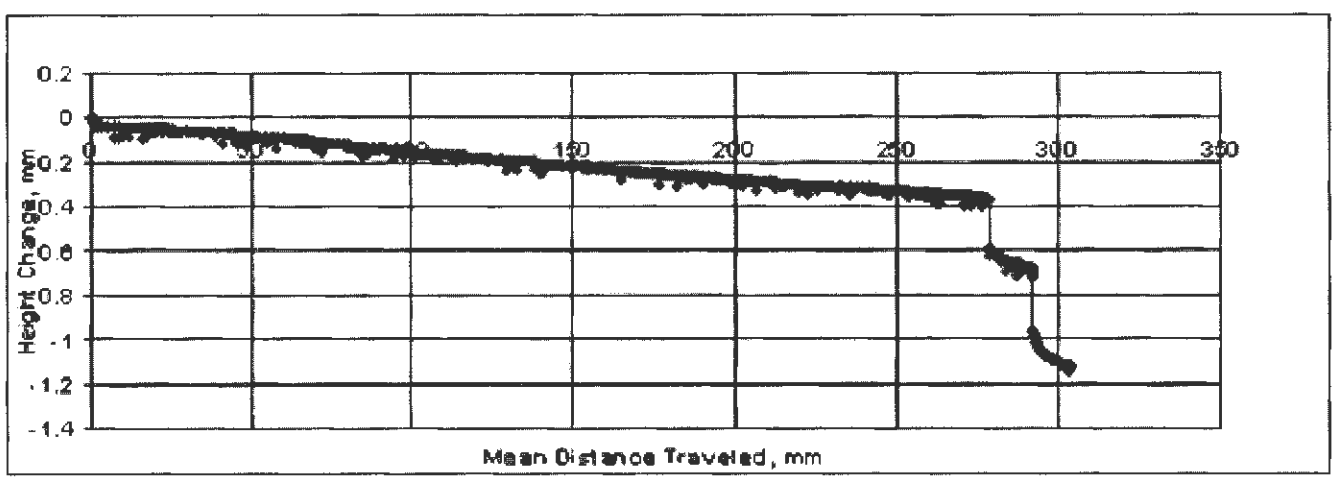

Figure A.30. 63.6 meter (210 ft), weathering cycle X5, Pierre Shale, Oahe Dam Site, PZT50-5.42, settlement plot

DETERMINATION OF THE RESIDUAL SHEAR STRENGTH
IN THE BROMHEAD RING SHEAR APPARATUS

Sample Description:	WEATHERED X0 PIERRE CLAY SHALE	Boring:	PZT50/5.42
Sample Location:	OAHE DAM SITE, SD, USA	Performed By:	MB
Sample No:	Weathering Cycle 232 foot	Date:	10/5/2004
Depth ft:	232	Depth, m:	70
Preparation :	Remoulded at	Initial water content (%)	38.3
		Remolded Dry Density (g/cm^3)	1.64
	Controls:	Hydrated	Multistage
		Material Passed #50	

Stage	Normal effective stress kPa	Residual Shear stress kPa	Tan phi
1	100.95	12.1	0.12
2	198.91	23.4	0.12
3	394.84	46.5	0.12

Dimensions:

Inner radius mm :	50
Outer radius mm :	35
Thickness mm :	5

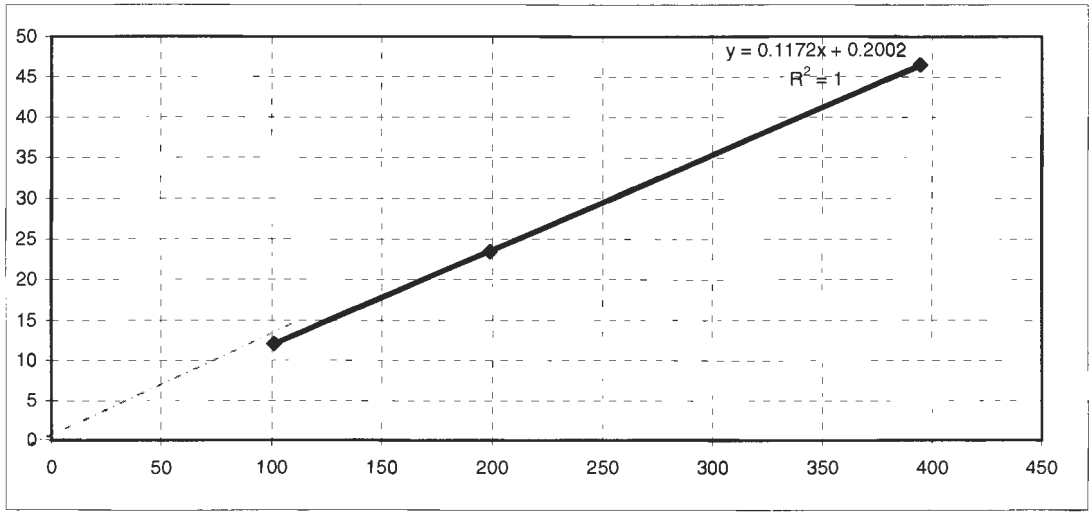

Shear parameters	c', kPa	ϕ'	r^2
Best fit straight line	0.2	6.7	1
Line through origin	0	6.7	0.999

Rate of Angular Displacement		
Shearing Stage for 1 revolution	0.12 mm/min	0.16 deg/min
Strain Rate for Normal Stresses	0.04 mm/min	0.048 deg/min

Figure A.31. 70.3 meter (232 ft), weathering cycle X0, Pierre Shale, Oahe Dam Site, PZT50-5.42, Bromhead Ring Shear report

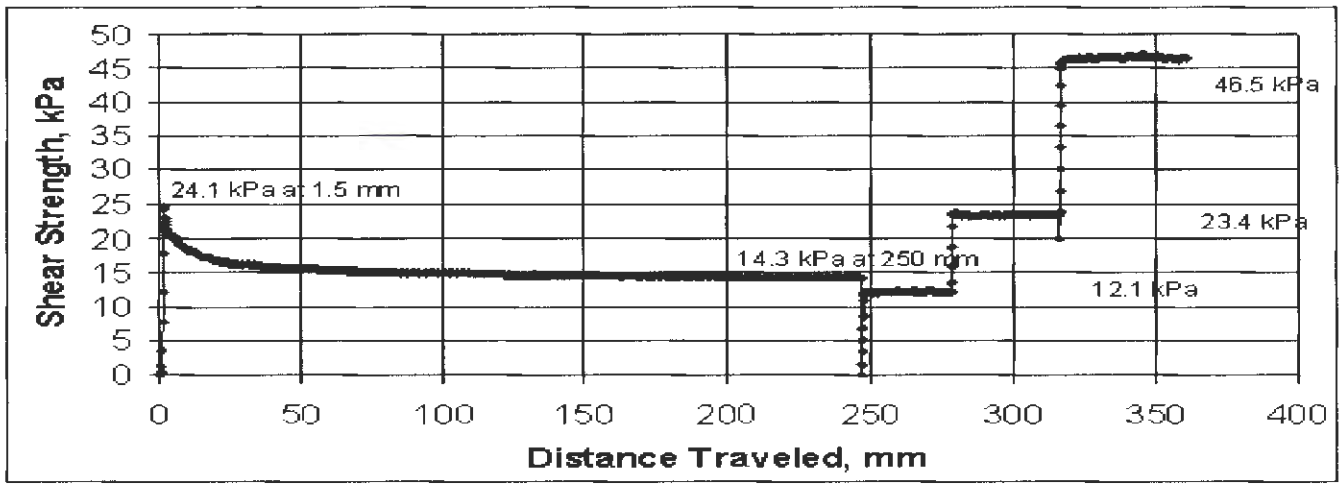

Figure A.32. 70.3 meter (232 ft), weathering cycle X0, Pierre Shale, Oahe Dam Site, PZT50-5.42, residual strength plot

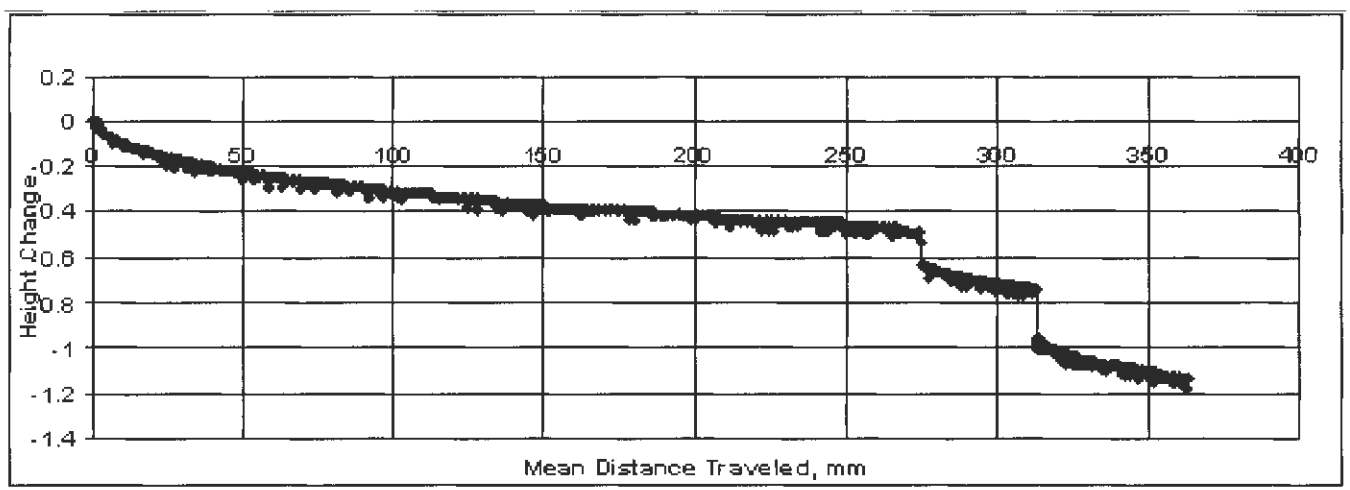

Figure A.33. 70.3 meter (232 ft), weathering cycle X0, Pierre Shale, Oahe Dam Site, PZT50-5.42, settlement plot

DETERMINATION OF THE RESIDUAL SHEAR STRENGTH
IN THE BROMHEAD RING SHEAR APPARATUS

Sample Description:	WEATHERED X1 PIERRE CLAY SHALE	Boring:	PZT50/5.42
Sample Location:	OAHE DAM SITE, SD, USA	Performed By:	MB
Sample No:	Weathering Cycle 232 foot	Date:	10/12/2004
Depth ft:	232	Depth, m:	70
Preparation :	Remoulded at	Initial water content (%)	34.7
		Remolded Dry Density (g/cm^3)	1.47
	Controls:	Hydrated	Multistage
		Material Passed #50	

Stage	Normal effective stress kPa	Residual Shear stress kPa	Tan phi
1	100.95	12.3	0.12
2	198.91	24.3	0.12
3	394.84	49.9	0.13

Dimensions:

Inner radius mm :	50
Outer radius mm :	35
Thickness mm :	5

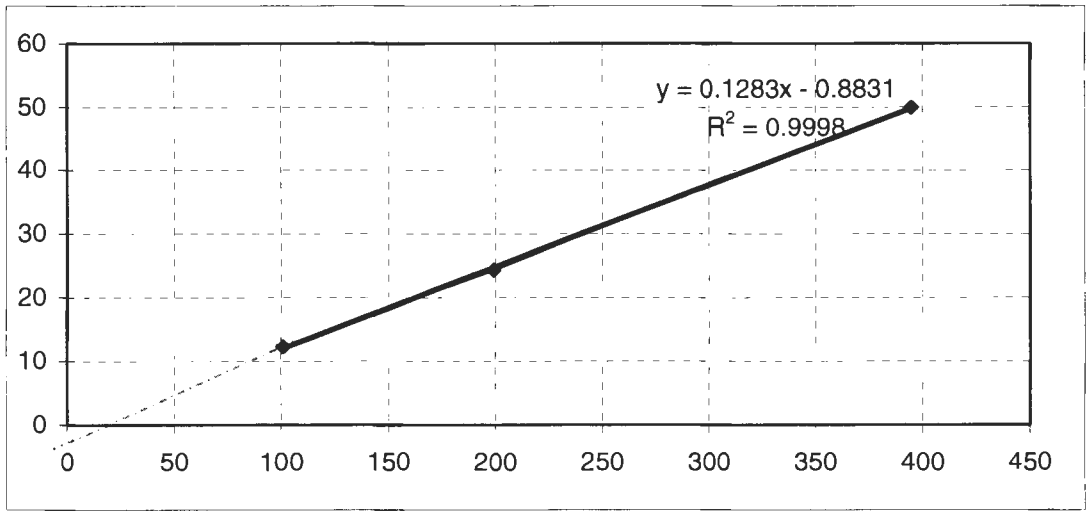

Shear parameters	c', kPa	φ'	r^2
Best fit straight line	~0	7.4	0.999
Line through origin	0	6.6	0.997

Rate of Angular Displacement		
Shearing Stage for 1 revolution	0.12 mm/min	0.16 deg/min
Strain Rate for Normal Stresses	0.04 mm/min	0.048 deg/min

Figure A.34. 70.3 meter (232 ft), weathering cycle X1, Pierre Shale, Oahe Dam Site, PZT50-5.42, Bromhead Ring Shear report

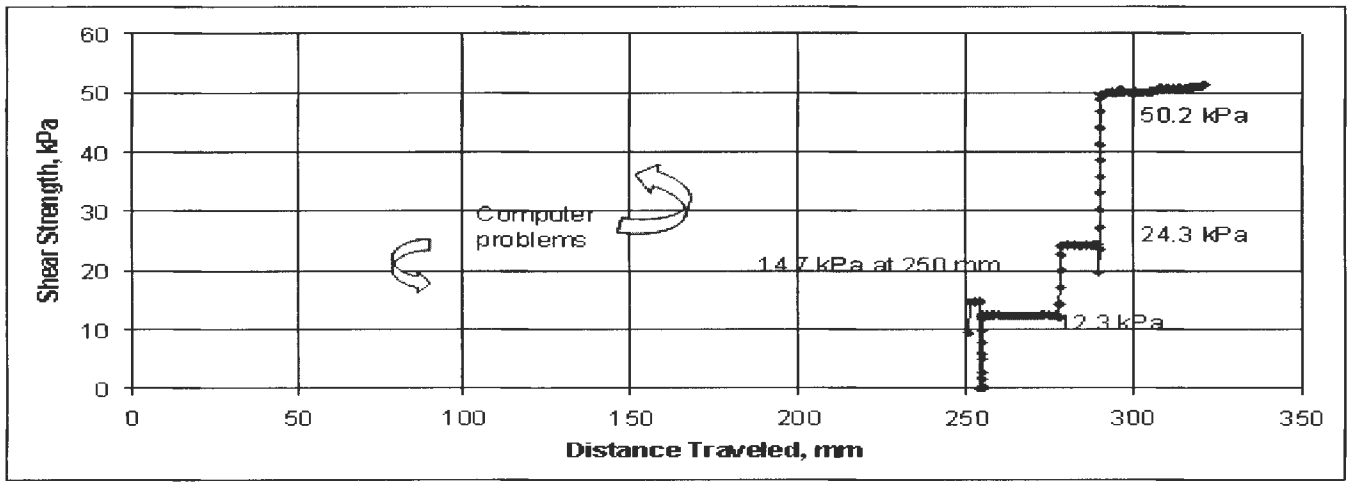

Figure A.35. 70.3 meter (232 ft), weathering cycle X1, Pierre Shale, Oahe Dam Site, PZT50-5.42, residual strength plot

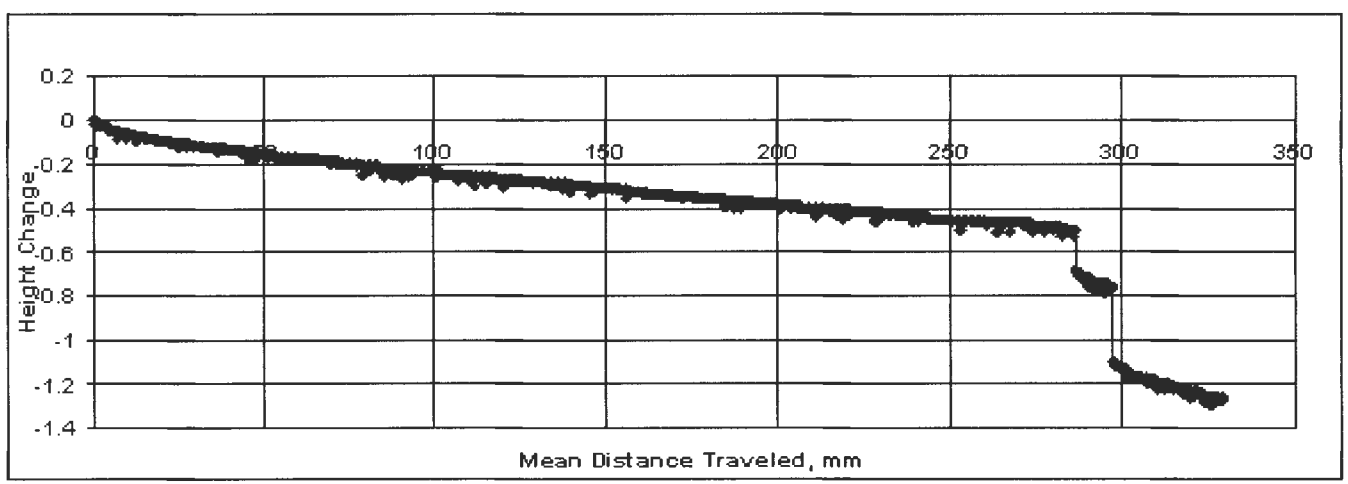

Figure A.36. 70.3 meter (232 ft), weathering cycle X1, Pierre Shale, Oahe Dam Site, PZT50-5.42, settlement plot

DETERMINATION OF THE RESIDUAL SHEAR STRENGTH
IN THE BROMHEAD RING SHEAR APPARATUS

Sample Description:	WEATHERED X2 PIERRE CLAY SHALE	Boring:	PZT50/5.42
Sample Location:	OAHE DAM SITE, SD, USA	Performed By:	MB
Sample No:	Weathering Cycle 232 foot	Date:	9/17/2004
Depth ft:	232	Depth, m:	70
Preparation :	Remoulded at	Initial water content (%)	36.2
		Remolded Dry Density (g/cm^3)	1.62
	Controls:	Hydrated	Multistage
		Material Passed #50	

Stage	Normal effective stress kPa	Residual Shear stress kPa	Tan phi
1	100.95	11.5	0.11
2	198.91	22.3	0.11
3	394.84	45.2	0.11

Dimensions:

Inner radius mm :	50
Outer radius mm :	35
Thickness mm :	5

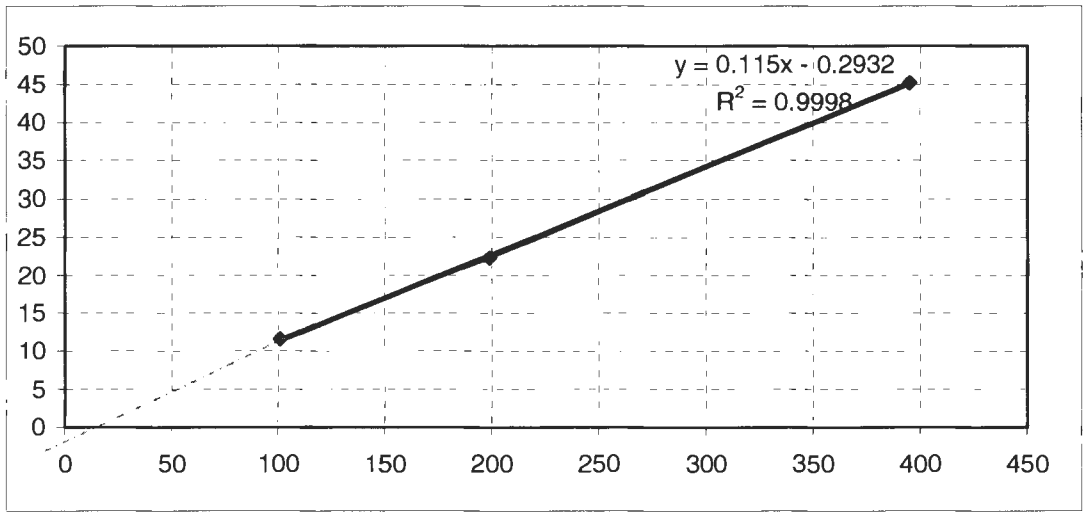

Shear parameters	c', kPa	ϕ'	r^2
Best fit straight line	~0	6.6	0.999
Line through origin	0	6.6	0.997

Rate of Angular Displacement		
Shearing Stage for 1 revolution	0.12 mm/min	0.16 deg/min
Strain Rate for Normal Stresses	0.04 mm/min	0.048 deg/min

Figure A.37. 70.3 meter (232 ft), weathering cycle X2, Pierre Shale, Oahe Dam Site, PZT50-5.42, Bromhead Ring Shear report

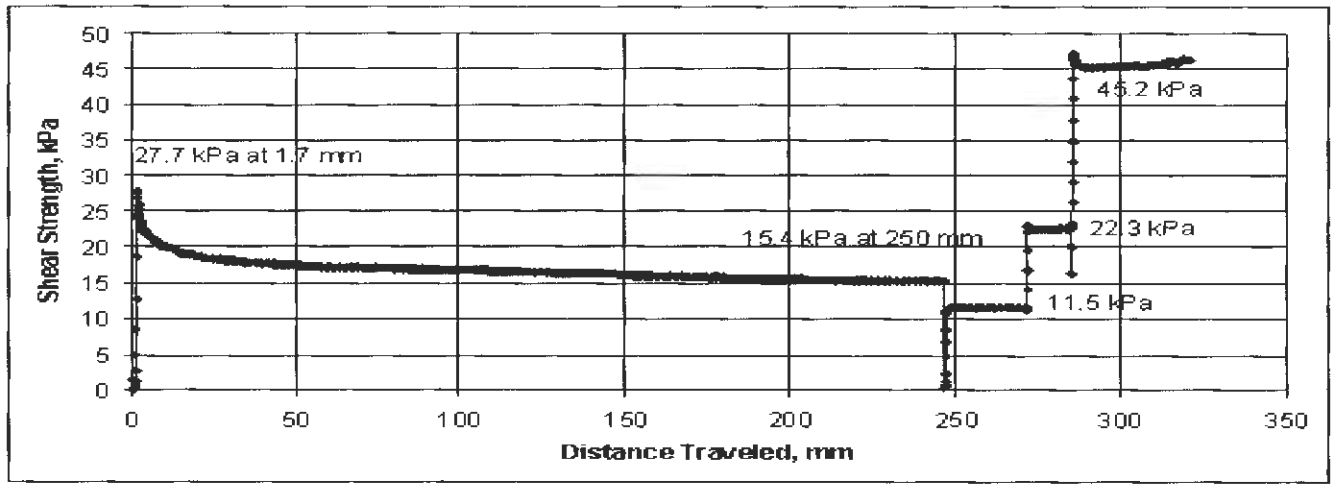

Figure A.38. 70.3 meter (232 ft), weathering cycle X2, Pierre Shale, Oahe Dam Site, PZT50-5.42, residual strength

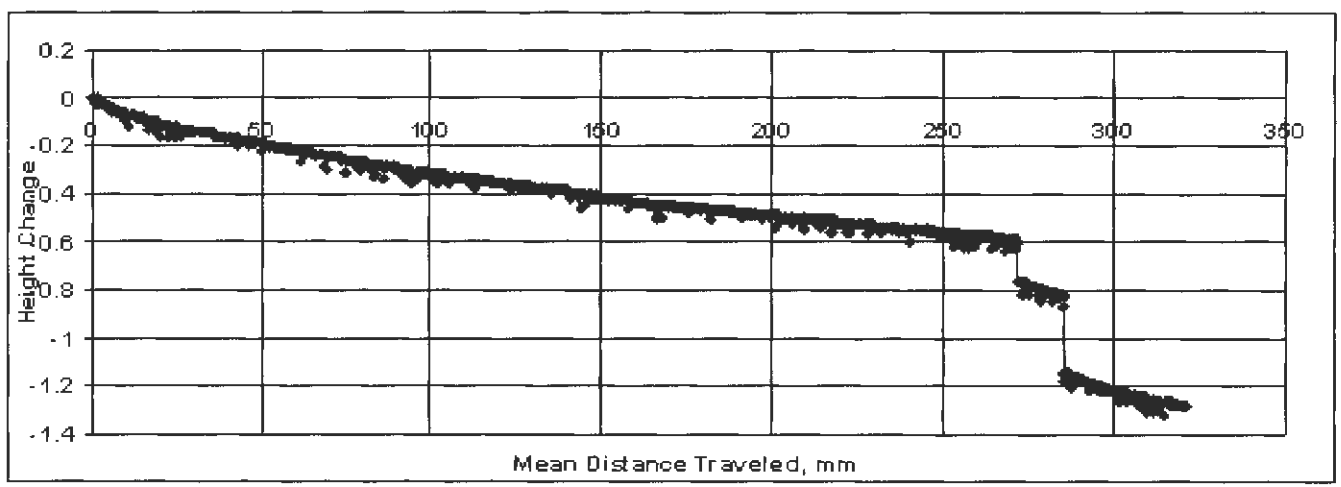

Figure A.39. 70.3 meter (232 ft), weathering cycle X2, Pierre Shale, Oahe Dam Site, PZT50-5.42, settlement plot

DETERMINATION OF THE RESIDUAL SHEAR STRENGTH
IN THE BROMHEAD RING SHEAR APPARATUS

Sample Description:	WEATHERED X3 PIERRE CLAY SHALE	Boring:	PZT50/5.42
Sample Location:	OAHE DAM SITE, SD, USA	Performed By:	MB
Sample No:	Weathering Cycle 232 foot	Date:	9/26/2004
Depth ft:	232	Depth, m:	70
Preparation :	Remoulded at	Initial water content (%)	31.1
		Remolded Dry Density (g/cm^3)	1.48
	Controls:	Hydrated	Multistage
		Material Passed #50	

Stage	Normal effective stress kPa	Residual Shear stress kPa	Tan phi
1	100.95	10.8	0.11
2	198.91	19.9	0.10
3	394.84	38.6	0.10

Dimensions:

Inner radius mm :	50
Outer radius mm :	35
Thickness mm :	5

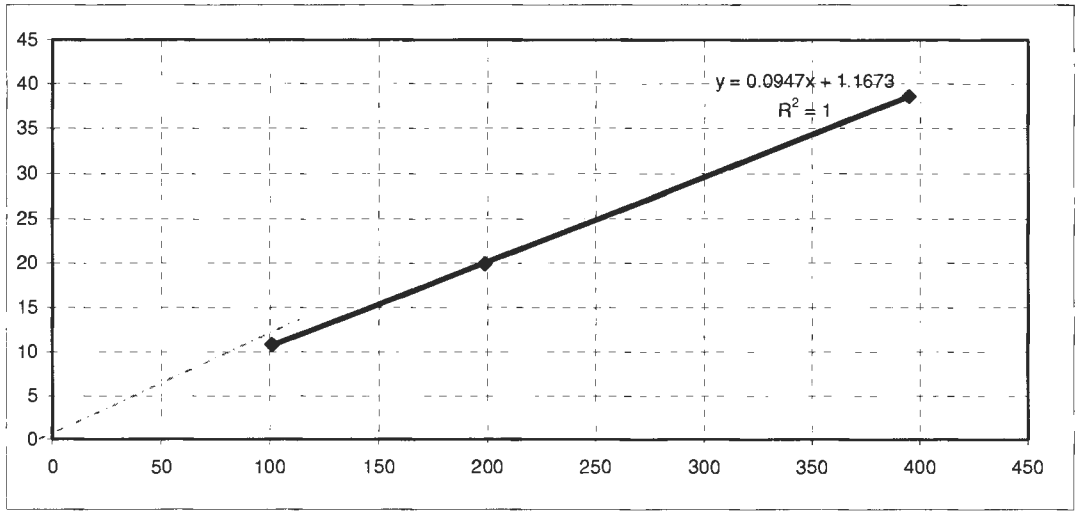

Shear parameters	c', kPa	ϕ'	r²
Best fit straight line	1.17	5.4	1
Line through origin	0	5.7	0.997

Rate of Angular Displacement		
Shearing Stage for 1 revolution	0.12 mm/min	0.16 deg/min
Strain Rate for Normal Stresses	0.04 mm/min	0.048 deg/min

Figure A.40. 70.3 meter (232 ft), weathering cycle X3, Pierre Shale, Oahe Dam Site, PZT50-5.42, Bromhead Ring Shear report

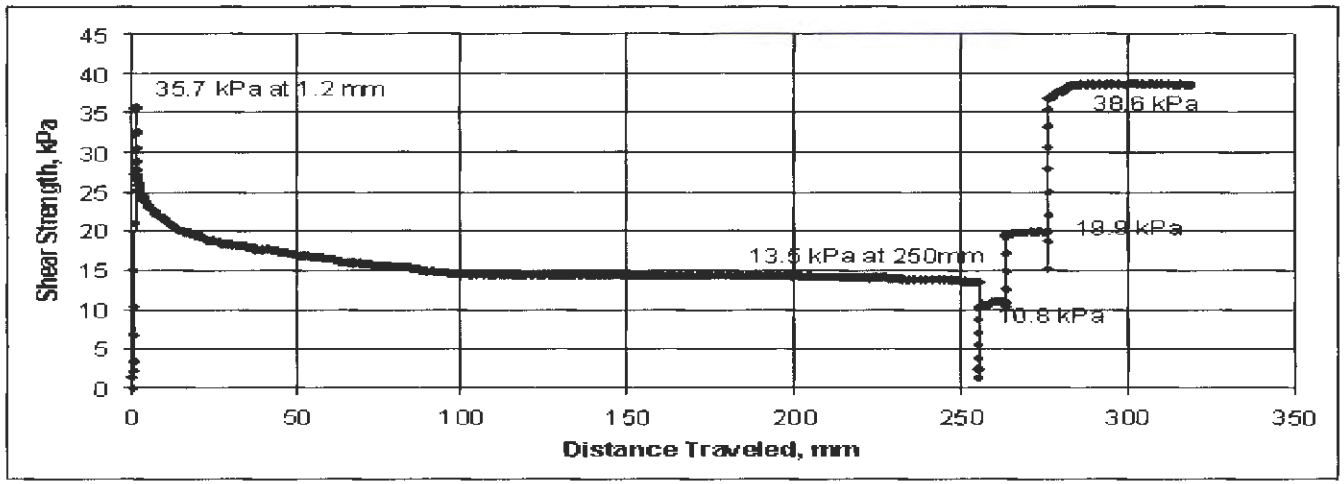

Figure A.41. 70.3 meter (232 ft), weathering cycle X3, Pierre Shale, Oahe Dam Site, PZT50-5.42, residual strength plot

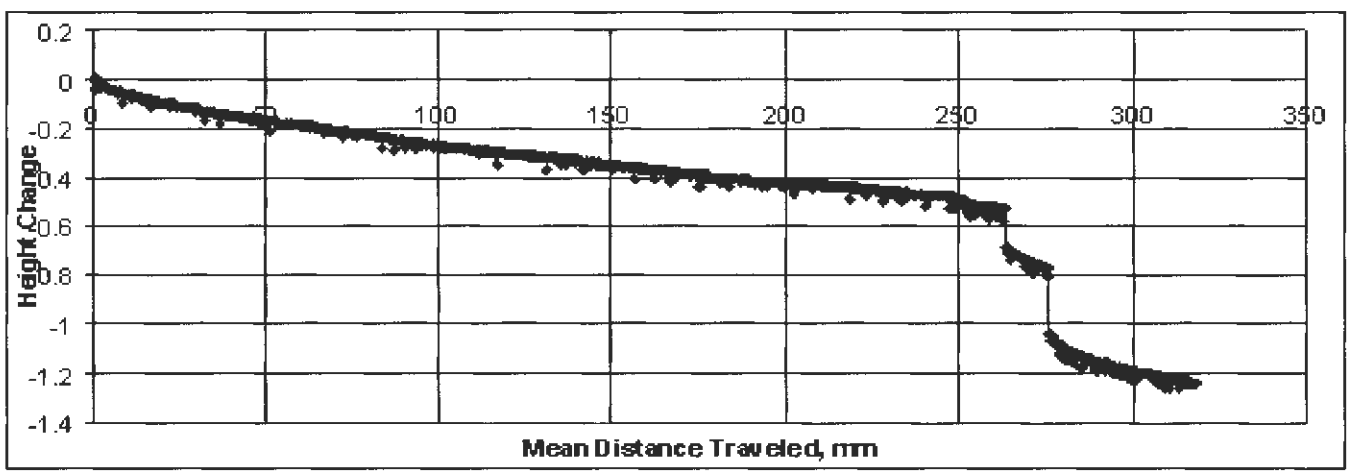

Figure A.42. 70.3 meter (232 ft), weathering cycle X3, Pierre Shale, Oahe Dam Site, PZT50-5.42, settlement plot

DETERMINATION OF THE RESIDUAL SHEAR STRENGTH
IN THE BROMHEAD RING SHEAR APPARATUS

Sample Description:	WEATHERED X4 PIERRE CLAY SHALE	Boring:	PZT50/5.42
Sample Location:	OAHE DAM SITE, SD, USA	Performed By:	MB
Sample No:	Weathering Cycle 232 foot	Date:	9/29/2004
Depth ft:	232	Depth, m:	70
Preparation :	Remoulded at	Initial water content (%)	34.1
		Remolded Dry Density (g/cm^3)	1.57
	Controls:	Hydrated	Multistage
		Material Passed #50	

Stage	Normal effective stress kPa	Residual Shear stress kPa	Tan phi
1	100.95	13.7	0.14
2	198.91	25	0.13
3	394.84	48	0.12

Dimensions:
Inner radius mm : 50
Outer radius mm : 35
Thickness mm : 5

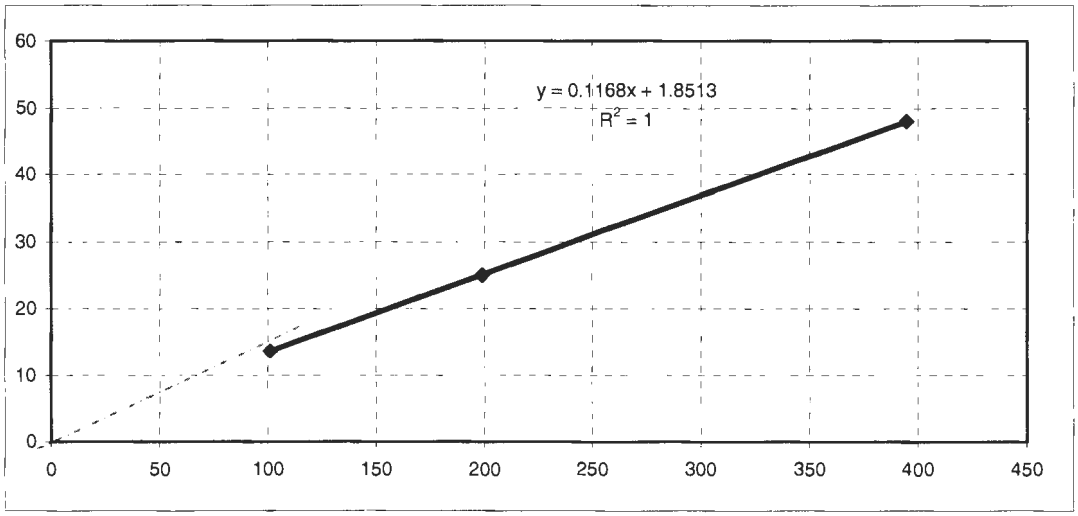

Shear parameters	c', kPa	ϕ'	r²
Best fit straight line	1.9	6.7	1
Line through origin	0	6.9	0.9963

Rate of Angular Displacement		
Shearing Stage for 1 revolution	0.12 mm/min	0.16 deg/min
Strain Rate for Normal Stresses	0.04 mm/min	0.048 deg/min

Figure A.43. 70.3 meter (232 ft), weathering cycle X4, Pierre Shale, Oahe Dam Site, PZT50-5.42, Bromhead Ring Shear report

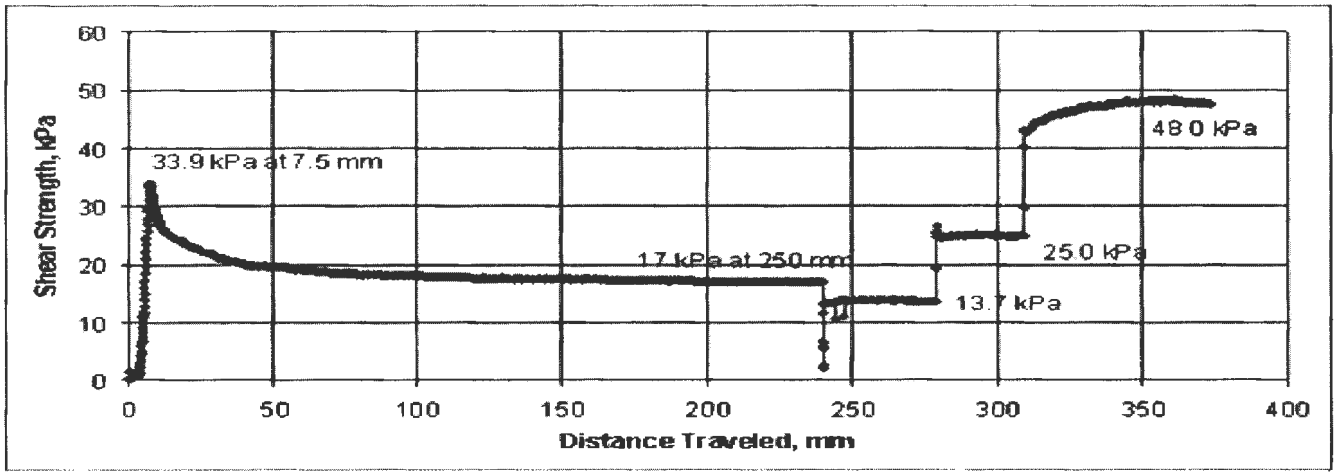

Figure A.44. 70.3 meter (232 ft), weathering cycle X3, Pierre Shale, Oahe Dam Site, PZT50-5.42, residual strength plot

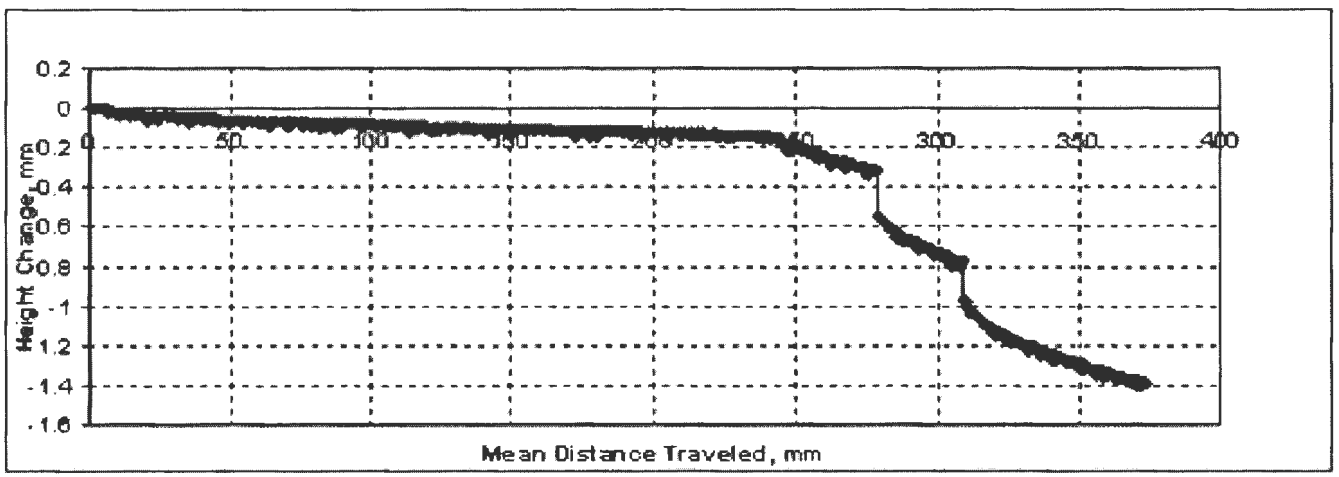

Figure A.45. 70.3 meter (232 ft), weathering cycle X3, Pierre Shale, Oahe Dam Site, PZT50-5.42, settlement plot

DETERMINATION OF THE RESIDUAL SHEAR STRENGTH
IN THE BROMHEAD RING SHEAR APPARATUS

Sample Description:	WEATHERED X5 PIERRE CLAY SHALE	Boring:	PZT50/5.42
Sample Location:	OAHE DAM SITE, SD, USA	Performed By:	MB
Sample No:	Weathering Cycle 232 foot	Date:	10/4/2005
Depth ft:	232	Depth, m:	70
Preparation :	Remoulded at	Initial water content (%)	38.2
		Remolded Dry Density (g/cm^3)	1.44
	Controls:	Hydrated	Multistage
		Material Passed #50	

Stage	Normal effective stress kPa	Residual Shear stress kPa	Tan phi
1	100.95	13.1	0.13
2	198.91	23.4	0.12
3	394.84	46.9	0.12

Dimensions:

Inner radius mm :	50
Outer radius mm :	35
Thickness mm :	5

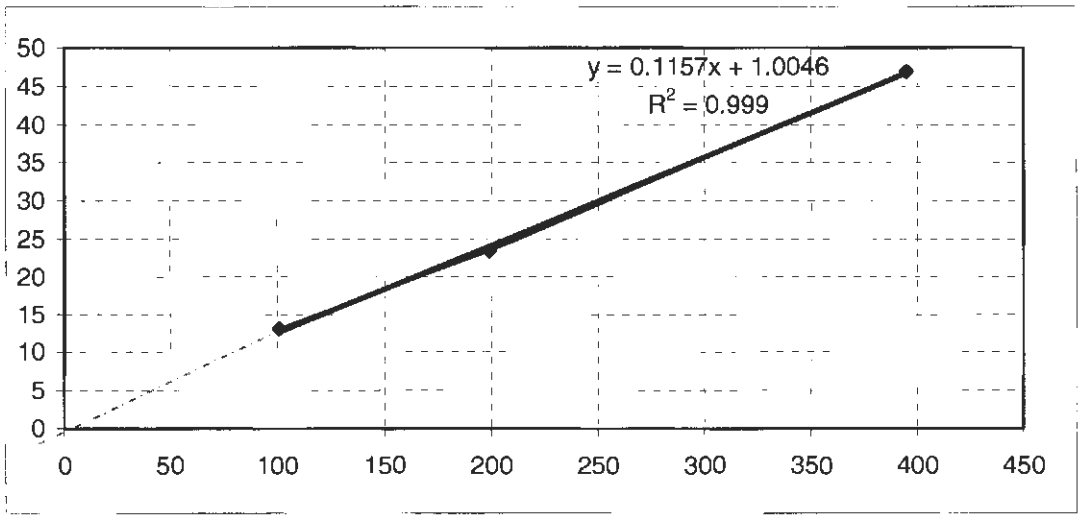

Shear parameters	c', kPa	ϕ'	r^2
Best fit straight line	1	6.6	0.999
Line through origin	0	6.8	0.9979

Rate of Angular Displacement		
Shearing Stage for 1 revolution	0.12 mm/min	0.16 deg/min
Strain Rate for Normal Stresses	0.04 mm/min	0.048 deg/min

Figure A.46. 70.3 meter (232 ft), weathering cycle X5, Pierre Shale, Oahe Dam Site, PZT50-5.42, Bromhead Ring Shear report

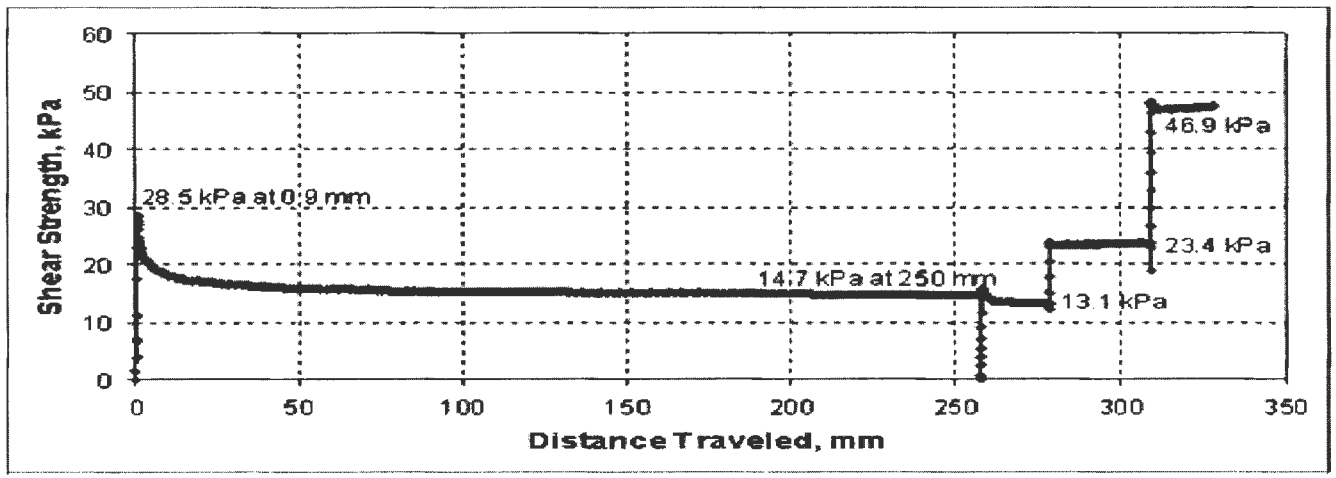

Figure A.47. 70.3 meter (232 ft), weathering cycle X5, Pierre Shale, Oahe Dam Site, PZT50-5.42, residual strength plot

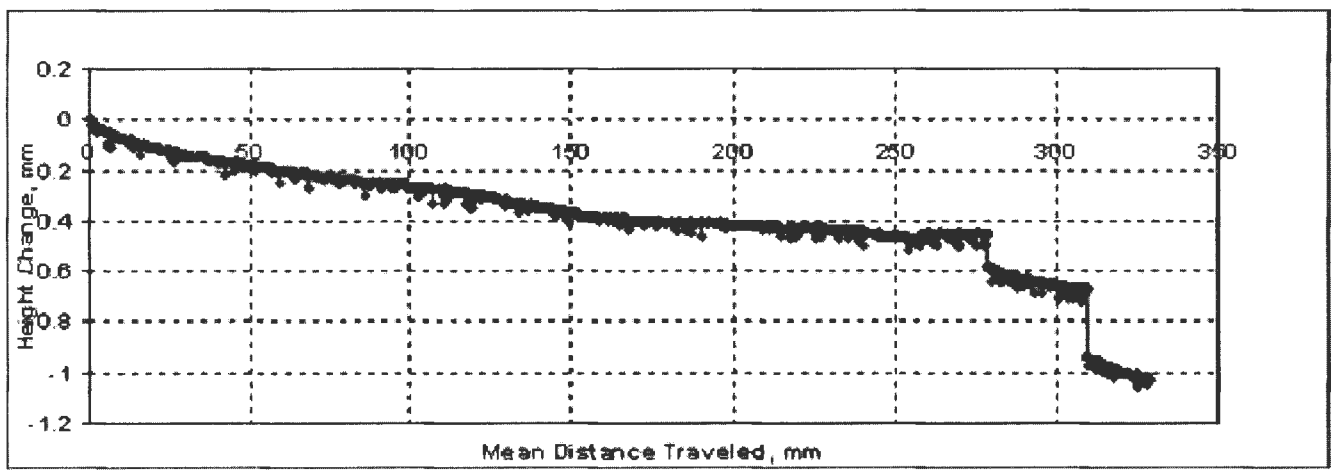

Figure A.48. 70.3 meter (232 ft), weathering cycle X5, Pierre Shale, Oahe Dam Site, PZT50-5.42, settlement plot

DETERMINATION OF THE RESIDUAL SHEAR STRENGTH
IN THE BROMHEAD RING SHEAR APPARATUS

Sample Description:	WEATHERED ZONE PIERRE CLAY SHALE	Boring:	PZT50/5.42
Sample Location:	OAHE DAM SITE, SD, USA	Performed By:	MB
Sample No:	PZT50-59	Date:	7/17/2004
Depth ft:	59	Depth, m	17.9
Preparation :	Remolded at:	Initial water content (%)	52.6
		Remolded Dry Density (g/cm^3)	1.37
	Controls:	Hydrated	Multistage
		Material Passed #50	

Stage	Normal effective stress kPa	Residual Shear stress kPa	Tan phi
1	100.95	11.2	0.11
2	198.91	21.4	0.11
3	394.84	41.2	0.10

Dimensions:

Inner radius mm :	50
Outer radius mm :	35
Thickness mm :	5

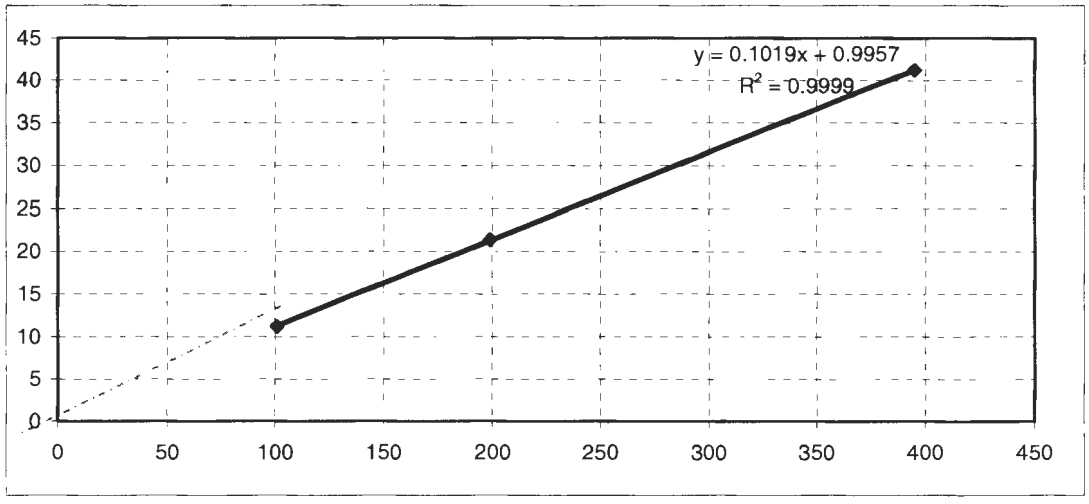

Shear parameters	c', kPa	φ'	r^2
Best fit straight line	1	5.8	0.9996
Line through origin	0	6.0	0.999

Rate of Angular Displacement

Shearing Stage for 1 revolution	0.12 mm/min	0.16 deg/min
Strain Rate for Normal Stresses	0.04 mm/min	0.048 deg/min

Figure A.49. 17.9 meter (59 ft), Pierre Shale, Oahe Dam Site, PZT50-5.42, Bromhead Ring Shear report

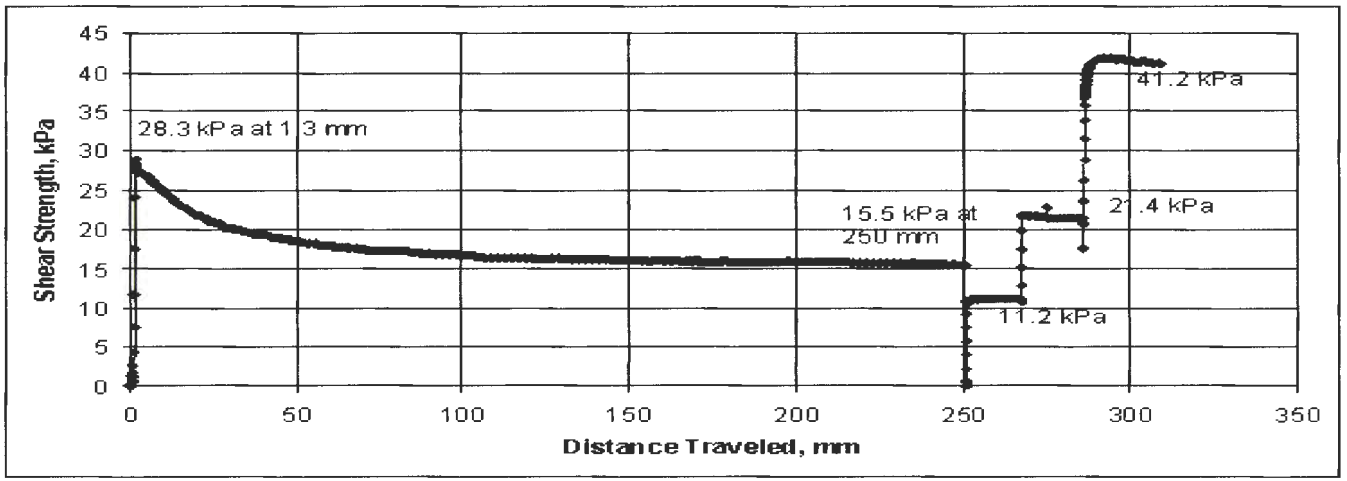

Figure A.50. 17.9 meter (59 ft), Pierre Shale, Oahe Dam Site, PZT50-5.42, residual strength plot

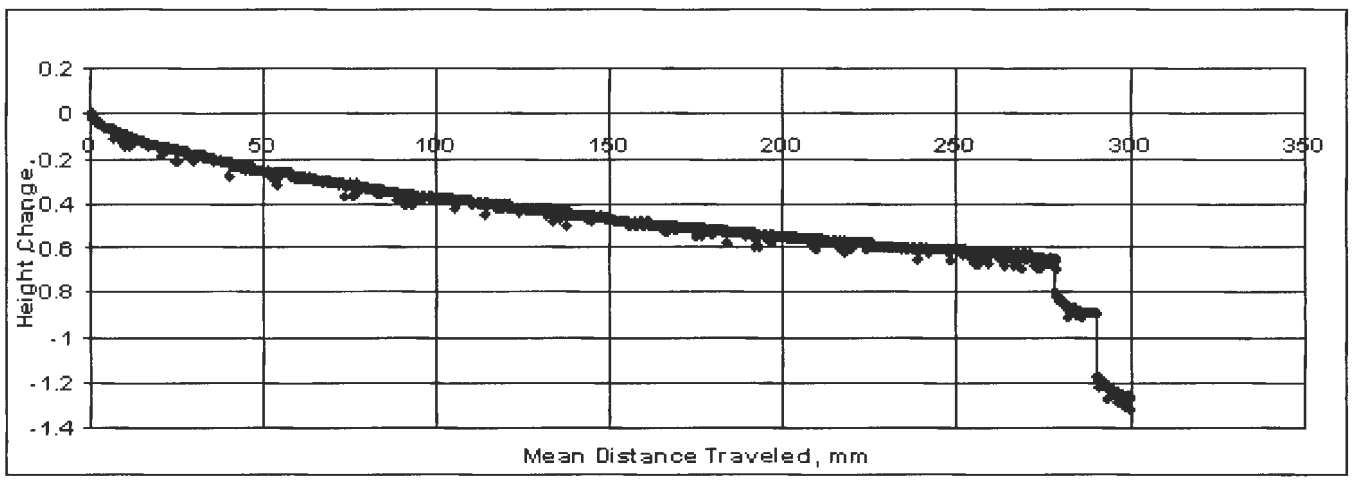

Figure A.51. 17.9 meter (59 ft), Pierre Shale, Oahe Dam Site, PZT50-5.42, settlement plot

DETERMINATION OF THE RESIDUAL SHEAR STRENGTH
IN THE BROMHEAD RING SHEAR APPARATUS

Sample Description:	WEATHERED ZONE PIERRE CLAY SHALE	Boring:	PZT50/5.42
Sample Location:	OAHE DAM SITE, SD, USA	Performed By:	MB
Sample No:	PZT50-60	Date:	12/11/2004
Depth ft:	60	Depth, m	18.2
Preparation :	Remolded at:	Initial water content (%)	38
		Remolded Dry Density (g/cm^3)	1.45
	Controls:	Hydrated	Multistage
		Material Passed #50	

Stage	Normal effective stress kPa	Residual Shear stress kPa	Tan phi
1	100.95	15.1	0.15
2	198.91	30.4	0.15
3	394.84	62.4	0.16

Dimensions:

Inner radius mm :	50
Outer radius mm :	35
Thickness mm :	5

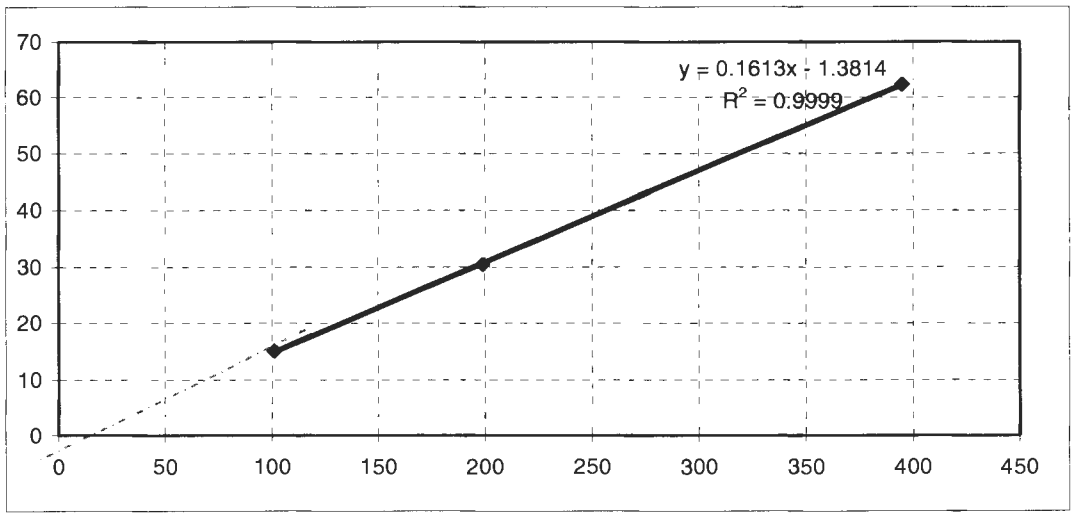

Shear parameters	c', kPa	ϕ'	r^2
Best fit straight line	~0	9.2	0.999
Line through origin	0	9.0	0.999

Rate of Angular Displacement		
Shearing Stage for 1 revolution	0.12 mm/min	0.16 deg/min
Strain Rate for Normal Stresses	0.04 mm/min	0.048 deg/min

Figure A.52. 18.2 meter (60 ft), Pierre Shale, Oahe Dam Site, PZT50-5.42, Bromhead Ring Shear report

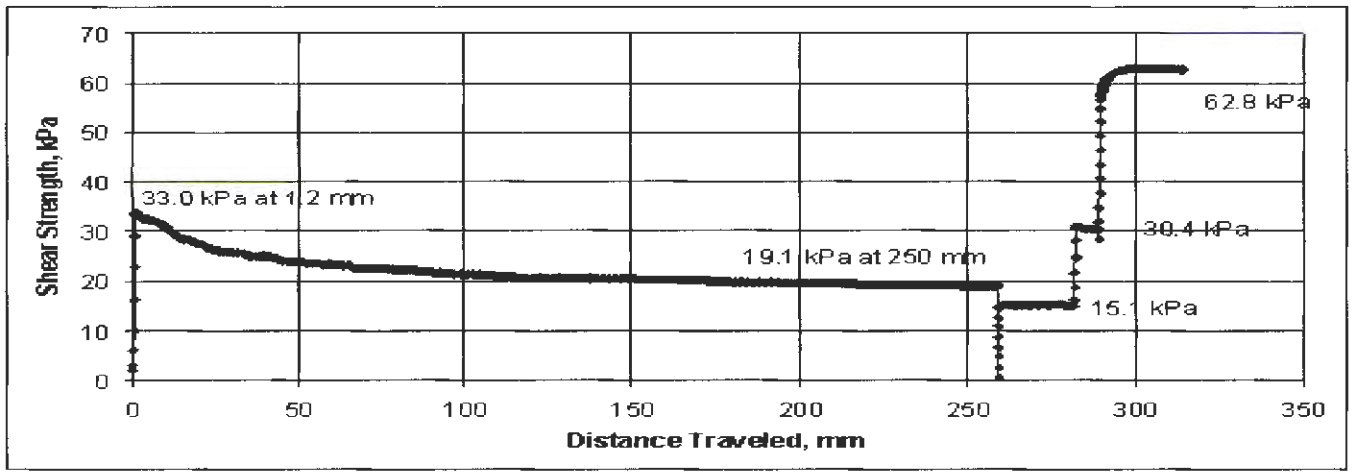

Figure A.53. 18.2 meter (60 ft), Pierre Shale, Oahe Dam Site, PZT50-5.42, residual strength plot

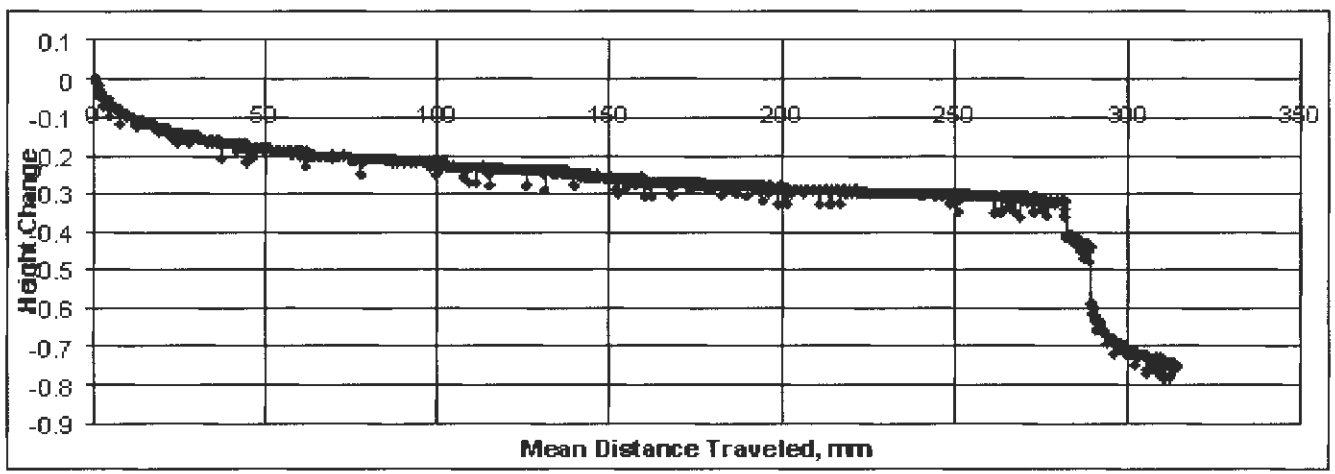

Figure A.54. 18.2 meter (60 ft), Pierre Shale, Oahe Dam Site, PZT50-5.42, settlement plot

DETERMINATION OF THE RESIDUAL SHEAR STRENGTH
IN THE BROMHEAD RING SHEAR APPARATUS

Sample Description:	WEATHERED ZONE PIERRE CLAY SHALE	Boring:	PZT50/5.42
Sample Location:	OAHE DAM SITE, SD, USA	Performed By:	MB
Sample No:	PZT50-61	Date:	6/24/2004
Depth ft:	61	Depth, m	18.5
Preparation :	Remolded at:	Initial water content (%)	44.7
		Remolded Dry Density (g/cm^3)	1.41
	Controls:	Hydrated	Multistage
		Material Passed #50	

Stage	Normal effective stress kPa	Residual Shear stress kPa	Tan phi
1	100.95	13.3	0.13
2	198.91	27.8	0.14
3	394.84	59.4	0.15

Dimensions:
Inner radius mm : 50
Outer radius mm : 35
Thickness mm : 5

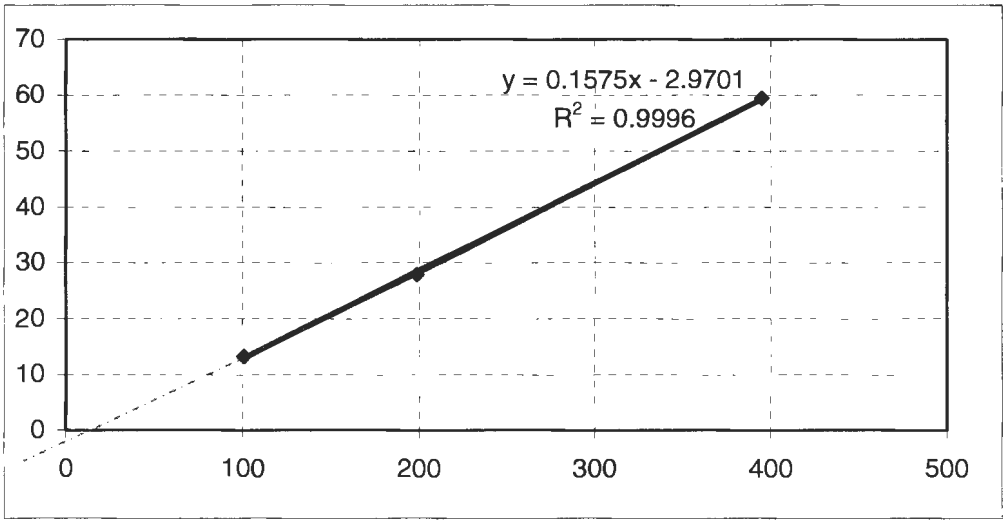

Shear parameters	c', kPa	ϕ'	r^2
Best fit straight line	~0	9.0	0.9996
Line through origin	0	8.5	0.994

Rate of Angular Displacement

Shearing Stage for 1 revolution	0.12 mm/min	0.16 deg/min
Strain Rate for Normal Stresses	0.04 mm/min	0.048 deg/min

Figure A.55. 18.5 meter (61 ft), Pierre Shale, Oahe Dam Site, PZT50-5.42, Bromhead Ring Shear report

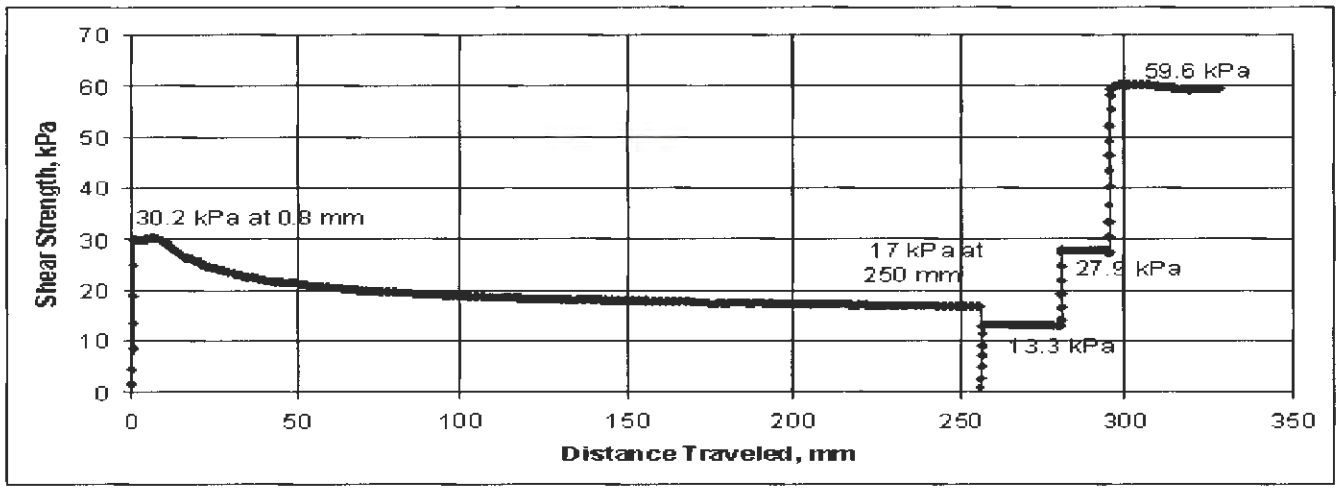

Figure A.56. 18.5 meter (61 ft), Pierre Shale, Oahe Dam Site, PZT50-5.42, residual strength plot

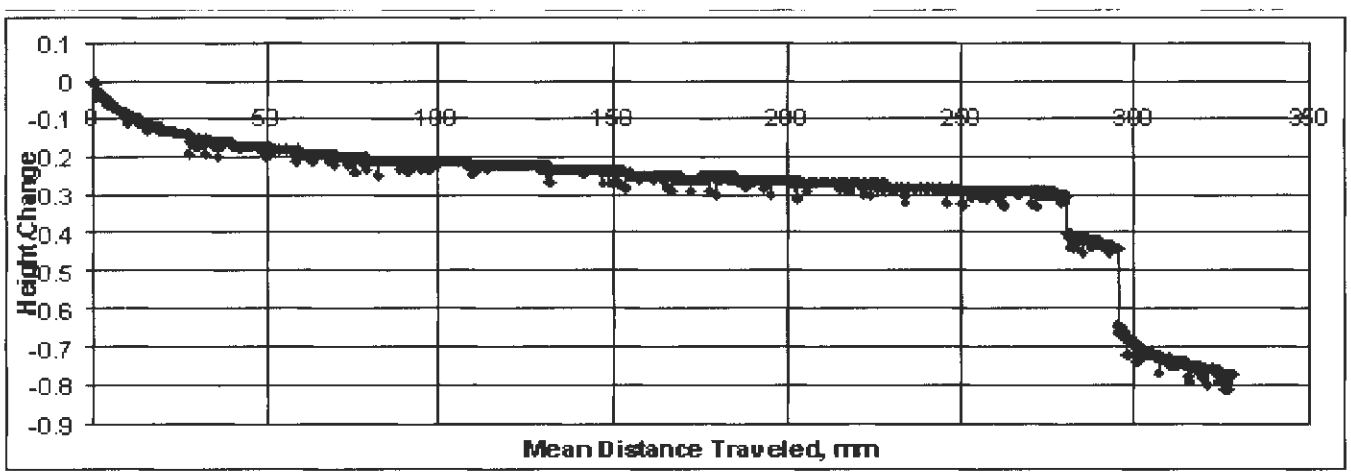

Figure A.57. 18.5 meter (61 ft), Pierre Shale, Oahe Dam Site, PZT50-5.42, settlement plot

DETERMINATION OF THE RESIDUAL SHEAR STRENGTH
IN THE BROMHEAD RING SHEAR APPARATUS

Sample Description:	WEATHERED ZONE PIERRE CLAY SHALE	Boring:	PZT50/5.42
Sample Location:	OAHE DAM SITE, SD, USA	Performed By:	MB
Sample No:	PZT50-63	Date:	6/8/2004
Depth ft:	63	Depth, m	19.1
Preparation :	Remolded at:	Initial water content (%)	44.1
		Remolded Dry Density (g/cm^3)	1.50
	Controls:	Hydrated	Multistage
		Material Passed #50	

Stage	Normal effective stress kPa	Residual Shear stress kPa	Tan phi
1	100.95	11	0.11
2	198.91	22.3	0.11
3	394.84	45.6	0.12

Dimensions:
Inner radius mm : 50
Outer radius mm : 35
Thickness mm : 5

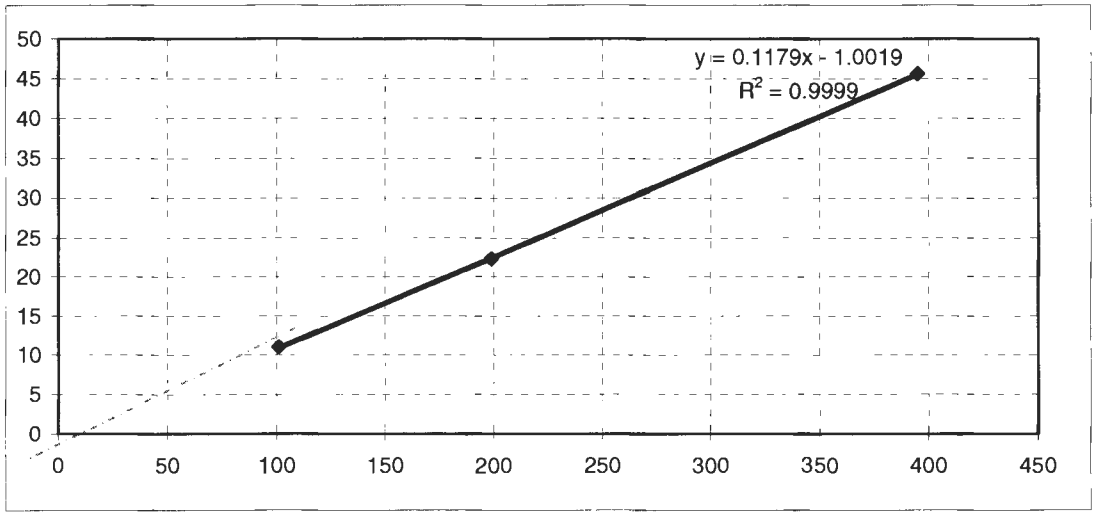

Shear parameters	c', kPa	ϕ'	r^2
Best fit straight line	~0	6.8	0.999
Line through origin	0	7.0	0.997

Rate of Angular Displacement		
Shearing Stage for 1 revolution	0.12 mm/min	0.16 deg/min
Strain Rate for Normal Stresses	0.04 mm/min	0.048 deg/min

Figure A.58. 19.1 meter (63 ft), Pierre Shale, Oahe Dam Site, PZT50-5.42, Bromhead Ring Shear report

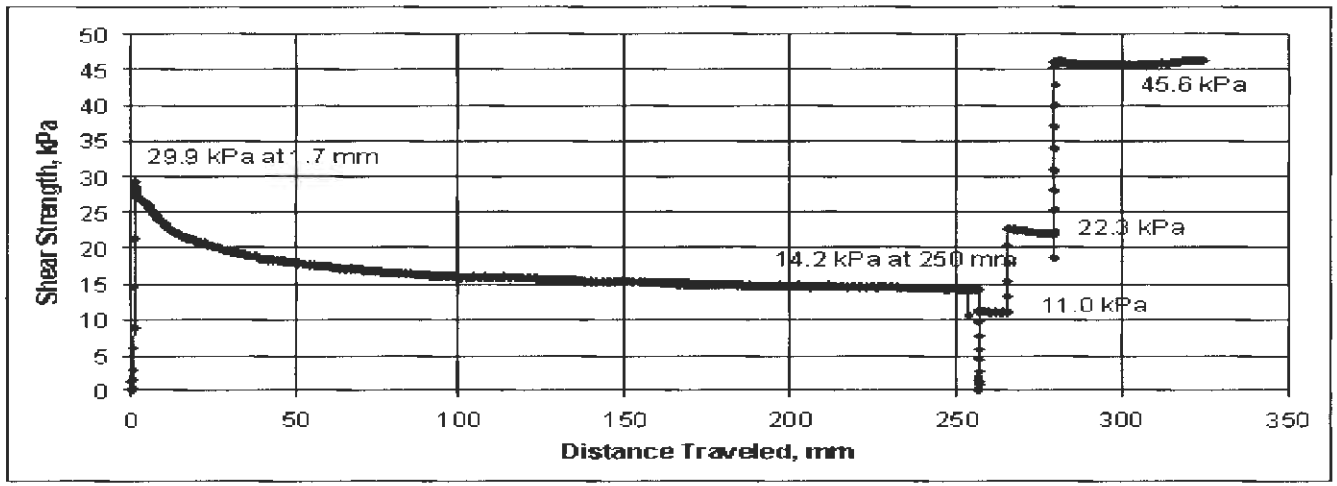

Figure A.59. 19.1 meter (63 ft), Pierre Shale, Oahe Dam Site, PZT50-5.42, residual strength plot

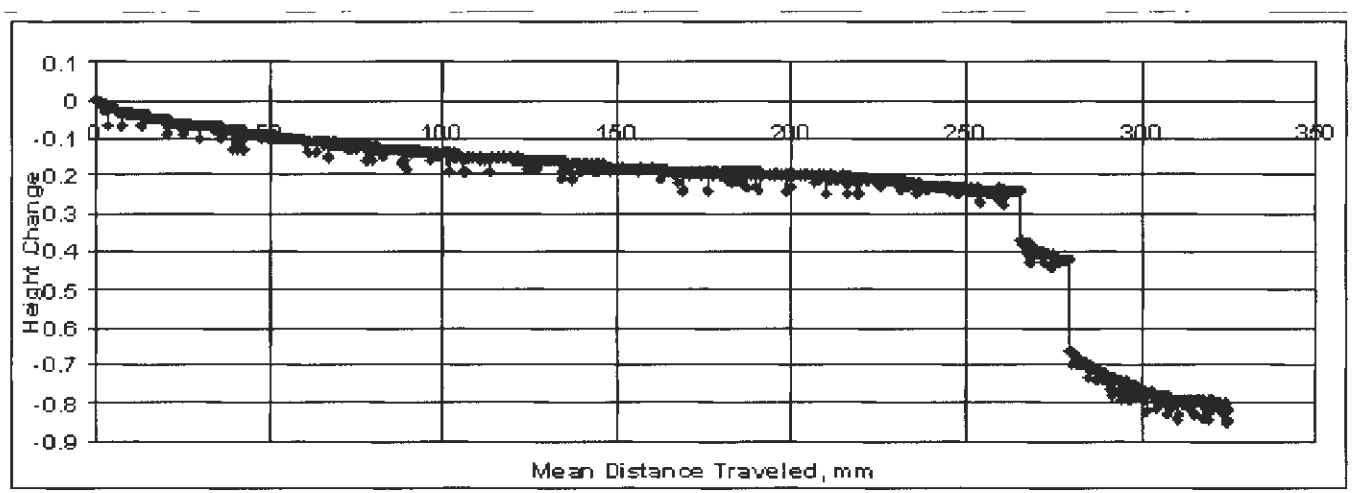

Figure A.60. 19.1 meter (63 ft), Pierre Shale, Oahe Dam Site, PZT50-5.42, settlement plot

DETERMINATION OF THE RESIDUAL SHEAR STRENGTH
IN THE BROMHEAD RING SHEAR APPARATUS

Sample Description:	WEATHERED ZONE PIERRE CLAY SHALE	Boring:	PZT50/5.42
Sample Location:	OAHE DAM SITE, SD, USA	Performed By:	MB
Sample No:	PZT50-65	Date:	7/9/2004
Depth ft:	65	Depth, m	19.7
Preparation :	Remolded at:	Initial water content (%)	44.1
		Remolded Dry Density (g/cm^3)	1.42
	Controls:	Hydrated	Multistage
		Material Passed #50	

Stage	Normal effective stress kPa	Residual Shear stress kPa	Tan phi
1	100.95	11	0.11
2	198.91	19.1	0.10
3	394.84	40.3	0.10

Dimensions:
Inner radius mm : 50
Outer radius mm : 35
Thickness mm : 5

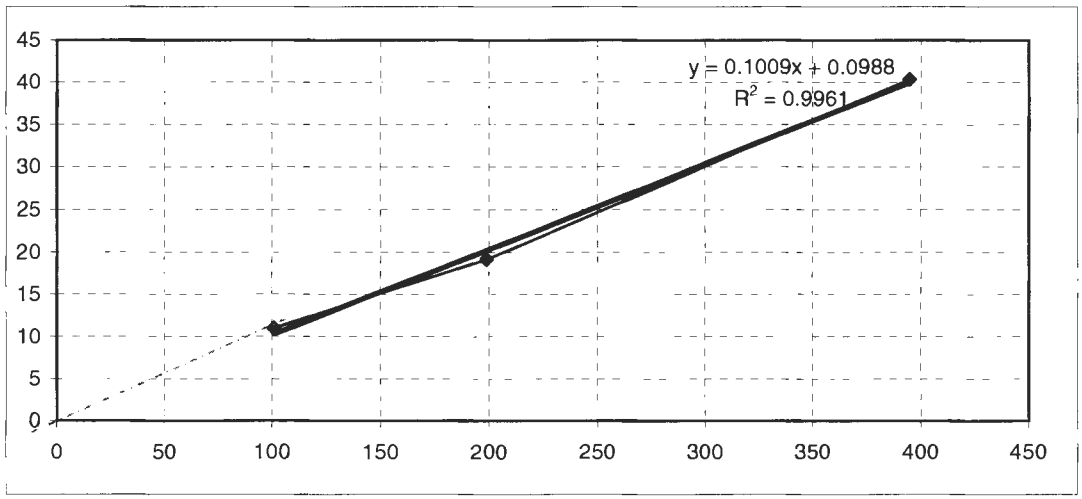

Shear parameters	c', kPa	ϕ'	r^2
Best fit straight line	0.1	5.8	0.996
Line through origin	0	5.7	0.996

Rate of Angular Displacement

Shearing Stage for 1 revolution	0.12 mm/min	0.16 deg/min
Strain Rate for Normal Stresses	0.04 mm/min	0.048 deg/min

Figure A.61. 19.7 meter (65 ft), Pierre Shale, Oahe Dam Site, PZT50-5.42, Bromhead Ring Shear report

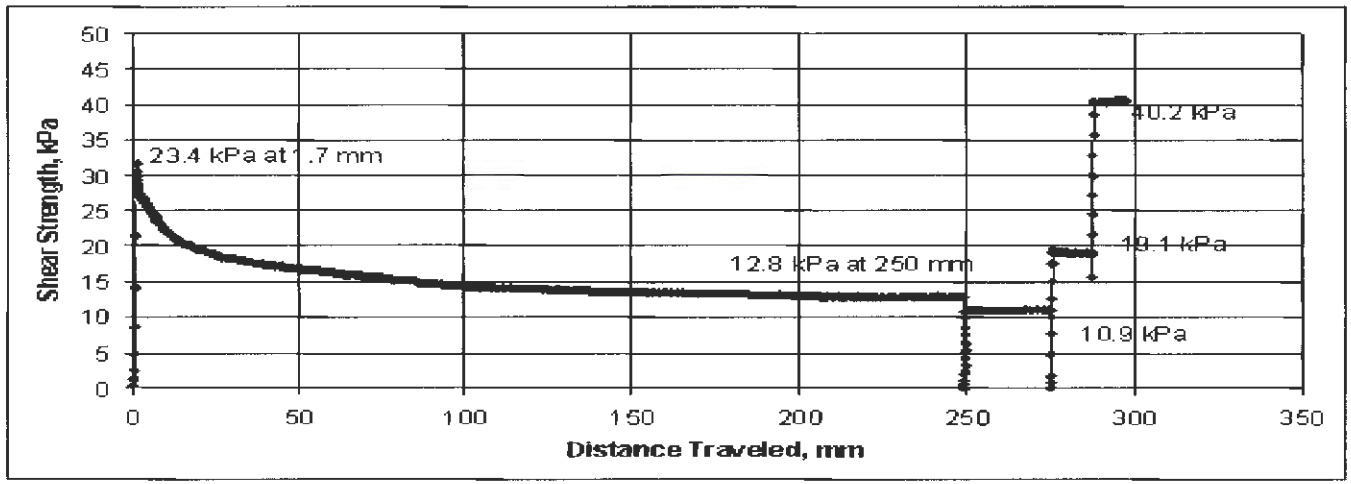

Figure A.62. 19.7 meter (65 ft), Pierre Shale, Oahe Dam Site, PZT50-5.42, residual strength plot

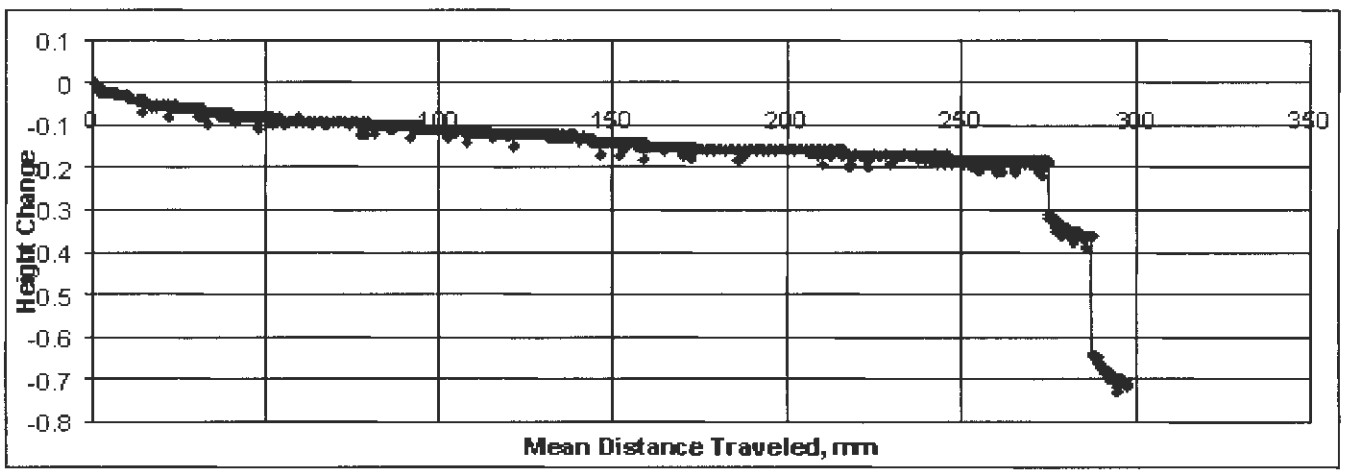

Figure A.63. 19.7 meter (65 ft), Pierre Shale, Oahe Dam Site, PZT50-5.42, settlement plot

DETERMINATION OF THE RESIDUAL SHEAR STRENGTH
IN THE BROMHEAD RING SHEAR APPARATUS

Sample Description:	WEATHERED ZONE PIERRE CLAY SHALE	Boring:	PZT50/5.42
Sample Location:	OAHE DAM SITE, SD, USA	Performed By:	MB
Sample No:	PZT50-72	Date:	7/15/2004
Depth ft:	72	Depth, m	21.8
Preparation :	Remolded at:	Initial water content (%)	44.2
		Remolded Dry Density (g/cm^3)	1.42
	Controls:	Hydrated	Multistage
		Material Passed #50	

Stage	Normal effective stress kPa	Residual Shear stress kPa	Tan phi
1	100.95	13.7	0.14
2	198.91	29.6	0.15
3	394.84	57.5	0.15

Dimensions:

Inner radius mm :	50
Outer radius mm :	35
Thickness mm :	5

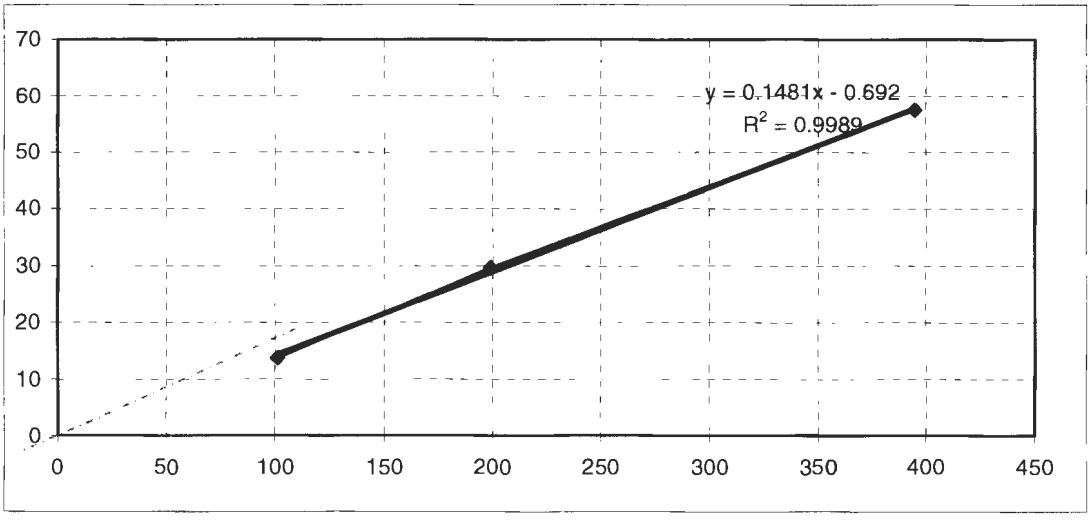

Shear parameters	c', kPa	ϕ'	r^2
Best fit straight line	~0	8.5	0.999
Line through origin	0	8.3	0.999

Rate of Angular Displacement		
Shearing Stage for 1 revolution	0.12 mm/min	0.16 deg/min
Strain Rate for Normal Stresses	0.04 mm/min	0.048 deg/min

Figure A.64. 21.8 meter (72 ft), Pierre Shale, Oahe Dam Site, PZT50-5.42, Bromhead Ring Shear report

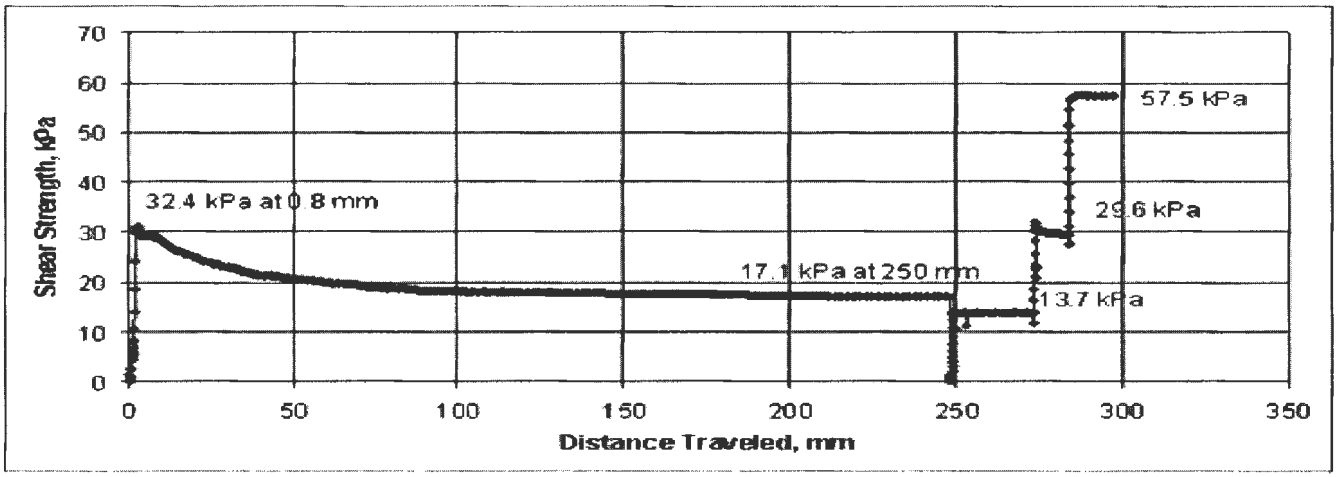

Figure A.65. 21.8 meter (72 ft), Pierre Shale, Oahe Dam Site, PZT50-5.42, residual strength plot

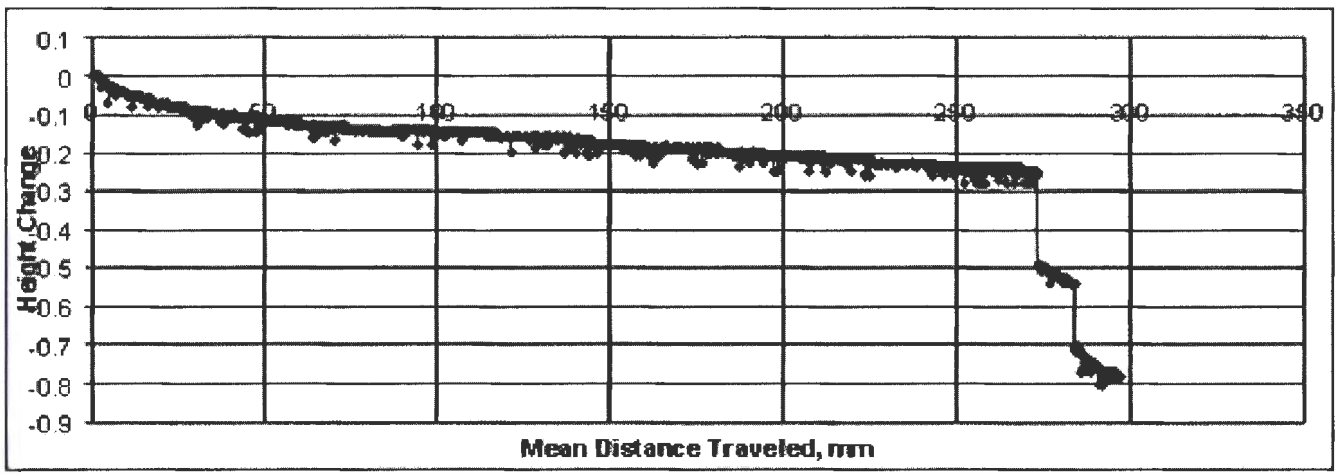

Figure A.66. 21.8 meter (72 ft), Pierre Shale, Oahe Dam Site, PZT50-5.42, settlement plot

DETERMINATION OF THE RESIDUAL SHEAR STRENGTH
IN THE BROMHEAD RING SHEAR APPARATUS

Sample Description:	TRANSITIONAL ZONE PIERRE CLAY SHALE	Boring:	PZT50/5.42
Sample Location:	OAHE DAM SITE, SD, USA	Performed By:	MB
Sample No:	PZT50-75	Date:	7/28/2005
Depth ft:	75	Depth, m	22.7
Preparation :	Remolded at:	Initial water content (%)	38.1
		Remolded Dry Density (g/cm^3)	1.45
	Controls:	Hydrated	Multistage
		Material Passed #50	

Stage	Normal effective stress kPa	Residual Shear stress kPa	Tan phi
1	100.95	18.9	0.19
2	198.91	36.6	0.18
3	394.84	75.8	0.19

Dimensions:

Inner radius mm :	50
Outer radius mm :	35
Thickness mm :	5

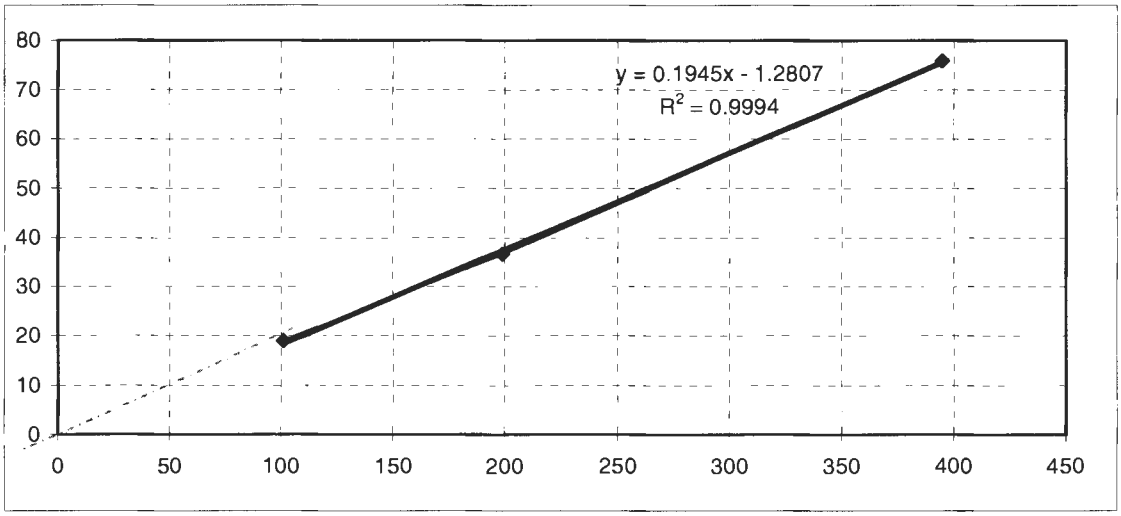

Shear parameters	c', kPa	ϕ'	r^2
Best fit straight line	~0	11.1	0.999
Line through origin	0	10.9	0.999

Rate of Angular Displacement		
Shearing Stage for 1 revolution	0.12 mm/min	0.16 deg/min
Strain Rate for Normal Stresses	0.04 mm/min	0.048 deg/mir

Figure A.67. 22.7 meter (75 ft), Pierre Shale, Oahe Dam Site, PZT50-5.42, Bromhead Ring Shear report

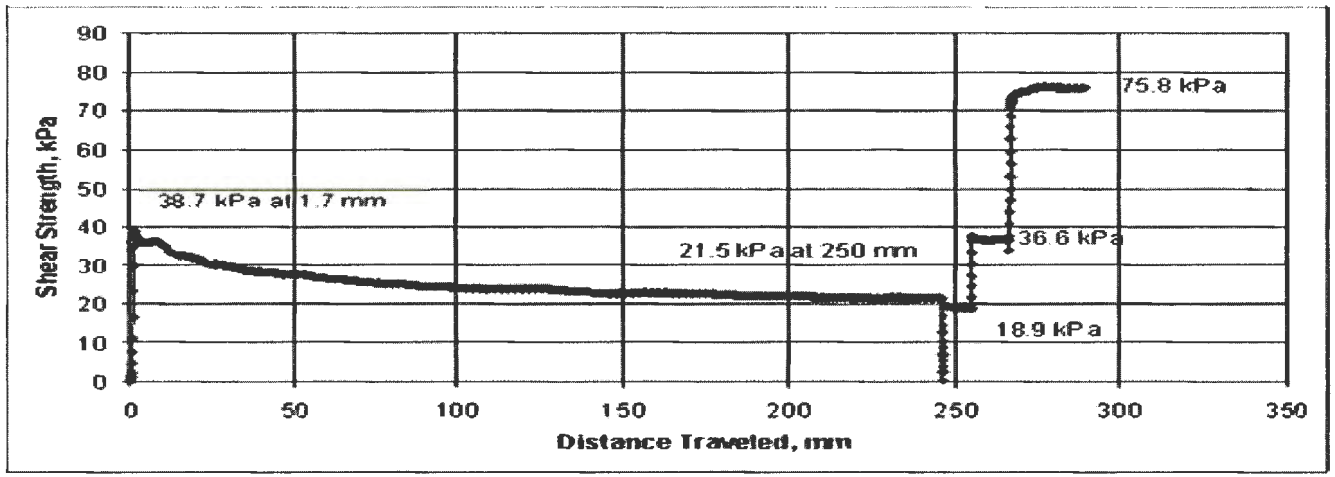

Figure A.68. 22.7 meter (75 ft), Pierre Shale, Oahe Dam Site, PZT50-5.42, residual strength plot

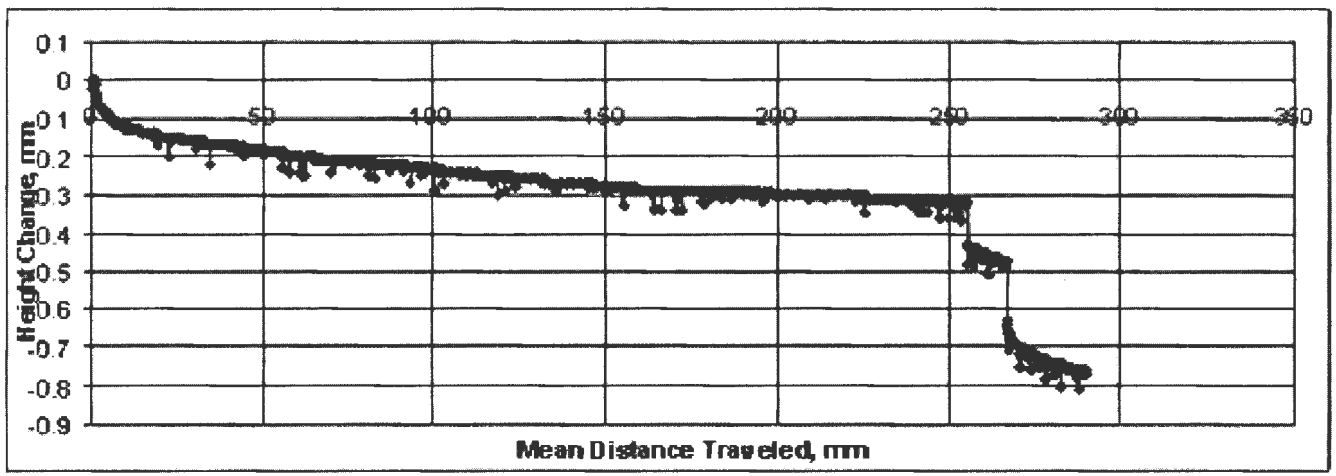

Figure A.69. 22.7 meter (75 ft), Pierre Shale, Oahe Dam Site, PZT50-5.42, settlement plot

DETERMINATION OF THE RESIDUAL SHEAR STRENGTH
IN THE BROMHEAD RING SHEAR APPARATUS

Sample Description:	TRANSITIONAL ZONE PIERRE CLAY SHALE	Boring:	PZT50/5.42
Sample Location:	OAHE DAM SITE, SD, USA	Performed By:	MB
Sample No:	PZT50-79	Date:	7/11/2004
Depth ft:	79	Depth, m	23.9
Preparation :	Remolded at:	Initial water content (%)	47.7
		Remolded Dry Density (g/cm^3)	1.50
	Controls:	Hydrated	Multistage
		Material Passed #50	

Stage	Normal effective stress kPa	Residual Shear stress kPa	Tan phi
1	100.95	16.8	0.17
2	198.91	36	0.18
3	394.84	74.5	0.19

Dimensions:

Inner radius mm :	50
Outer radius mm :	35
Thickness mm :	5

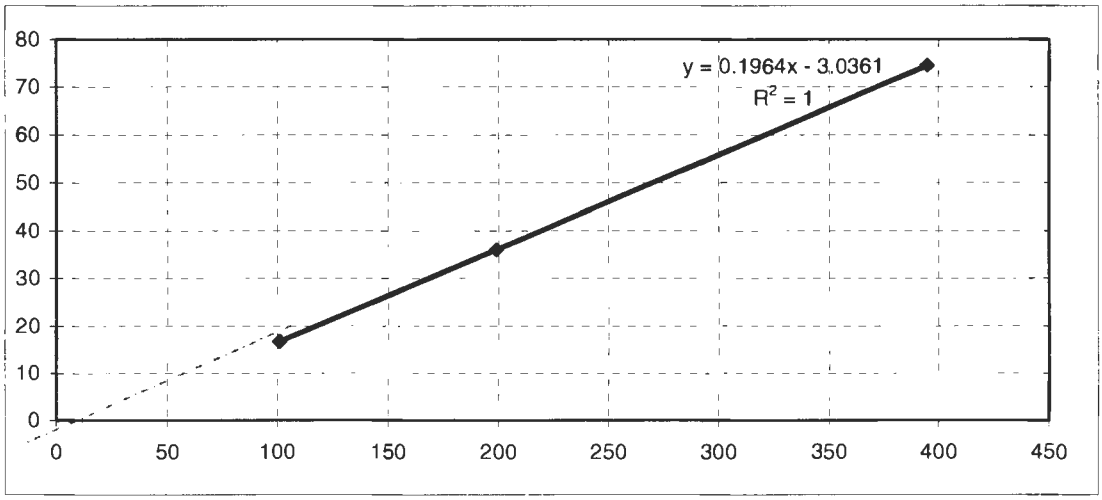

Shear parameters	c', kPa	ϕ'	r^2
Best fit straight line	~0	11.3	1
Line through origin	0	10.7	0.997

Rate of Angular Displacement

Shearing Stage for 1 revolution	0.12 mm/min	0.16 deg/min
Strain Rate for Normal Stresses	0.04 mm/min	0.048 deg/min

Figure A.70. 23.9 meter (79 ft), Pierre Shale, Oahe Dam Site, PZT50-5.42, Bromhead Ring Shear report

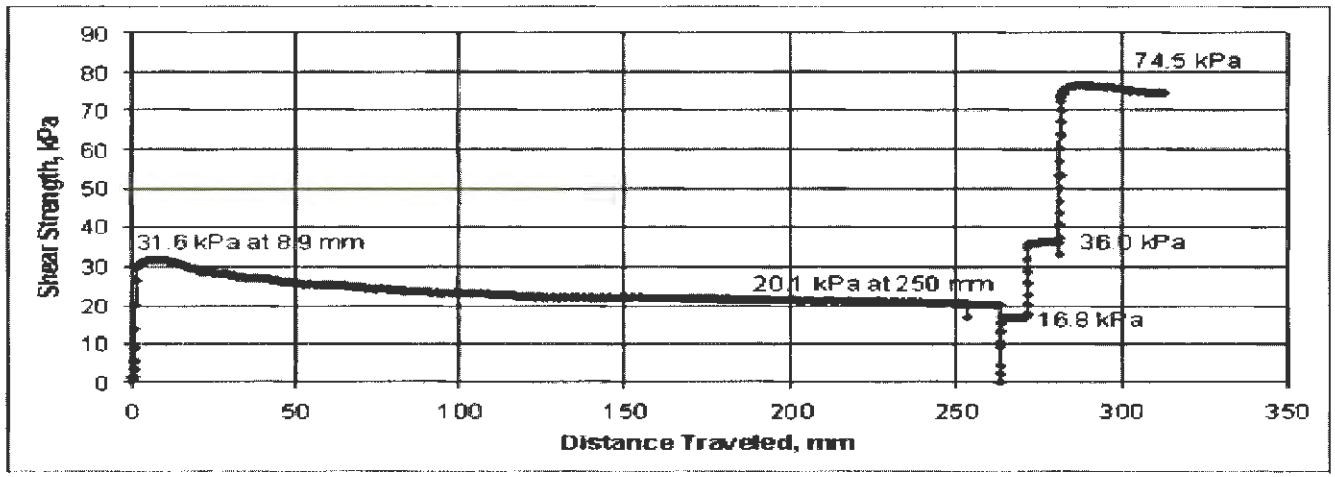

Figure A.71. 23.9 meter (79 ft), Pierre Shale, Oahe Dam Site, PZT50-5.42, residual strength plot

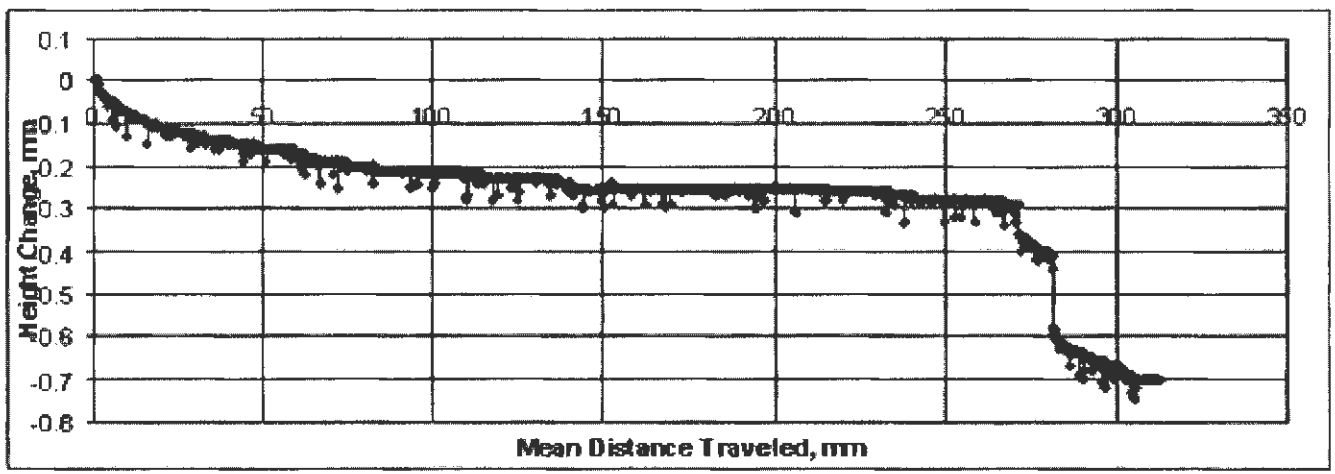

Figure A.72. 23.9 meter (79 ft), Pierre Shale, Oahe Dam Site, PZT50-5.42, settlement plot

DETERMINATION OF THE RESIDUAL SHEAR STRENGTH
IN THE BROMHEAD RING SHEAR APPARATUS

Sample Description:	TRANSITIONAL ZONE PIERRE CLAY SHALE	Boring:	PZT50/5.42
Sample Location:	OAHE DAM SITE, SD, USA	Performed By:	MB
Sample No:	PZT50-85	Date:	7/1/2004
Depth ft:	85	Depth, m	25.8
Preparation :	Remolded at:	Initial water content (%)	38.5
		Remolded Dry Density (g/cm^3)	1.45

Controls: Hydrated Multistage
Material Passed #50

Stage	Normal effective stress kPa	Residual Shear stress kPa	Tan phi
1	100.95	14	0.14
2	198.91	26.6	0.13
3	394.84	58.3	0.15

Dimensions:
Inner radius mm : 50
Outer radius mm : 35
Thickness mm : 5

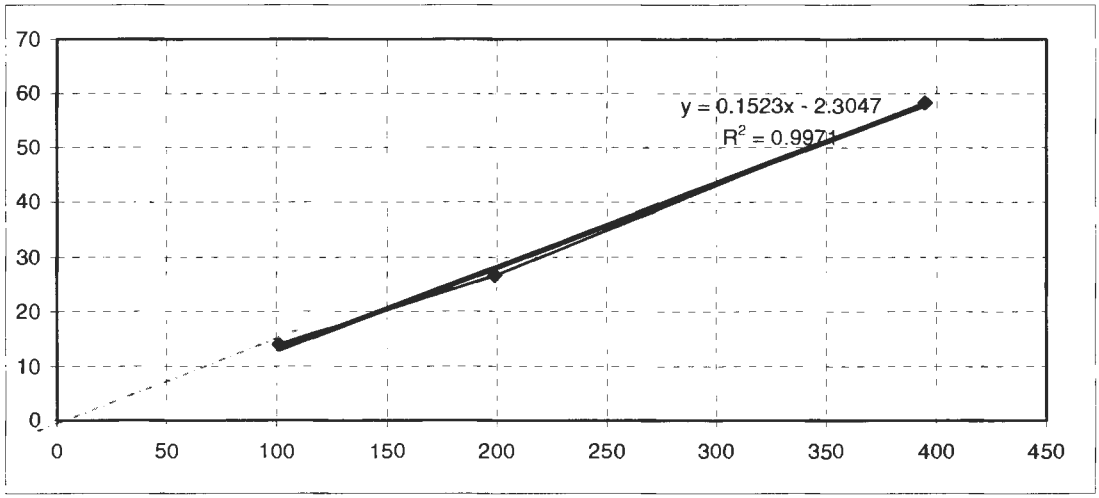

Shear parameters	c', kPa	φ'	r^2
Best fit straight line	~0	8.7	0.997
Line through origin	0	8.3	0.994

Rate of Angular Displacement

Shearing Stage for 1 revolution	0.12 mm/min	0.16 deg/min
Strain Rate for Normal Stresses	0.04 mm/min	0.048 deg/min

Figure A.73. 25.8 meter (85 ft), Pierre Shale, Oahe Dam Site, PZT50-5.42, Bromhead Ring Shear report

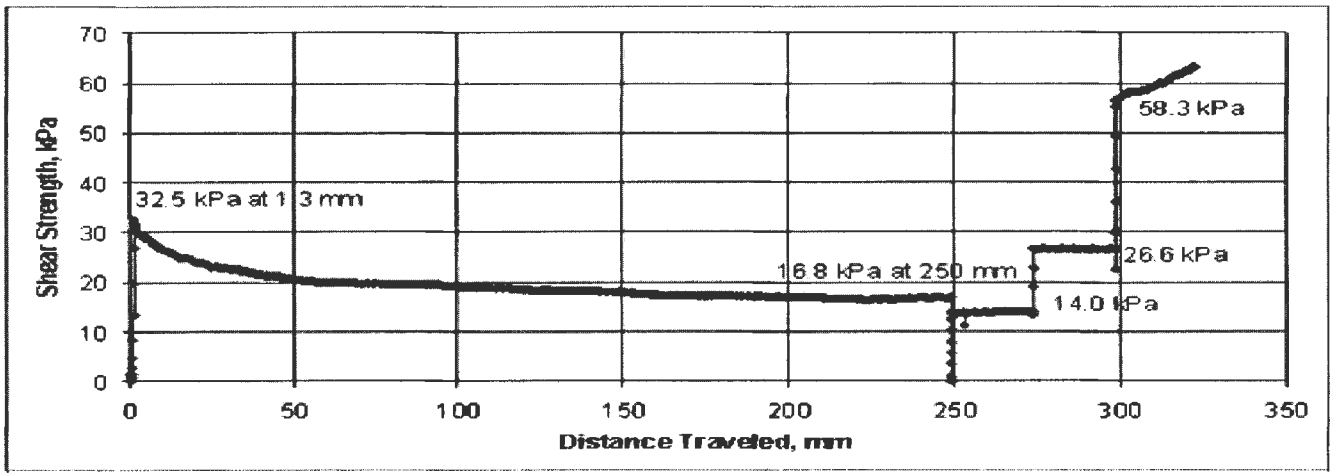

Figure A.74. 25.8 meter (85 ft), Pierre Shale, Oahe Dam Site, PZT50-5.42, residual strength plot

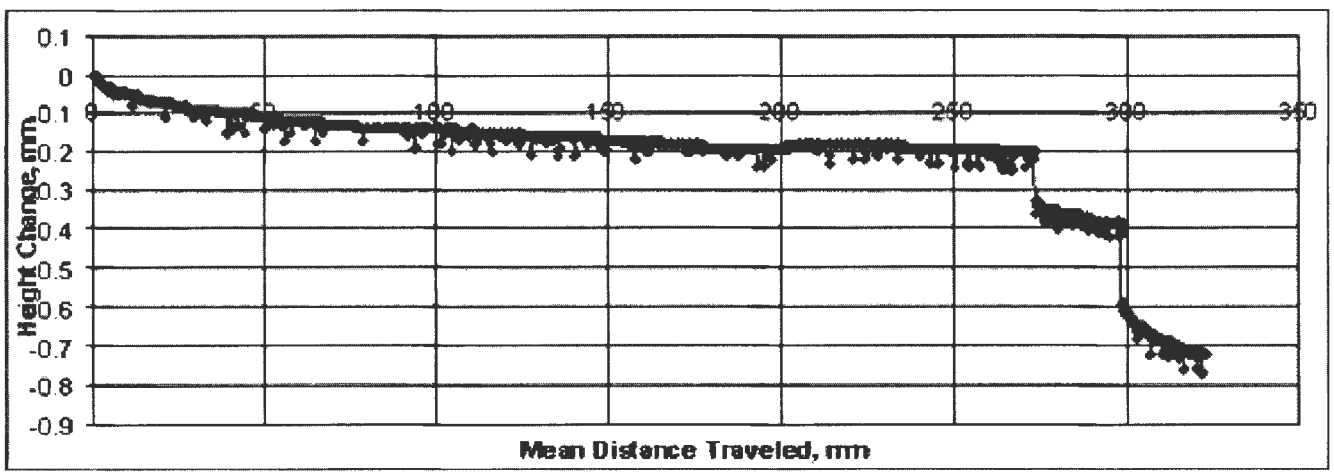

Figure A.75. 25.8 meter (85 ft), Pierre Shale, Oahe Dam Site, PZT50-5.42, settlement plot

DETERMINATION OF THE RESIDUAL SHEAR STRENGTH
IN THE BROMHEAD RING SHEAR APPARATUS

Sample Description:	TRANSITIONAL ZONE PIERRE CLAY SHALE	Boring:	PZT50/5.42
Sample Location:	OAHE DAM SITE, SD, USA	Performed By:	MB
Sample No:	PZT50-89	Date:	7/8/2004
Depth ft:	89	Depth, m	27
Preparation :	Remolded at:	Initial water content (%)	44.1
		Remolded Dry Density (g/cm^3)	1.47
	Controls:	Hydrated	Multistage
		Material Passed #50	

Stage	Normal effective stress kPa	Residual Shear stress kPa	Tan phi
1	100.95	13.3	0.13
2	198.91	25.7	0.13
3	394.84	50.8	0.13

Dimensions:

Inner radius mm :	50
Outer radius mm :	35
Thickness mm :	5

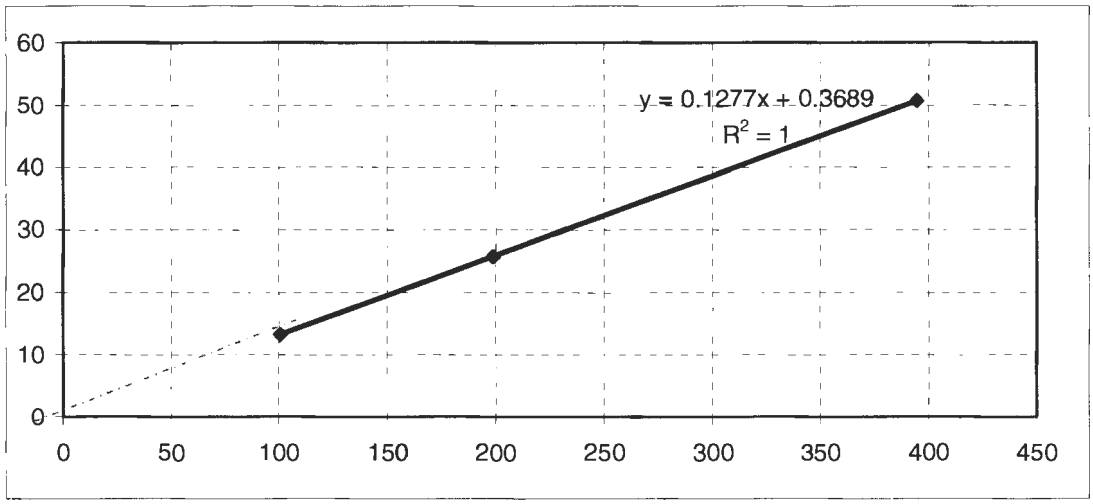

Shear parameters	c', kPa	ϕ'	r^2
Best fit straight line	0.4	7.3	1
Line through origin	0	7.4	0.999

Rate of Angular Displacement		
Shearing Stage for 1 revolution	0.12 mm/min	0.16 deg/min
Strain Rate for Normal Stresses	0.04 mm/min	0.048 deg/min

Figure A.76. 27.0 meter (89 ft), Pierre Shale, Oahe Dam Site, PZT50-5.42, Bromhead Ring Shear report

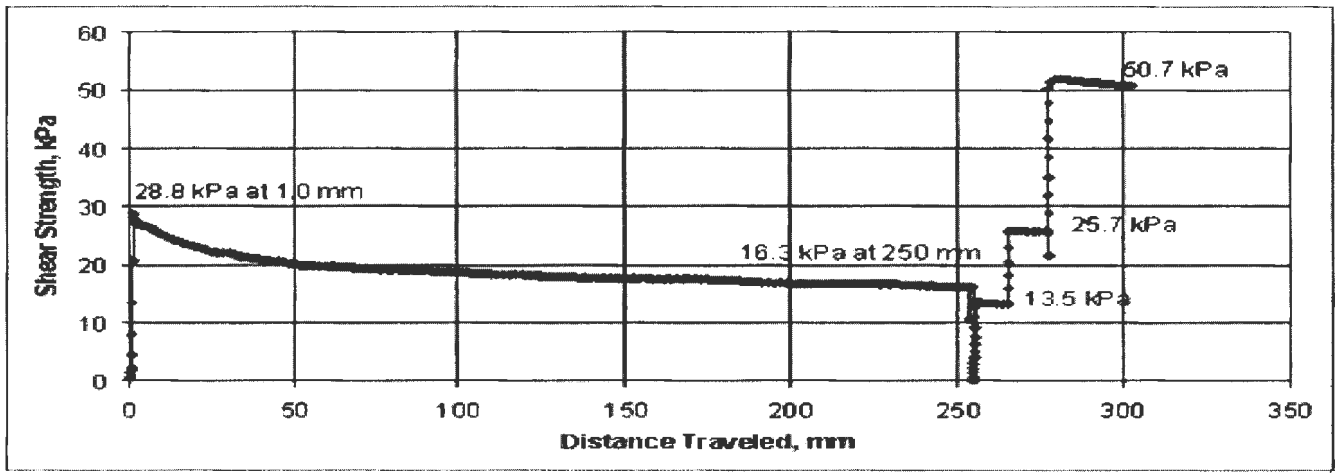

Figure A.77. 27.0 meter (89 ft), Pierre Shale, Oahe Dam Site, PZT50-5.42, residual strength plot

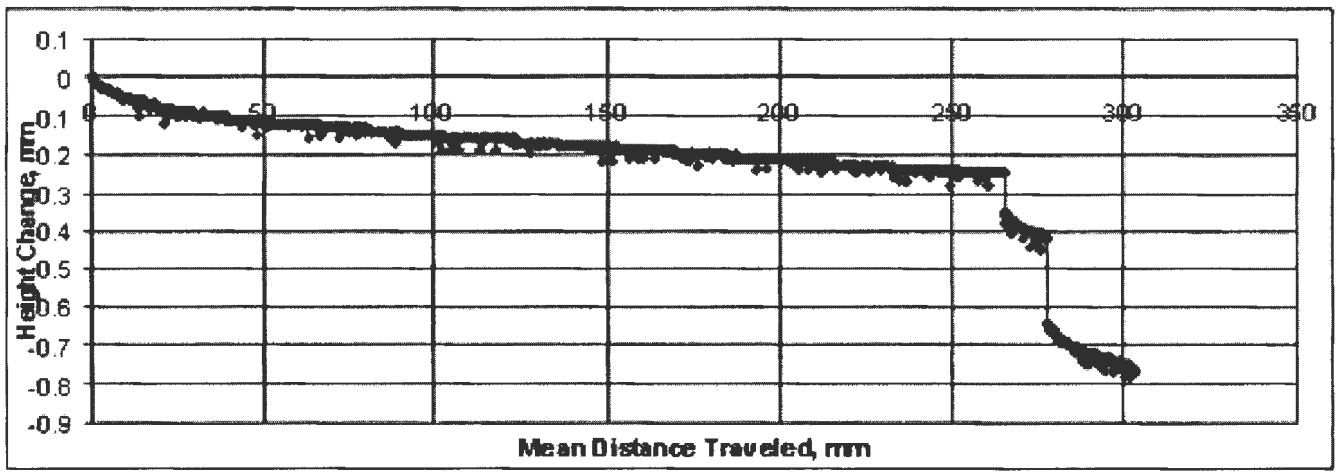

Figure A.78. 27.0 meter (89 ft), Pierre Shale, Oahe Dam Site, PZT50-5.42, settlement plot

DETERMINATION OF THE RESIDUAL SHEAR STRENGTH
IN THE BROMHEAD RING SHEAR APPARATUS

Sample Description:	UNWEATHERED ZONE PIERRE CLAY SHALE	Boring:	PZT50/5.42
Sample Location:	OAHE DAM SITE, SD, USA	Performed By:	MB
Sample No:	PZT50-95	Date:	6/8/2004
Depth ft:	95	Depth, m	28.8
Preparation :	Remolded at:	Initial water content (%)	44.1
		Remolded Dry Density (g/cm^3)	1.50
	Controls:	Hydrated	Multistage
		Material Passed #50	

Stage	Normal effective stress kPa	Residual Shear stress kPa	Tan phi
1	100.95	10.9	0.11
2	198.91	22.3	0.11
3	394.84	46.7	0.12

Dimensions:

Inner radius mm :	50
Outer radius mm :	35
Thickness mm :	5

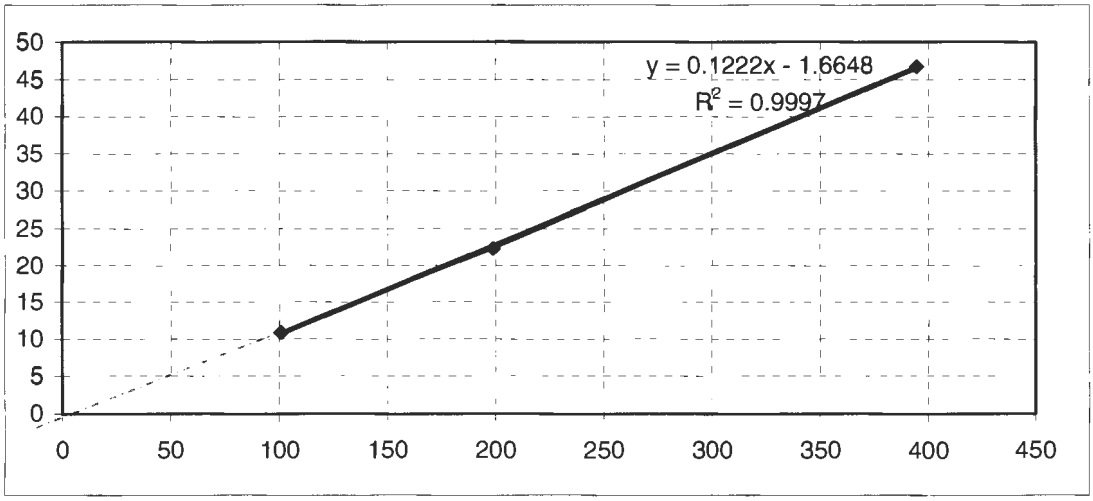

Shear parameters	c', kPa	φ'	r^2
Best fit straight line	~0	7.0	0.999
Line through origin	0	6.7	0.997

Rate of Angular Displacement

Shearing Stage for 1 revolution	0.12 mm/min	0.16 deg/min
Strain Rate for Normal Stresses	0.04 mm/min	0.048 deg/min

Figure A.79. 28.8 meter (95 ft), Pierre Shale, Oahe Dam Site, PZT50-5.42, Bromhead Ring Shear report

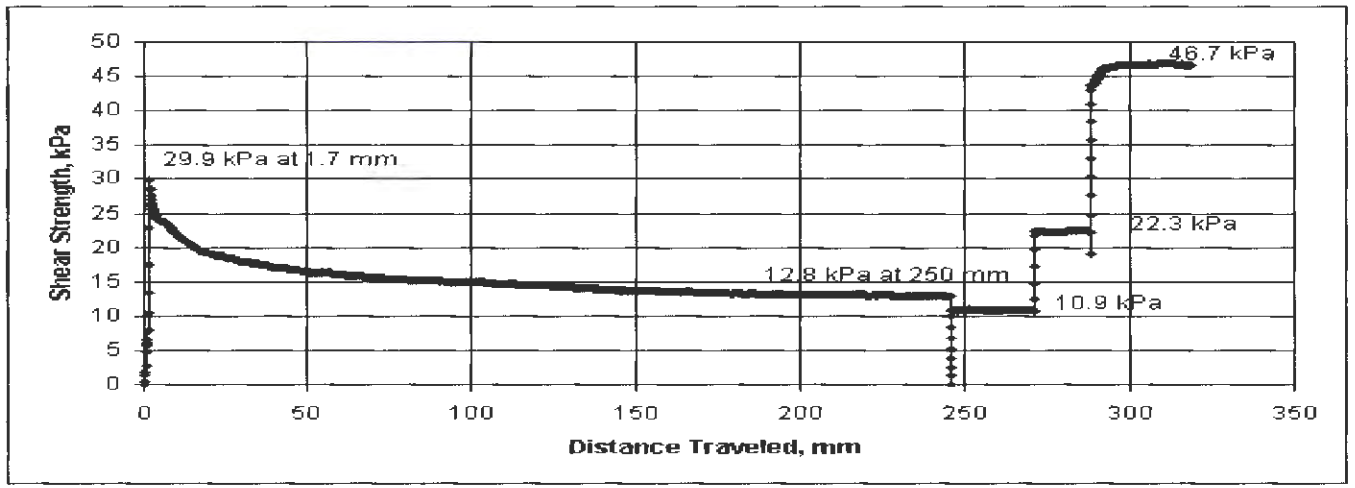

Figure A.80. 28.8 meter (95 ft), Pierre Shale, Oahe Dam Site, PZT50-5.42, residual strength plot

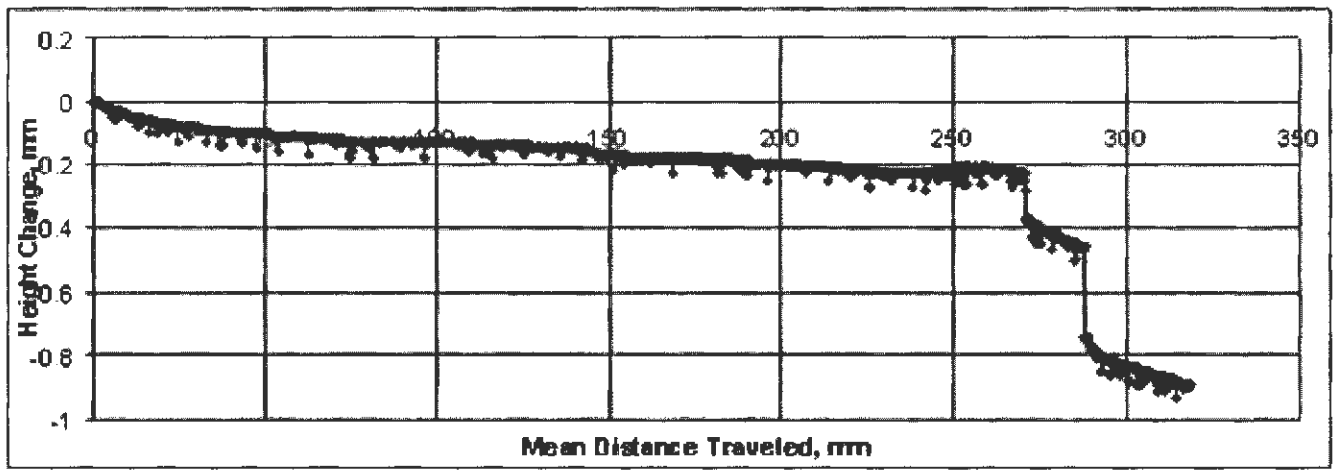

Figure A.81. 28.8 meter (95 ft), Pierre Shale, Oahe Dam Site, PZT50-5.42, settlement plot

DETERMINATION OF THE RESIDUAL SHEAR STRENGTH
IN THE BROMHEAD RING SHEAR APPARATUS

Sample Description:	UNWEATHERED ZONE PIERRE CLAY SHALE	Boring:	PZT50/5.42
Sample Location:	OAHE DAM SITE, SD, USA	Performed By:	MB
Sample No:	PZT50-105	Date:	6/12/2004
Depth ft:	105	Depth, m	31.8
Preparation :	Remolded at:	Initial water content (%)	42.1
		Remolded Dry Density (g/cm^3)	1.49
	Controls:	Hydrated Material Passed #50	Multistage

Stage	Normal effective stress kPa	Residual Shear stress kPa	Tan phi
1	100.95	11.3	0.11
2	198.91	23.5	0.12
3	394.84	48.9	0.12

Dimensions:

Inner radius mm :	50
Outer radius mm :	35
Thickness mm :	5

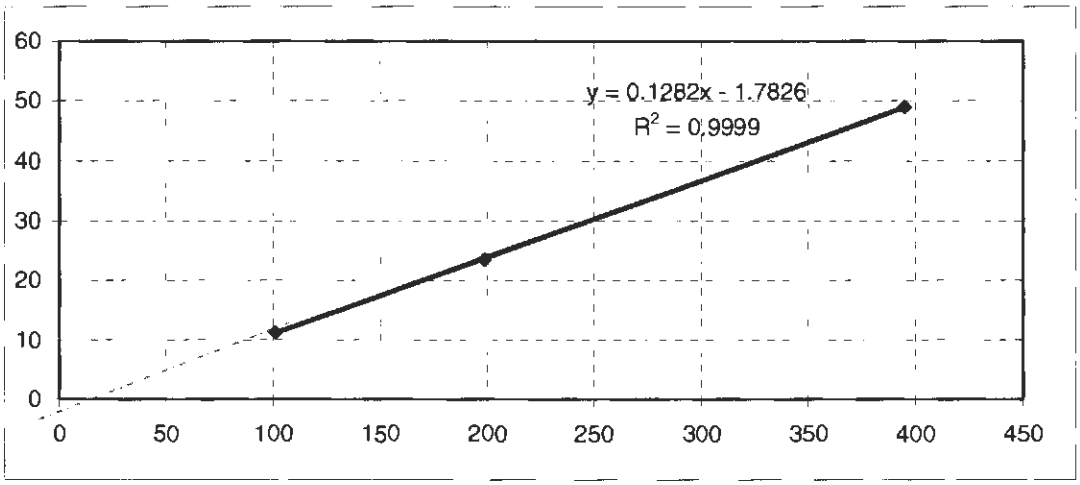

Shear parameters	c', kPa	ϕ'	r^2
Best fit straight line	~0	7.3	0.999
Line through origin	0	7.0	0.997

Rate of Angular Displacement

Shearing Stage for 1 revolution	0.12 mm/min	0.16 deg/min
Strain Rate for Normal Stresses	0.04 mm/min	0.048 deg/min

Figure A.82. 31.8 meter (105 ft), Pierre Shale, Oahe Dam Site, PZT50-5.42, Bromhead Ring

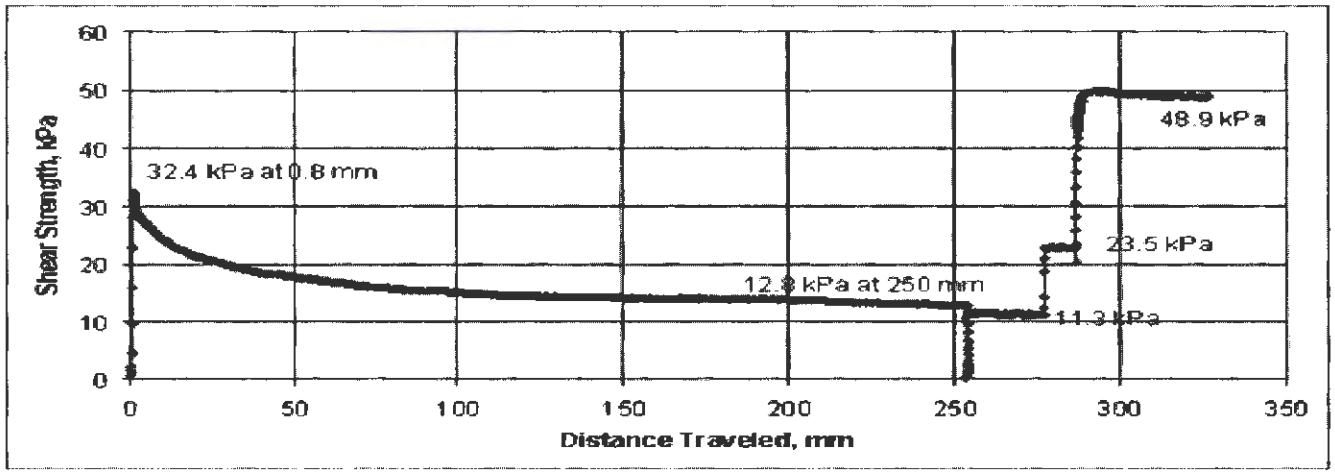

Figure A.83. 28.8 meter (95 ft), Pierre Shale, Oahe Dam Site, PZT50-5.42, residual strength plot

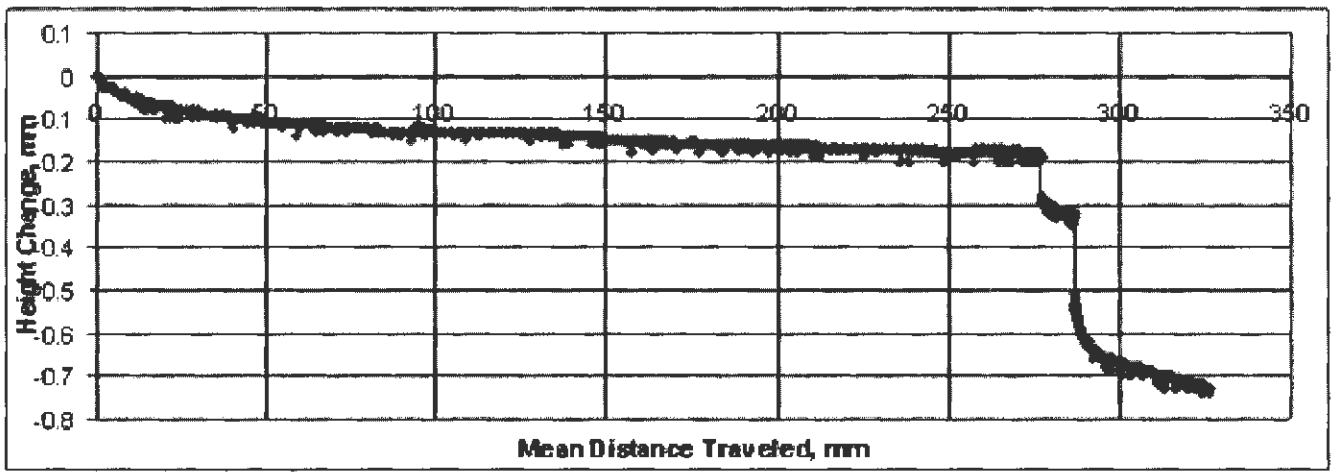

Figure A.84. 28.8 meter (95 ft), Pierre Shale, Oahe Dam Site, PZT50-5.42, settlement plot

DETERMINATION OF THE RESIDUAL SHEAR STRENGTH
IN THE BROMHEAD RING SHEAR APPARATUS

Sample Description:	UNWEATHERED ZONE PIERRE CLAY SHALE	Boring:	PZT50/5.42
Sample Location:	OAHE DAM SITE, SD, USA	Performed By:	MB
Sample No:	PZT50-113	Date:	7/5/2004
Depth ft:	113	Depth, m	34.2
Preparation :	Remolded at:	Initial water content (%)	45.1
		Remolded Dry Density (g/cm^3)	1.54

Controls: Hydrated Multistage
Material Passed #50

Stage	Normal effective stress kPa	Residual Shear stress kPa	Tan phi
1	100.95	10.6	0.11
2	198.91	22.2	0.11
3	394.84	45.2	0.11

Dimensions:
Inner radius mm : 50
Outer radius mm : 35
Thickness mm : 5

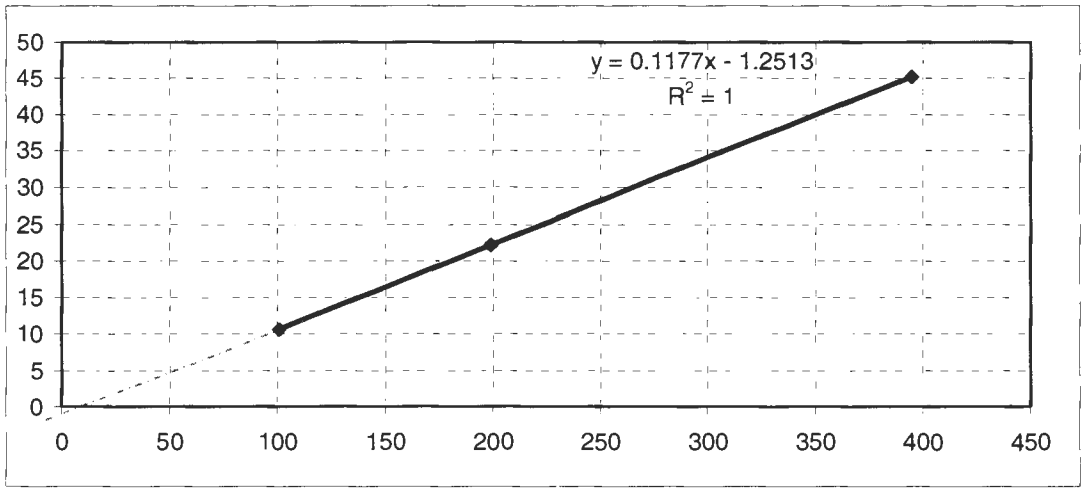

Shear parameters	c', kPa	ϕ'	r^2
Best fit straight line	~0	6.7	1
Line through origin	0	6.5	0.999

Rate of Angular Displacement		
Shearing Stage for 1 revolution	0.12 mm/min	0.16 deg/min
Strain Rate for Normal Stresses	0.04 mm/min	0.048 deg/min

Figure A.85. 34.2 meter (113 ft), Pierre Shale, Oahe Dam Site, PZT50-5.42, Bromhead Ring

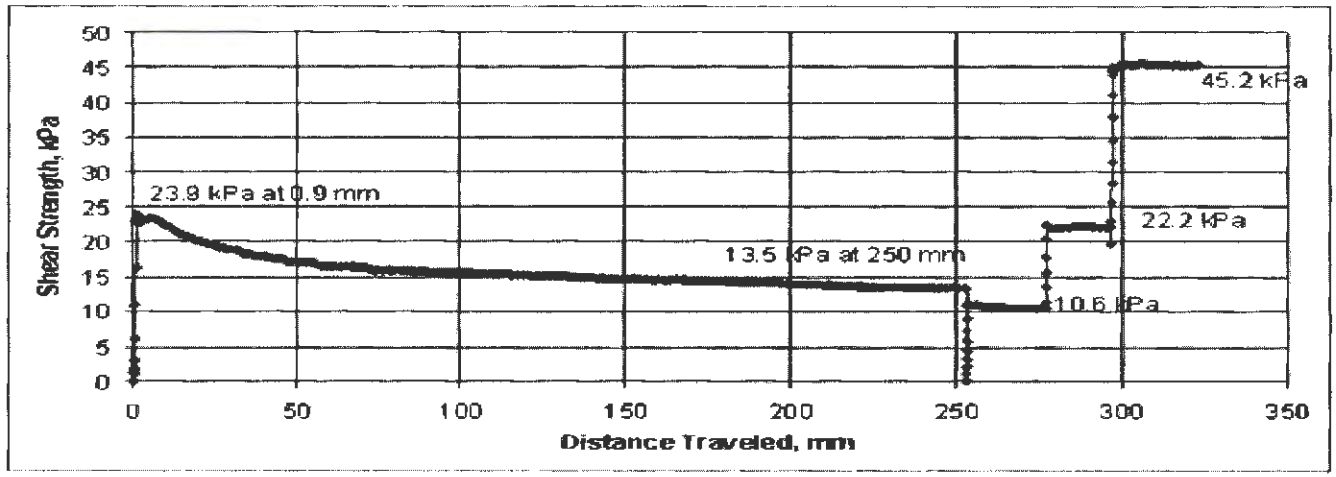

Figure A.86. 34.2 meter (113 ft), Pierre Shale, Oahe Dam Site, PZT50-5.42, residual strength plot

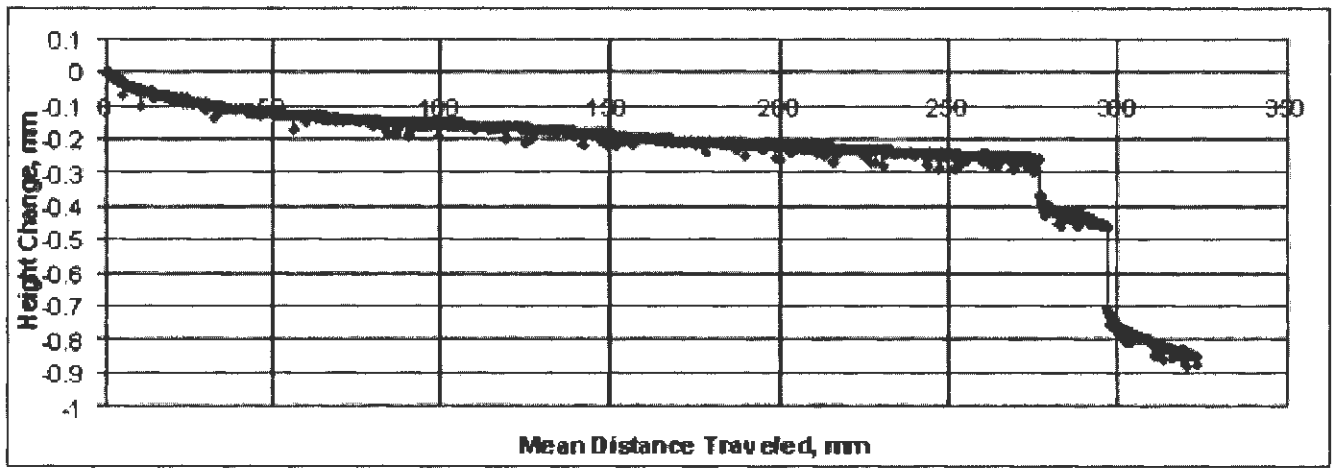

Figure A.87. 34.2 meter (113 ft), Pierre Shale, Oahe Dam Site, PZT50-5.42, settlement plot

DETERMINATION OF THE RESIDUAL SHEAR STRENGTH
IN THE BROMHEAD RING SHEAR APPARATUS

Sample Description:	UNWEATHERED ZONE PIERRE CLAY SHALE	Boring:	PZT50/5.42
Sample Location:	OAHE DAM SITE, SD, USA	Performed By:	MB
Sample No:	PZT50-105	Date:	6/12/2004
Depth ft:	105	Depth, m	31.8
Preparation :	Remolded at:	Initial water content (%)	42.1
		Remolded Dry Density (g/cm^3)	1.49
	Controls:	Hydrated Material Passed #50	Multistage

Stage	Normal effective stress kPa	Residual Shear stress kPa	Tan phi
1	100.95	11.3	0.11
2	198.91	23.5	0.12
3	394.84	48.9	0.12

Dimensions:

Inner radius mm :	50
Outer radius mm :	35
Thickness mm :	5

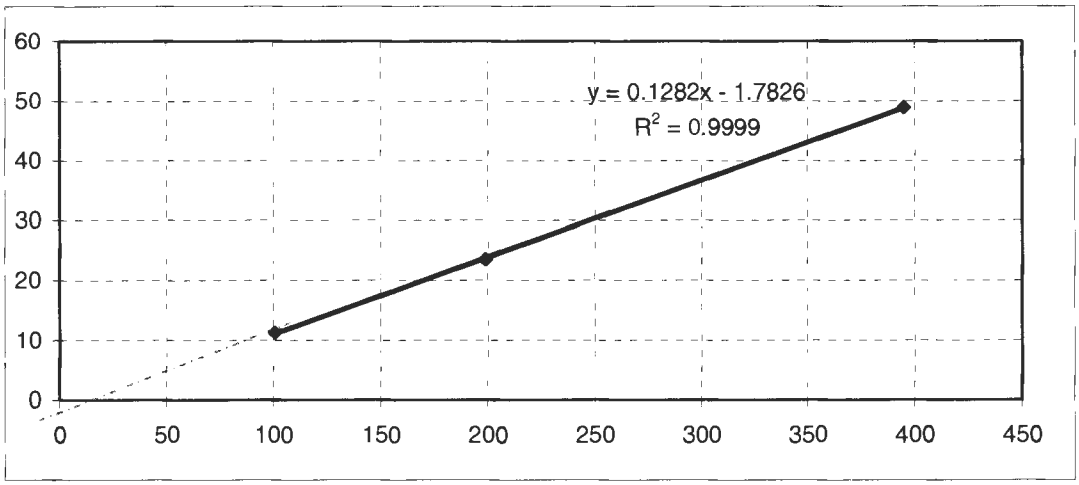

Shear parameters	c', kPa	ϕ'	r^2
Best fit straight line	~0	7.3	0.999
Line through origin	0	7.0	0.997

Rate of Angular Displacement

Shearing Stage for 1 revolution	0.12 mm/min	0.16 deg/min
Strain Rate for Normal Stresses	0.04 mm/min	0.048 deg/min

Figure A.88. 31.8 meter (105 ft), Pierre Shale, Oahe Dam Site, PZT50-5.42, Bromhead Ring

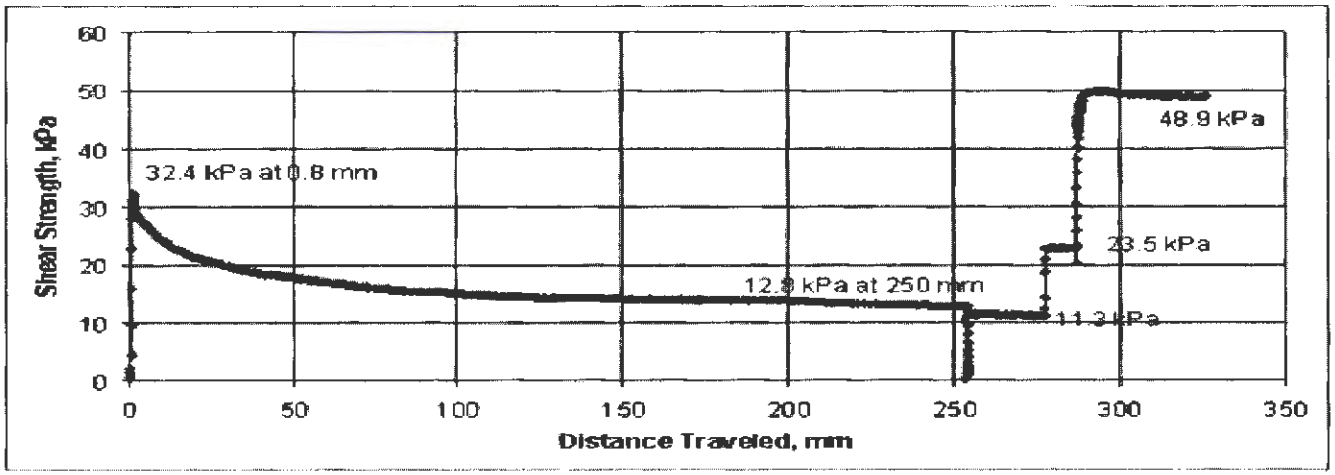

Figure A.89. 31.8 meter (105 ft), Pierre Shale, Oahe Dam Site, PZT50-5.42, residual strength plot

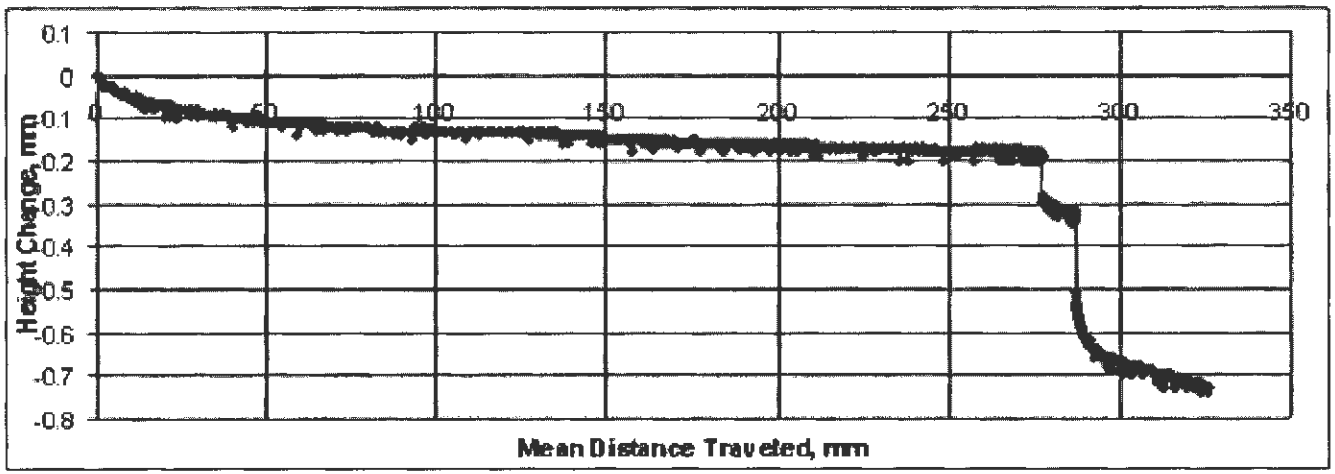

Figure A.90. 31.8 meter (105 ft), Pierre Shale, Oahe Dam Site, PZT50-5.42, settlement plot

APPENDIX B

MULTISTAGE BROMHEAD RING SHEAR PROCEDURE AFTER ASTM D6467

Authors: Birchmier, M.A. and Voros, S.

1. A 1-kilogram sample is taken out of the bulk sample at a known depth.
   Use enough soil for multiple tests, do not necessarily need 1 kg.
   Air-dry sample

2. The clay/shale is crushed by mortar and pestle until material passes the #50 sieve. Be careful not to crush large individual particles into smaller particles.
   Need at least 50g of passing #50 per test.
   Crushing causes artificial surfaces, which have been shown to influence the residual strength. Too much crushing is similar to ball milling, which affects the clay particles themselves.

3. Obtain the material that passes the #50 sieve and increase the soil's water content with distilled water or other chemically prepared water to the soil's plastic limit
   ASTM D6467 says liquid limit—LL was used mostly with the other types of ring shear, not with the Bromhead Ring Shear Device (Bromhead 1979). Excessive settlement of the top platen occurs for wetter materials. The final moisture content of the material is also near the PL.

4. Hydrate the soil for a minimum forty-eight hours or other time as necessary.

5. Mold the hydrated soil into the annular sample recess of the sample container by hand, tamping carefully.
   • The sample container disc should be saturated with water before soil is added.

6. Using a spatula knife, trim the excess molded soil flush with the surface of the sample container in the direction of shearing.
   Direction of shearing = clockwise.

7. Obtain the moisture content of the soil using the excess soil shavings. Note the weight of the apparatus and molded soil on the data form.
   For moisture content, about 15 g of soil is needed.
   Typical weight of apparatus and soil is 1890 g; this weight should be measured after each test. Record the weight on the data form.
   Remolded dry density is obtained from the moisture content and the soil's volume and weight.

8. Place the sample container in position on the locating studs. Replace and tighten knurled retaining nuts.

9. Place the torque arm assembly on top of sample container.

10. Swing loading yoke into position above the torque arm assembly.

11. Flood the sample by filling perspex water bath with distilled or chemically prepared water.
- Water bath – covers lower portion of torque arm assembly.

12. Place initial seating load on sample. .

13. Place the vertical load transducer on the loading yoke. Start the Datalogger on the computer.
Open the Wykeham Ferrance folder on desktop, open the DataLogger2000 folder and open DataLogger2000.exe.
Ensure the Data Logger is on.
Open the Logger drop-down menu and click Connect.
Open the Tests drop-down menu click Load and open RingShear.tst file.

14. Note the parameters (Sample ID, Stage, Comments) of the test in the program. See Figure 1.
Sample ID – will be the file name
Stage = 1
Comments – date, test depth, moisture content info, amount of load and/or shearing rate, testing stage description (consolidation or shearing w/ rate).

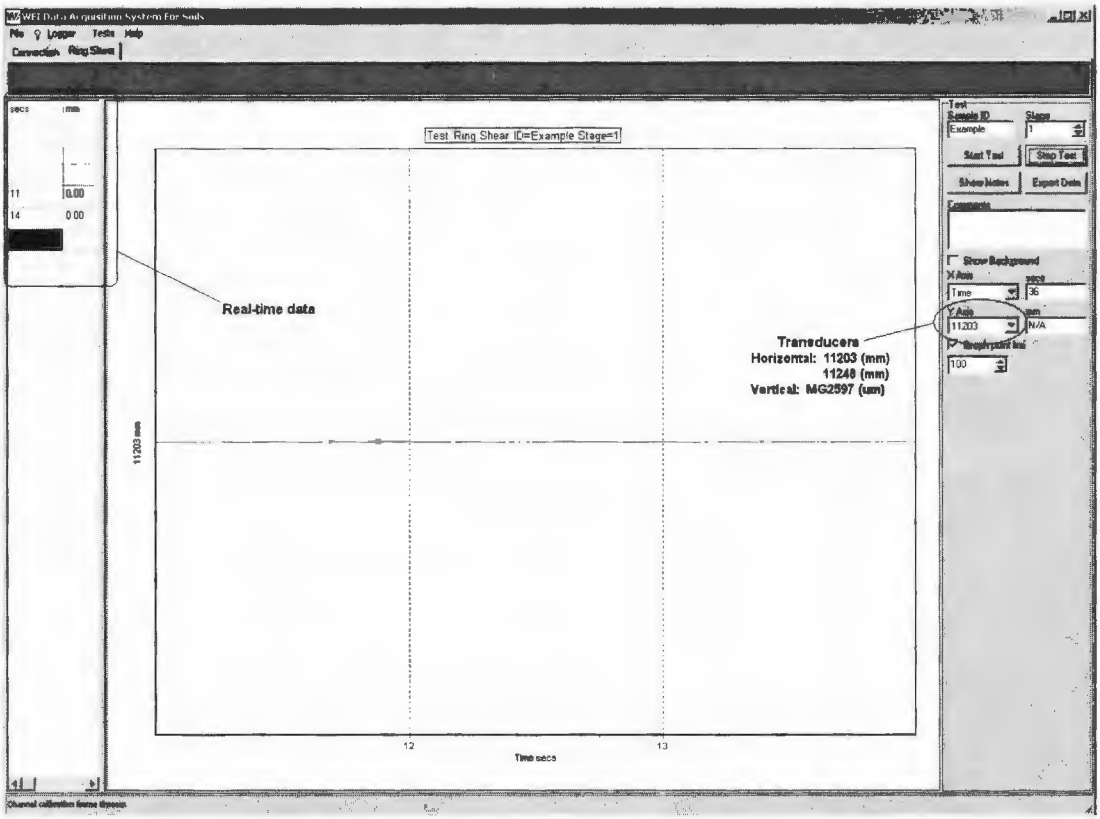

Figure 1. Display screen.

15. Start the consolidation process of the remolded soil with the initial normal stress to be used for loading.

Place vertical transducer on top of loading yoke.

Click Start Test and add the initial weight to load hanger – almost simultaneously

- For a 50.5 kPa normal stress, place 2 kg on the hanger.

For a 101 kPa normal stress, place 4 kg on the hanger.

Lower stresses tend to give higher friction angles. By starting at 101-kPa stress, you can work your way up to 400-kPa stress. Too large of stresses cause excessive settlement, causing skin friction to be excessive.

16. Consolidate the soil for approximately one hour.

Consolidation is found to be a minor part of the test. As we are working with such a small thickness drained on both sides, t_b is negligible.

Consolidation can be monitored directly (view data from transducer MG2597).

We have found that with small sample size, consolidation is complete in an hour or less.

17. Export and *always* save the consolidation stage as an Excel file (not as a .csv file).

Click Stop Test.

Click Export Data.

Click Show in Excel and save as an .xls file

Data filtering not needed for stage 1.

18. To form the initial shear surface, adjust the displacement rate to 0.16 deg/min.
Refer to machine template or data in WF Manual to adjust gears.
The rate of 0.16 deg/min is to shear the sample to align the particles in orientation with movement, the first part of obtaining the residual shear.
Higher rates influence the residual strength greatly and cause excessive settlement.
Lower speeds can be used but take longer.

19. Lock in, turn on, and zero the load dials. Ensure that the load dial end is perpendicular to the top platen. Place a small load on each side, giving a reading of approximately 0.03 to 0.09 on the load dial. This ensures contact is made between the dial end and the top platen.

20. Input the information for this stage into the Datalogger program
Stage = 2. This is the first shearing stage.
In the comments area, input the shearing rate (0.16 deg/min) and the load (101 kPa, or other initial load).

21. Start the Datalogger and shearing at 0.16 deg/min
Click Start Test while turning on machine.

22. Shear the soil at 0.16 deg/min for approximately 36 hours (~1.5 rev)
37.5 hrs provides for exactly 1.5 rev.
Check level of water in the water bath at least once every 24 hours.

23. At the end of this stage, turn off machine and click Stop Test to end test stage and export data into Excel
Export process - filter the data by 50 (by percent of travel)

24. Reduce the rate to 0.048 deg/min, input the new data for next stage into the Datalogger
When changing strain rate –move the dials from torque arm and replace them after changing rate.
When replacing dials, lock in, and zero the load dials. Ensure that the load dial end is perpendicular to the top platen. Place a small load on each side, giving a reading of approximately 0.03 to 0.09 on the load dial. This ensures contact is made between the dial end and the top platen.
New data is Stage 3, and 0.048 deg/min – load is still 101 kPa (or other initial load)

25. Restart the Datalogger, and run the test until constant residual shear strength is obtained for 0.5-1 hour. This step takes approximately 4-6 hours.
It is necessary to monitor the values on both load transducers (11203 and 11248) to ensure a constant residual strength is obtained.
Turn off the ring shear machine, click Stop Test and export data into Excel
Export process - filter the material by 50 (by travel)

26. Increase the normal stress to 198 kPa (8kg) and let consolidate for approximately one hour; input the new data for next stage into the Datalogger
Add an additional 4 kg to lever arm
New data is Stage = 4, and 198 kPa (8 kg)

27. Restart the Datalogger, maintaining rate of 0.048 deg/min and run until a constant residual shear strength is obtained for 0.5-1 hour. This step takes approximately 4-6 hours.
Turn off the ring shear machine, click Stop Test and export data into excel
Export process - filter the material by 50 (by travel)

28. Increase the normal stress to 394 kPa (16kg) and let consolidate for approximately one hour; input the new data for next stage into the Datalogger
Add an additional 8 kg to lever arm
New data is Stage = 5, and 394 kPa (16 kg)

29. Restart the Datalogger, maintaining rate of 0.048 deg/min and run until a constant residual shear strength is obtained for 0.5-1 hour. This step takes approximately 4-6 hours.
Turn off the ring shear machine, click Stop Test and export data into excel
Export process - filter the material by 50 (by travel)

30. Remove the load from soil, remove the load yoke, remove the apparatus from the water bath and turn off load cells

31. Use a knife and carefully remove the sheared material from the ring shear apparatus.
Keep the sheared material for later analysis if desired
Try to keep the sample intact for analysis in the SEM, store in plastic bag
32. Carefully and thoroughly clean the machine with distilled water.

Other notes:
Check oil three to four times a year, dependent on use. Do not overfill.
Grease inside gears once to twice a year, dependent on use.

APPENDIX C

OAHE DAM, STATION 50+00: BORING AND ENGINEERING CLASSIFICATION

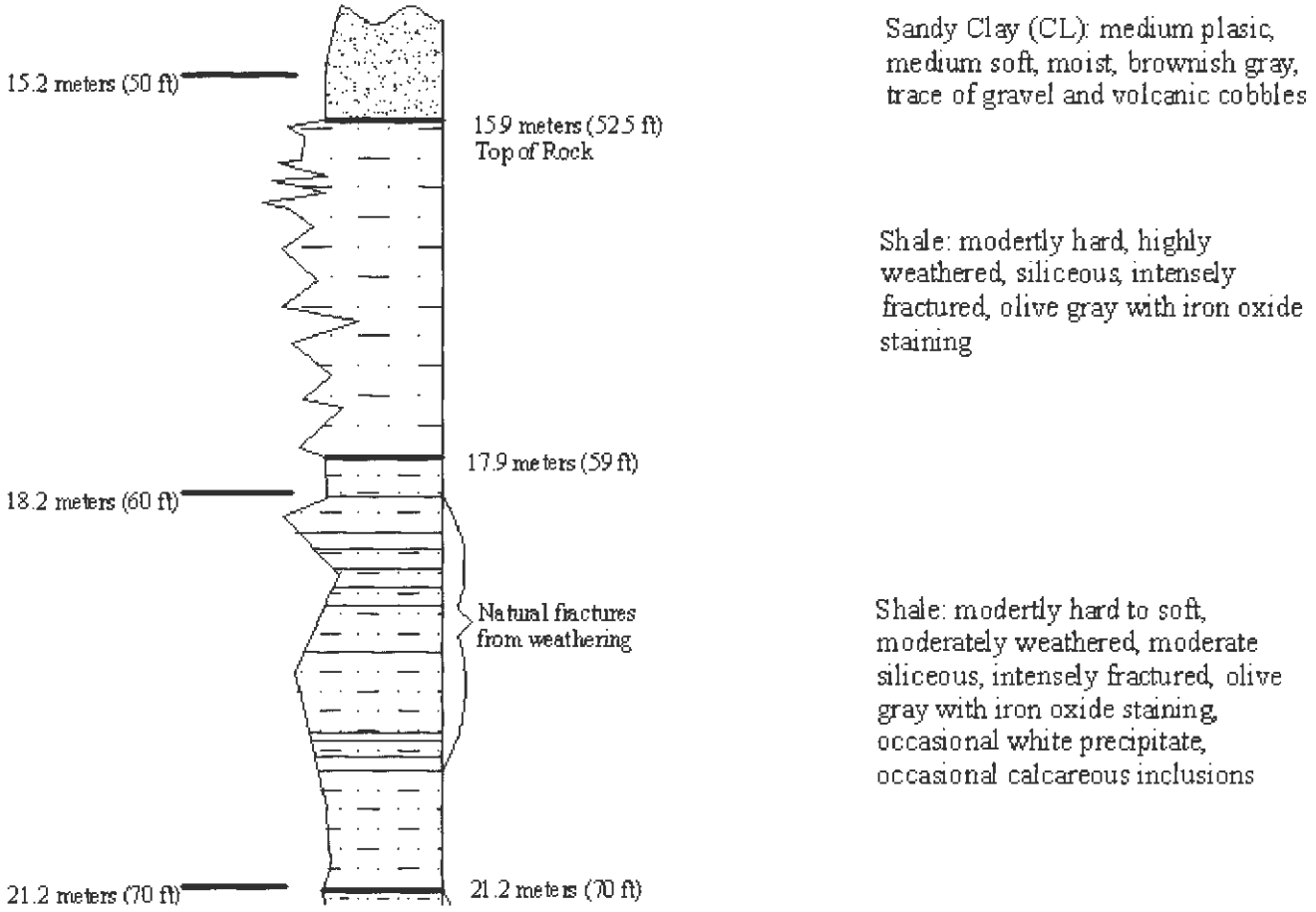

Figure C.1. Boring Information: Boring- PZT50/5.42; Location: Oahe Dam, Pierre, SD; Elevation: 475.95 meters (1570.62 ft); Drill Date: June 13-21, 2001

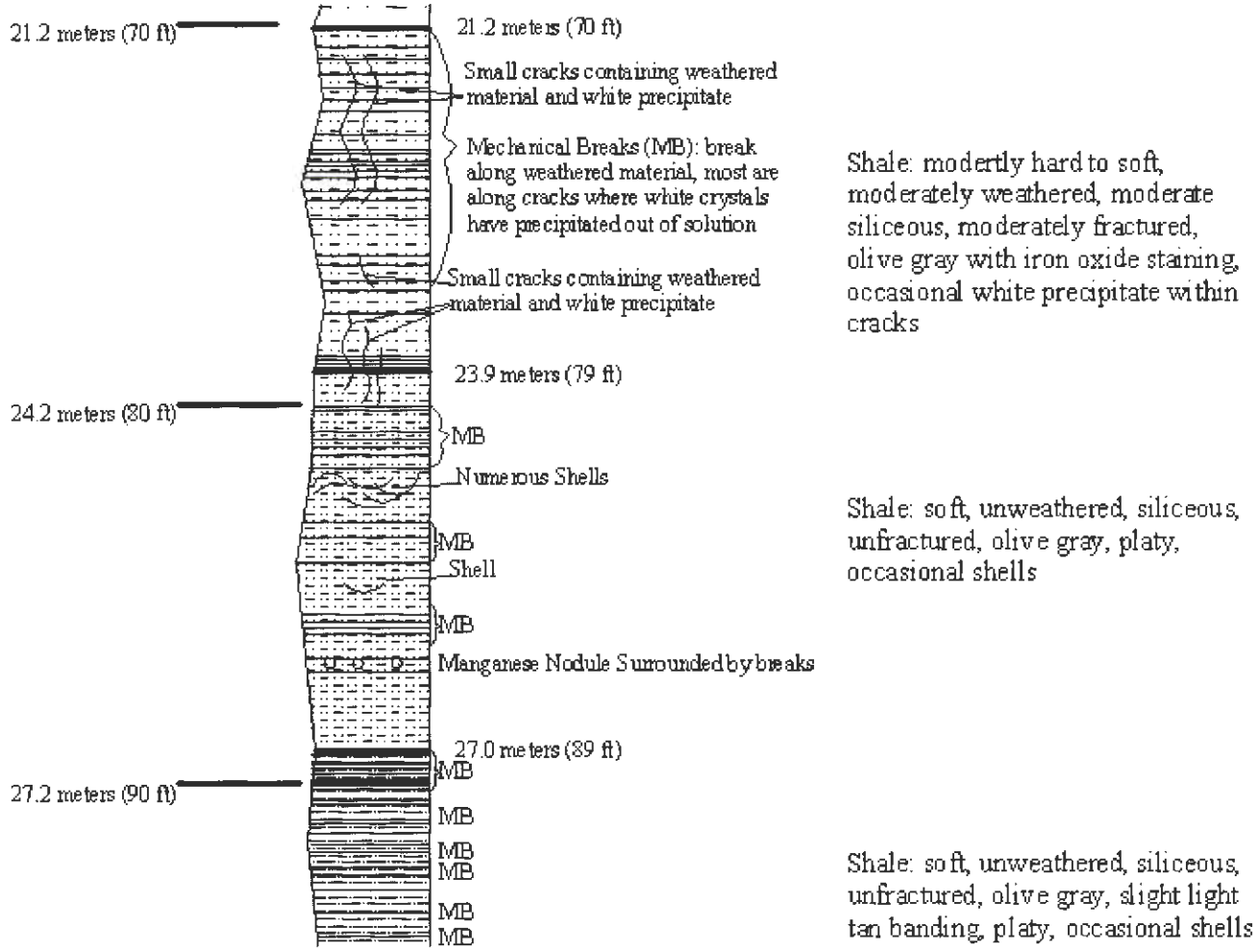

Figure C.1. con't. Boring Information: Boring- PZT50/5.42; Location: Oahe Dam, Pierre, SD; Elevation: 475.95 meters (1570.62 ft); Drill Date: June 13-21, 2001

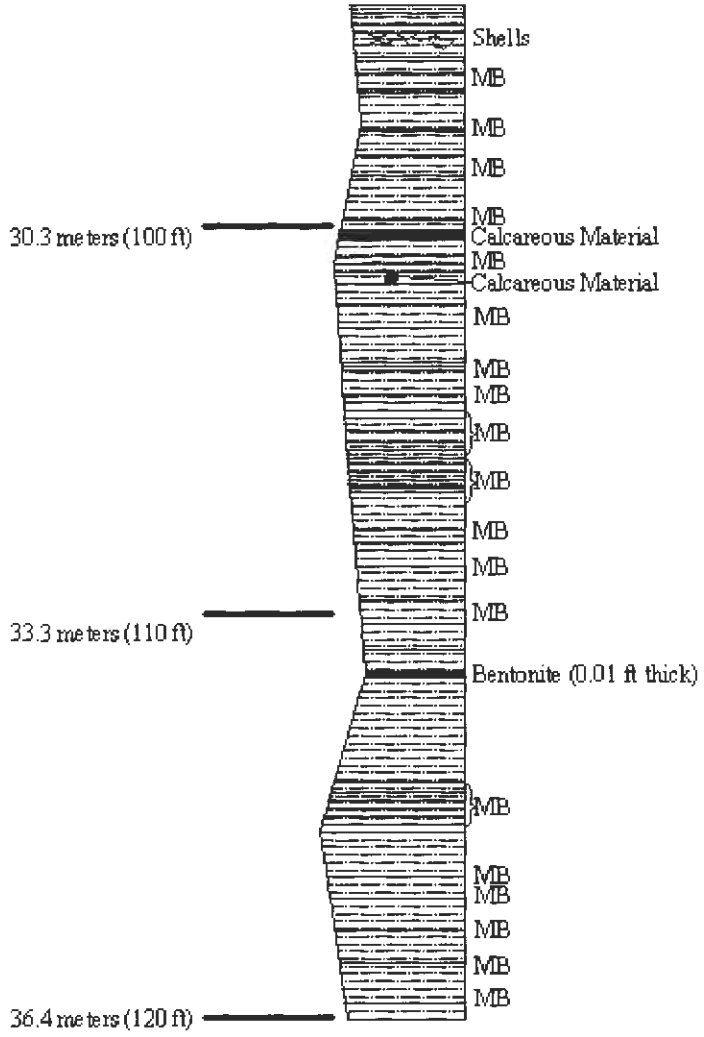

Shale: soft, unweathered, siliceous, unfractured, olive gray, light tan calcareous banding, platy, trace shells

Figure C.1. con't. Boring Information: Boring- PZT50/5.42; Location: Oahe Dam, Pierre, SD; Elevation: 475.95 meters (1570.62 ft); Drill Date: June 13-21, 2001

Table C.1. PZT50-5.42 Atterberg Limit

Depth (m)	Depth (ft)	Liquid Limit (%)	Plastic Limit (%)	Plastic Index (%)
17.9	59	76.4	46.6	29.8
18.5	61	66.2	41.6	24.6
19.1	63	75.0	45.7	29.3
19.7	65	76.3	43.6	32.7
21.8	72	65.5	44.4	21.1
22.7	75	71.1	41.2	29.9
23.3	77	66.7	41.1	25.6
23.9	79	71.4	41.5	29.9
24.8	82	82.0	46.0	36.0
25.8	85	68.2	44.2	23.2
26.4	87	61.5	40.0	21.5
27.0	89	63.8	41.5	22.3
28.8	95	88.2	42.4	45.8
31.8	105	71.2	43.5	27.7
33.9	112	74.2	46.6	27.6

Table C.2. PZT50-5.42 particle size analysis (hydrometer)

Depth m	Depth ft	>0.074 mm	0.074-0.002 mm	<0.002 mm
17.9	59	7.8	42.2	50.0
18.5	61	4.2	49.8	46.0
19.1	63	2.2	65.8	32.0
19.4	64	5.0	65.0	30.0
19.7	65	1.5	48.5	50.0
21.2	70	5.9	43.1	51.0
22.7	75	25.5	62.5	12.0
23.3	77	30.9	53.1	16.0
23.9	79	23.1	56.9	20.0
24.8	82	9.3	75.7	15.0
25.8	85	9.3	74.7	16.0
27.3	90	2.0	62.0	36.0
28.8	95	4.7	67.3	28.0
31.8	105	5.1	67.9	27.0
33.9	112	3.0	75.0	22.0

Table C.3. Weathering cycle Atterberg Limit

Depth m	Depth ft	Weathering Cycle	Liquid limit (%)	Plastic limit (%)	Plastic index (%)
63.0	208	0	79.0	33.1	45.9
63.0	208	1	85.0	34.7	50.3
63.0	208	2	88.2	35.5	52.7
63.0	208	3	100.0	40.4	59.6
63.0	208	4	113.0	40.2	72.8
63.0	208	5	125.0	42.9	82.1
63.6	210	0	62.8	31.9	30.9
63.6	210	1	78.3	34.4	43.9
63.6	210	3	79.0	35.4	43.6
63.6	210	5	85.9	36.1	49.8
70.3	232	0	71.5	30.9	40.6
70.3	232	1	71.6	30.4	40.9
70.3	232	2	72.1	30.8	41.3
70.3	232	3	74.2	32.1	42.1
70.3	232	4	68.0	29.2	38.8
70.3	232	5	70.9	30.8	40.1

APPENDICES D & E

SYSTEM REQUIREMENTS

CD

These appendixes are located on a CD-ROM and contain data regarding the micromorphology, mineralogy and chemistry of the tested material. Micromorphology and EDS results are located on the file labeled Appendix D. X-ray diffraction and x-ray fluorescence analyses are in the file labeled Appendix E.

System requirements for the CD: IBM PC or 100% compatible; Windows 95, 98, NT, 2000, Me, or XP; Pentium® 166 Mhz or faster; 32 MB RAM; CD-ROM; Microsoft Word 2000 or higher.